POLITECNICO DI MILANO

Scuola di Ingegneria Industriale e dell'Informazione

Corso di Laurea Magistrale in Ingegneria Energetica Orientamento Idrocarburi

Foam Assisted Water Alternating Gas Injection Optimization Under Uncertainties on a Real Reservoir

Relatore:	Prof. Giovanni LOZZA
Co-relatore:	Prof. Martin Julian BLUNT
Tutor Aziendale:	Ing. Caterina TOPINI
Tutor Aziendale:	Dott. Andrea Luigi LAMBERTI

Tesi di Laurea di:	Massimo MONTES
Matricola:	800425

Anno Accademico 2013-2014

Acknowledgements

Milan, 3rd October 2014

I wish to offer my sincerest gratitude to many persons who contributed positively to this work.

Foremost, I express my thankfulness to my advisor Professor Giovanni Lozza who has been always helpful since I applied for the ENI scholarship and during my academic career. He also allowed me to be followed by Professor Martin J. Blunt who provided me many suggestions with his knowledge and patience during the development of the thesis and, therefore, as much gratitude is addressed to him.

Besides my advisors, I thank my company-supervisors Andrea Lamberti and Caterina Topini for their share of experience and their unfailing help. They hugely improved my knowledge about reservoir engineering, guided me throughout many problems and gave me suggestions to successfully complete this work.

Furthermore, during the last months, two persons have inordinately contributed to my breakthrough in the dissertation and became key players of my internship: Ernesto Della Rossa and Riccardo Sabatino. They spent much time providing relentless help and, without their participation, I would not have arrived so far. This is the reason why undeniable thankfulness has to be addressed to them.

Also Marco Rotondi played a central role, as he allowed me to join the reservoir engineering department at ENI after I had pro-actively sought out the best sector to keep my interests burning. Thus, special thanks are due to him.

Then, huge gratitude is directed to my mother, because of her incommensurate love and help provided during these years spent far away from my hometown, and to my uncle and aunt, who have always supported me like second parents. With regards to this fact, I would like to thank my father for having always inspired me since I was a child and after he passed away.

Last but not least, I thank my colleagues and, at the same time, friends Marco, Luca and Riccardo, for the great moments shared with them during this exciting path, and all my friends who have always been very close to me, especially Carlo and Andrea, with whom I spent a significant part of my life.

Massimo Montes

Abstract

In recent years, injections of surfactant have been studied in the oil industry to generate foam inside the reservoir in order to mitigate the negative effects on the production, due mainly to the high mobility of the gas injected during enhanced oil recovery processes. Several applications, conducted at both pilot and field scales, led to extremely beneficial results from an economic point of view, by improving the exploitation of the selected reservoirs. Laboratory experiments have been carried out in parallel to empirical simulation models, in order to examine in more detail the effects of this process and the behavior of the foam inside the reservoir.

The aim of this work is to suggest an approach to achieve optimal results in terms of future reservoir management and control, at the same time, the uncertainties related to the foam behavior. The methodology has been applied to a real field through the available simulation model.

The chosen greenfield is an off-shore reservoir located in the West Africa region. It will be earmarked for enhanced oil recovery techniques (WAG – Water Alternating Gas) aimed at associated gas disposal and oil production improvement. In order to mitigate the possible negative effects coming from the gas production, the surfactant injection is proposed to generate the foam inside the reservoir. Thus, the reported approach consists of a robust oil and gas production optimization, consequent to foam application, through proxy model applied to an optimized WAG base case. Once that ranges of uncertain parameters coming from the simulation model have been proactively selected, optimal possible averaged values have been obtained shaping a Pareto frontier.

The positive results achieved show the possibility to improve the oil recovery and minimize the gas production. Anyhow, it is necessary to plan detailed laboratory analyses (core-floods and surfactant selection) to verify the surfactant injection efficacy inside the selected reservoir.

Keywords: Enhanced Oil Recovery; Robust Optimization; Reservoir Simulation; Foam-Assisted-Water-Alternating-Gas; Uncertainty; Proxy.

Sommario

Negli ultimi anni, iniezioni di tensioattivo sono state studiate nell'industria petrolifera allo scopo di generare schiuma in giacimento per mitigare le ripercussioni negative sulla produzione, dovute principalmente all'alta mobilità del gas iniettato durante processi di recupero avanzato. Diverse applicazioni, condotte sia a livello pilota che di campo, hanno portato a risultati estremamente vantaggiosi in termini economici, migliorando lo sfruttamento dei giacimenti selezionati. Allo scopo di analizzare con maggior dettaglio gli effetti derivanti da tale processo ed il comportamento della schiuma in giacimento, sono stati sviluppati in parallelo esperimenti di laboratorio e modelli di simulazione empirici.

L'obiettivo di questo lavoro è quello di proporre un approccio che verta a conseguire risultati ottimali in termini di gestione futura del giacimento, governando le incertezze relative al comportamento della schiuma. La metodologia è stata applicata ad un campo reale tramite il modello di simulazione disponibile.

Il giacimento selezionato, è un campo off-shore del West Africa non ancora entrato in produzione. Il campo è destinato ad essere sviluppato con tecniche di recupero avanzato (WAG – Water Alternating Gas) finalizzate allo smaltimento del gas associato e all'incremento della produzione di petrolio. L'iniezione di tensioattivo per la formazione di schiuma in giacimento è stata proposta per mitigare i possibili effetti negativi legati alla produzione di gas. Partendo quindi dall'ottimizzazione del caso WAG, l'approccio si basa su un'ottimizzazione robusta della produzione di petrolio e gas a seguito dell'applicazione di schiuma in giacimento tramite l'utilizzo di modelli proxy. Dopo aver preventivamente selezionato i range di incertezza dei parametri del modello di simulazione, si sono ottenuti possibili valori ottimali mediati con la formazione di una frontiera Paretiana.

I risultati positivi così conseguiti mostrano la possibilità di incrementare la produzione di petrolio minimizzando la produzione di gas. Sarà però necessario pianificare analisi di laboratorio di dettaglio (selezione di tensioattivo e flussaggi in carota) per confermare l'efficacia dell'iniezione di tensioattivo nel giacimento selezionato.

Parole chiave: Recupero Avanzato di Petrolio; Ottimizzazione Robusta; Simulazione di Giacimento; Foam-Assisted-Water-Alternating-Gas; Incertezza; Proxy.

Extended summary

1. Introduction

Traditionally, three stages characterize chronologically the oil production process: primary, secondary and tertiary recovery. During primary recovery, the fluid rise is due to natural factors or artificial mechanisms applied at the wellbore-level and, the obtainable recovery factors are usually small. On the other hand, during the secondary recovery either water or gas is injected inside the reservoir to displace and produce a higher amount of oil, increasing in this way the recovery factors until economically feasible. Then, tertiary recovery can be started at any time of the productive life of a reservoir depending on affordability. This process aims to further increase oil production by altering the physic-chemical properties of hydrocarbons and rock.

2. WAG Injection processes

WAG (Water-Alternating-Gas) processes allow an improvement of the oil production by injecting water alternating gas from the same well. The benefits obtainable compared to a simple gas or water injection are a combination of microscopic and macroscopic effects, which are more or less evident depending on the selected case. From a microscopic point of view, despite an initial preferential channeling, the alternation of injected phases leads to a discontinuity of the same phases inside the porous medium, improving the obtained recovery. On the other hand, from a macroscopic point of view, favorable ratios water/gas volumes injected avoid formation of tongues within the advancing front. Additionally, gravitational phenomena lead to a better displacement inside the reservoir, as the gas, which tends to rise toward the upper-layers, displaces a volume of water that would have not otherwise been displaced by water.

The main difference among WAG techniques is the distinction between miscible and immiscible injections. The former are characterized by low values of surface tension between oil and gas and by a process of microscopic enlargement of the preferential path made by the continuous gas/oil phase. However, in the case of immiscible injections the gas phase tends to follow the same microscopic preferential pathway and no channel enlargements are noticeable.

The decision-parameters choice during WAG processes is essential to ensure improved oil recoveries. First and foremost, the choice of the gas to be injected (mainly differentiated between hydrocarbon, non-hydrocarbon and CO2) is important for both technical and

economic feasibility of the process. Key roles are also partly attributable to injection patterns and heterogeneity of the reservoirs. Furthermore, a good water/gas injected ratio allows a good control of the mobility and the advancement of the displacing front.

Operational problems may arise from the continued alternation of injected phases. In fact, a premature production of the injected gas may take place and cause the producers shut-off. Moreover, the wells-injectivity may be compromised due to both the fragmentation of the phases and the entrapment of gas inside the pores. Finally, corrosion, asphaltenes and hydrates may affect the productive life and damage the economics of the projects.

3. Fundamentals of Foam Assisted WAG

Foams can be used to solve displacement problems due to either thief zones or gravity over-ride. In this regard, three classes of foam can be identified according to their action on the gas and their scale of application (well or reservoir): in-depth mobility control foams (MCF), blocking/diverting foams (BDF) and gas-to-oil ratio foams (GOR). Furthermore, depending on the generation and injection methods (which involve different degrees of mobility reduction), a further classification can be implemented: pre-formed foams, co-injection foams and surfactant-alternating-gas foams.

At reservoir conditions, a foam is considered to be a dispersion of gas in a continuous liquid phase (surfactant and water), where the gas flow-paths are made discontinuous by thin liquid lamellae. These lamellae collapse when their thickness drops below a critical value in correspondence to critical values of water saturation, capillary pressure and foam quality (f_g) (ratio between injected gas and water flow-rates). Three states inside the porous media can then be classified: foam absence; weak foam (low gas-mobility reductions); strong foam (many lamellae and high gas-mobility reductions).

Once the surfactant has been selected, special attention must be paid to the process variables, as they have large effect on the application effectiveness. In particular, the most important ones are: permeability, injection rates, pressure, surfactant-type, oil interactions, adsorption and temperature.

4. Full field analysis

The reservoir is modeled through the 3-D simulation software ECLIPSE by a black-oil model, namely the hydrocarbon components are simply differentiated between oil and gas phases and the only compositional information is represented by the two densities.

The subject of this work is an under-saturated deep-water offshore Angolan reservoir (FIELD α). Thus, the oil is immiscible with the gas and, data collected, the oil-water contact is close to the perforations of the producers, suggesting possible premature gas breakthroughs. In terms of development, the field involves the use of an FPSO (Floating, Production, Storage and Offloading) unit for the production, which is connected to two producers and two injectors. Moreover, the produced gas (in addition to the gas coming from neighboring fields) must be re-injected due to no-flaring policies, for gas disposal purposes in the absence of other solutions.

A simulation base-case characterized by water-injection only is useful to check whether it is convenient to select FIELD α as a good candidate for WAG. At the end of the selected time frame, the producer P-302 closes prematurely because of high values of water cut. Moreover, by visually analyzing the reservoir fluid saturations, it becomes evident the presence of an undisplaced oil-cap, endorsing the possible application of the considered enhanced oil recovery technique.

The decision variables analyzed during the WAG optimization process are:

- injection slug time-length (3 to 12 months for operational constraints);
- injection-well starting the first gas slug injection after 2-years of continuous water injection;
- voidage replacement ratio (VRR), i.e. the ratio between injected water and produced liquids, in order to evaluate the injected water effect.

The influence of each one of these variables is then evaluated by a full-factorial experimental design, i.e. all the 60 possible combinations (3 values of VRR are selected) are simulated. From an initial analysis, it appears that low VRR values (0,7) lead to a premature producers shut-off. Moreover, the choice of injector I-402 as the one starting with the first gas slug, leads to generally greater oil recoveries. Thus, once the ranges have been reduced, the apparently best case is taken into account (12 months long-lasting injection) and the possible VRR variation for each injection is studied (8 injections for the selected time frame). Since it would be unreasonable and impossible to simulate all the possible combinations of variables, a 150 cases sample is obtained by means of the Latin Hypercube Sampling technique (LHS) in order to try to best represent the space of possible simulations. The resulting distribution shows that the maximum variation of total oil produced (FOPT) at the end of the 10-years time-frame is very small (about 0,3%). Furthermore, the several VRRs, with the exception of the first one, exhibit a weak or even very weak correlation with the results. These observations endorse the futility of long and accurate optimizations. Before drawing any conclusion, a set of 250 simulations is run for the 8-months lasting injections (those with shorter injections show premature shut-offs), representing the other possible cases with injections shorter than 12 months. Anyhow, this latter distribution lies clearly below the other one (12 months, thus selected as the best case).

Subsequently, through a comparison with the simple VRR=1 case, the latter appears to generate the best results in terms of NPV, due to the anticipated production. The VRR=1 case is therefore defined as the optimal one. A comparison with the simple water-injection case shows good results in terms of recovery factors (ΔRF=+2,41%), but, at the same time, it exhibits a substantial increase of the gas production.

By having a look at the production profiles, the problems due to the gas are evident and underlined by a visual analysis of the fluids (water, gas and oil) saturations. In fact, the gravity-override is evident inside the reservoir during production. This is why producers experience early-gas breakthrough.

5. Foam-Assisted-WAG Optimization

The used ECLIPSE model considers the foam as a surfactant concentration in the aqeous phase. It is subject to natural decay and adsorption and it changes the gas mobility through the following direct multiplier:

$$M_{rf} = \frac{1}{1 + M_r^{ref} F_w F_s F_o F_c} \quad \text{(I)}$$

where:
M_r^{ref} represents the reference mobility reduction factor;
F_w, F_s, F_o, F_c are factors affecting the foam strength.
In particular, F_w represents the weakening due to an excessive reduction of the water saturation, F_s represents the negative effects of an exaggerated reduction of surfactant concentration, F_o represents the instability created by the oil and F_c represents the mobility alteration due to shear-thinning behaviors at a low foam-quality. Each of these factors is then decomposable in a term representing the limiting value of the parameter controlling the physical event, i.e. S_w^{lim} (limiting water saturation), C_s^{ref} (reference surfactant concentration), S_o^m (maximum oil saturation), N_c^r(reference capillary number), and exponents controlling the abruptness of the transition in the limiting stage, i.e. f_w, e_s, e_o and e_c. Anyway, decay and F_c are excluded from the reported analysis.

Thus, the two objectives of the presented analysis are minimization of the gas and maximization of the oil produced. The problem variables are divided into two groups: operative decisional variables and uncertain variables. The former are concentration and injection time-length of three surfactant injections, namely six variables are considered (C_{s1}, C_{s2}, C_{s3}, T_{s1}, T_{s2}, T_{s3}), whereas the latter are the same terms considered in the foam model, i.e. eight variables. For all of them, from a probabilistic point of view, a reasonable uniformly distributed range is chosen (with a base case, maximum and minimum values), in order to take into account the maximum level of uncertainty.

The problem is then subdivided into two parts: a first analysis focused on the oil and a following complete robust analysis which takes into account the outcomes of the previous analysis.

Based on the analysis of the oil, a stepwise regression of the decision variables is executed on a 126-simulated samples obtained through LHS. It shows a certain importance with regard to the parameters of the first and second injection, while it is reasonable to neglect the variation of variables of the third slug (C_{s3}, T_{s3}), but not their presence.

A nominal optimization is implemented to find the best values of the remaining four decision variables, by means of a proxy modeling technique which approximates the objective function (FOPT) and its relationship with the inputs. For this purpose, the Universal Kriging interpolation method is selected. Since it cannot exist without a validation stage, 70% of the samples resulting from LHS is randomly selected for the building process and the remaining 30% is used to verify the accuracy. Once the proxy is considered valid, a nominal optimization can be performed. 10000 predicted evaluations are carried through LHS. The best 40 ones are then really simulated and then the best 10 out of 40 are analyzed to reduce the decision variables range.

Subsequently, a sensitivity analysis of uncertainties is executed by varying one variable at a time (OVAT) and setting it equal to the minimum or maximum value of the range (the others are set to the base case). In this way, 17 simulations are performed and the results show a tiny change of oil recovery, which allows to avoid further detailed analyses focused on one outcome only. Thus, the ranges are kept tight to allow a complete robust analysis of both gas and oil.

The stepwise regression of the 126 sites coming from LHS reported for the FOPT is repeated for the total gas produced (FGPT) in order to check whether it is possible to reduce the ranges and neglect the variability of the parameters characterizing the third slug. The results are slightly better than the ones obtained for the oil case in terms of determination coefficient (R^2). Anyhow, the relevant parameters are exactly the same. A trade-off between the objective functions thus exists, since a reduction of the volume of gas produced implies generally a reduction of oil produced as well. The OVAT analysis is repeated as well as sensitivity analysis for the uncertain variables e the same parameters, this time much more impactful on the outcomes, are relevant.

Up to this point, once the ranges are reduced, it is possible to build the proxy functions. For this purpose, however, since 9 variables are considered (both uncertain and decision variables simultaneously), a rich cluster of simulations is necessary. Thus, 2000 runs are executed (of which 1990 are not corrupted), requiring a considerable computational effort which leads to the following output distribution:

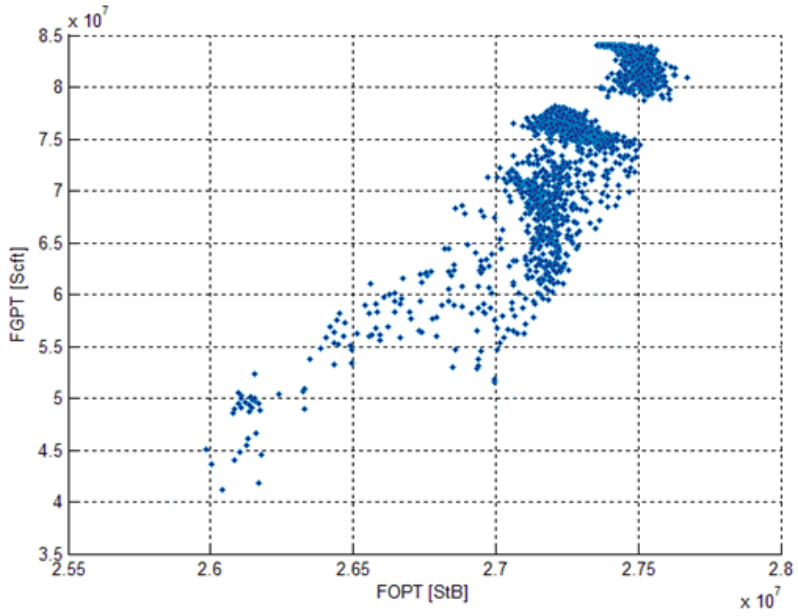

Figure I - Illustration of the FGPT and FOPT values resulting from the 1990 simulations run

The distributions of decision variables do not follow any particular and noticeable trend, whereas this is true for some uncertain variables, supporting the most effect on the outcomes given by the uncertainties and the need of a robust optimization. So, the proxies are obtained by a multilinear regression method. The superiority of the one built for the gas is clear if compared to the one built for the oil in terms of R^2 and normalized error.

10000 sites are then predicted through the proxy functions, resulting from 100 random sets of values of decision variables combined with as many sets of values of uncertain variables (obtained by LHS). All the uncertain variables are then averaged for each set of decision ones, so that 100 predicted sites robust with respect to the uncertainties are obtained. In fact, what is evident from the new distribution (significantly reduced compared to Fig. I) is that the trends for three of four decision variables (C_{s1}, C_{s2}, T_{s1}) are much more underlined. The optimization of the objective functions can be expressed, in terms of aggregate functions, as follows:

$$F_{max} = \max(\overline{FOPT}_{\boldsymbol{u}} - \lambda \cdot \overline{FGPT}_{\boldsymbol{u}})$$

where $\overline{FOPT}_{\boldsymbol{u}}$ and $\overline{FGPT}_{\boldsymbol{u}}$ represent the outcomes averaged on the uncertainties, whereas λ represents the weight (in terms of economic benefits) of the gas reduction compared to the increase of oil produced. Thus, by varying the values of λ, several possible optimal sites are obtained, shaping in this way a Pareto frontier inside the frame of interest. An assessment of the results obtained by simulating 300 cases is then made. These 300 simulations correspond to the values of decision variables of the three intermediate sites of the predicted Pareto frontier (the extremes are dominated sites). They are averaged as well and the outcomes (both predicted and simulated) are shown in the following figure:

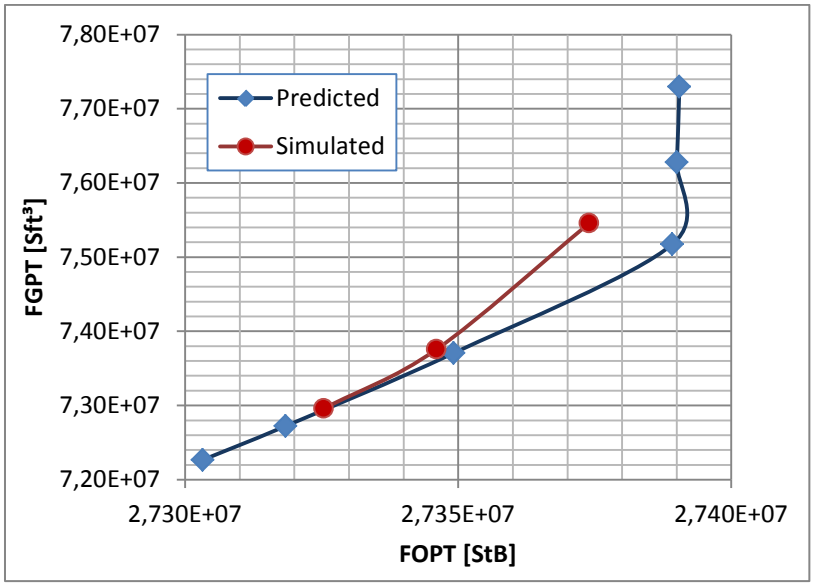

Figure II - Illustration of the comparison between simulated and predicted frontier

Through an analysis of the percentage errors related to the averaged outcomes and through an evaluation of the dispersion by means of the relative standard deviation (RSD), it is clear that the gas-proxy is much more accurate than the oil-proxy. Values obtainable on the Pareto frontier, however, demonstrate significant benefits in terms of produced gas reduction compared to the optimal WAG case, whereas oil recovery shows a very limited increase, representing rather a constraint for possible high reduction of produced gas. Furthermore, in order to better visualize the beneficial effects of foam application, a case very close to one of the three averaged optimal sites is simulated for a profiles-analysis. The result is a clear decrease of volumes of gas produced and of GOR, while the oil appears to remain at values on average higher than the WAG case in terms of produced rates until the third surfactant injection occurs. This is due to the closure of both wells within the selected time frame because of the non-optimal choice of values for the parameters of the third slug. This fact supports the need of further analyses for the optimization of the whole field-life instead of the 10-years time frame. Moreover, more in-depth analyses carried in the laboratories will be necessary to select the optimal surfactant (within the chosen range for the parameters) and possible remedial actions must be analyzed in order to better address potential problems during the foam application.

6. Conclusions

This dissertation is focused on the application of foam to enhance the production of oil and reduce the gas produced. For the selected field, the WAG technique has been selected to obtain the benefits just mentioned and to dispose the gas produced from other fields. Thus, the analysis proceeds through the selection of an optimal WAG case. Then, the foam

application is evaluated. 2000 runs are executed and an optimal robust analysis is performed, leading to a Pareto frontier of optimal sites.

So far, one of the main assumption is to consider only uncertainties related to the foam model. Furthermore, the model might be improved by minimizing the variances of the outcomes (GOPT and FGPT), in case the uncertainties are reduced, and by dealing with net-present values (NPV), which might, however, provide a modest added value.

Additional laboratory tests are needed before a real full-field application and the proposed analysis can be repeated to investigate possible foam application in other reservoirs.

Riassunto esteso

1. Introduzione

Tre fasi tradizionalmente caratterizzano cronologicamente la produzione di petrolio: recupero primario, secondario e terziario. Durante il recupero primario, la risalita di fluido è data da fattori naturali oppure da meccanismi artificiali applicati a livello di pozzo e i fattori di recupero ottenibili sono generalmente bassi. Durante il recupero secondario, invece, acqua o gas vengono iniettati a livello di giacimento per spiazzare e produrre una maggiore quantità di petrolio, incrementando in questo modo i fattori di recupero, fintantoché il processo risulti economicamente vantaggioso. Infine, il recupero terziario, che può comunque essere avviato o meno in qualunque momento della vita produttiva del giacimento a seconda della convenienza economica, punta ad incrementare ulteriormente la produzione di petrolio tramite alterazione delle proprietà chimico-fisiche degli idrocarburi e della roccia.

2. Processi di iniezione WAG

I processi WAG (Water-Alternating-Gas) permettono un miglioramento della produzione di petrolio tramite iniezione, da stesso pozzo, di gas alternato ad acqua. I benefici ottenibili rispetto ad una semplice iniezione di gas o acqua risultano così una combinazione di fattori microscopici e macroscopici più o meno evidenti a seconda dei casi. Da un punto di vista microscopico, nonostante un iniziale incanalamento preferenziale, l'alternanza delle fasi iniettate porta ad una discontinuità delle stesse nel mezzo poroso, migliorando in tal modo il recupero ottenuto. Invece, da un punto di vista macroscopico, rapporti favorevoli di acqua/gas iniettati portano ad evitare la formazione di lingue in corrispondenza del fronte di avanzamento. In aggiunta, i fenomeni gravitativi portano ad un migliore spiazzamento di tutto il giacimento, in quanto il gas che tende a salire verso la parte alta strutturale spiazza una quantità di olio che non sarebbe stata prodotta dall'acqua.

La principale differenziazione tra le tecniche WAG prevede la distinzione tra iniezioni miscibili e iniezioni immiscibili. Le prime sono caratterizzate da bassi valori di tensione superficiale tra gas e petrolio e da un processo microscopico di ingrossamento del cammino preferenziale della fase continua gas/olio dopo la prima iniezione gassosa. Nel caso di iniezioni immiscibili, invece, il gas tende a ripercorrere lo stesso cammino preferenziale a livello microscopico senza alcun ingrossamento del canale.

La scelta dei parametri decisionali durante i processi WAG è fondamentale al fine di garantire un recupero addizionale di petrolio. Innanzitutto, la scelta del gas da iniettare

(principalmente differenziato in idrocarburico, non idrocarburico e CO_2) risulta fondamentale per la fattibilità tecnico-economica del processo. Ruoli importanti sono poi attribuibili anche al pattern di iniezione e all'eterogeneità del giacimento. Infine, un buon rapporto acqua su gas iniettati permette il controllo della mobilità e dell'avanzamento del fronte di spiazzamento.

Problemi operativi possono nascere dalla continua alternanza di fasi iniettate. Infatti, una prematura produzione di gas iniettato può avvenire e causare la chiusura dei pozzi produttori. Inoltre, l'iniettività dei pozzi può essere compromessa a causa della frammentazione delle fasi e dell'intrappolamento del gas nei pori. Infine, anche corrosione e formazione di asfalteni e idrati possono compromettere la vita produttiva e danneggiare le economie dei progetti.

3. Fondamenti di Foam Assisted WAG

Le schiume possono essere utilizzate per risolvere problemi di spiazzamento dovuti a zone ladre o over-ride gravitazionale. A tal proposito, sono identificabili tre classi di schiuma a seconda della loro azione sul gas e della loro applicazione a livello di pozzo o giacimento. Esistono, quindi, schiume per controllo della mobilità (MCF), per blocco/deviazione del gas (BDF) e per controllo del rapporto gas/olio (GOR). Inoltre, a seconda del metodo di generazione e iniezione, implicanti diversi gradi di riduzione di mobilità, può essere attuata un'ulteriore classificazione: schiume pre-formate; schiume da co-iniezione; schiume per iniezioni di tensioattivo-alternante-gas (SAG).

In condizioni di giacimento, una schiuma è considerata una dispersione di gas in una fase continua di liquido (formata da tensioattivo e acqua), dove i percorsi di flusso del gas sono resi discontinui da sottili lamelle liquide. Queste ultime collassano allorquando il loro spessore scenda al di sotto di un valore critico, riconducibile a valori critici di saturazione dell'acqua, di pressione capillare e di foam-quality (f_g) (rapporto tra portate di gas iniettato e acqua iniettata). Possono quindi essere categorizzati tre stati nel mezzo poroso: assenza di schiuma; schiuma debole (con ridotte riduzioni della mobilità del gas); schiuma forte (con presenza di molte lamelle e alte riduzioni della mobilità del gas).

Una volta selezionato il miglior tensioattivo da utilizzare, particolare attenzione deve essere posta alle variabili di processo, le quali hanno largo effetto sull'efficacia dell'applicazione. In particolare, le più importanti sono: permeabilità, portate di iniezione, pressione, tipo di surfattante, interazioni con il petrolio, adsorbimento e temperatura.

4. Analisi a scala di campo

Il giacimento viene modellizzato il tramite software di simulazione 3-D ECLIPSE, in cui si ricorre ad un modello black-oil, ovvero le componenti idrocarburiche vengono distinte semplicemente in fase olio e fase gas e l'unica informazione composizionale è data dalle densità delle due fasi.

Il soggetto di studio è un giacimento sotto-saturo deep-water off-shore Angolano (FIELD α). Il petrolio risulta quindi immiscibile con il gas e, dai dati rilevati, il livello in cui petrolio e acqua entrano in contatto risulta prossimo alle perforazioni dei pozzi produttori, suggerendo possibili fenomeni di prematuro gas breakthrough. A livello di sviluppo, il giacimento prevede l'utilizzo di un'unità FPSO (Floating, Production, Storage and Offloading) per la produzione, connessa ad un layout di due pozzi produttori e due iniettori. Inoltre, il gas prodotto deve essere re-iniettato per politiche no-flaring insieme a quello di giacimenti confinanti, per scopi di smaltimento gas in assenza di altre soluzioni.

Un caso base di simulazione con semplice iniezione di acqua è utile per verificare se sia conveniente o meno selezionare FIELD α come candidato a tecniche WAG. Alla fine del riquadro temporale selezionato, si nota come il produttore P-302 chiuda precocemente a causa di un elevato water-cut. Inoltre, da un'analisi visiva del giacimento in termini di saturazioni, è evidente la presenza di una cappa di petrolio non spiazzato, che motiva il possibile utilizzo del metodo di recupero avanzato considerato.

Le variabili decisionali analizzate nel processo di ottimizzazione del caso WAG sono tre:

- tempo di durata di uno slug di iniezione (da 3 a 12 mesi per motivi operativi);
- iniettore di inizio con la prima iniezione a gas dopo i primi 2 anni di iniezione ad acqua;
- voidage replacement ratio (VRR), ovvero il rapporto tra acqua iniettata e liquidi prodotti, al fine di valutare l'effetto che ha il volume di acqua iniettata.

L'influenza di ognuna di queste viene quindi valutata con un design sperimentale di tipo fattoriale, ovvero tutte le 60 possibili combinazioni (con 3 valori di VRR) vengono simulate. Da una prima analisi, si nota come valori bassi di VRR (0,7) portino a chiusura prematura dei pozzi produttori e come iniziare la prima iniezione a gas tramite l'iniettore I-402 porti in generale ad un maggiore recupero di petrolio. A questo punto, una volta ristretti i range di variazione, viene preso in considerazione il caso apparentemente migliore (12 mesi di durata di ogni iniezione) e si analizza la possibile variazione di VRR per ogni iniezione (8 iniezioni per il riquadro temporale selezionato). Poiché sarebbe irragionevole e impossibile simulare tutte le possibili combinazioni di variabili, viene utilizzato un campionamento (150 casi) di tipo Latin Hypercube (LHS) per cercare di rappresentare al meglio lo spazio delle possibili simulazioni. La distribuzione risultante mostra che la variazione massima in petrolio prodotto (FOPT) alla fine dei 10 anni risulta essere molto piccola (circa 0,3%). Inoltre, i vari VRR delle iniezioni, ad esclusione del primo, mostrano una debole se non debolissima correlazione con i risultati. Queste osservazioni rendono idea dell'inutilità di effettuare un'ottimizzazione costosa ed accurata.

Prima di trarre conclusioni, un set di altre 250 simulazioni viene eseguito per il caso con iniezioni da 8 mesi (quelli con iniezioni più brevi mostravano chiusura prematura dei pozzi), a rappresentazione degli altri possibili casi con iniezioni più brevi di 12 mesi. Tuttavia, quest'ultima distribuzione è nettamente al di sotto di quella con iniezioni da 12 mesi, dalla quale è quindi selezionato il caso migliore in termini di recuperi finali.

A valle di questa selezione, tramite un confronto con il semplice caso a VRR=1, quest'ultimo risulta come apportante i maggiori benefici in termini economici, dato che la produzione viene anticipata. È quindi definito quale ottimale il caso con VRR=1 e un paragone con il caso a semplice iniezione di acqua mostra buoni risultati in termini di recovery factor (ΔRF=+2,41%), ma allo stesso tempo un sostanziale aumento di produzione di gas dovuto alle stesse iniezioni.

Dando uno sguardo ai profili di produzione, i problemi dati dal gas risultano manifesti e sono sottolineati da un'analisi visiva delle saturazioni dei tre fluidi (acqua, gas e olio). Infatti, fenomeni di over-ride gravitazionale sono evidenti all'interno del giacimento durante la fase produttiva, motivo per cui i produttori subiscono un break-through precoce di gas.

5. Ottimizzazione di Foam-Assisted-WAG

Il modello utilizzato in ECLIPSE tratta la schiuma come una concentrazione di tensioattivo in fase acquosa. Essa è soggetta a decadimento naturale e ad adsorbimento e modifica la mobilità del gas tramite il seguente fattore moltiplicativo diretto:

$$M_{rf} = \frac{1}{1 + M_r^{ref} F_w F_s F_o F_c} \qquad \text{(I)}$$

dove:
M_r^{ref} rappresenta il fattore di riduzione della mobilità di riferimento;
F_w, F_s, F_o, F_c sono tutti fattori che interessano la robustezza della schiuma.
In particolare, F_w si riferisce all'indebolimento dovuto alla riduzione eccessiva di saturazione dell'acqua, F_s si riferisce all'effetto negativo che ha una diminuzione eccessiva di concentrazione di tensioattivo, F_o si riferisce all'instabilità creata dalla presenza di olio ed F_c all'alterazione di mobilità data da comportamenti pseudoplastici a basse foam-quality. Ognuno di questi fattori è poi composto da un termine rappresentante il valore limite del parametro controllante il fenomeno fisico, ovvero S_w^{lim} (saturazione limite dell'acqua), C_s^{ref} (concentrazione di riferimento di tensioattivo), S_o^m (saturazione massima di olio), N_c^r (numero capillare di riferimento), e da esponenti controllanti la repentinità della transizione nel punto limite, ovvero f_w, e_s, e_o ed e_c. Dei fattori presentati, il decadimento ed F_c sono stati esclusi dall'analisi riportata.

I due obbiettivi dell'analisi presentata sono quindi la minimizzazione del gas e la massimizzazione del petrolio prodotti. Le variabili del problema sono suddivise in due gruppi: variabili operative decisionali e variabili incerte. Le prime sono concentrazione e tempo di iniezione di tre iniezioni di tensioattivo, ovvero sei variabili (C_{s1}, C_{s2}, C_{s3}, T_{s1}, T_{s2}, T_{s3}), mentre le seconde sono i termini presi in considerazione del modello di schiuma, ovvero otto variabili. Per tutte queste è stato scelto un sensato range di variazione distribuito uniformemente a livello probabilistico (con caso base e valori minimi e massimi), per tenere conto del massimo livello di incertezza.

Il problema viene quindi suddiviso in due parti: una prima analisi focalizzata sul solo petrolio e una seconda analisi robusta completa che tenga in considerazione i valori ottenuti nella precedente.

Partendo dall'analisi del petrolio, una regressione stepwise delle variabili decisionali è eseguita su un campione (a seguito di LHS) di 126 sensate simulazioni. Essa mostra una certa rilevanza per quanto riguarda i parametri della prima e seconda iniezione, mentre per la terza è ragionevole trascurare le variazioni delle variabili (C_{s3}, T_{s3}), ma non la loro presenza.

Viene quindi effettuata un'ottimizzazione nominale per trovare i valori migliori delle quattro variabili decisionali rimanenti, ricorrendo ad una tecnica di proxy modeling che approssimi la funzione obbiettivo (massima FOPT) ed il suo legame con gli input. A tal fine viene selezionato il metodo di interpolazione Universal Kriging. Poiché esso non può esistere senza una fase di validazione, il 70% dei campioni derivanti da LHS è casualmente selezionato per la costruzione e il restante 30% è utilizzato a verifica dell'accuratezza. Una volta considerato valido il proxy risultante, un'ottimizzazione nominale può essere effettuata. Vengono quindi avviate 10000 valutazioni fittizie campionate tramite LHS, da cui sono estratte le migliori 40 per essere realmente simulate e, di queste ultime, le migliori 10 sono analizzate per una riduzione dei range di variazione delle variabili decisionali.

Successivamente, un'analisi di sensitività viene eseguita sulle incertezze variando una variabile incerta alla volta (OVAT) e ponendola uguale al valore minimo o al massimo del range (le altre sono poste al caso base). Vengono effettuate così 17 simulazioni e i risultati mostrano una variazione molto ridotta di recupero di petrolio, che permette di evitare ulteriori analisi approfondite focalizzate su un solo output. I range ristretti vengono quindi mantenuti per permettere un'analisi completa robusta sia sul gas che sul petrolio.

L'analisi stepwise dei 126 dati da LHS riportata per l'FOPT viene ripetuta per il gas prodotto (FGPT) al fine di verificare se sia possibile o meno restringere i range selezionati e trascurare la variabilità dei parametri della terza iniezione. I risultati sono un po' migliori di quelli del petrolio in termini di coefficiente di determinazione (R^2), tuttavia i parametri rilevanti risultano esattamente gli stessi del caso a petrolio. Le due funzioni obbiettivo si trovano quindi in trade-off dato che una riduzione del gas porta in linea generale anche ad una riduzione del petrolio prodotto. Anche l'OVAT viene poi ripetuta come analisi di

sensitività per le variabili incerte e gli stessi parametri, molto più impattanti sull'output questa volta, risultano rilevanti.

Arrivati a questo punto e ristretti i range di variazione, è possibile la costruzione delle funzioni proxy. Per far ciò, tuttavia, avendo 9 variabili in gioco (vengono trattate contemporaneamente variabili incerte e decisionali stavolta), è necessario avere a disposizione un sostanzioso cluster di simulazioni. A tal scopo vengono avviati 2000 run (di cui 1990 non corrotti), richiedenti un notevole sforzo computazionale, che portano alla seguente distribuzione degli output:

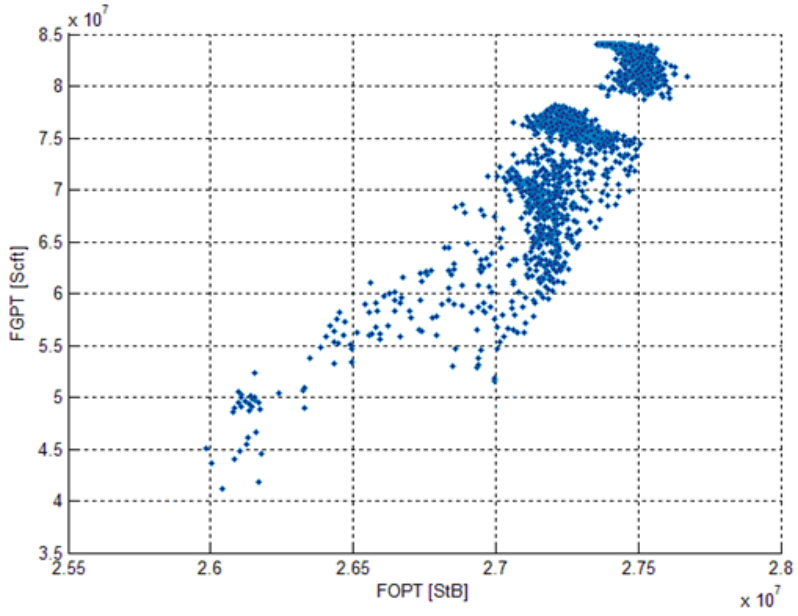

Figura I - Rappresentazione di FGPT ed FOPT dei 1990 run selezionati

Le distribuzioni delle variabili decisionali non seguono alcun trend particolare ed evidente, mentre ciò risulta vero per alcune variabili incerte, supportando il maggior effetto sugli output dato dalle incertezze e la necessità di un'ottimizzazione robusta. Quindi, si ottengono i proxy tramite un metodo di regressione multilineare, da cui si nota la netta superiorità di quello ottenuto per il gas rispetto a quello del petrolio in termini di R^2 e di errore normalizzato sulla finestra di variazione.

Con le funzioni proxy si valutano, così, 10000 siti predetti risultanti dalle combinazioni di 100 set casuali di valori delle variabili decisionali con altrettanti set di valori per quelle incerte (tutte ottenute da LHS). Si mediano, poi, tutte le variabili incerte per ogni set di decisionali, così da ottenere 100 siti predetti robusti sulle incertezze. Infatti, ciò che si nota dalla nuova distribuzione (nettamente ridotta rispetto a Fig. I) è che i trend per tre di quattro variabili decisionali (C_{s1}, C_{s2}, T_{s1}) sono stavolta molto più evidenti. L'ottimizzazione delle funzioni obbiettivo si può tradurre, in termini di funzione aggregata, nella seguente espressione:

$$F_{max} = \max(\overline{FOPT}_{\boldsymbol{u}} - \lambda \cdot \overline{FGPT}_{\boldsymbol{u}})$$

Dove $\overline{FOPT}_{\boldsymbol{u}}$ ed $\overline{FGPT}_{\boldsymbol{u}}$ rappresentano i valori mediati sulle incertezze degli output, mentre λ rende conto del peso (in termini di benefici economici) che ha la riduzione di gas comparata con un incremento del petrolio. Si ottengono, così, al variare dei valori di λ, diversi possibili casi ottimali, che formano quindi una frontiera Paretiana all'interno del riquadro di interesse. Una verifica dei risultati ottenuti viene quindi fatta simulando 300 casi corrispondenti agli stessi valori di variabili decisionali dei tre punti intermedi della frontiera Paretiana predetta (considerando quelli estremi come dominati) e facendone quindi le medie. I risultati (predetti e simulati) ottenuti sono mostrati nella seguente figura:

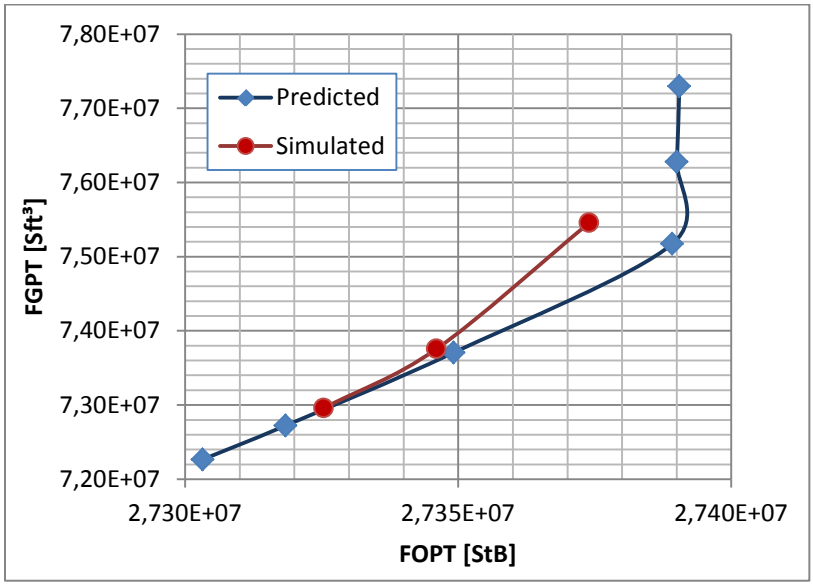

Figura II – Rappresentazione comparativa tra frontiera simulata e frontiera predetta

Da un'analisi degli errori percentuali relativi agli output mediati e da una valutazione della dispersione tramite deviazione standard relativa, si nota come effettivamente il proxy fatto sulla produzione di gas sia molto più affidabile di quello fatto sul petrolio. I valori ottenibili sulla frontiera di Pareto, comunque, dimostrano sensibili benefici in termini di riduzione di gas rispetto al caso WAG ottimale, mentre il petrolio mostra un incremento molto limitato, rappresentando piuttosto un vincolo per riduzioni elevate di gas prodotto. Inoltre, al fine di visualizzare meglio gli effetti benefici della schiuma, viene simulato un caso molto prossimo, in termini di output, a uno dei tre mediati ottimali simulati, per un'analisi dei profili. Il risultato è un'evidente diminuzione di volumi di gas prodotto in gioco e di GOR, mentre il petrolio sembrerebbe rimanere sempre a valori mediamente superiori rispetto al caso WAG in termini di portate prodotte fino a poco prima della terza iniezione. Ciò è dovuto alla chiusura di entrambi i pozzi entro il riquadro temporale selezionato a causa della scelta non meditata di valori per la terza iniezione. Ciò supporta il fatto che ulteriori analisi saranno richieste per l'ottimizzazione durante la vita totale del giacimento e non solo di 10 anni. In generale, poi, più approfondite analisi in laboratorio saranno necessarie per la selezione ottimale del surfattante (che stia quindi entro i range

selezionati) e possibili interventi risolutivi dovranno essere meglio analizzati per poter risolvere possibili problemi in fase di applicazione della schiuma.

6. Conclusioni

Questa tesi è focalizzata sull'applicazione di schiuma per migliorare la produzione di petrolio e ridurre quella di gas. Per il giacimento selezionato, la tecnologia di recupero avanzato WAG è stata selezionata per ottenere i benefici appena accennati e per smaltire il gas prodotto da altri campi. L'analisi, quindi procede dapprima attraverso la selezione di un caso ottimo di WAG e poi con la valutazione dell'applicazione della schiuma. 2000 simulazioni vengono quindi avviate e sulla base di queste si effettua un'analisi ottimale robusta che porta ad una risultante frontiera di Pareto di valori medi ottimali di output.

In tutto ciò, una delle principali assunzioni è quella di considerare solo le incertezze relative al modello di schiuma. Inoltre, il modello potrebbe essere migliorato andando ad effettuare una minimizzazione delle varianze degli output (FGPT ed FOPT), in caso di riduzione delle incertezze, e un'analisi degli NPV, che tuttavia rischierebbe di apportare solo un modesto valore aggiunto.

Ulteriori analisi di laboratorio sono necessarie prima di una reale applicazione a scala di campo e l'analisi proposta può essere ripetuta per investigare possibili applicazioni di schiuma in altri giacimenti.

Table of Contents

Acknowledgements i
Abstract ii
Sommario iii
Extended summary iv
Riassunto esteso xii
Table of Contents xx
List of Figures xxiii
List of Tables xxvi
List of acronyms xxvii
1. Introduction 1
2. WAG Injection processes 4
2.1. Mechanisms of Water Alternating Gas injection in oil reservoirs 4
2.2 Classification of WAG processes 8
2.2.1. Miscible injection 9
2.2.2. Immiscible injection 11
2.2.3. Other injection techniques 13
2.3 Design parameters for WAG projects 15
2.3.1. Injection gas 15
2.3.2. Injection pattern 16
2.3.3. Reservoir heterogeneity 16
2.3.4. WAG ratio 17
2.4. Operational problems 17
3. Fundamentals of Foam Assisted WAG 20
3.1. Introduction to foam application 20
3.2. Foam in porous media 21
3.2.1. Foam states 23
3.2.2. Foam generation mechanisms 24
3.2.3. Foam termination mechanisms 26
3.2.4. Foam flow regimes 26

3.3. Process Variables 28
4. Full Field Analysis 31
4.1. Simulation environment 31
4.2. Reservoir characterization 32
4.3. Water Injection case 36
4.4. WAG Injection Optimization 39
4.4.1. Parameters Selection 41
4.4.2. Sensitivity analysis 42
4.4.3. Range improvement 43
4.4.4. Pre-screening sampling 46
4.4.5. Best starting case selection 49
4.4.6. Best WAG scenario 52
4.5. Issues characterization 56
5. Foam Assisted WAG Optimization 59
5.1. Foam model 59
5.2. Analysis setup 63
5.2.1. Variables selection and problem formalization 64
5.2.2. Range selection 66
5.2.3. Problem split 68
5.3. FOPT Analysis 68
5.3.1. Decision variables sensitivity 69
5.3.2. Proxy construction 73
5.3.3. Nominal proxy optimization 76
5.3.4. Uncertain variables sensitivity 77
5.3.5. Ranges improvement 79
5.4. Complete robust analysis 80
5.4.1. Decision variables sensitivity 80
5.4.2. Uncertain variables sensitivity 83
5.4.3. Proxies construction 84
5.4.4. Robust proxy optimization 90
5.5. Foam-effects visualization 98
5.6. Future developments 101

6. Conclusions 103
Appendix A 105
A.1. ECLIPSE data file 105
A.2. MATLAB data file 117
Appendix B 119
References 126

List of Figures

Figure 1 . 1 - Driving mechanisms during primary recovery: solution gas (a), gas-cap (b) and natural water drive (c) 1
Figure 1 . 2 – Gas injection in the gas cap 2
Figure 1 . 3 - Water injection below the water-oil contact (WOC) 2
Figure 2 . 1 - Illustration of the efficiency factors [6] 4
Figure 2 . 2 – Illustration of a miscible WAG process [7] 5
Figure 2 . 3 – Oil recovery in a water-wet rock as percentage of initial trapped oil due to consecutive WAG slugs [8] 5
Figure 2 . 4 – Microscopic visualization of gas (yellow), water (blue) and oil (red) phases during three WAG cycles [8] 6
Figure 2 . 5 – Stable (red) and unstable (black) oil sauration contours (S=0,5) depicted after 100 (left), 300 (middle), 500 (right) days [11] 7
Figure 2 . 6 – Gas three phase relative permeability diagram 8
Figure 2 . 7 – Visual comparison between three experimental MWAG micromodel applications: (a) gas-flood of the first WAG cycle after water-flooding; (b) gas flood of the second WAG cycle; (c) 12-hrs continued gas flooding of the first WAG cycle after the water-flood [16] 10
Figure 2 . 8 – Visual comparison between three experimental IWAG micromodel applications: (a) gas-flood of the first WAG cycle after water-flooding; (b) water-flood of the first WAG cycle after gas-flooding; (c) gas-flood of the second WAG cycle [19] 11
Figure 2 . 9 – Oil saturation profiles indicating the decreasing recovery during five IWAG cycles [20] 12
Figure 2 . 10 – (a) Gas-flood of the second IWAG cycle; (b) gas-flood of the fifth cycle [19] 12
Figure 2 . 11 – Injectivity during: (a) cyclic WAG injection, with 29 days water injection and 10 days gas injection (0,059 PV/cycle); (b) cyclic SAG injection, with 40 days water injection and 60 days gas injection (0,015 PV/cycle). 14
Figure 2 . 12 – Illustration of the three zones formed during WAG injection 14
Figure 2 . 13 – Injection-gas types distribution among WAG applications 15
Figure 2 . 14 – Possible regular patterns for injection 16
Figure 2 . 15 – Typical pressures and temperatures for solid formation in generic petroleum production [28] 18
Figure 3 . 1 - Schematic of a foam system [32] 21
Figure 3 . 2 – Pressure distribution in the water phase 22
Figure 3 . 3 – Ideal disjoining pressure trend as a function of film thickness [33] 22
Figure 3 . 4 – Plot showing the unstable and stable regions for foams 23
Figure 3 . 5 – Comparison between the three foam states [32] 24

Figure 3 . 6 – Schematic of leave-behind mechanism showing gas invasion (A) and foaming film (B) 25
Figure 3 . 7 – Schematic of lamella division showing branch point (A) and two resulting bubbles (B) 25
Figure 3 . 8 – Schematic of snap-off mechanism showing gas penetrating a throat(A) and a new bubble formed (B) 25
Figure 3 . 9 – Pressure drop (psi) across 2-ft sandpack as a function of gas and liquid flow rates [37] 27
Figure 3 . 10 – Ideal representation of the flow regimes 27
Figure 3 . 11 – Apparent viscosities of a CO2 foam vs. foam quality at different permeabilities [38] 28
Figure 4 . 1 – Angolan Reservoirs [47] 32
Figure 4 . 2 – Illustration of saturations distribution of the FIELD α model 34
Figure 4 . 3 – Illustration of the good facies channel in an intermediate layer 35
Figure 4 . 4 – Well oil production rates and water cuts (P-301 and P-302) 37
Figure 4 . 5 – Plane slice comparing the depths reached by P-301 and P-302 38
Figure 4 . 6 – Top-view after 10 years of water injection 38
Figure 4 . 7 – Cross-section in the near-well area of P-302 (top) and P-301 (bottom) 39
Figure 4 . 8 – Logical scheme applied for the analyses 40
Figure 4 . 9 – Plot showing the 60 possible cases in terms of Field Oil Produced vs. Timestep Cases 43
Figure 4 . 10 – BHP and THP profiles of P-301 and P-302 44
Figure 4 . 11 – Illustration of VLP and IPR for P-301 45
Figure 4 . 12 – VRR Discrete density function 47
Figure 4 . 13 – VRR Cumulative distribution function 47
Figure 4 . 14 – 2-variables example of LHS 48
Figure 4 . 15 – Scatter-plot and Box-plot showing the distribution of FOPT amongst the simulations 49
Figure 4 . 16 – FOPT vs. first VRR value 50
Figure 4 . 17 – Simultaneous plot of FOPT vs. Time for all the 150 simulations 51
Figure 4 . 18 - Scatter-plot and Box-plots (cases #6 and #10 [cyan]) of FOPT amongst the simulations 52
Figure 4 . 19 – Comparison of FOPT trend for the two cases VRR=1 and VRR variable . 53
Figure 4 . 20 – NPV trends for both VRR=1 and Optimal LHS cases 55
Figure 4 . 21 – Field oil production rate and water cut profiles 56
Figure 4 . 22 – Field oil and gas production rates and GOR profiles 57
Figure 4 . 23 – P-301/I-402 cross section at 01/01/2020 57
Figure 4 . 24 – P-302/I-401 cross section at 01/01/2021 58
Figure 4 . 25 – P-301/P-302 cross section at 01/01/2021 58
Figure 5 . 1 – Steps analyzed throughout this section 64
Figure 5 . 2 – List of objective functions 65
Figure 5 . 3 - List of decision variables 65

Figure 5 . 4 - List of uncertain variables..... 66
Figure 5 . 5 - Scheme representing the steps throughout the FOPT-analysis..... 68
Figure 5 . 6 - Plot showing the 150 LHS runs with the threshold at 27,4 million StB..... 69
Figure 5 . 7 – First (top) and last (bottom) steps of the stepwise regression analysis..... 71
Figure 5 . 8 - Representation of FOPTs as functions of slug time-length and concentration for: 1st slug (upper-left), 2nd slug (upper right), 3rdslug (bottom)..... 72
Figure 5 . 9 – Illustration of predicted vs. simulated data and 1% error lines..... 76
Figure 5 . 10 – Illustration of Cs versus Ts of the two slugs for the 10 best simulated cases 77
Figure 5 . 11 – OVAT analysis conducted at 6,16 (a), 8,16(b) and 10(c) years..... 78
Figure 5 . 12 – Scheme representing the steps throughout the FGPT-analysis..... 80
Figure 5 . 13 - First (top) and last (bottom) steps of the stepwise regression analysis..... 81
Figure 5 . 14 – Representation of FGPTs as functions of slug time-length and concentration for: 1st slug (upper-left), 2nd slug (upper right), 3rdslug (bottom)..... 82
Figure 5 . 15 – OVAT analysis conducted at 6,16 (a), 8,16(b) and 10(c) years..... 83
Figure 5 . 16 – Illustration of the FGPT and FOPT values resulting from the 1990 simulations run 85
Figure 5 . 17 – FOPTs and FGPTs as functions of each variable..... 86
Figure 5 . 18 – Illustration of the FGPT and FOPT values within the frame of interest..... 87
Figure 5 . 19 – FOPT values simulated and predicted by the proxy and validation sites (red) 89
Figure 5 . 20 – FGPT values simulated and predicted by the proxy and validation sites (red) 89
Figure 5 . 21 – Illustration of the concept of dominance..... 91
Figure 5 . 22 – Average predicted values of FOPT and FGPT plotted 92
Figure 5 . 23 – Illustration of the averaged predicted sites as functions of the decision variables..... 93
Figure 5 . 24 – Average values inside the frame of interest and approximated Pareto frontier (red) 94
Figure 5 . 25 – Illustration of a comparison between simulated and predicted frontier..... 96
Figure 5 . 26 – Comparison between the foam-case and the best WAG case in terms of FOPR and FGPT..... 99
Figure 5 . 27 – Comparison between the foam-case and the best WAG case in terms of GOR..... 99
Figure 5 . 28 – Comparison between the foam-case and the best WAG case in terms of water cuts of each producer..... 100
Figure 5 . 29 – Comparison between the foam-case and the best WAG case in terms of field water injection rates 101

List of Tables

Table 1 – Post-risk FIELD α data 33
Table 2 – Facies characteristics 35
Table 3 – Reservoir constraints 36
Table 4 – Forecasted data of gas to be disposed 41
Table 5 – BHP and THP data of P-301 and P-302 44
Table 6 – Pearson's coefficients 50
Table 7 – Best case #10 scenario characteristics 52
Table 8 – Parameters used for calculations 54
Table 9 – Comparison between the results of the WI-only and best-WAG cases 55
Table 10 - Ranges of the variables analyzed in the work 67
Table 11 – Averaged best values after the proxy optimization 77
Table 12 – New values selected for the decision variables 79
Table 13 – Maximum errors and coefficients of determination for each proxy 90
Table 14 – Equivalent barrels of reduced gas for the computation of λ and corresponding average FOPT and FGPT 95
Table 15 – Decision parameters of the four Pareto-optimal sites used to generate the simulations 95
Table 16 – Decision parameters of the four Pareto-optimal sites used to generate the simulations 95
Table 17 – relative standard deviations of FGPT and FOPT in both simulated and predicted cases 97
Table 18 – Values selected to run the simulation with the foam injection 98

List of acronyms

Av.	Average
BDF	Blocking diverting foam
BHP	Bottom hole pressure
EOR	Enhanced oil recovery
ERR	Error
FAWAG	Foam assisted water alternating gas
FGOR	Field gas to oil ratio
FGPT	Field gas production total
FOPR	Field gas production rate
FOPT	Field oil production total
FPSO	Floating production storage and offloading
FWCT	Field water cut
FWIR	Field water injection rates
GOR	Gas to oil ratio
HSE	Health safety and environment
HWAG	Hybrid water alternating gas
IAM	Integrated asset model
IFT	Interfacial tension
IOR	Improved oil recovery
IPR	Inflow performance relationship
IWAG	Immiscible water alternating gas
LHS	Latin hypercube sampling
LIQ	Liquid
MCF	In-depth mobility control foam
MMP	Minimum miscible pressure
MStcft	Thousand standard cubic feet
MWAG	Miscible water alternating gas
OVAT	One variable at a time
OWC	Oil water contact
RB	Reservoir barrel
RF	Recovery factor
RSD	Relative standard error
SAG	Surfactant alternating gas
StB	Standard barrel
Stcft	Standard cubic feet
SWAG	Simultaneous water alternating gas
THP	Tubing head pressure
VLP	Vertical lift performance
VRR	Voidage replacement ratio
WAG	Water alternating gas
WBHP	Well bottom hole pressure
WTHP	Well tubing head pressure
WOPR	Well oil production rate
WWCT	Well water cut

1. Introduction

Traditionally, crude oil production from reservoirs is divided, in a chronological sense, into three distinct phases: primary, secondary and tertiary recovery.

During primary recovery, the driving forces, which allow oil to rise to the surface, come from the oil itself (in terms of density of the hydrocarbon due to different percentages of its components) or from reservoir natural over-pressure. These mechanisms include fluid expansion, rock expansion, solution gas drive (*Fig. 1.1a*), gas-cap drive (*Fig. 1.1b*), natural water drive (*Fig. 1.1c*) and gravity drainage. In addition to the above mentioned exploitation mechanisms, the drive may be supported by the use of artificial lift techniques (such as pumps or gas lift). Typically only about 10-20% of a reservoir original oil in place (OOIP) is produced during primary recovery.

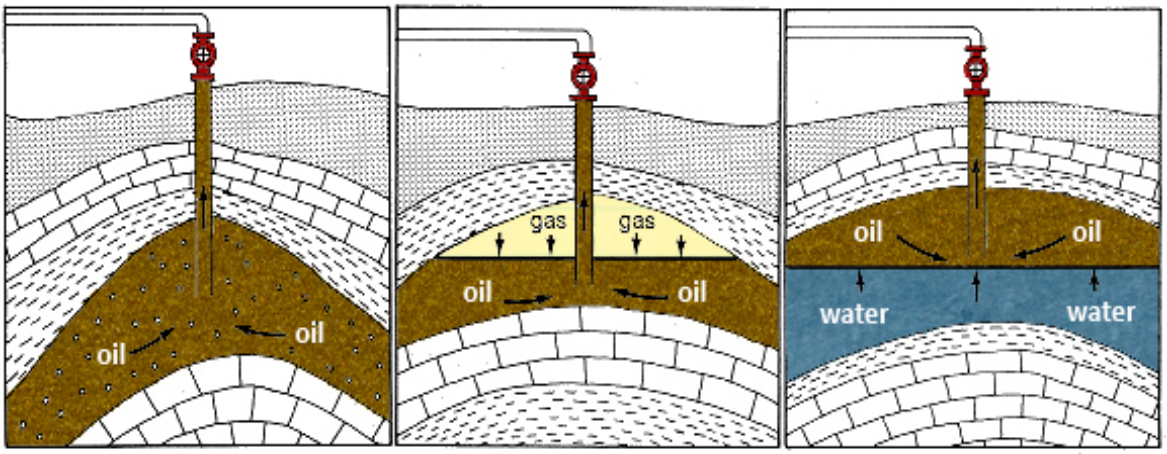

Figure 1 . 1 - Driving mechanisms during primary recovery: solution gas (a), gas-cap (b) and natural water drive (c)

Secondary recovery increases field-productivity adding energy into the reservoir by injecting water or gas in the pore spaces to displace oil and easily produce it. In order to form a continuous phase and fluid communication, gas is injected into the gas cap (if present) (*Fig 1.2*), while water can be injected below the water-oil-contact (WOC) level (*Fig. 1.3*) to sweep oil from the pore-spaces. This stage reaches its limit when the injected fluid (water or gas) starts being produced in significant amounts, making the exploitation of the reservoir no longer economically worthwhile. According to the US Department of Energy, the recovery factor, in case of secondary recovery, most likely amounts to 20-40% of the oil originally in place combined with the primary recovery [1].

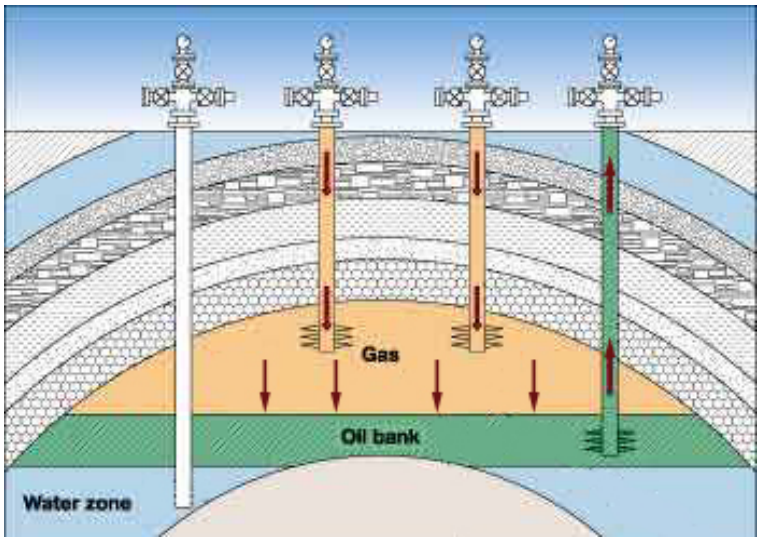

Figure 1 . 2 – Gas injection in the gas cap

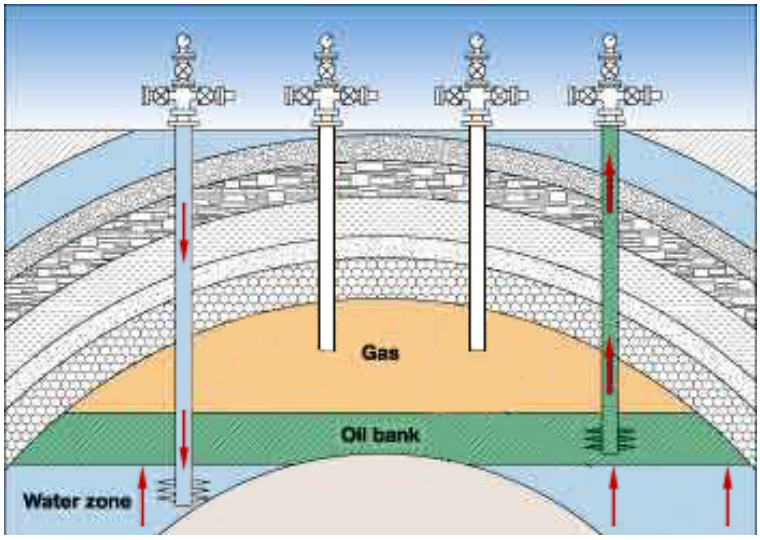

Figure 1 . 3 - Water injection below the water-oil contact (WOC)

Tertiary recovery is the way to further increase oil production by altering the reservoir hydrocarbon physical and chemical properties, the rock-fluid interaction or the reservoir rock properties. It represents the third stage of oil production, even if it can be initiated at any time during the production of a reservoir. The term is often replaced by the most common Enhanced Oil Recovery (EOR). Moreover, the term EOR is sometimes substituted by Improved Oil Recovery (IOR), which actually refers to recovery techniques where energy is added into the reservoir, without any changes in the original properties of oil and rock. Anyway, this is not really a strict definition and these terms are rather similar.

EOR techniques cannot be blindly applied on all reservoirs because of the costs. Therefore, economic evaluations must be carried out together with technical analyses to determine which type of EOR will work best on the reservoir and which could be the gain from an economic point of view obtained by applying the selected technique. Taking into account these considerations, EOR can increase total recovery factors up to 75% [2].

Despite several classifications of EOR techniques which can be found in literature, the following categories are considered thorough for the purposes of this work [3]: gas injection, chemicals injection, mobility-control processes, thermal recovery and other processes.

- *Gas injection* involves the injection of hydrocarbon gases, non-hydrocarbon gases (such as nitrogen) or carbon dioxide into the reservoir. The objective is to inject fluids which are either miscible or immiscible with the oil. Carbon dioxide EOR is a method that is gaining popularity and it is nowadays including the injection of CO_2 obtained as a byproduct from industrial processes, even if the most common gas injection process remains the one using hydrocarbon gases because of their availability.
- *Chemical injection* helps to free trapped oil within reservoir pores. This technique can involve the use of detergent-like surfactants to decrease the residual oil saturation inside the rock pores and, as a result, lower the amount of oil left behind the water front.
- *Mobility-control processes* are those based on maintaining a sufficiently favorable mobility ratio to improve the macroscopic displacement efficiency. Examples of this category are the gas-mobility reduction due to foam injection and the use of long-chained molecules (polymers) into the reservoir to increase the mobility.
- *Thermal recovery* involves the introduction of heat (such as steam injection or in-situ combustion) into the reservoir to reduce the viscosity of the oil and improve its ability to flow through the reservoir.
- "*Other processes*" refers to all the methods not included in the above mentioned categories, such as microbial-based techniques.

Although EOR applications are predominantly employed onshore, technologies are being developed to expand EOR to offshore developments. The main challenges existing for offshore applications include economics of the development, weight, space and power limitations and fewer wells that are more widely spaced.

2. WAG Injection processes

2.1. Mechanisms of Water Alternating Gas injection in oil reservoirs

Water-Alternating-Gas (WAG) processes represent an enhanced oil recovery method consisting of injecting a gas slug followed by a water slug through the same well. It was initially proposed in 1950's to improve the displacement of gas injection, essentially by means of water controlling the mobility and stabilizing the advancing front of displacement [4] [5].

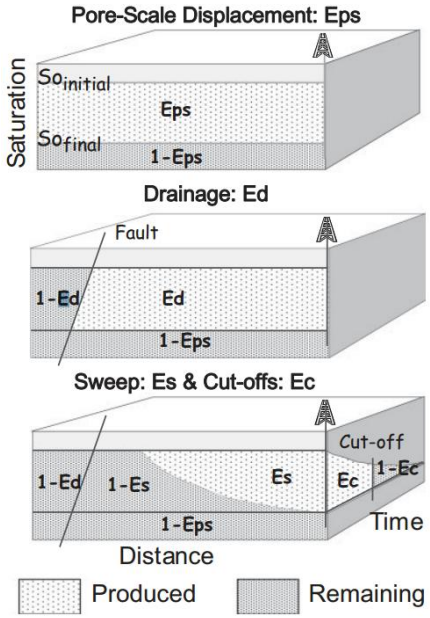

Figure 2 . 1 - Illustration of the efficiency factors [6]

In order to better understand the improved recovery given by WAG methods, it is convenient to introduce an oil recovery factor as the product of four terms [6] (*Fig. 2.1*):

$$R_f = E_{ps} \cdot E_d \cdot E_s \cdot E_c \qquad (2.1)$$

E_{ps} is the pore-scale displacement efficiency, i.e. the microscopic efficiency of the recovery process, which represents also the theoretical maximum recovery factor in case the process could be perfectly applied throughout the entire field; E_d is the drainage efficiency referred to the connectedness to a production well and it is most likely close to 1; E_c represents a cut-off efficiency, that is the loss of recovery related to reaching critical economic thresholds before the theoretical maximum production; E_s is the total volumetric (macroscopic) sweep efficiency referred to the movement of oil towards producers within the drained volume. This last parameter can be decomposed into two additional terms, E_v and E_h, representing the vertical and the horizontal sweep efficiency respectively.

WAG injection combines the microscopic-scale benefits (E_{ps}) of gas-flooding (in miscible or immiscible conditions) with the macroscopic efficiency (E_s) given by both gas and water-flooding, resulting in improved recovery of oil if compared to either secondary water injection or gas injection alone. In fact, the first benefit is evident both in miscible and immiscible processes where gas displaces oil and the residual oil saturation in the flooded areas is lower than after water-flooding [4]. The increase in macroscopic efficiency is very clear when gravity effects are predominant, thus water and gas displace oil from unswept regions, resulting in improved recovery if compared to either secondary water injection or gas injection alone. In addition, the presence of a previously injected amount of gas in the porous medium reduces the water relative permeability (k_{rw}) in three-phase zones favoring water diversion to new areas and improving the volumetric sweep efficiency (*Fig. 2.2*).

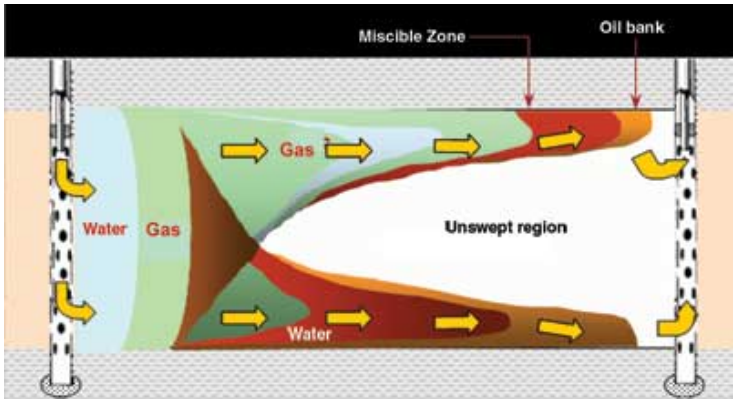

Figure 2 . 2 – Illustration of a miscible WAG process [7]

In a water-flooded reservoir, gas flooding can improve oil recovery by connecting the so called trapped gas volumes after water-flooding and mobilizing some of the remaining oil contained in the pore spaces. Subsequently, the injected water will further reduce the oil saturation (S_o) by displacing some of both remaining oil and gas in the pores. A maximum theoretical improvement in oil recovery after WAG can be obtained by repeating the process until asymptotical values are reached, which make the process not economically-feasible anymore [8] (*Fig. 2.3*). In fact, most of the recovery, regarding experimental results shown below, is achieved at the second WAG cycle.

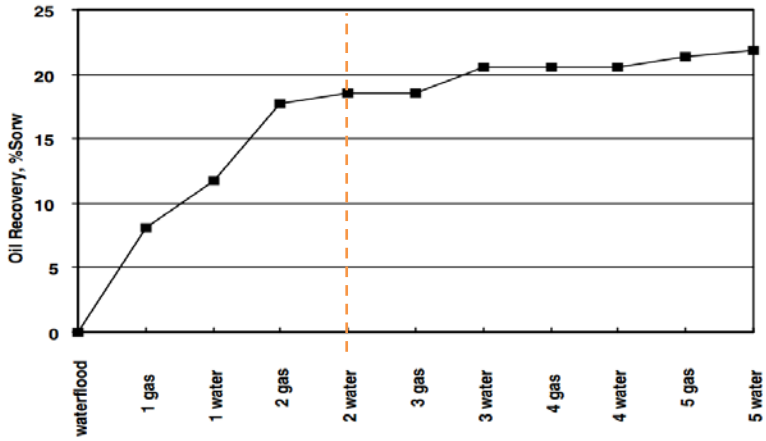

Figure 2 . 3 – Oil recovery in a water-wet rock as percentage of initial trapped oil due to consecutive WAG slugs [8]

From a microscopic point of view, during the first water-flood (which simulates a secondary recovery), oil is displaced by corner filament flow and thickening rather than by piston-like sweep, as a result of a capillary dominated flow. When the gas injection of the first WAG cycle occurs, the gas channels through the oil because of its low interfacial tension and viscosity and does not significantly improve recovery. Despite this, small drops of oil move ahead of the advancing front and reach more oil, resulting in a mobility improvement due to oil phase continuity. Then, when water injection follows gas injection in water-wet cases, water filaments snap-off the gas phase making a following gas injection more effective and increasing the recovery if compared to a continuous gas injection. This process can be repeated several times with the same working principles until the recovery is asymptotically increased [8] (*Fig. 2.4* – red=oil; blue=water; yellow=gas).

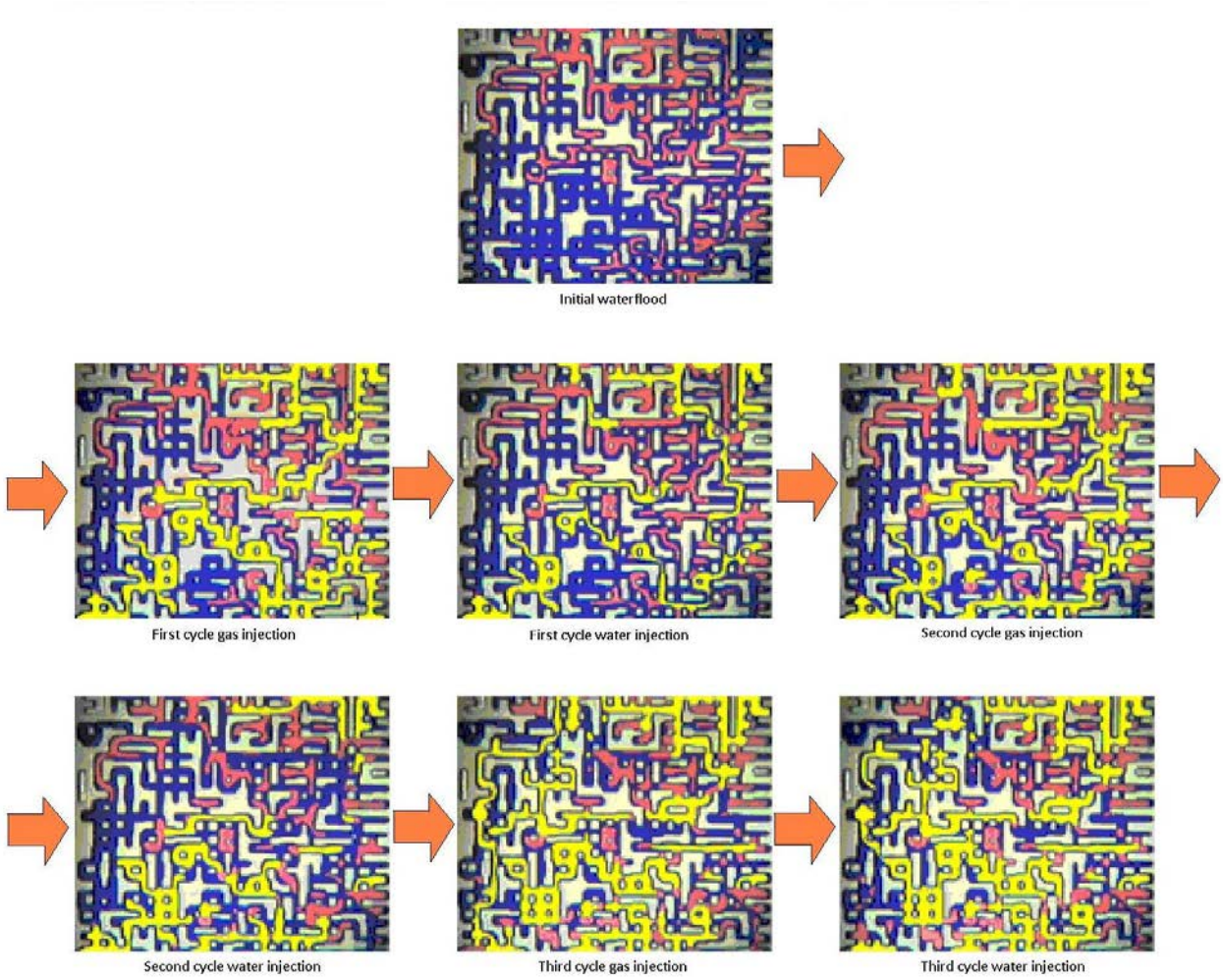

Figure 2 . 4 – Microscopic visualization of gas (yellow), water (blue) and oil (red) phases during three WAG cycles [8]

On the other hand, from a macroscopic point of view, it has been shown experimentally that WAG floods lower residual oil saturation in three-phase zones and influence viscosities and densities due to compositional exchanges [9]. The process outperforms continuous-gas-injections in terms of unit pore volumes of gas injected and returns of recovery [10]. In fact, the high mobility of the injected gas during a WAG process can lead

to an instability of the displacing front due to the tendency for a gas tongue to be formed at the top of the targeted area, if an adverse gas-to-water injection ratio is chosen [11]. This can be seen in *Fig. 2.5*, where a 2D reservoir simulation shows stable (red line) and unstable (black line) fronts at different time-steps.

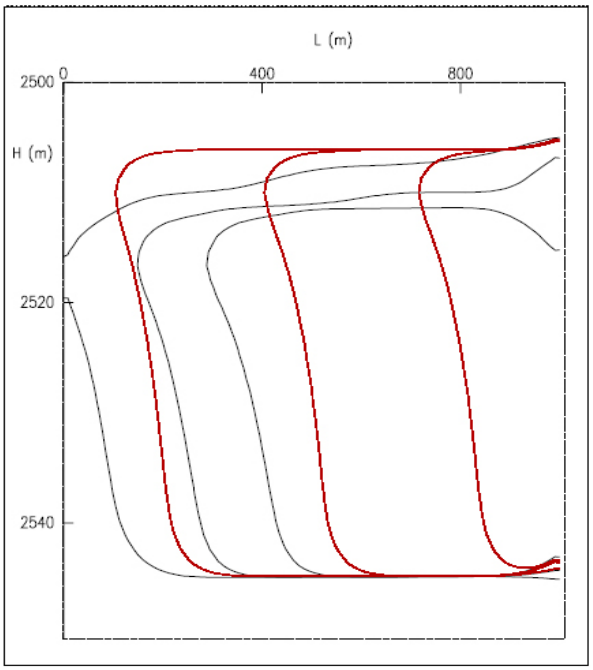

Figure 2 . 5 – Stable (red) and unstable (black) oil saturation contours (S=0,5) depicted after 100 (left), 300 (middle), 500 (right) days [11]

However, simulations have highlighted some disadvantages, too. Some of them are particularly evident if the complete process is described as a sequence of drainage and imbibition phenomena, resulting in relative permeability hysteresis. As a matter of fact, an irreparable change to relative permeability occurs due to permanent alterations of reservoir properties. When a gas slug is released into a water-wet reservoir, a drainage process occurs (gas saturation (S_g) and relative permeability (k_{rg}) increase), followed by imbibition during the successive water slug (water saturation (S_w) and relative permeability (k_{rw}) increase), and so on for the other WAG cycles. As can be seen in *Fig. 2.6*, the gas end-values of saturation and relative permeability are different for each cycle, providing evidence that a permanent change in reservoir properties has occurred due to trapping of the oil and gas in the pore spaces [12]. Similar considerations can be stated as well for water and oil in three-phase situations.

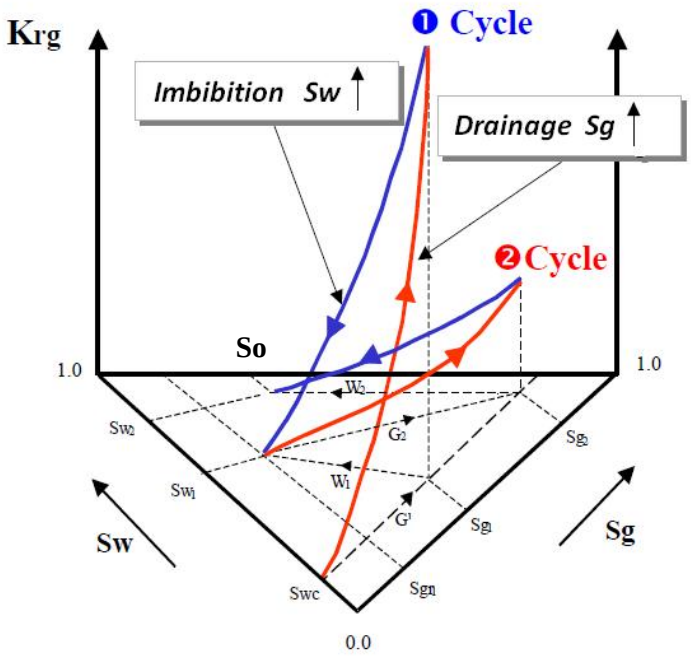

Figure 2 . 6 – Gas three phase relative permeability diagram

In field case simulations, hysteresis led to a reduced oil recovery compared to other simulations performed neglecting this phenomenon. This is supposed to happen mainly because of gas injectivity reduction resulting from gas trapping near the injection well [13].

In the end, from an HSE point of view, reinjection of gas also helps avoiding concerns such as flaring and CO_2 emissions, especially in cases where gas export is not economically or technically feasible (such as in several offshore applications). Anyway, based on the history of applications up to 1996 [4], the common trend for successful injections was an increased oil recovery ranging between 5% and 10% of the oil initially in place. It is then obvious that the process feasibility is strongly influenced by oil prices. As a matter of fact, when the commodity price took a tumble in 1985, problems in WAG projects arose leading to several premature closures and a descending trend in WAG startups during the following years [4]. Nowadays, the oil price is three to four times higher than the average discounted back price in 1990's, supporting a regained high level of interest for WAG processes.

2.2 Classification of WAG processes

Several WAG techniques exist and they can be grouped in many ways. Anyhow, the most common and applied processes are miscible and immiscible injections, leading to a classification which mainly distinguishes between these two categories. Other techniques referring to simultaneous and hybrid injection will be grouped as "other injection techniques":

- Miscible injection
- Immiscible injection
- Other injection techniques

A brief description of each injection technique is worthwhile to better understand the aims and the characteristics of this work.

2.2.1. Miscible injection

The term “miscible WAG injection” (MWAG) refers to the behavior of the gas in the presence of a contacting oil phase. As the injected gas initially contacts the reservoir oil, it is not at equilibrium yet and the contact between the fluids results in mass transfer and properties change. But, since their properties become quickly similar and eventually equal, the two phases achieve complete miscibility and the interface between them vanishes. This phenomenon implies, at the microscopic pore level and in case of first contact miscibility, a practically 100% efficient displacement due to the absence of physical interfaces, which allow a complete purge of the oil detained in the pores. Anyway, since first contact miscibility is quite rare, what usually happens during WAG processes is a multi-contact miscibility that makes gas and oil miscible through consecutive steps or contacts [14]. The considerations reported in this subsection are valid for both processes.

Miscible injection is a widely applied process in oil fields [4]. Thus, the injection pattern strongly affects the WAG performances, because overall field pressure has to be accurately controlled through injectors positioning and maintained as close as possible to the so called minimum miscible pressure (MMP), that can be defined as the minimum required pressure to achieve miscibility of oil and gas [15].

Although the process is not fully understood yet, it is possible to observe through network models and experimental micro-models that when a gas injection of a first-cycle WAG is carried out after water-flooding, the gas follows a preferential pathway, endorsing the capillary dominated propagation, and just a little redistribution of the gas-finger occurs during the following cycles, producing essentially the same single pathway. Rather if a single gas injection is prolonged, the gas-finger grows because of the thick oil layer formation and the subsequent complete contacted-oil drainage along the gas-path [16] (*Fig. 2.7* – white=oil; blue=water; yellow=gas).

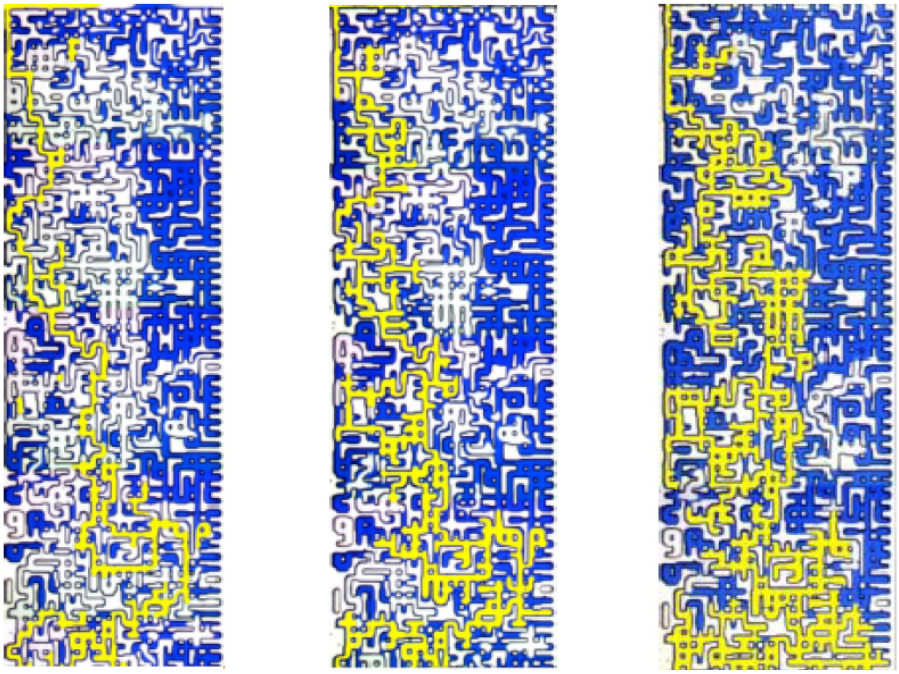

(a) (b) (c)

Figure 2 . 7 – Visual comparison between three experimental MWAG micromodel applications: (a) gas-flood of the first WAG cycle after water-flooding; (b) gas flood of the second WAG cycle; (c) 12-hrs continued gas flooding of the first WAG cycle after the water-flood [16]

This is due to the fact that, close to the miscibility critical point, any third non-critical phase (such as water) will be covered by a layer of multi-contact miscible phase. Thus, the oil perfectly wets the solid surface (in case of an oil-wet system) or the water substrate (in water-wet systems) and, when bypassed by the gas, it remains connected to the oil clusters contained in the pores already swept by the gas. Moreover, due to very low interfacial tension (IFT) between oil and gas phases, the capillary forces are not dominant and thus the gas can easily move the interface into the bypassed oil. This happens because gas prefers to enter pores filled with oil instead of those filled with water, as the IFT between gas and oil is lower than the IFT between gas and water. The process then provides a good driving force for the clusters to be pushed into the miscible oil-gas flow stream, so that the drainage will occur efficiently. In this case the amount of gas injected is not really an important issue as long as it is enough to connect the isolated groups of oil and to ensure a continuous pathway [17].

It has also been shown experimentally that “water blocking” is an important factor as a lower initial water saturation leads to higher oil recovery. Additionally, in a “weakly water-wet” system, the continued gas injection is not as efficient as in water-wet or oil-wet cases, while a path snap off has been rather noticed, leading to gas-fingers diversion (in the same way as in an immiscible WAG process) [18].

2.2.2. Immiscible injection

In case the multiple contact miscibility cannot be achieved by the gas slug during the WAG process because of the impossibility to reach the critical point, the correct term to refer to is “immiscible WAG injection” (IWAG). Even though its physical displacement mechanism is still not perfectly understood yet, it is possible to state good observations on what happens experimentally, as done previously with miscible processes.

Immiscible and miscible gas injection behave differently on the microscopic scale. In fact, if the gas injection is continued after the establishment of the first gas finger, the highly mobile fluid follows the same pathway without any expansion or growth of the finger and no further oil recovery can be noticed. On the other hand, the subsequent water-flood of the first WAG cycle causes a fragmentation of both the gas and oil phases, as can be seen in *Fig. 2.8* (red=oil; blue=water; yellow=gas). In this case, the second WAG cycle gas injection draws different pathways in the microscopic scale, that is a finger diversion occurs improving the oil displacement [16].

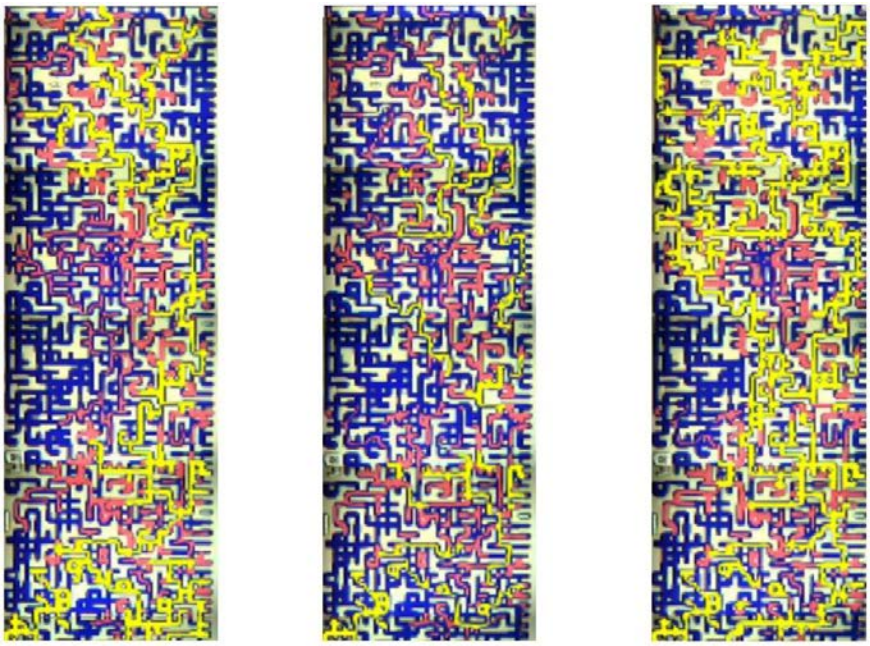

Figure 2 . 8 – Visual comparison between three experimental IWAG micromodel applications: (a) gas-flood of the first WAG cycle after water-flooding; (b) water-flood of the first WAG cycle after gas-flooding; (c) gas-flood of the second WAG cycle [19]

However, after a few cycles of injection, the incremental oil recovery decreases until no more additional oil is produced with further WAG cycles (*Fig. 2.9*) [20].

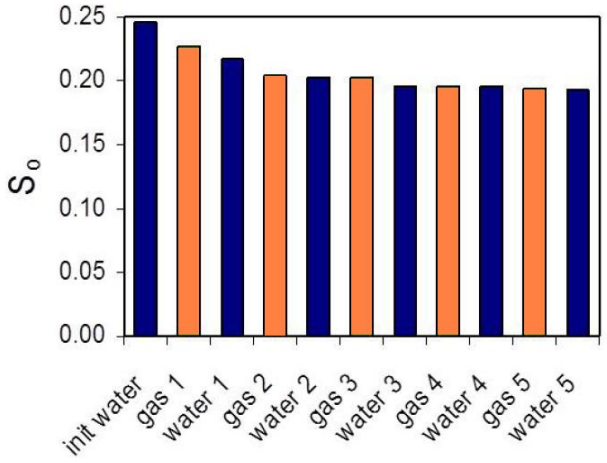

Figure 2 . 9 – Oil saturation profiles indicating the decreasing recovery during five IWAG cycles [20]

This does not imply that nothing is happening during the cycle. A mere redistribution of fluids rather occurs at the pore level without any additional oil production, as can be noticed in *Fig. 2.10* (red=oil; blue=water; yellow=gas), where the amount of oil present in the core after the 5th cycle is more or less the same of the one shown after the 2nd cycle.

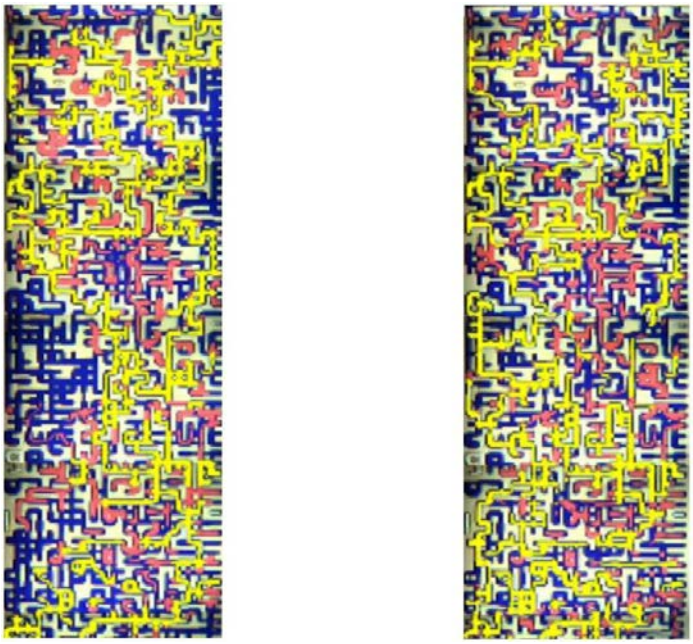

(a) (b)

Figure 2 . 10 – (a) Gas-flood of the second IWAG cycle; (b) gas-flood of the fifth cycle [19]

These results are endorsed by three main experimental observations in a water-wet system [21]:

- Gas trapping – Water imbibition during WAG cycles in the presence of a gaseous phase leads to trapping part of the gas in the pores. As several pores contain residual oil which is not mobile in a water-oil system, the gas trapping results in both mobilizing a fraction of this previously static oil, even at low saturations, and reducing three-phase residual oil saturation.

- Hysteresis – During WAG cycles, hysteresis phenomena occur. As seen in *Fig. 2.6*, the gas saturation increases after each WAG cycle in a three-phase environment, so that different secondary drainage profiles are drawn and gas relative permeability values (k_{rg}) decrease as well. This results in effective improvement of mobility control of gas.
- Modest gas dissolution – It causes oil swelling and viscosity reduction leading to less residual oil, increased recovery and more favorable water-oil mobility ratio, in case original conditions were very undersaturated with gas.

Anyhow, a successful IWAG injection can achieve a good recovery just maintaining the reservoir pressure instead of trying to reach the minimum miscible pressure.

2.2.3. Other injection techniques

Basically, there are two other minor injection processes that are reported in some field history applications: Simultaneous WAG (SWAG) and Hybrid WAG (HWAG).

SWAG is a technique in which water and gas are co-injected into a portion or the entire thickness of the formation, by using either a single wellbore or a dual completion injector where the two phases enter the pore zone at different depths (also called Selective SWAG - SSWAG). SWAG process appears to provide a better control over the gas mobility than a traditional WAG, resulting in improved sweep efficiency and steadiness of gas production and GOR (gas to oil ratio) response [17]. In fact, considering that injected water and gas are at the same pressure, the injection process seems more uniform, gravity effects are less evident and, as a consequence, a better mobility control can be achieved. Moreover, from a "producer" point of view, the producing gas-oil-ratio is expected to have a smoother profile, since the presence of big slugs, which increase the well-head pressure, are avoided. On the other hand, gas and water at the same pressure must be injected through the well avoiding hydrates formation. Furthermore, 1-D simulations have shown that a traditional WAG injection has a better injectivity than a SWAG process (from 12% with small slugs to 30% with larger slugs), especially in case of foam formation through Surfactant-Alternating-Gas (SAG) processes (50% to 150% increase in injectivity) because of the reduced mobility of three flowing phases – gas, oil and water – in SWAG (*Fig. 2.11*) [22].

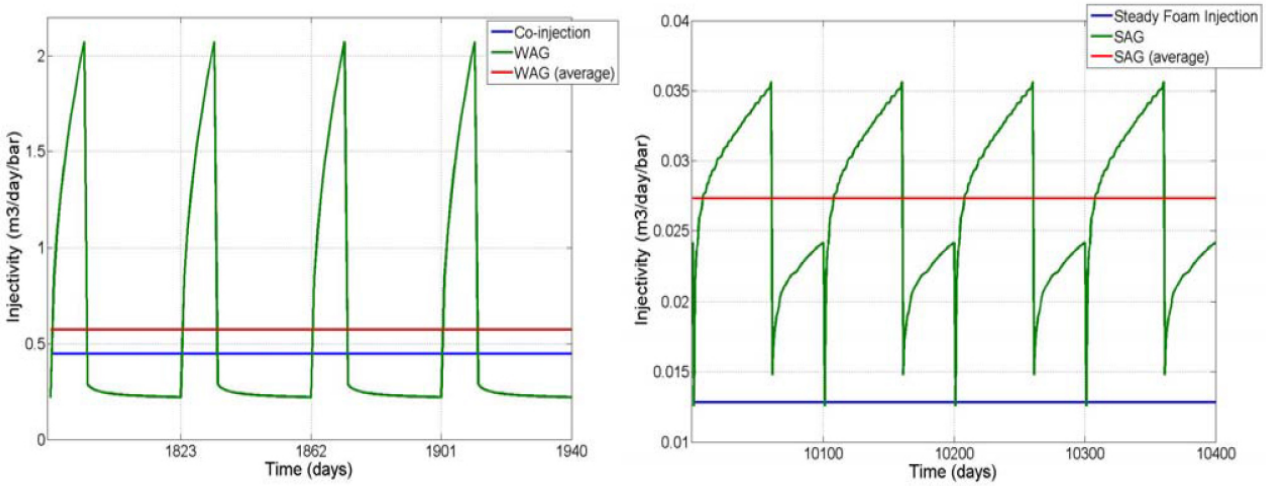

Figure 2 . 11 – Injectivity during: (a) cyclic WAG injection, with 29 days water injection and 10 days gas injection (0,059 PV/cycle); (b) cyclic SAG injection, with 40 days water injection and 60 days gas injection (0,015 PV/cycle).

This WAG-advantage, analyzed more in depth through a 2-D simulation, leads to an increase in the distance that the water-gas mixture travels before complete segregation, resulting in a further increase in the volume swept. [22] (*Fig. 2.12*).

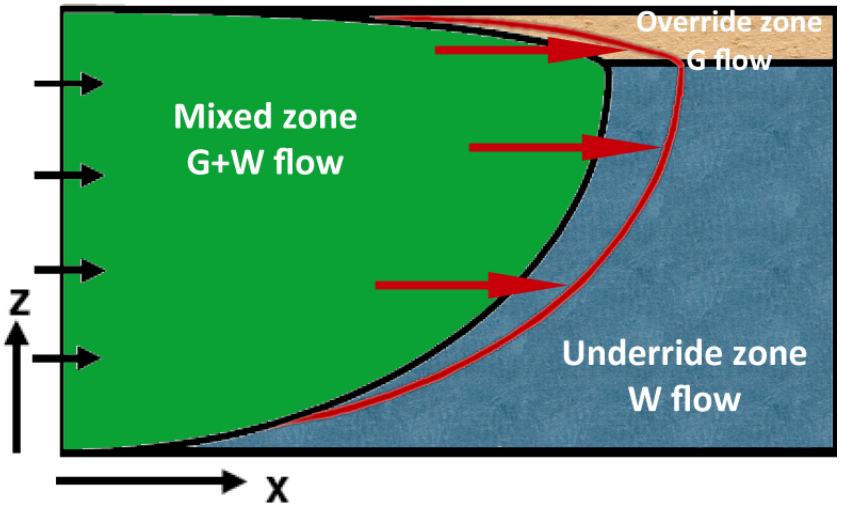

Figure 2 . 12 – Illustration of the three zones formed during WAG injection

Some field applications have been reported in literature [4] highlighting different results and reasons for applying SWAG injection.

In addition to Simultaneous WAG, another injection technique, called Hybrid WAG injection, has been applied during the last 30 years. This process consists in injecting a large slug of gas followed by small slugs of water alternating gas. Even though the results might be different, the same considerations as those reported for traditional WAG can be applied.

2.3 Design parameters for WAG projects

The main objective during WAG injections is obviously to achieve additional recovery compared to other possible operations. These processes have been applied in several reservoirs with different operational characteristics. Thus, some important parameters should be carefully analyzed from an operational point of view during the project design, in addition to the obvious role that fluid characteristics play.

2.3.1. Injection gas

One of the first issues is the selection of the injection gas to use. The decision is mainly based on economic considerations and availability [4]. Gas properties are critical in WAG injection because they determine whether the process will be miscible or immiscible under the prevailing conditions of pressure and temperature within the reservoir. Injection gases can be roughly divided into three groups: 1) carbon dioxide, 2) hydrocarbons and 3) non-hydrocarbons (CO_2 excluded). *Fig. 2.13* shows the distribution of injection gas types among the existing WAG projects [4].

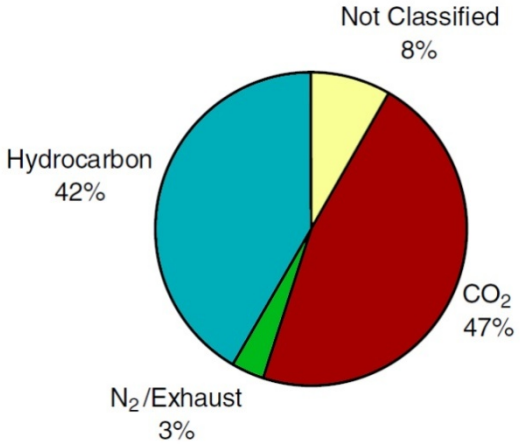

Figure 2 . 13 – Injection-gas types distribution among WAG applications

The first solution is mostly applied when miscibility should be achieved or in case of special delivery options, since CO_2 is a very expensive gas. Moreover, problems related to corrosion are often reported for this application.

Hydrocarbons injection is rather mainly applied in case of direct availability of gas during production. This is the reason why this technique is applied almost just for offshore plants, even if studies concerning the possibility of injecting CO_2 have been investigated [4]. Since the properties of the produced gas cannot be largely varied (only slightly improve the miscibility through gas enrichment with ethane, propane or butane), it is usually difficult to control the miscibility characteristics of the injection.

Only few applications can be found concerning the third solution, where the injection process recurs to non-hydrocarbon gases such as nitrogen or flue gases (CO_2 excluded), mainly because of the proximity of special supplies.

Once the gas has been selected, the optimal amount of gas to be injected during WAG floods should be estimated and applied, in order to avoid gas recycling due to gas-excess that leads to a reduction in additional recovery.

2.3.2. Injection pattern

The injection pattern is another important design parameter and the five-spot one seems to be the most popular [4]. As a rule of thumb, an increase in the number of injectors is supposed to give a better control of the field pressure, which has to be maintained above the minimum miscible pressure to achieve miscibility, and hence of the WAG-injection performance Regular patterns are suitable for onshore fields, while they are seldom used offshore. In fact, in offshore field cases, the wells are usually placed on the basis of geological considerations.

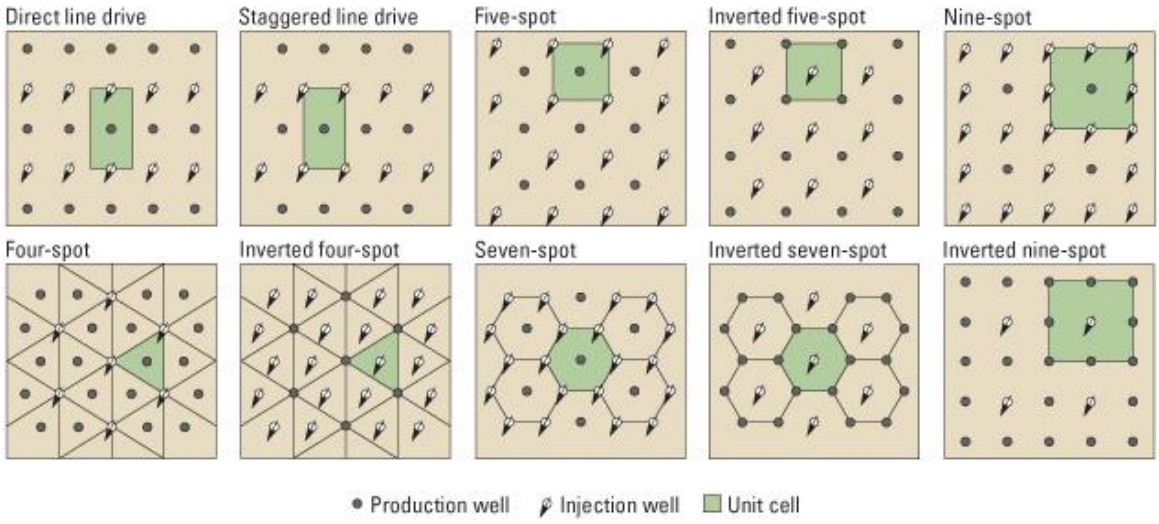

Figure 2 . 14 – Possible regular patterns for injection

A recent study [23] showed that a 4-spot pattern on an Iranian fractured reservoir gives higher recoveries than a 5-spot configuration, meaning that increasing the number of injection wells does not necessarily imply an increased recovery.

2.3.3. Reservoir heterogeneity

Most reservoirs have a non-uniform pore-size distribution and a varying degree of pore interconnectivity. Their vertical heterogeneity can be in part easily modeled in the form of heterogeneous layers.

Layers with high vertical permeability are influenced by cross-flow perpendicular to the bulk flow direction. This phenomenon may increase the vertical sweep, but generally it appeared to be detrimental for oil recovery, mainly due to gravity segregation effects and thus low flooding velocity in the reservoir. This leads to reduced frontal advancement in less permeable layers reducing recovery factors [10].

Heterogeneous permeabilities can severely affect the WAG process design and the resulting recovery rates. The situation worsens as the ratio between vertical and horizontal permeability (k_v/k_h) increases [24].

2.3.4. WAG ratio

The WAG ratio is defined as the ratio of injected water ($q_{w,inj}$) to injected gas ($q_{g,inj}$):

$$W_R = \frac{q_{w,inj}}{q_{g,inj}} \tag{2.2}$$

An optimum value of WAG ratio allows a good mobility and thus avoids problems caused by either an excess of water injected that may lead to poor microscopic sweep and water tongue at the bottom of the reservoir, or an excess of gas injected, which may rather result in a gas tongue development (override) at the top of the reservoir and a very early gas breakthrough [12]. A WAG ratio of 1:1 is normally used in field applications [4]. However, its optimal value depends on the gas availability and rock wettability of the reservoir [25], in order to achieve a stable front in which gas and water are moving at the same speed . In general, the amount of fluids to be injected at the desired pressures affects the cost of surface facilities, like compressors and pumps, which in turn may become an economic constraint for WAG applications, affecting also the optimal WAG ratio itself [24]. At the same time, “tapering” occurs when the water to gas ratio varies throughout the flood. In many reported cases it was not a planned process, but it was rather a consequence of increased recycling during the WAG process. However, the relative volume of water can be increased in order to give a better control on channeling and override phenomena. Tapering becomes more important proportionally to the cost of the gas used [4].

2.4. Operational problems

As a switch in the injection fluids frequently occurs, the WAG injection is more demanding than a pure gas or water injection an thus, some operational problems must be avoided during the production life of an oil field. Most common problems in WAG applications are listed below, on the basis of operational reports of field applications [4].

- ***Early gas breakthrough***
  Due to its very high mobility, the injected gas can break through one or more production wells earlier than expected if close attention is not paid during WAG processes. In fact, channeling and override may occur leading to possible premature shut-off of the producers. Moreover, override is a critical issue, especially for offshore fields, because of limited number of wells and gas handling facilities.
- ***Reduced injectivity***
  Reduced injectivity implies less water or gas injected in the reservoir, leading to a steeper pressure drop and thus affecting displacement and production. Experimental evidence has shown that water slugs injected after gas slugs cause fragmentation and trapping of the gas in the pores, reducing areas available to water flow and hence reducing relative permeability. As more WAG cycles are injected, more gas is trapped and thus the water flow is more restrained [26].
- ***Corrosion***
  Corrosion is an important issue for many projects. As WAG processes are normally applied as tertiary recovery methods, the project will then have to take over old injection and production facilities originally not properly designed for this application. However, only processes using CO_2 as injected gas have reported severe problems, further worsened by scale formation (inorganic salts, such as sulphates or carbonates) and precipitation in production equipment.
- ***Asphaltenes and hydrates formation***
  Asphaltenes and hydrates may lead to problems in production (delays or stops) and hence affect the economics of projects.
  Asphaltenes precipitation and deposition effects should be anticipated at earlier stages of each project. Unfortunately, asphaltenes nature is not properly understood yet and thus its modeling remains dubious [27]. Anyhow, the problem could be remediated in many cases with solvent treatment at proper intervals.
  On the other hand, hydrates are formed when liquid water and natural gas are present at "wrong" side of equilibrium line (*Fig. 2.15*).

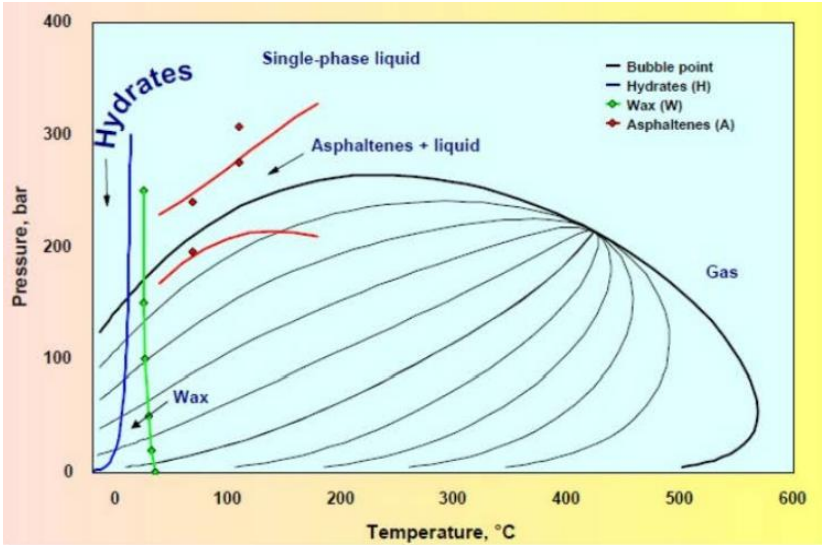

Figure 2 . 15 – Typical pressures and temperatures for solid formation in generic petroleum production [28]

Water molecules are stabilized by small gas molecules so that the physical process of hydrates formation can occur at quite high temperatures. Historically, hydrate formation in wells caused sometimes freezing of the wellhead during nights and cold periods. Normally, the problem can be controlled by methanol treatments (or other antifreezes such as ethylene glycol), but due to high expenses associated to the antifreeze injection, new solutions are being studied and applied at pilot-scale [29].

3. Fundamentals of Foam Assisted WAG

3.1. Introduction to foam application

Foam can be applied to solve conformance problems caused by either thief zones or gravity override, improving therefore the sweep efficiency of a WAG injection. In all cases, an unfavorable mobility ratio between the displacing fluids and density differences mainly affect the problem. A proper identification of causes and "offending production wells" experiencing a premature breakthrough of injection fluids is required to the definition of the problem.

Presence and position of high and low permeable layers, their permeability contrast, structural dip and gas segregation are factors to consider during the selection of the best foam process. On this basis, in addition to the manners of foam placement (around an injection well or a production well), three classes of foam can be identified:

- In-depth Mobility Control Foam (MCF)
- Blocking/Diverting Foam (BDF)
- Gas-Oil-Ratio (GOR) control foam

While MCF and BDF are used for injection wells treatments, a GOR control foam is applied to producers to directly and temporarily protect near-well producing zones from gas influx. Treating the producer, of course, does not give as large field-scale recoveries as injector treatments do, but the chemical volumes used are much smaller, so that the process may become technically and economically practical [30]. On the other hand, the distinction between MCF and BDF is to some extent arbitrary and not strict at all. In fact, BDF foams are usually used in small volumes, relating to the small swept volume (no matter if due to overriding or thief zones), whereas MCFs propagate all the way from injectors to producers without decaying [31]. Therefore, the conditions for the application of the latter class of foams are the most demanding.

In field pilots and applications, diverse manners of foam placement have been used and all of them are closely associated with the way by which foam is generated. Thus, three types of foam generation can be found as well:

- *Pre-formed foam* - generated outside the porous medium before entering the pay zone, i.e. at the surface, during the downward flow through the tubing or in the perforations.
- *Co-injection foam* – formed in situ in the first entrance segment of the porous medium during co-injection of surfactant solution and gas.

- *Surfactant-Alternating-Gas (SAG) foam* – generated by alternate injection of gas and surfactant solution during drainage of the surfactant solution by gas in the whole invaded zone.

There are some differences between the above reported types of foam. As a matter of fact, a SAG foam cannot completely block the porous medium and its mobility reduction effect is lower than that for the other two types. Furthermore, while a pre-formed foam develops a high gas mobility reduction soon after the entrance into the porous medium, a co-injection foam has a weaker effect at the entrance segment, which then acts as a foam generation zone [31].

3.2. Foam in porous media

The main goal for a foam assisted EOR process is mobility control throughout the formation, by creating a foam-filled region which spans large distances over periods of months or even years and potentially redirects flow pathways to unswept areas. It is essentially a mixture of gas, water and surfactant (foaming agent), without which foams are unstable and quickly collapse. In fact, foam at reservoir conditions is defined as a dispersion of gas in liquid such that the liquid phase is continuous and at least some gas flow paths are made discontinuous by thin liquid films called lamellae (*Fig. 3.1*). The junction encompassed by a dotted circle and connected by three lamellae is called "Plateau" border.

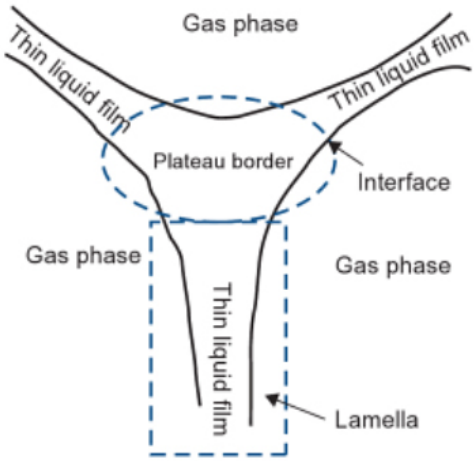

Figure 3 . 1 - Schematic of a foam system [32]

In porous media, foam exists as gas bubbles whose shapes conform to the solid matrix. Each lamella contains two gas-liquid interfaces separated by the thin film, and each lamella has a surface tension. This is the variable which is significantly lowered when a surfactant is added to water.

Moreover, in a water-wet porous medium it is possible to notice the presence of water as both bulk water in small pores and lamellae between gas bubbles (*Fig. 3.2*).

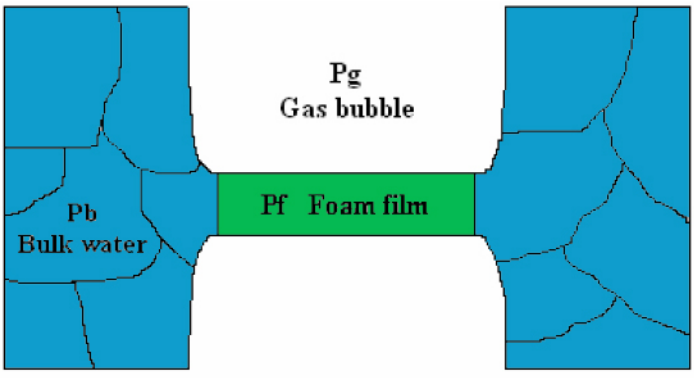

Figure 3 . 2 – Pressure distribution in the water phase

The pressure difference between the bulk water and the gas bubble is expressed as capillary pressure p_c:

$$p_c = p_g - p_b \tag{3.1}$$

Where p_g is the pressure inside the gas bubble and p_b the bulk water pressure. At equilibrium, the value of p_c should be balanced by the disjoining pressure, Π:

$$\Pi(h) = p_g - p_f \tag{3.2}$$

Where h represents the film thickness and p_f the average pressure inside the liquid film. The disjoining pressure is characterized by attractive forces between molecules, which lead to attraction between film surfaces, and repulsive forces, due to the interaction of two same-sign charged interfaces. If Π exceeds the maximum value Π_{max}, then the thickness becomes lower than its critical value h_{cr} and the film collapses (*Fig. 3.*3).

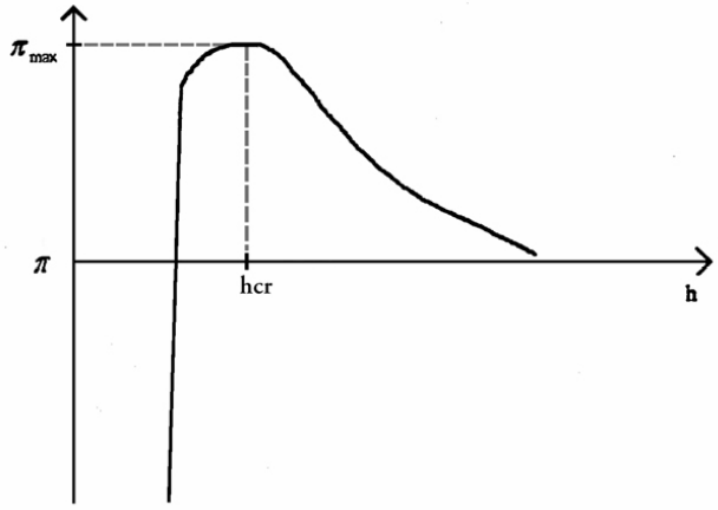

Figure 3 . 3 – Ideal disjoining pressure trend as a function of film thickness [33]

Thus, at equilibrium, this curve together with the capillary pressure determines the equilibrium thickness of the film. In the figure below, it is shown the capillary pressure as a function of water saturation (S_w) to better understand the relationship between Π_{max}, p_c and S_w (*Fig. 3.4*).

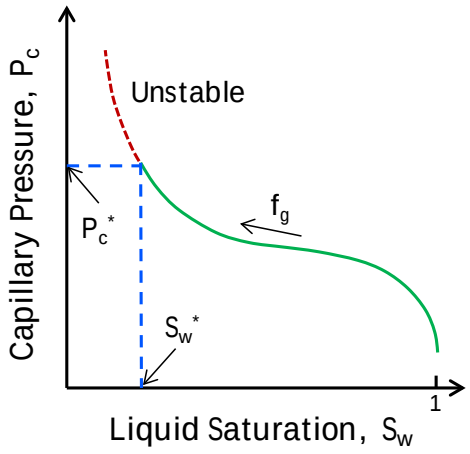

Figure 3 . 4 – Plot showing the unstable and stable regions for foams

It is important to notice the critical water saturation S_w* below which no foam exists because of the high capillary pressure. Obviously, the limiting capillary pressure p_c* for foam stability in porous media is lower than the value of Π_{max} for static films measured in laboratories. Anyway, another parameter is shown in the figure. In fact, foam generation in porous media depends on injection rates of the fluids and on foam quality, defined as:

$$f_g = \frac{injected\ gas\ flow\ rate}{total\ injected\ fluid\ flow\ rate} \tag{3.3}$$

This definition allows to understand the significance of the arrow f_g pointing to the opposite direction of S_w in *Fig. 3.4*, that is to say an increase in the gas fraction will cause a decrease in the water saturation.

Foam states, creation and termination mechanisms, together with flowing regimes inside porous media, will be introduced in the following subsections.

3.2.1. Foam states

Foam is typically categorized into three different states while flowing inside a porous medium.

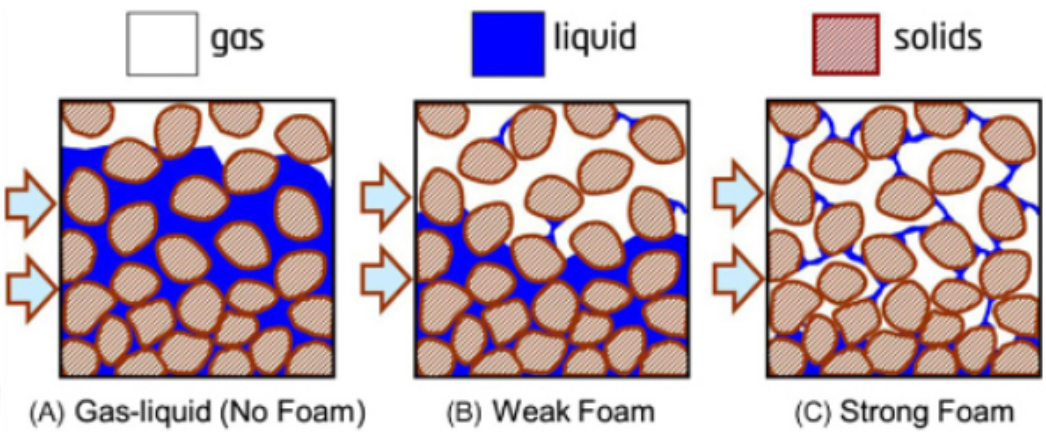

Figure 3 . 5 – Comparison between the three foam states [32]

As illustrated in *Fig. 3.5*, the first case (A) is representative of conditions where no foams are present initially or, in case there were pre-existing foams, they have been destabilized and destroyed, for instance, by a high oil saturation. In this case, the flow is characterized by two conventional gas-liquid phases without films, resulting in high saturation of liquid. In the second case (B), a "weak" foam is formed exhibiting a moderate gas mobility reduction and thus a moderate pressure gradient increase. Lastly, in the third case (C), the presence of many foam films leads to a very fine-textured foam which is referred to as "strong" foam. Once this foam is formed, its structure implies a decrease in effective gas mobility which can reach even several orders of magnitude, exhibiting a dramatic increase in pressure gradients.

3.2.2. Foam generation mechanisms

In field applications, three different flow regimes have been encountered in porous media and each of them results in totally different flow behaviors and generation mechanisms [32]:

- Surface facilities and well itself, where inertial flow may create bulk foam;
- Near-wellbore region, where flow rates and pressure gradients are high;
- Formation, far away from the injection well, where flow rates and pressure gradients are much lower.

It is commonly accepted that, on the basis of what just said above, lamellae are created by the three following mechanisms inside real porous media:

- ***Leave behind***
  This mechanism consists of the creation of stabilized liquid films as two gas menisci invade adjacent liquid-filled pore bodies from different directions, as shown in *Fig. 3.6*. A film is left behind as two menisci converge downstream. It is an important mechanism at low velocities and, although it is usually a source of weak foams, a large number of lamellae are created to block gas pathways.

Nevertheless, it cannot account alone for the large reduction in gas mobility usually seen with foams.

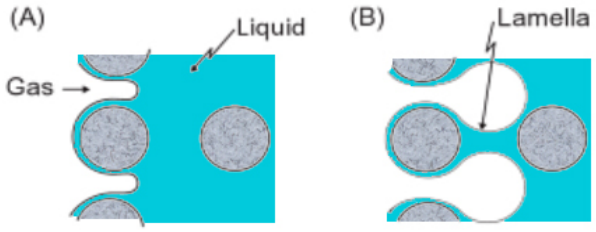

Figure 3 . 6 – Schematic of leave-behind mechanism showing gas invasion (A) and foaming film (B)

- ***Lamella division***

  Lamella division occurs when a gas bubble approaches a branch point so that two or more lamellae are generated from a single one (*Fig. 3.7*) This is mainly a high-velocity mechanism.

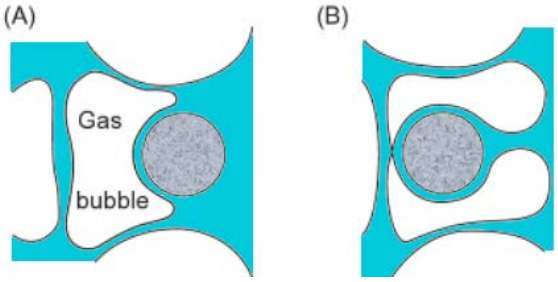

Figure 3 . 7 – Schematic of lamella division showing branch point (A) and two resulting bubbles (B)

- ***Snap-off***

  Snap-off occurs when a gas bubble penetrates a pore throat and a new smaller bubble is formed from the first one (*Fig. 3.8*). It has been shown experimentally that this mechanism happens if the local capillary pressure falls to about half the capillary entry pressure of the throat [34]. The gas-phase is then transformed into discontinuous form and, as it can occur repeatedly at the same site, this mechanism can affect a relatively large portion of the field [32]. This is believed to be the predominant foam generation mechanism.

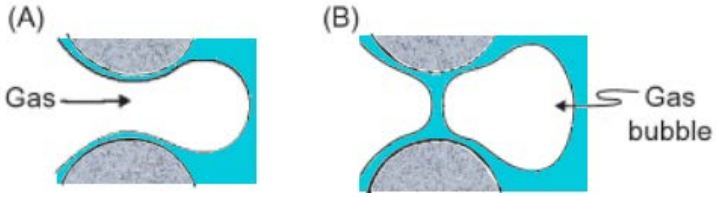

Figure 3 . 8 – Schematic of snap-off mechanism showing gas penetrating a throat(A) and a new bubble formed (B)

3.2.3. Foam termination mechanisms

In absence of oil, two mechanisms are mainly responsible for the foam coalescence [35]. Both mechanisms result in the formation of one big bubble from two smaller bubbles which were initially occupying the pore space.

- ***Capillary suction***
  Moving lamellae coalesce when they are rapidly stretched across large pore bodies. For a given gas flow rate and capillary pressure, pore-throats/pore-bodies combinations with large aspect ratios serve as termination sites. Moreover, as the gas velocity or capillary pressure increases, an increasing number of pores become termination sites [34].
- ***Gas diffusion***
  Gas diffusion coalescence occurs when two bubbles with different curvatures are in contact. As the pressure on the concave side of a curved foam film is higher than that on the convex side, gas diffuses through the film and dissolves in the liquid present in the convex side. Thus, the gas diffuses from smaller bubbles to less curved (bigger) ones.

While the first mechanism happens through a fast physical process, the latter takes place through a slow diffusion process [34].

3.2.4. Foam flow regimes

Strong-foams exhibit two distinct steady-state flow regimes as functions of foam quality f_g. As illustrated in *Fig. 3.9* below, at high foam qualities (upper-left portion of the figure) pressure gradients ∇p are nearly independent of gas flow rates u_g. This "high-quality" regime is controlled by bubble coalescence at the "limiting capillary pressure" P_c^*, that is to say both capillary pressure and water saturation remain at P_c^* and $S_w = S_w(P_c^*)$ respectively, independently of gas flow rates. In this regime, as a function of the total flow rate $(u_g + u_w)$, the foam behavior can be shear-thinning, Newtonian or even shear thickening [36]. On the other hand, the "low-quality" regime (lower-right portion of the figure) is characterized by a shear-thinning behavior and the pressure gradient ∇p is rather independent of liquid flow rates u_w, due to bubble trapping and mobilization [32]. Different opinions are reported on literature whether these regimes characterize only strong foams [32] or possibly also weak foams [36].

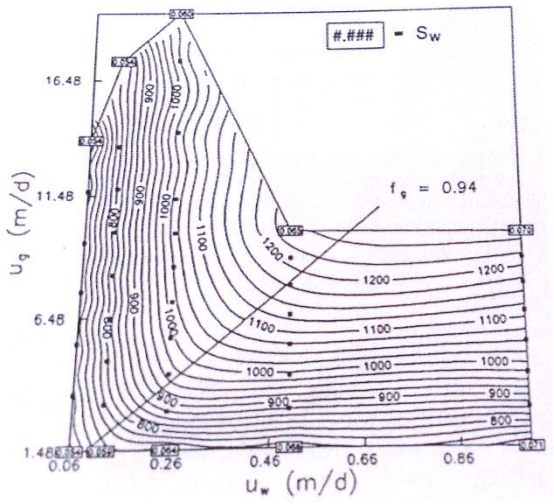

Figure 3 . 9 – Pressure drop (psi) across 2-ft sandpack as a function of gas and liquid flow rates [37]

The idealized representation of the pressure drop vs. flow rates given in *Fig. 3.10* gives a better idea of what said in the lines above.

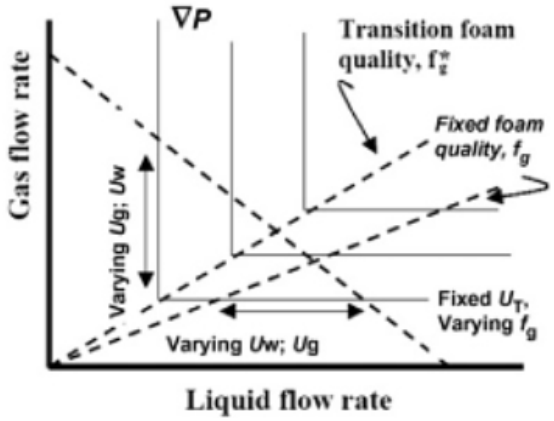

Figure 3 . 10 – Ideal representation of the flow regimes

Fixed foam qualities are represented as straight lines starting from the origin, as obvious by the definition given in the previous pages, while experiments conducted at fixed overall flow rates are represented as inclined lines crossing the ones of fixed qualities. In the ideal case of an abrupt transition from low quality to high quality, all the "transition" points lie on a straight line with a constant foam quality f_g^*, whose slope depends on compositional factors and permeability. As a matter of fact, f_g^* decreases according to an increase in permeability k, as noticeable from both *Fig. 3.9* and *Fig. 3.10* where, for a fixed total velocity and varying values of foam quality, the maximum pressure gradient is reached at the transition foam quality.

3.3. Process Variables

Once a good surfactant has been chosen, several variables affect the propagation (in both reservoirs and cores, which are required to be 40-50 cm long at least) and, as a consequence, the effectiveness of mobility control by foam in porous media [34]. A list of the most important process variables is reported below:

- ***Permeability***
  Permeability is the most important parameter affecting foam propagation in porous media. Experimental evidence indicates that foam reduces gas mobility more in high permeability media than in low permeability media. This fact can be inferred by having a look at the change of apparent viscosities (μ_f^{app}) at fixed foam qualities by changing the permeability values (k) (*Fig. 3.11*).

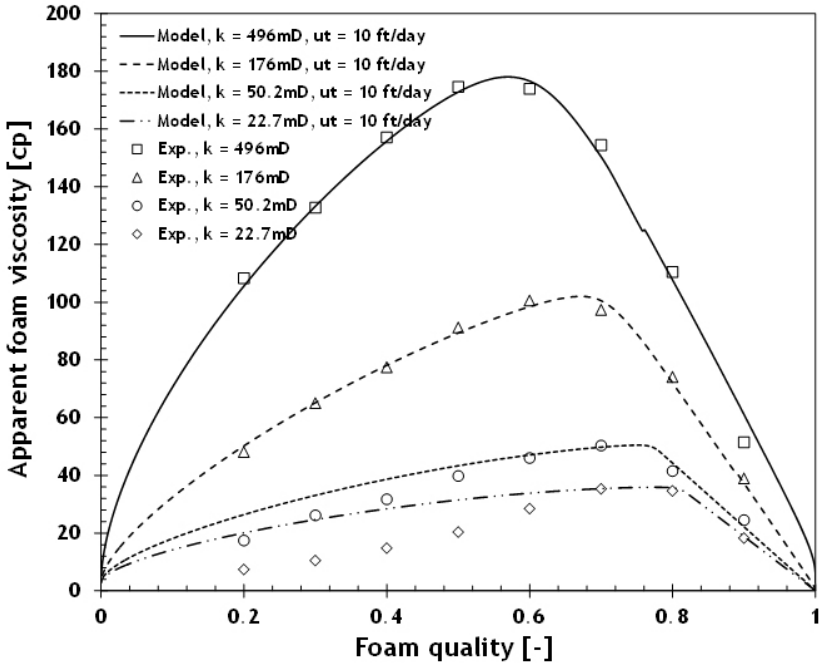

Figure 3 . 11 – Apparent viscosities of a CO2 foam vs. foam quality at different permeabilities [38]

The apparent viscosity μ_f^{app} is defined as the viscosity one would infer for foam at a given fractional flow if foam were treated as a single phase fluid. Thus, for a given water saturation, its expression becomes as follows:

$$\mu_f^{app} = \frac{1}{\frac{k_{r,w}(S_w)}{\mu_w} + \frac{k_{r,g}^f(S_w)}{\mu_g}} \tag{3.4}$$

Experimental data and best fitting curves of corefloods are reported on *Fig. 3.11* for different foam qualities and permeabilities at a given concentration of a certain surfactant (2000 ppm Chaser CD-1050). Higher values of apparent viscosity for higher values of permeability are evident from the figure, supporting what said

above, i.e. a higher efficacy in mobility reduction is noticeable in high permeability rocks.

- ***Injection rate***

  Gas and liquid injection rates determine the foam quality in porous media. Thus, they represent important parameters responsible of a good propagation and mobility characteristics. A good number of experimental studies [38] have shown that foams with qualities above $f_g = 95\%$ are too dry to be stable, while below $f_g = 45\%$ they lose their rheological consistency reflecting a liquid behavior. Furthermore, the overall velocity $(u_t = u_g + u_w)$ affects slightly the process of matching coreflood data with models [38].

- ***Pressure***

  Foam flooding experiments at variable pressures in an oil free porous medium have demonstrated that the foam strength steeply increases with increasing system pressures. For instance, the strength of C_{16} Alfa-Olefin-Sulfonate (AOS) based foams was reduced when the system pressure was relaxed, due to the same mechanisms that destabilizes foams in the absence of oil and previously described. Anyway, foam stability and oil-foam interactions vary differently with pressure depending on the surfactant selected [39].

- ***Surfactant***

  It is conceivable that the surfactant used has an important role in generation and stability of foams inside porous media at reservoir conditions. In addition to these roles, it should be characterized by low adsorption and decomposition losses and by increasing-effect on sweep efficiency. It should also be commercially available and inexpensive [40]. Furthermore, its concentration is inversely proportional to coalescence forces, i.e. the foam weakens and the displacement efficiency decreases with decreasing surfactant concentration, affecting the sizes of foam bubbles as previously mentioned in the foam termination mechanisms [41].

  Many types of surfactant have been identified in lab tests as viable candidates. Nevertheless, different types of water soluble anionic α-olefin-sulfonates (AOS) have frequently been cited as excellent agents for different foam based EOR processes [34].

- ***Oil***

  An important parameter to consider regarding the stability and effectiveness of foams is the effect of oil. Generally, two mechanisms of foam-oil interaction are possible, i.e. either the oil penetrates and destabilizes the foam film, or the foam film slides over a film of water covering the oil. Studies about these concerns are comparatively rare and greater efforts to collect experimental results and correlate them to the stability of foams in oil saturated porous media are required [42]. In fact, although different models have been successfully applied to different situations, translating the fundamental mechanisms of foam/oil interaction into generally applicable rules for field application remains very difficult [34] and carries a good amount of uncertainties.

- ***Adsorption***

  Adsorption of surfactant into the rock surface is one of the biggest unwanted destabilizing effects in foam based EOR processes. A basic rule consists on avoiding the employment of cationic surfactants in negative charged sandstone rock and of anionic surfactants in positive charged carbonate rocks [34]. Adsorption is a difficult effect to be modeled as it is a function of surfactant formulation, crude oil and brine compositions, rock mineralogy, reservoir pressure and temperature. At the same time it is an important parameter since it is frequently found that the amount of surfactant adsorbed accounts for most of the cost of the surfactant itself [43].

- ***Temperature***

  Temperature is a parameter which cannot be altered during a foam flood, so just few studies, in which temperature is systematically varied, have been carried out. Nonetheless, it is apparent that foam flooding above 80°C may require more careful design than low temperature floods. But, a benefit of high temperature formations is the lower surfactant adsorption recorded [34].

4. Full Field Analysis

4.1. Simulation environment

Reservoir simulations represent a form of numerical modeling used to quantify the flow of fluids through porous media and predict hydrocarbon field productions. Finite difference simulators are usually used in reservoir simulations. The reservoir is divided into a finite number of 3-D cells in which fluids behavior is modeled within discretized time steps. Simulations are underpinned by three physical concepts:

- Material balance equations
- Isothermal fluid phase behavior
- Darcy's law

ECLIPSE 100, a three phase, three dimensional black oil modeling simulator, is used for the purposes of this work. The term "black oil" refers to the fluid model, in which water is explicitly modeled together with two hydrocarbon components: oil phase and gas phase [44]. As a black oil simulator, ECLIPSE 100 does not consider changes in composition of the hydrocarbons as the field is produced and densities of oil and gas phases are the only compositional information taken into account. Thus, water and oil phases are always assumed to be immiscible and mass exchanges may occur between gas and oil phases only. The mathematical framework of the simulator consists of the following set of partial differential equations:

$$\frac{\partial}{\partial t}\left[\phi\left(\frac{S_o}{B_o}+\frac{R_v S_g}{B_g}\right)\right]+\nabla\cdot\left(\frac{1}{B_o}\vec{u}_o+\frac{R_v}{B_g}\vec{u}_g\right)=0 \tag{4.1}$$

$$\frac{\partial}{\partial t}\left[\phi\left(\frac{S_w}{B_w}\right)\right]+\nabla\cdot\left(\frac{1}{B_w}\vec{u}_w\right)=0 \tag{4.2}$$

$$\frac{\partial}{\partial t}\left[\phi\left(\frac{R_s S_o}{B_o}+\frac{S_g}{B_g}\right)\right]+\nabla\cdot\left(\frac{R_s}{B_o}\vec{u}_o+\frac{1}{B_g}\vec{u}_g\right)=0 \tag{4.3}$$

Where:
ϕ is the porosity of the porous medium,
the subscripts *o, g, w* represent oil, gas and water phase respectively,
B is the formation volume factor for a specific fluid, that is to say the ratio of the fluid reservoir volume to the volume at standard conditions,
S is the fluid saturation, i.e. the fraction of porosity of a zone occupied by that fluid,
R_s and R_v are the solution gas in oil phase and the vaporized oil in gas phase respectively;
$\vec{u}$ terms are the Darcy velocities of the three phases and can be expressed by following equation:

$$\vec{u} = -\frac{k}{\mu}(\vec{\nabla}p - \rho\vec{g}) \tag{4.4}$$

where k is the permeability of the medium to the considered fluid, μ is the dynamic viscosity of the fluid, p is the pressure, ρ is the fluid density and $\vec{g}$ the gravity vector. This expression results from the Navier-Stokes equation simplified with the assumptions of stationary, incompressible flow, linear dependence between viscous resisting force and velocity, and slow flow in a porous medium.

All the information needed by ECLIPSE is given by the user through keywords, tables and maps of property distributions in a single data input file. This data file contains a complete reservoir description in terms of fluid and rock properties, initial conditions characteristics of wells and surface facilities conditions (if needed). ECLIPSE outputs various resulting information at dates predefined by the user that can be examined using text editors and post-processing software of various degrees of sophistication [45].

4.2. Reservoir characterization

This work is focused on the application of foam to improve the effect of WAG injection in an offshore deepwater oil reservoir in Angola, here called FIELD α (*Fig 4.1*). This is a sandstone reservoir characterized by, like most of the Angolan ones, the presence of meandering turbiditic channels in which the hydrocarbon accumulation occurred.

Figure 4 . 1 – Angolan Reservoirs [47]

The following data set is needed to populate the reservoir model:

FIELD α Characteristics		
	UNITS	**MEAN VALUES**
RESERVOIR		
Start-up date		01/11/2014
Rock type		Sandstone
Area	[km^2]	16
Datum depth	[m]	2543,2
Datum pressure	[psia]	3769,3
Oil water contact (OWC)	[m]	2605,2
Minimum depth	[m]	2199,99
Maximum depth	[m]	3002,43
Reservoir temperature	[°C]	65
Average reservoir pressure	[psia]	3696,75
Average permeability	[mD]	575
Av. best sands permeability	[mD]	1050
Average porosity	[%]	18
Best sands porosity	[%]	21
Bubble point pressure (T_{res})	[psia]	2684
Minimum miscible pressure	[psia]	7005,0
Water depth	[m]	1320
Water salinity	[g/l] NaCl	130
OIL		
Field oil in place	[StB]	$63{,}23 \cdot 10^6$
Gravity	[°API]	32,9
Viscosity	[cP]	0,9
Oil Formation Volume Factor	[RB/StB]	1,31

Table 1 – Post-risk FIELD α data

A few preliminary observations can be made by perusing the data:

- FIELD α is an initially undersaturated sandstone reservoir in which oil is immiscible with its and nearby fields' gas due to the very high value of minimum miscible pressure.
- Since the OWC lies at 2065m, it results quite close in terms of vertical depth from the bottom perforations of the production wells, suggesting a probable premature water breakthrough and high water cuts during the oil recovery processes, even if analyses conducted on analogues fields, which take into account the presence of an Angolan regional aquifer, show its weaknesses.
- Moreover, as the sea-water depth is well above 800m, this is considered a deep water reservoir, implying a more challenging production stage. This is the reason why an FPSO has been selected as the most suitable solution to exploit FIELD α and consistent constraints are outlined in the field model.

The reservoir model is represented in *Fig. 4.2* (top and front sides) by a 67x53x30 grid (x, y, z maximum ranges) showing a ternary representation of fluids saturation distribution in the reservoir.

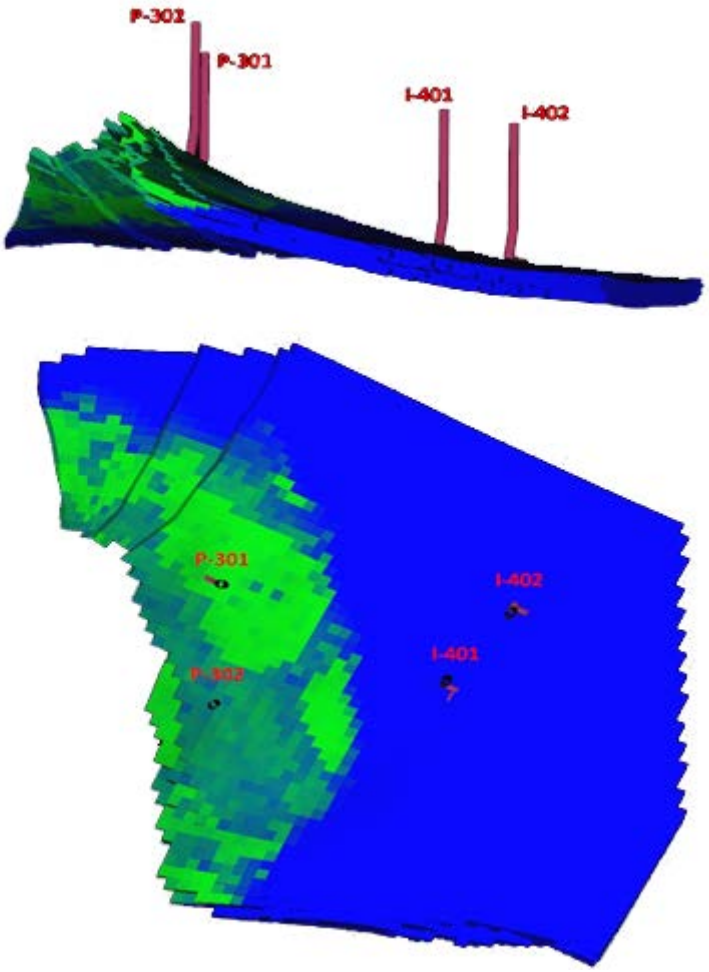

Figure 4 . 2 – Illustration of saturations (water-blue, oil-green, gas-red) distribution of the FIELD α model

Coherently with the reported data, it is palpable that no free gas is present at the beginning, as no red cells, representing gas saturated regions, are visualized in the figure. As already mentioned, the reservoir is characterized by the presence of turbiditic sandstone channels that are reported in the model by splitting the reservoir into three facies differing from each other because of the rock characteristics from a static point of view (i.e. porosity and permeability) and from a dynamic point of view (i.e. relative permeabilities). An illustration of the three facies is shown in *Fig. 4.3*, where an intermediate layer of the reservoir is represented from a top view. The channel characterized by good facies connecting the injectors I-401 and I-402 with both the producers is well-rendered in red color.

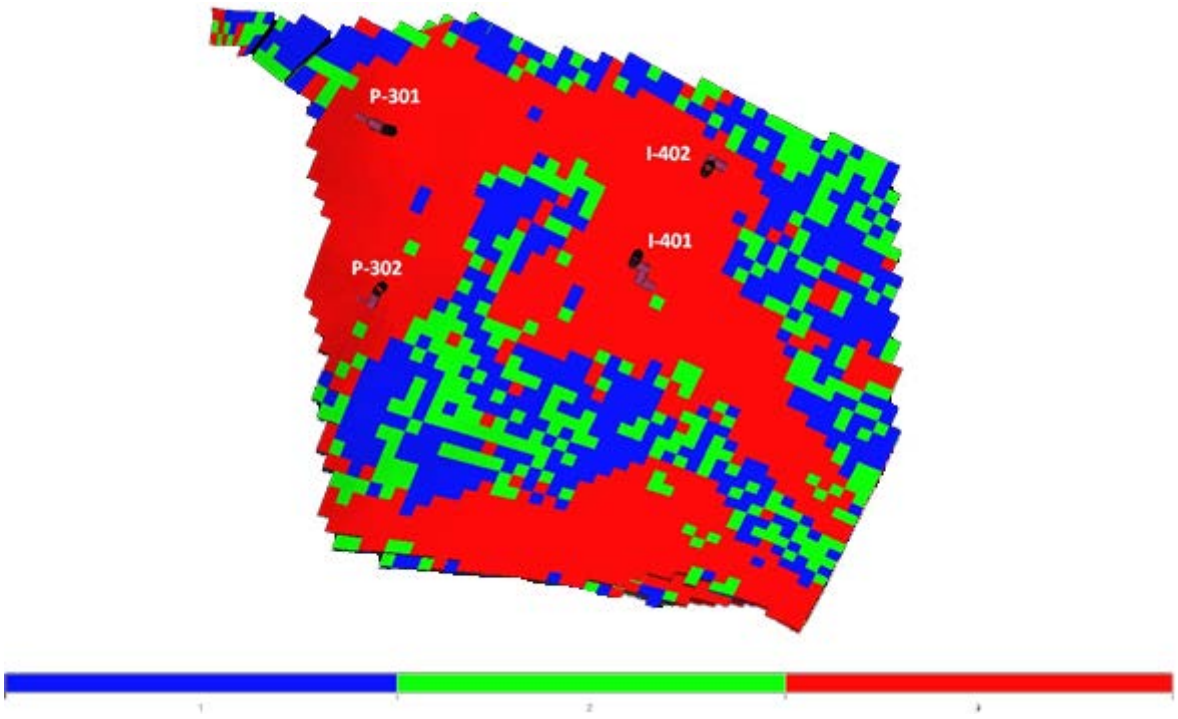

Figure 4 . 3 – Illustration of the good facies channel in an intermediate layer

Data about the dynamic features of the three regions are reported in the following table:

Facies	Fig. 4.3 color	$k_{r,o}^{max}$	k_v/k_h	$k_{r,w}^{res}$	$S_{ow,cr}$
Bad	**Blue**	0,196	0,01	0,038	0,134
Intermediate	**Green**	0,585	0,114	0,216	0,112
Good	**Red**	0,820	0,703	0,461	0,107

Table 2 – Facies characteristics

$k_{r,o}^{max}$ represents the maximum oil relative permeability, k_v/k_h is the ratio between vertical and horizontal absolute permeabilities, $k_{r,w}^{res}$ is the residual water relative permeability and $S_{ow,cr}$ is the critical oil-in-water saturation.

Regarding the reservoir development plan several assumptions can be made:

- as already mentioned, a floating production, storage and offloading (FPSO) vessel is used to receive and store hydrocarbons produced together with the hydrocarbon of other fields located in the surroundings
- the well layout consists of two oil producers, P-301 and P-302, and two injectors, I-401 and I-402;
- water injection, as secondary recovery stage, is applied since the start-up date, as primary recovery processes are not sufficient to guarantee the economically feasible production;
- the development plan was originally to apply a water-injection-only process until a second field start-up after 2 years of FIELD α production life, but in this work this constraint has been modified to study the effect of shortening this period;

- gas produced from FIELD α and other nearby fields has to be reinjected due to the no-flaring policy [46] and to the absence of other utilities for gas disposal;
- reservoir production life is constrained at 10 years due to operational choices.

In addition, other constraints have been added and are reported in the following table:

FIELD α Model constraints		
	UNITS	**MEAN VALUES**
RESERVOIR		
Gas consumption rate	[$Stft^3/d$] $\cdot 10^3$	7500
Oil production rate target	[StB/d]	20000
Gas production upper limit	[$Stft^3/d$] $\cdot 10^3$	30000
Liquid production upper limit	[StB/d]	25000
P-301		
Limiting oil production rate	[StB/d]	11000
Limiting gas production rate	[$Stft^3/d$] $\cdot 10^3$	15000
Minimum tubing head pressure	[psia]	1450
Artificial lift injection	[$Stft^3/d$] $\cdot 10^3$	0,6
Economic production threshold	[StB/d]	200
Length down tubing of gas-lift injection	[m]	1107
Limiting well water cut	[%]	0,95
P-302		
Limiting oil production rate	[StB/d]	9000
Limiting gas production rate	[$Stft^3/d$] $\cdot 10^3$	15000
Minimum tubing head pressure	[psia]	1450
Artificial lift injection	[$Stft^3/d$] $\cdot 10^3$	0,4
Economic production threshold	[StB/d]	200
Length down tubing of gas-lift injection	[m]	1316
Limiting well water cut	[%]	0,95
I-401/I-402		
Bottom hole pressure upper limit (water)	[psia]	5100
Tubing head pressure upper limit (water)	[psia]	3000
Bottom hole pressure upper limit (gas)	[psia]	5100
Tubing head pressure upper limit (gas)	[psia]	5000

Table 3 – Reservoir constraints

4.3. Water Injection case

The water-injection-only scenario can be used as a baseline to show the possible advantages achievable with an EOR application. In fact, even if it is mandatory to re-inject the dissolved gas as previously described, it may be found that FIELD α is not a good candidate for gas injection. A voidage replacement ratio VRR = 1 has been used for the simulations, honoring all the constraints already reported in the previous pages.

The following figures show the output data profiles for the simulated 10-years time frame.

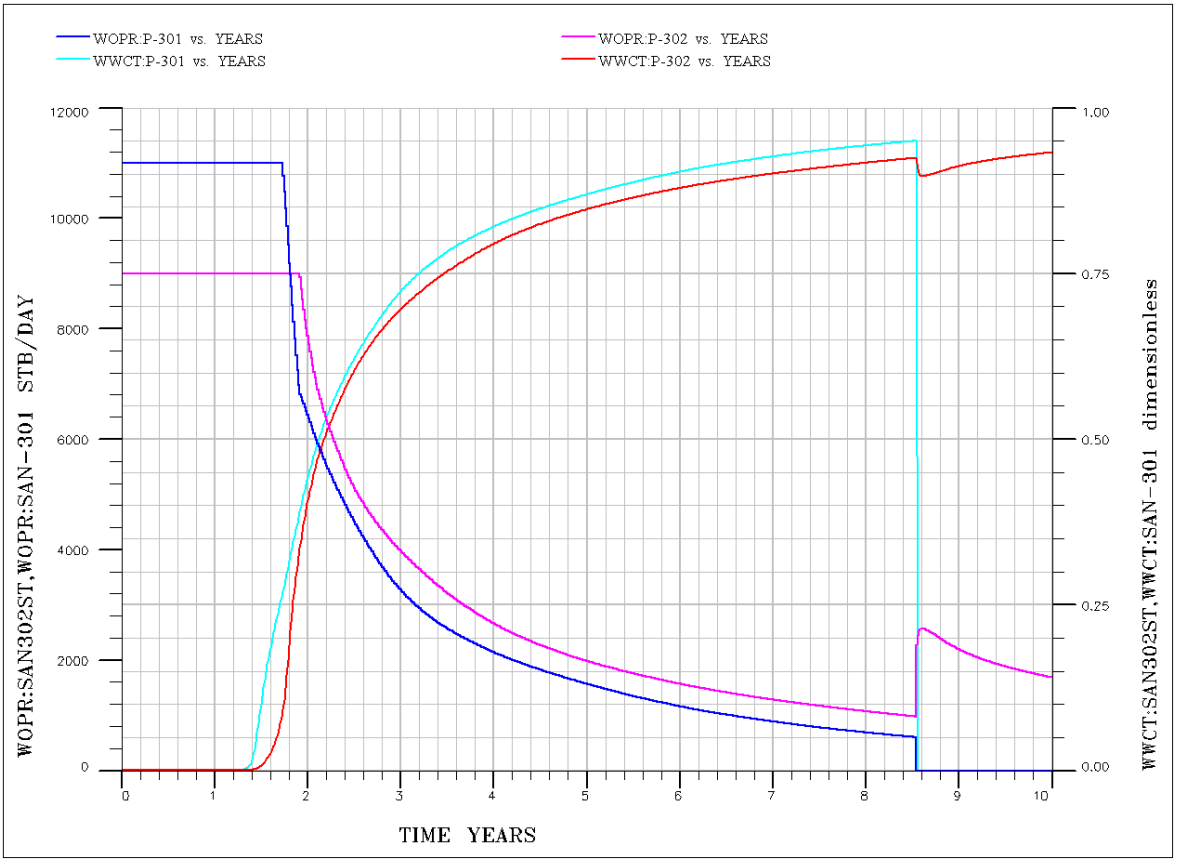

Figure 4 . 4 – Well oil production rates and water cuts (P-301 and P-302)

After a first period of well-maintained oil plateau for both production wells, production decreases due to the increasing WWCT (well water cut – water produced compared to the volume of total liquids produced) that leads the total liquid production rate (FLPR) to reach its limiting value (25000 StB/d). The producer P-301 undergoes a premature shut-off at 8,5 years due to the high water cut value reached, corresponding to the limiting well water cut (95%) already reported. By the end of the simulation period, the P-302 WOPR (well oil production rate) immediately rises once that P-301 is shut. This is coherent with *Fig. 4.3*, where the good-facies channel connects both the injectors with P-301 first, and then it subsequently reaches P-302. So, once that P-301 is shut, all the injected water affects P-302, which instantaneously increases its production rates. A few reasons can be outlined to explain the earlier water breakthrough and subsequent shut-off of P-301: it reaches a deeper layer compared to P-302 (*Fig. 4.5*); it is the producer which covers the whole thickness range; as the first producer encountered by the channel flow, it is more susceptible to injected fluids effects.

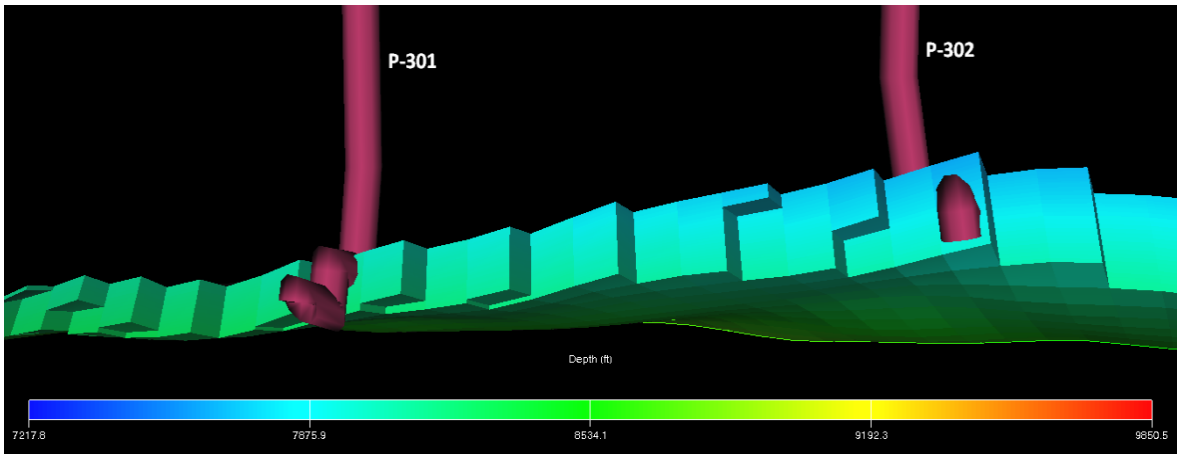

Figure 4 . 5 – Plane slice comparing the depths reached by P-301 and P-302

A saturations analysis of near-well regions can clearly outline, from a qualitative point of view, whether WAG processes represent an interesting solution or not. A top-view (*Fig. 4.6*) and two cross-sections (*Fig. 4.7*) in the near-well area at time 10 years are shown to verify the presence of unswept oil in the upper layers after water-injection if compared to Fig. 4.2.

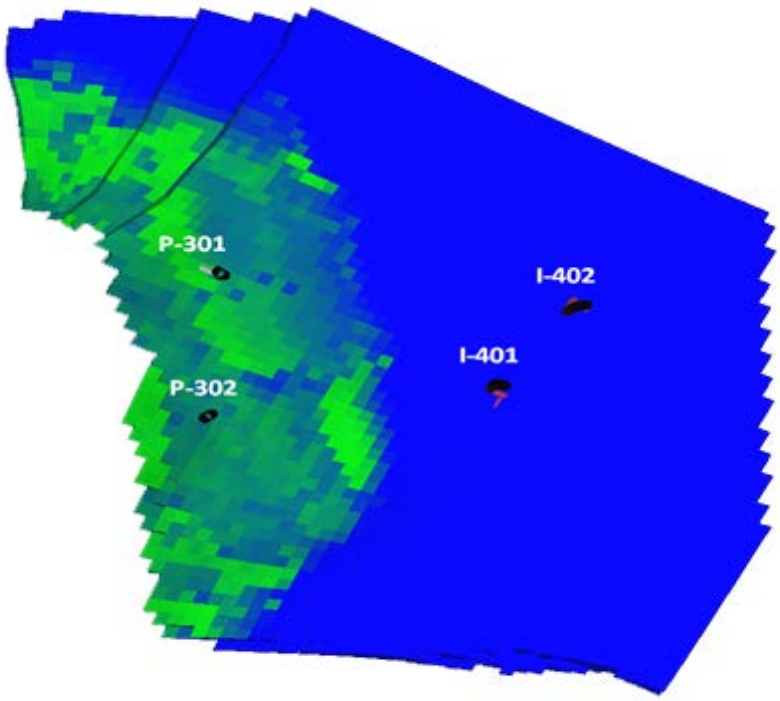

Figure 4 . 6 – Fluids saturation (water-blue, oil-green, gas-red), top-view after 10 years of water injection

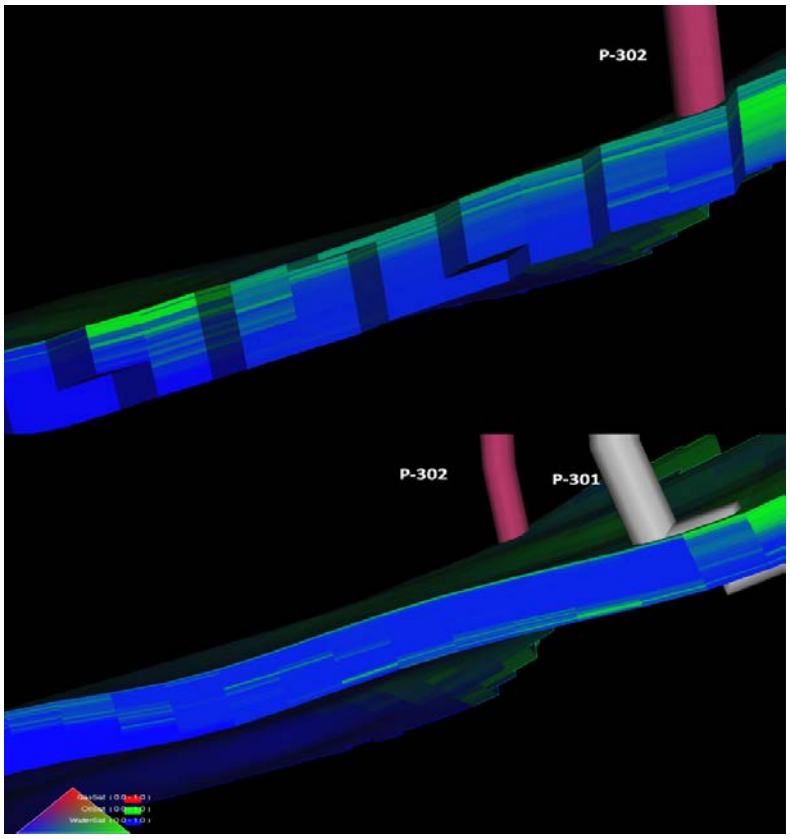

Figure 4 . 7 – Cross-section in the near-well area of P-302 (top) and P-301 (bottom)

The top-view of the reservoir clearly shows the presence of an unswept oil cap after water injection, endorsing a possible recovery increase by WAG processes. This is further noticeable in the near-well cross-sections, where (especially for P-302) a significant number of layers still have a high oil saturation (green).

Total oil produced (FOPT) and recovery factor (RF) after 10 years are:

FOPT [StB]	RF [%]
$25{,}77 \cdot 10^6$	40,76%

As can be seen, the recovery factor is quite high compared to usual values of secondary oil recovery techniques (see Introduction). Nevertheless, the reported observations are sufficient to support the analyses outlined in the following paragraphs, especially if we compare them with recovery factors already reached by analogue fields in the same area.

4.4. WAG Injection Optimization

Once that a Water-Alternating-Gas injection has been demonstrated to be probably effective in increasing the oil production of FIELD α compared to the water-injection-only case, a WAG optimization is required for sake of comparison with the final Foam-Assisted-WAG case. For this purpose a commercial software called MEPO is used.

The software is applied in the following as a reservoir optimization tool and it is applied to study uncertainties in WAG and foam application on the selected reservoir. MEPO is able to automatically modify the starting data file and to launch multiple simulations in parallel, providing powerful analyses and speeding up computational times.

After variables selection, MEPO allows the user to select methods to populate the input parameters and generate simulations through ECLIPSE runs (see Appendix A.1). These methods can be divided into two main categories:

- Experimental Design Methods – typically used to produce a single set of simulations to obtain tips about how input parameters relate to response parameters;
- Optimization Methods – produce multiple sets of simulations in order to achieve an objective by applying a smart process which reduces the number of samples needed and tries to reach the optimized objective functions in a minimum number of simulations.

Due to the characteristics of the selected reservoir and the constraints to both the productions and injections previously described, the chosen procedure to analyze and optimize the injections for the WAG case follows the structure below represented:

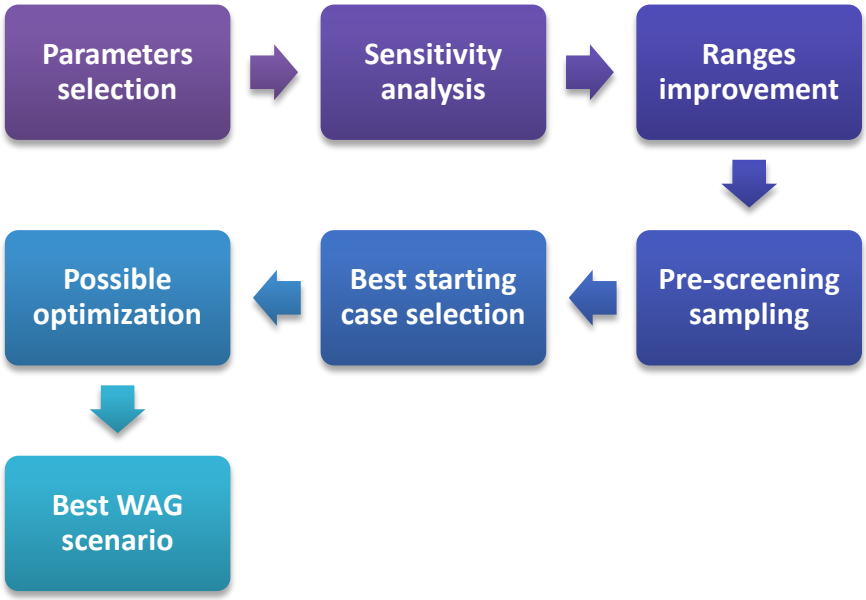

Figure 4 . 8 – Logical scheme applied for the analyses

In the following subsections, an accurate description of the analyses performed to obtain an optimal WAG injection is reported.

4.4.1. Parameters Selection

The main variables to be investigated for the optimization process are the following ones:

- Switch time-step
- Injection-well starting the first gas slug injection after continuous water injection, referring to the fact that gas injection can be started either by I-401 or I-402
- Voidage replacement ratio for water slugs

The term "switch time-step" refers to the time that elapses between two consecutive switches of injected slugs. This variable is taken into account because it is necessary to decide how long each slug (water or gas one) should last. Its values have been considered constant amongst every case because of operational problems in changing it arbitrarily on an ongoing basis for a real process. Thus, injections of 3 to 12 months between two consecutive switches have been studied. The injection of gas coming from other fields for gas disposal purposes represents a strong constraint because the injection rates have to respect the forecasted amounts of gas to be disposed in FIELD α. Table B1 in Appendix B shows all the cases varying from 3 to 12 months-long lasting slugs in both cases of I-401 and I-402 as starting-well with the first gas injection (20 cases overall represented).

All the possible cases are represented because of the difficulties of isolating, in a single script, the time-steps from the gas disposed which varies every year following previously forecasted quantities. This problem is due to the fact that each WAG case has a different number of slugs and, as a consequence, a different number of possible values of voidage replacement ratio, which is described below. Forecasted data of gas to be disposed in FIELD α are shown below (Table 4):

Starting-Date	Consumption Rate [MScf/d]	Import Rate [MScf/d]
04/2016-01/2017	7500	17641
01/2018	7500	15220
01/2019	7500	12974
01/2020	7500	9897
01/2021	7500	7503
01/2022	7500	6200
01/2023	7500	5151
01/2024	7500	4405

Table 4 – Forecasted data of gas to be disposed

As can be noticed, the constant value of consumption rate is due to the fact that a large amount of gas is consumed to assure all the operations on the FPSO. The water injection lasts for at least 1,5 years before the WAG process starts. In fact it is not convenient to start with the gas injection before 04/2016 because of premature loss of oil plateau due to premature gas production. Thus, also the effect of extending the water injection plateau is

examined amongst all the cases by considering 1,2 years of consecutive water injection with both the injectors and adding 3 to 12 months of further water injection after which the first gas slug is injected, taking into account the gas from other wells. This is the reason why in the table above the starting date of the first gas slug varies from 04/2016 to 01/2017, depending on which case is considered. Moreover, in order to outline a consistent comparison among the cases, the time length of each slug is not really constant for a same case because the gas coming from other fields is reported every year and the final slug is broken off to allow a possible continuation of the EOR process since the economic threshold is expected to be not reached yet after 10 years.

Also the amount of water injected has to be examined to best fulfill a thorough WAG optimization. As the water is usually injected also to support the pressure of the reservoir in addition to a displacement scope, the best way to vary the amount of water injected and find its optimal value for each water slug is by varying the values of voidage replacement ratio (VRR), that is the ratio of reservoir barrels of injected water to reservoir barrels of fluid produced. The VRR values examined are:

$$VRR_1 = 0{,}7 \qquad VRR_2 = 1 \qquad VRR_3 = 1{,}3$$

These values make physical sense as a VRR value lower than 0,7 would lead to a too high pressure drop which could result in much lower oil recoveries On the other hand, a VRR value higher than 1,3 would cause a too high water cut (ratio of water produced compared to the volume of total liquids produced) leading to a premature production wells shut-off.

4.4.2. Sensitivity analysis

The influence of each of the chosen parameters and, as a consequence, whether it is reasonable to optimize them, is evaluated by launching pre-screening runs. It is required to evaluate the total number of previously described cases. Thus, a “Full Factorial” experimental design has been selected to include all the possible parameters combinations:

$$3\ VRR\ values \cdot 10\ timesteps \cdot 2\ WAG\ starting\ wells = 60\ cases = 60\ simulations$$

The resulting values from simulations are shown in the following exhibit:

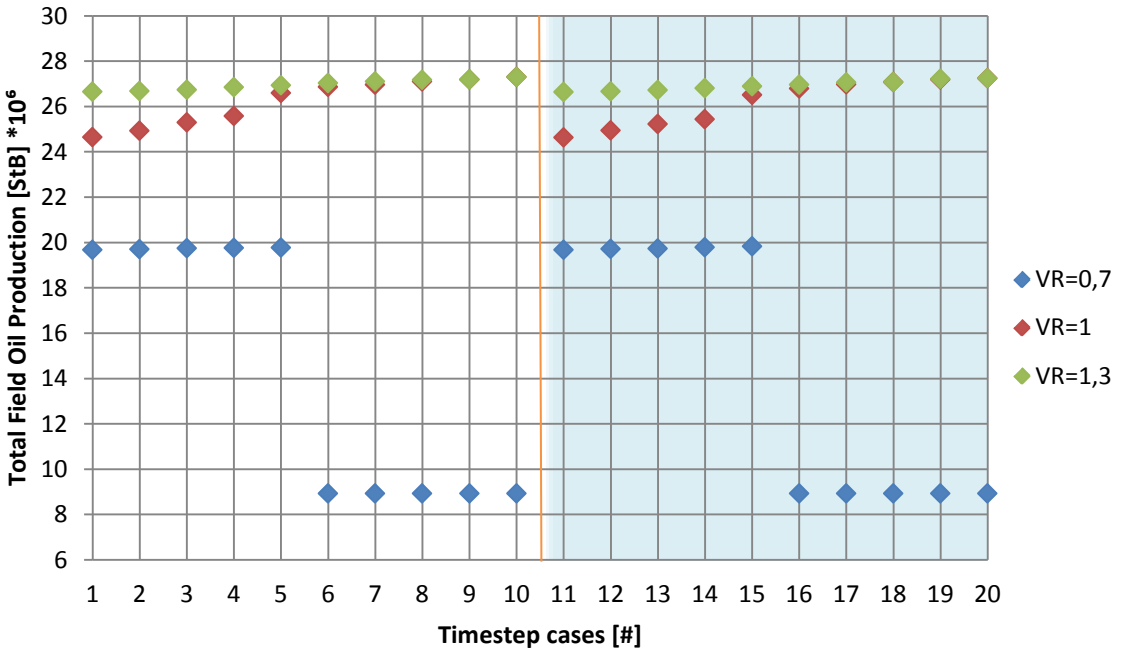

Figure 4 . 9 – Plot showing the 60 possible cases in terms of Field Oil Produced vs. Timestep Cases

The grid is divided into two areas including 30 cases each: the white left-hand one refers to the case of injector I-402 starting with the first gas slug injected, whereas the pale-blue right-hand one refers to the case of the first gas slug injected by I-401.

4.4.3. Range improvement

The plot represented on the previous page, in addition to the data reported in Table B2 (Appendix B), allows to outline some noticeable observations.

It is evident that a VRR = 0,7 leads to much lower values of total recovered oil. As a matter of fact, in case of slug time-lengths of 8 to 12 months (cases #6÷10 and #16÷20), both the producers P-302 and P-301 are prematurely shut off. For example, as shown in Fig. 4.9, for the case with VRR = 0,7 and slug time-length = 9 months (for other cases with VRR = 0,7 the profiles are exactly the same), both production wells reach the tubing head pressure constraint of THP = 1450 psi and, once that the THP is set to this constant value, the BHPs go on decreasing until they reach values which are not sufficient to maintain oil production. At the same time, the water production increases making the fluid column to be brought to surface heavier. In the end, the pressure drops along the tubing and the gravity are not balanced out by the difference between THP and BHP anymore (see *Fig. 4.10* and Table 5).

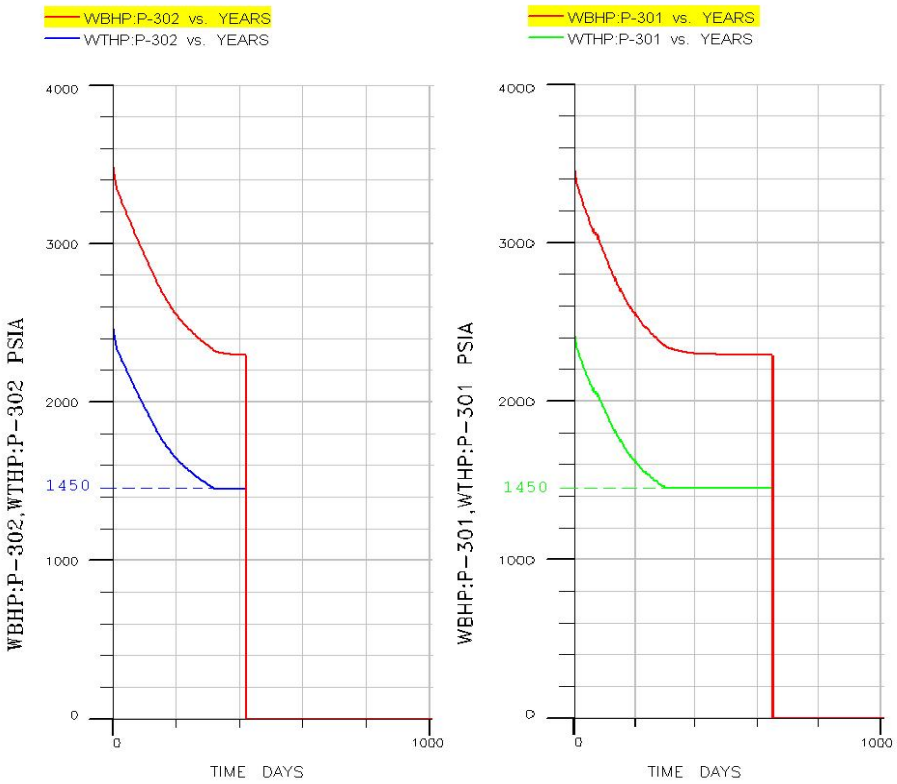

Figure 4 . 10 – BHP and THP profiles of P-301 and P-302

P-302			P-301		
TIME [d]	THP [psia]	BHP [psia]	TIME [d]	THP [psia]	BHP [psia]
300,79	1480,25	2356,62	279,81	1480,41	2380,74
324,18	1450	2319,55	304,79	1450	2339,83
369,75	1450	2300,19	470,68	1450	2294,24
389,73	1450	2296,51	535,63	1450	2292,07
419,71	1450	2295,96	645,56	1450	2291,89
422,71	0	0	650,55	0	0

Table 5 – BHP and THP data of P-301 and P-302

For instance, the vertical lift performance (VLP) and inflow performance relationship (IPR) curves can be plotted for the producer P-302 in order to highlight the loss of operating point at time 420 days, that is the time at which the producer is shut (the same observations can be made for P-301 as well). So, data are selected for day 300,79 and day 419,71 in order to compare the profiles before and in close proximity to the loss of the operating point.

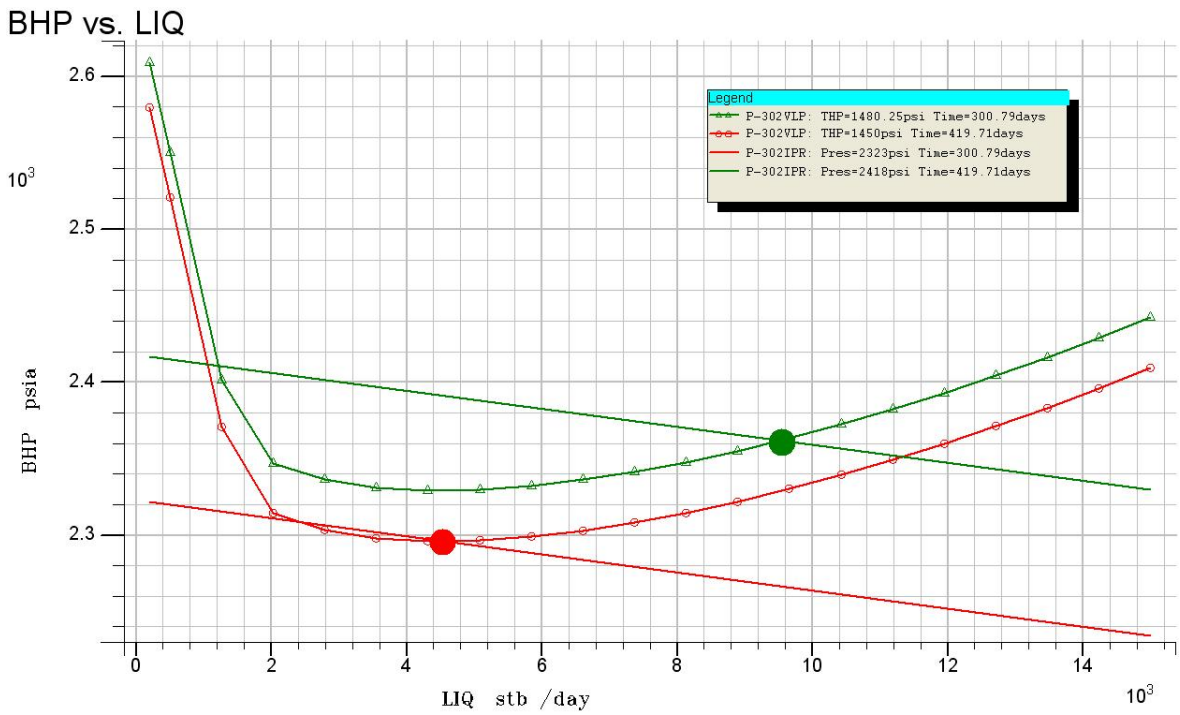

Figure 4 . 11 – Illustration of VLP and IPR for P-301

The green profiles represent the operating situation at time 300,79 days, whereas the red profiles represent time 419,71 days. It is noticeable that, as the shut-time gets closer, the operating point tends toward a tangential intersection between VLP and IPR curves.

The VLP curve is based on the mechanical energy equation for flow between two points in a system:

$$\frac{p_1}{\rho} + gz_1 + \alpha\frac{v_1^2}{2} = \frac{p_2}{\rho} + gz_2 + \alpha\frac{v_2^2}{2} + W + E_l \qquad (4.5)$$

where p is the pressure; ρ is the fluid density; g is the gravitational acceleration; z is the elevation; α is the dimensionless kinetic energy correction factor; v is the velocity; W is the work done by the flowing fluid per unit mass; E_l is the irreversible energy loss per unit mass including viscous and friction losses. For most practical application, there is no work done by or on the fluid and the kinetic energy correction factor is usually assumed to be one. Considering the top and the bottom of the tubing, it is possible to make the BHP expression explicit and to obtain the profile represented in *Fig. 4.11*.

On the other hand, the IPR curve is approximated by a straight line having as y-intercept the instantaneous reservoir pressure ($\bar{p}_R$) and as slope the well productivity index (*WPI*). Thus, the IPR linear expression is given by:

$$BHP = \bar{p}_R - \frac{q_{LIQ}}{WPI} \qquad (4.6)$$

where $\bar{p}_R$ is the static average pressure around the wellbore [48], q_{LIQ} is the total liquid flow rate and *BHP* is the flowing bottom hole pressure. The last equation is derived from Darcy's law for the steady-state radial flow of a single incompressible fluid. The same situation is found for P-301 and for all the other cases with VRR=0,7, so further representations are omitted. Instead, for the cases with slug time-lengths of 3 to 7 months, the producer P-302 is not shut, because of less water amount in the wellbore column, and goes on producing for the entire 10-years period. Anyway, the total amount of oil produced in these cases is much lower than the amount produced for VRR>0,7 (*Fig. 4.9*).

As a consequence, just cases of VRR values equal or higher than 1,0 are taken into account for the following analyses. It is worthwhile to sort all the remaining cases by ascending values of time-step case and matching, at the same time, slug time-length and VRR for the two scenarios of either I-401 or I-402 starting with the first gas slug (see Table B3 in the Appendix). Even if the difference after outlining this comparison is weak, it is visible that in almost all cases, starting the first gas slug injection with I-402 implies a better recovery. Furthermore, the few cases which are not consistent with this observation are weakly negative ($\Delta_{I402\text{-}I401}$) and their trend is rapidly inverted when increasing the VRR values from 1 to 1,3. This allows to neglect the right hand side of *Fig. 4.9*, focusing the analyses on the left-hand side cases only.

As can be noticed from both Table B3 and *Fig. 4.9*, the total oil production (FOPT) increases going from 3 to 12 months of slug-duration for a same value of VRR and the difference in FOPT values between VRR=1,3 and VRR=1 cases ($\Delta_{VRR:1,3\text{-}1}$) decreases following the same trend. It is reasonable to imagine the best case to be the one corresponding to a slug-time of 12 months. But, due to the decreasing values of $\Delta_{VRR:1,3\text{-}1}$, it is possible to have a resulting leverage effect from changing the VRR values for each slug. So, the next step is to evaluate the effect of changing VRRs for each slug in every slug-duration case and to verify whether a wider range in FOPT when varying VRRs can lead to a higher final recovery for the optimized case.

4.4.4. Pre-screening sampling

So far, the number and the ranges of variables have been reduced. As previously stated, the main problem is the number of slugs which is obviously not constant during the time of 10 years. As a consequence, ten different analyses should be carried out to verify which combination of VRRs is the one guaranteeing the higher total oil production. But, before proceeding with any optimization methods, it is worthwhile to smartly sample a limited number of possible cases to simulate, in order to have a sampled "best-case" to start with for optimization, saving much time during this last process. It is possible to start with the case of 12 months-lasting slugs with 8 VRR-dependent slugs. Actually, as can be noticed from Table B1, 9 slugs are injected inside the reservoir taking into account also the first water injection. But, as the oil production reaches its limiting value during the first period, only 8 slugs starting from the first gas injection are considered. Moreover, the distribution

of VRRs is considered to be discrete and uniform varying from 1 to 1,3 with a finite step of 0,1 because of the operational impossibility to inject voidage replacing slugs with higher precision. Thus, the following illustrations show the discrete density and the cumulative distribution functions:

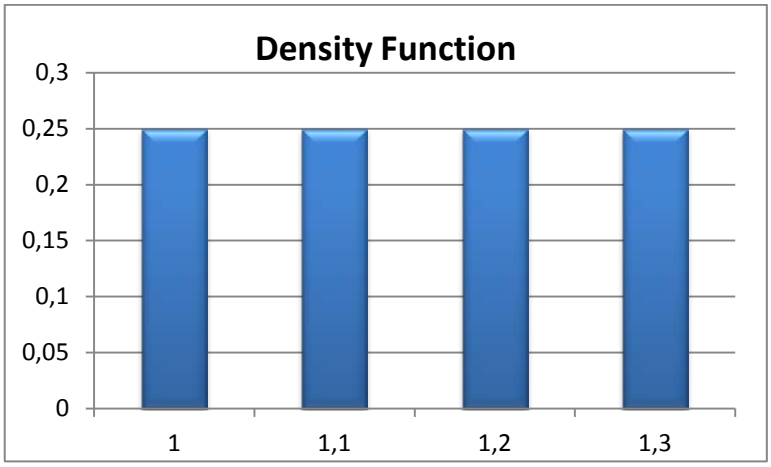

Figure 4 . 12 – VRR Discrete density function

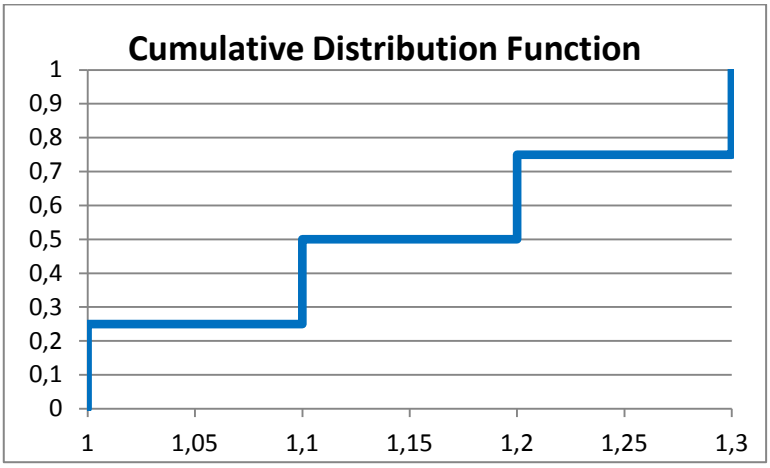

Figure 4 . 13 – VRR Cumulative distribution function

Where the cumulative distribution function of a real-valued discrete random variable X is defined as:

$$F_X(x) = P(X \leq x) \tag{4.7}$$

The right-hand side of the Eq. 4.7 represents the probability that the random variable X takes on a value less than or equal to x.

All the cases resulting from the combination of VRRs and number of slugs injected are almost impossible to be simulated in a reasonable time. In fact, a full-factorial design would require:

$$(4\ posssible\ VRR\ values)^{8\ slugs} = 65536\ simulations$$

An efficient and "cheap" extensive exploration of the model space can be achieved by random sampling of the density function. Among the many different methods of selecting the values of input variables, the "**Latin Hypercube Sampling**" (LHS) has been chosen due to its considerable intuitive appeal. For any selections of K input variables (VRRs) $\boldsymbol{X} = (X_1, \dots, X_j, \dots, X_K)$, where $K = 8$ in this case, an output variable $Y = f(\boldsymbol{X})$ is produced, representing the total oil produced after 10 years. LHS ensures that each input variable X_j has all portions of its distribution represented by input values. So, the range of each X_j is divided into N strata of equal probability $1/N$ and the sampling process occurs randomly once from each stratum [49]. The number of strata is selected by the user and its value coincides with the total number of runs selected. In this case a value of 150 runs has been used. As the distribution of VRRs is discrete, the codomain of the CDF is divided into 150 sections and each randomly sampled value will be rounded off to the closest VRR possible value.

The N values thus obtained for X_1 are paired at random without replacement with the N values randomly obtained for X_2. These N pairs are then combined in a random manner without replacement with the N values of X_3 as well to form N triples. This process is continued until a set of N K-tuples is formed [50], where K is 8 for the case considered. A scatterplot is not shown here as it would not be fully illustrative since 8 dimensions should be considered. Even a 3-D scatterplot would not have enough values to outline the efficiency of the LHS method, because of the discrete nature of the variable distributions. But, it is possible to show a graphical representation (*Fig. 4.14*) of LHS considering just two variables (VRR_1 and VRR_2):

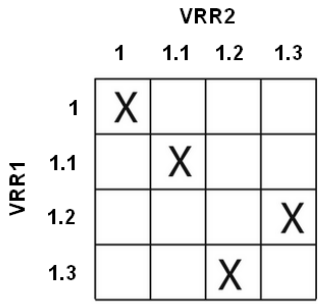

Figure 4 . 14 – 2-variables example of LHS

In literature, almost no recommendations or estimates for the sampling size of LHS were proposed. Anyway, based on the examples analyzed by Matala [51] for cases with up to 10 variables, it is possible to assume that reliable results can be obtained by a number of samples conform to, at least, the following ratio:

$$\frac{N}{K} = 10 \div 15 \tag{4.8}$$

In this case, a total number of $N = 150$ simulations has been selected and, considering the number of variables equal to $K = 8$, the selected ratio becomes $\frac{N}{K} = 18.75$, well above the

suggested reliability-related threshold. The following image shows the distribution of the output values obtained.

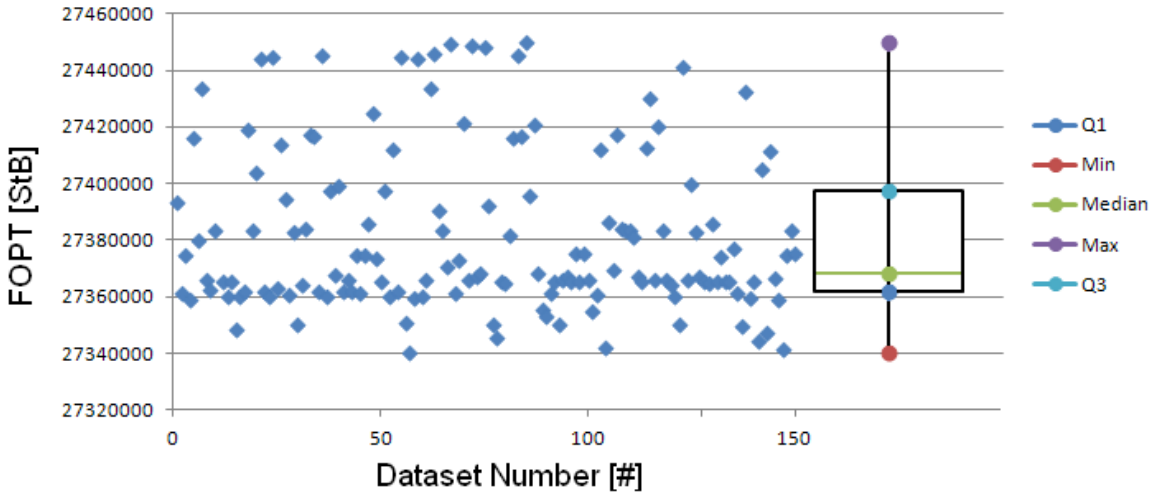

Figure 4 . 15 – Scatter-plot and Box-plot showing the distribution of FOPT amongst the simulations

4.4.5. Best starting case selection

As can be noticed from the plots, the range of variation for the total oil produced is very small and the maximum value is just 0,3% higher than the median. It is also worthwhile to look at the correlations between the input parameters and the response parameter (FOPT). Thus, the Pearson's correlation coefficient r_j is used as measure of the linear correlation between the input variables X_j and the output Y. When applied to a population, the Pearson's coefficient is represented by:

$$\rho_{X,Y} = \frac{cov(X,Y)}{\sigma_X \sigma_Y} \tag{4.9}$$

where cov is the covariance, σ_X is the standard deviation of X and σ_Y is the standard deviation of Y. When the coefficient is instead applied to a sample, the formula becomes the following one by substituting estimates of the covariances and variances:

$$r_j = \frac{\sum_{i=1}^{N}(X_{j,i} - \bar{X}_j)(Y_i - \bar{Y})}{\sqrt{\sum_{i=1}^{N}(X_{j,i} - \bar{X}_j)^2}\sqrt{\sum_{i=1}^{N}(Y_i - \bar{Y})^2}} \tag{4.10}$$

Where $\bar{X}_j = \frac{1}{N}\sum_{i=1}^{N} X_i$ is the sample mean of the j-th input variable (same for the output variable Y). The following table shows the Pearson's coefficients for all the VRRs, each of which is compared to the FOPT values:

	FOPT
VRR1	-0,852
VRR2	-0,300
VRR3	0,082
VRR4	0,049
VRR5	0,212
VRR6	-0,038
VRR7	-0,099
VRR8	0,124

Table 6 – Pearson's coefficients

The VRR values are sorted following the injection timeline, i.e. VRR1 and VRR8 correspond to the first and the last injection slugs after the water injection-only period respectively. The results show a weak correlation for all the VRRs ($|r_j| < 0{,}3$) but VRR1, which shows a strong inverse correlation, i.e. a low value of the VRR (=1,0) for the first slug leads to a higher FOPT, following a trend similar to a straight line (*Fig. 4.16*).

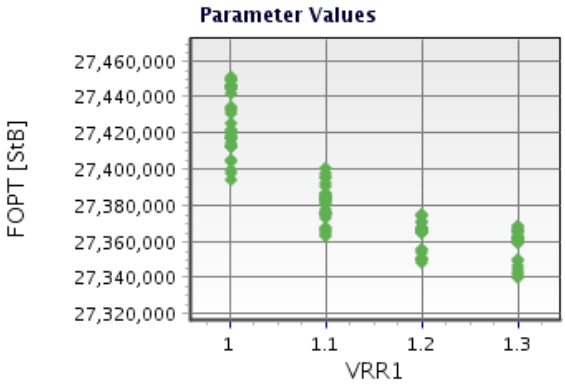

Figure 4 . 16 – FOPT vs. first VRR value

These observations support the needlessness of an accurate and slow method to improve the WAG optimization, since the expected optimal FOPT value will be very close to the maximum value found with the LHS and the values of voidage replacement ratio for each slug will not follow a real "rule". But, in order to have a more accurate evaluation of the effect of changing the VRR values, the "historical" effect should be taken into account. Thus, *Fig. 4.17* illustrates the simultaneous plot of all the FOPT values at every time step. It is evident how the final FOPT value is almost the same for all the simulations, while the history of the simulations shows a certain difference in oil recovery amongst the different cases between the 3rd and the 7th year. Obviously, the FOPTs during the first 3 years match perfectly because only water is injected for all the cases.

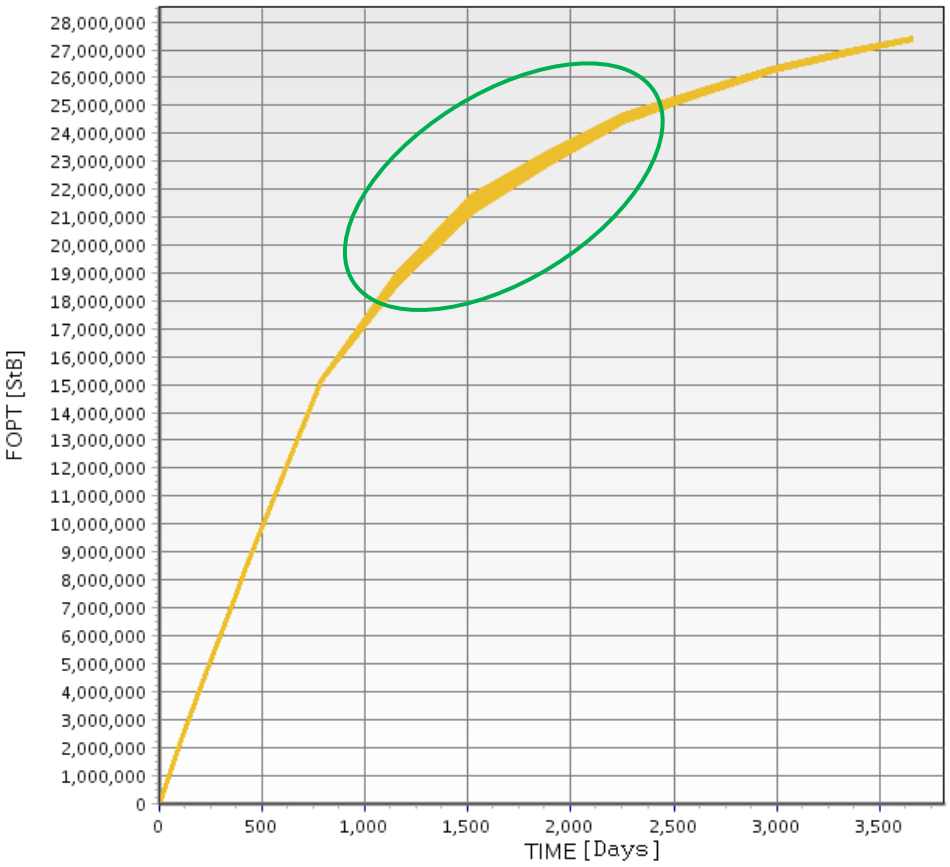

Figure 4 . 17 – Simultaneous plot of FOPT vs. Time for all the 150 simulations

Before drawing any conclusions, it is necessary to verify whether positive leverage effect will be observed in cases with shorter slugs and higher variation of FOPT. For this purpose, case #6 (8 months slug time-step; see Table B1) has been selected, as cases #1 to #5 experience a producer shut-off before 10 years with VRR=1. As the total number of slugs and, as a result, the number of input variables (VRRs) are very high, reasonable simplifications can reduce considerably the simulation-time requested. Table B2 in Appendix B represents the best 10 simulations obtained from case #10 (12 months slug time-step). As can be seen, all of them have the first and the second VRR set to 1, in agreement with the correlation coefficients shown in Table 6. So, for case #6, the VRR is set equal to 1 until year 2018, corresponding to INJ7. In this way, the simulations are run with 10 input variables. Following the same line of reasoning described above with Eq. 4.8, a total number of $N = 250$ simulations is chosen, taking into account the non-linear increase of complexity with an increasing number of variables. The resulting cloud of final values is shown in *Fig. 4.18* together with a comparison of both the box-plots of cases #6 and #10 (cyan area).

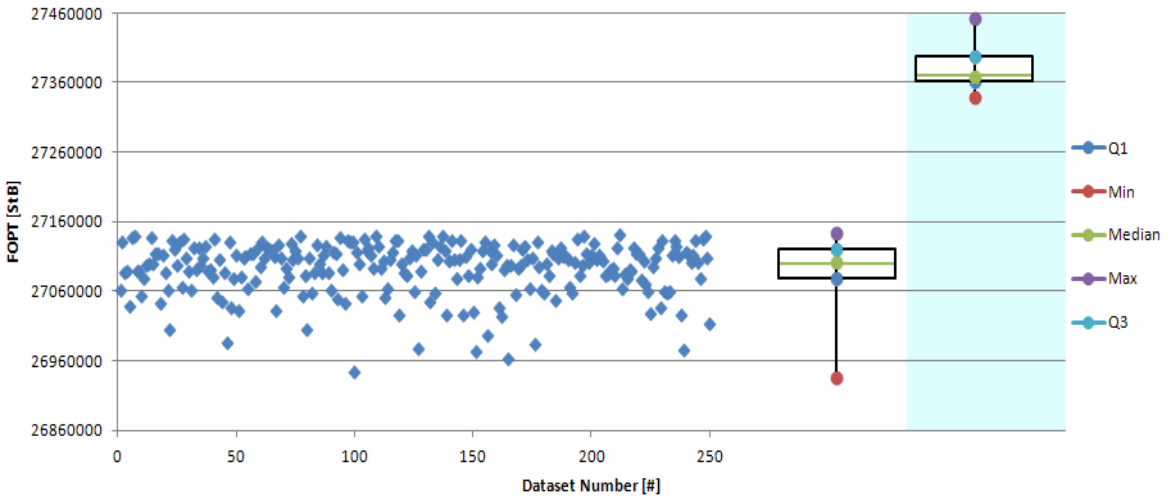

Figure 4 . 18 - Scatter-plot and Box-plots (cases #6 and #10 [cyan]) of FOPT amongst the simulations

It is evident that the FOPT values reachable by case #6 are lower than the ones of case #10, even if the range of variation is higher, as previously revealed. Thus, it would be worthless to proceed with further analyses. Moreover, assuming that this observation will be followed by the intermediate cases as well, it is possible to evaluate only case #10 to obtain the best WAG scenario without unnecessary optimization methods.

4.4.6. Best WAG scenario

The decision of not going through a proper optimization method to find the best WAG scenario is explained in this subsection. The best case among the simulated LHS runs is the one with the characteristics represented in the following table (blue row):

FOPT [StB]	VRR1	VRR2	VRR3	VRR4	VRR5	VRR6	VRR7	VRR8	RF [%]
27.449.968	1,00	1,00	1,30	1,20	1,30	1,20	1,00	1,10	43,41
27.297.784	1,00	1,00	1,00	1,00	1,00	1,00	1,00	1,00	43,17

Table 7 – Best case 12-months long-lasting slugs scenario characteristics

It is interesting to compare its FOPT vs. time profile with the one of the case with a VRR=1 for the whole 10-years period (white row), which has been simulated during the sensitivity analysis. *Fig. 4.19* shows this comparison. While the difference between the FOPTs at the end of the 10 years period is small, in the range 3-7 years this difference is quite evident and was already introduced in *Fig. 4.17*. From a technical point of view, the best case is the one obtained with the LH sampling of course. But, the increase of the total recovery factor is very small, i.e. just 0,2% higher. Moreover, from the operator point of view, the VRR=1 scenario is more attractive, as it is most important to maximize the Net Present Value (NPV) over the short term period.

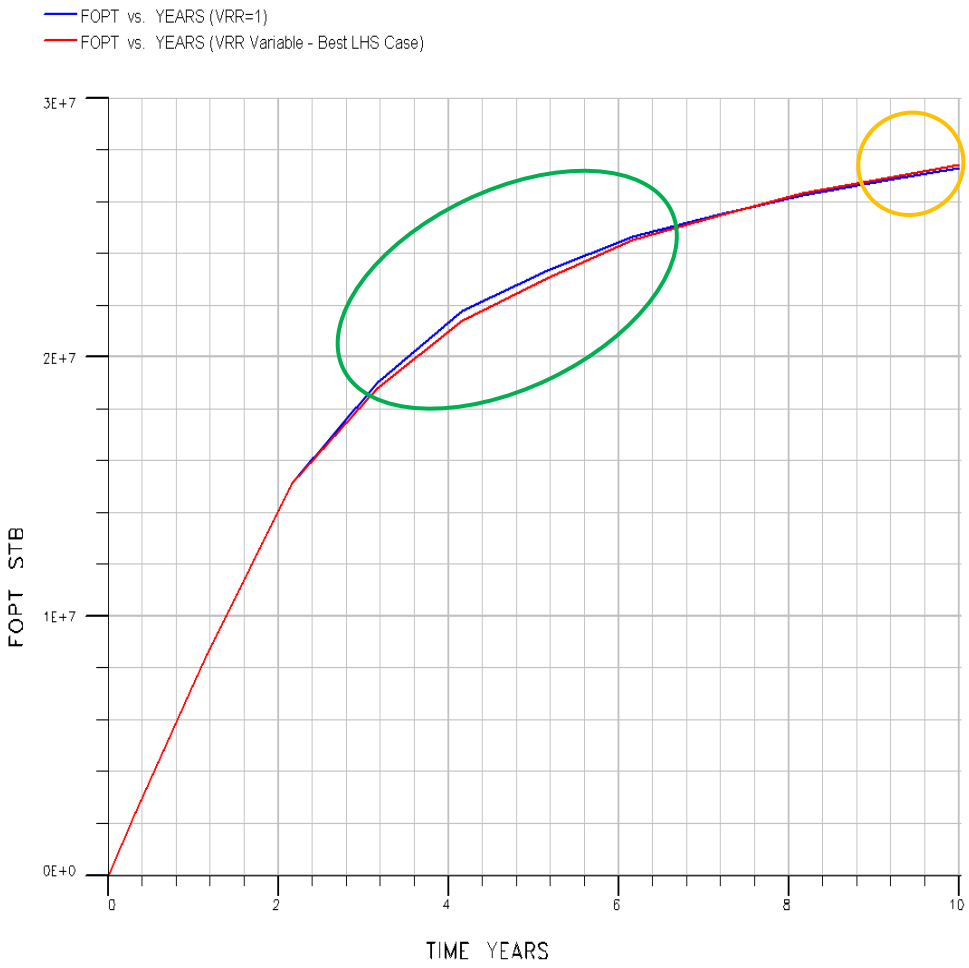

Figure 4 . 19 – Comparison of FOPT trend for the two cases VRR=1 and VRR variable

Thus, it is possible to compute its value through a simplified formula [52], neglecting the gas injection/production costs (due to disposal purposes) and other OPEX or CAPEX which are assumed the same for the two cases:

$$NPV = \sum_{n=1}^{N_L} \left[\sum_{i=1}^{N_p} \left(r_o^n q_{o,i}^n - r_w^n q_{w,i}^n \right) - \sum_{j=1}^{N_{wi}} r_{wi}^n q_{wi,j}^n \right] \frac{\Delta t^n}{(1+b)^{t^n/365}} \qquad (4.11)$$

Where:

N_L is the total number of simulation time steps;
N_p is the total number of producers;
N_{wi} is the total number of water injection wells;
the superscript n denotes the n-th simulation step;
r_o is the oil revenue ($/StB);
r_w is the water production cost ($/StB);
r_{wi} is the water injection cost ($/StB);
$q_{o,i}^n$ is the average oil production rate over the n-th time step of the i-th producer (StB/day);

$q_{w,i}^n$ is the water production rate over the n-th time step of the i-th producer (StB/day);
$q_{wi,j}^n$ is the water injection rate over the n-th time step of the j-th water injector (StB/day);
b is the weighted average cost of capital;
t^n is the cumulative time up to the n-th simulator time step (days);
Δt^n is the length of the n-th simulator time step (days).

The production and injection rates are easily obtained by simulations at the several time-steps and are reported in Appendix B (Table B 3) together with the calculations. On the other hand, the oil revenue is calculated by the following common and simplified linear formula [53] taking the Brent crude oil trends as reference:

$$r_o = r_{o,base} + A \cdot (°API) - B \cdot (\%S) \tag{4.12}$$

where $r_{o,base}$ is the base price for 0°API oil; A is the scale factor for API gravity (°API); B is the markdown factor for presence of Sulfur (%S). By applying Eq. 4.12 to both the reference Brent and FIELD α oil prices and by assuming the three factors ($r_{o,base}, A, B$) as the same for the two oils, it is possible to express the FIELD α oil price as follows:

$$r_{o,FIELD\alpha} = r_{o,Brent} + A \cdot (°API_{Brent} - °API_{FIELD\alpha}) - B \cdot (\%S_{Brent} - \%S_{FIELD\alpha}) \tag{4.13}$$

The factors A and B are assumed to be the ones reported in Table 8 below and suggested by Seba [54]. The values for the fixed data necessary to calculations are reported in the following table:

Parameters	Values
N_L	13
N_p	2
N_{wi}	1-2
b [%]	7,8
A	0,19
B	0,77
$°API_{Brent}$	38,1
$°API_{FIELD\alpha}$	32,9
$\%S_{Brent}$ [%]	0,37
$\%S_{FIELD\alpha}$ [%]	0
r_w [$/StB]	1,59
r_{wi} [$/StB]	0,3

Table 8 – Parameters used for calculations

r_w and r_{wi} are considered constant and equal for both injectors and producers because no significant differences can be noticed. As shown in Table B4, the final NPV values endorse the case with VRR=1 as the best one. Moreover, the trends of Table B4 which are represented in *Fig. 4.20* show that the $NPV_{VRR=1}$ is higher at each time step and that the

present value of the optimal LHS case of the last year is negative, underlining even more the convenience of pursuing the scenario with a constant VRR=1.

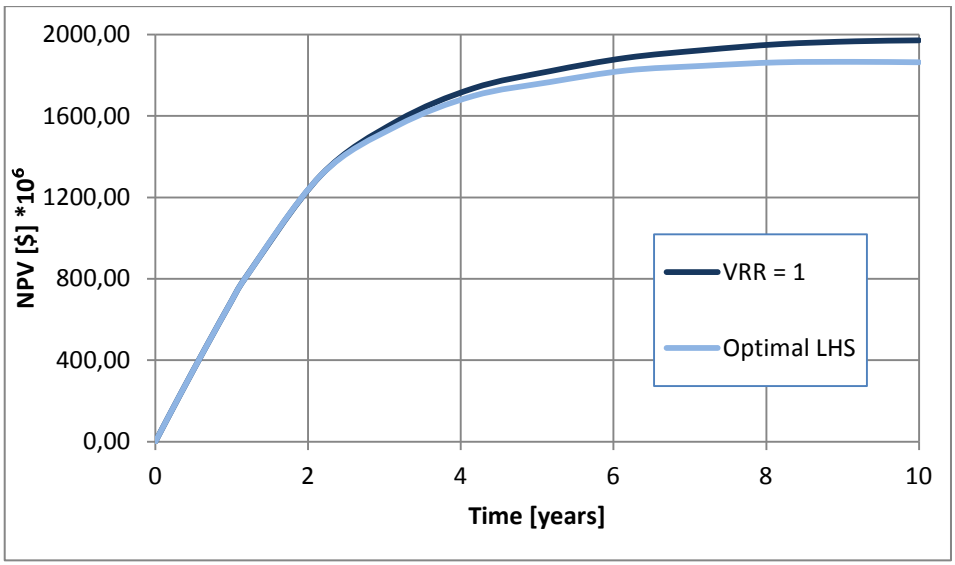

Figure 4 . 20 – NPV trends for both VRR=1 and Optimal LHS cases

Other scenarios with VRR>1 are not taken into account as the increased value of oil recovery obtainable is negligible (see Table B4) compared to the increased amount of water injected and produced. Other cases with even better NPVs are not taken into account, as the range is quite small and further unnecessary complications, such as using a variable VRR even if the effect is negligible, should be avoided for future perspectives of dealing with many variables while analyzing foam injection.

It is interesting also to briefly compare the selected case with the values coming from the water-injection-only case.

FOPT [StB]	FGPT [Sft^3]	RF [%]
25.775.480	15.851.310	40,76
27.297.784	84.113.576	43,17

Table 9 – Comparison between the results of the WI-only and best-WAG cases

As can be seen, an increase in the recovery factor of +2,41% is obtained, supporting the benefits of the WAG injection. But it is also interesting the huge difference between the values of total gas produced, which are due to the amount of gas injected inside the reservoir.

4.5. Issues characterization

So far, a WAG best scenario has been selected, but a few observations should be drawn to endorse the application of foam in FIELD α before proceeding with the analyses. Firstly, it should be highlighted that this is a reservoir used also for gas disposal purposes and, as a consequence, the considerations for application of foam reported in Chapter 3 have to be weighed with the fact that the produced-gas reduction is almost as important as the sweep efficiency increase. Secondly, a deeper look at the field production profiles can give a good overview of what is happening during the WAG process.

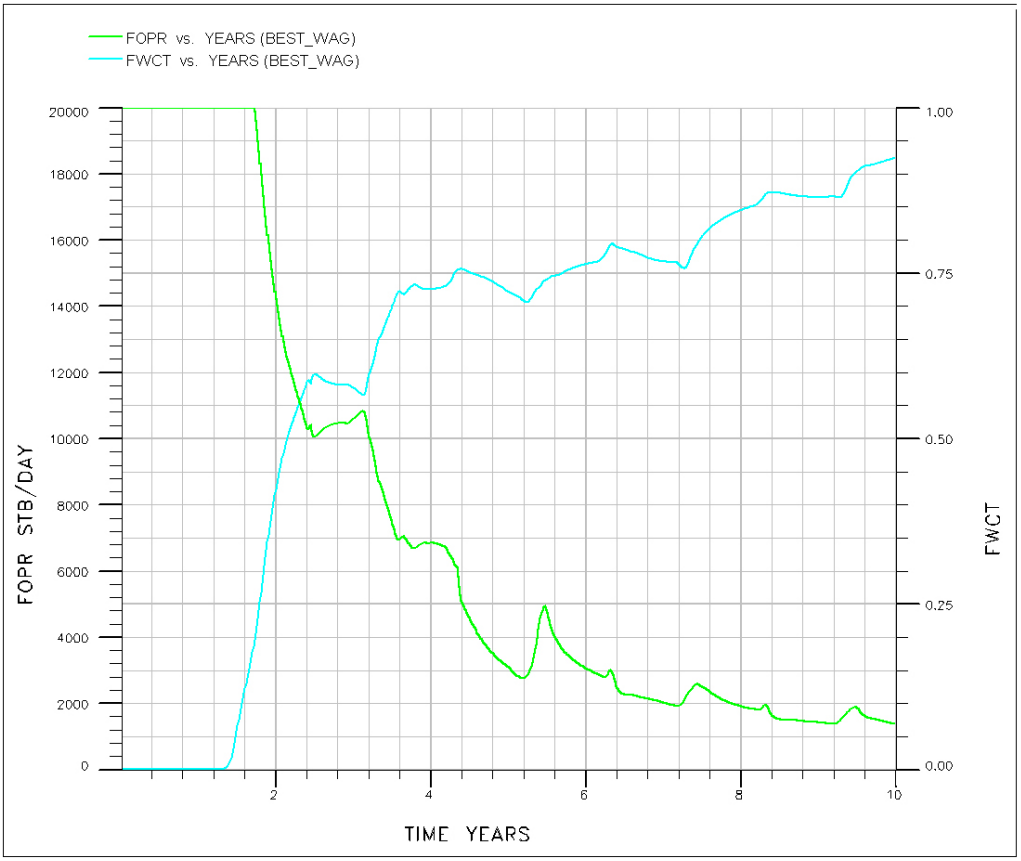

Figure 4 . 21 – Field oil production rate and water cut profiles

Fig. 4.21 plots the field water cut (FWCT) and oil production rate (FOPR). It is evident that once the plateau is lost, the steep decrease in oil production is due to water production, as the water injected increases the aquifer level which reaches the production wells at time 2 years more or less. Then, when the gas injection starts, the steep drop stops and the oil production profile settles on a more constant value. Anyway, until year 4 the water cut represents the specular negative profile of oil production rates. Thus, the decrease will probably not be solvable by a possible foam application before that date.

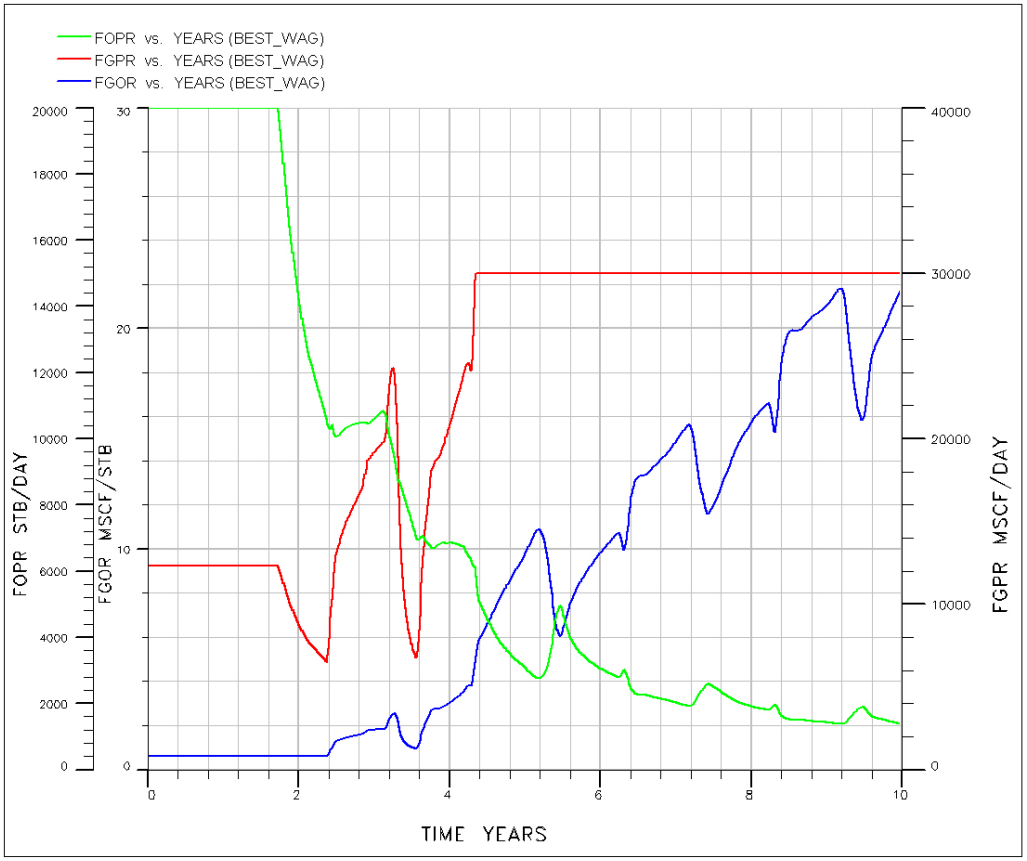

Figure 4 . 22 – Field oil and gas production rates and GOR profiles

In fact, as noticeable also from *Fig. 4.22*, the GOR profile is stable at values corresponding to the dissolved gas until that same date and then it follows a specular profile compared to the FOPR. This is due to both producers reaching the limiting gas production rate ($30 \cdot 10^6$ Sft^3 as overall value) and, as a consequence, the GOR becoming dependent only on the FOPR.

So far, the presence of a "gas-issue" is evident, but it is necessary to localize the problem in terms of reservoir graphic interface. For this purpose, three meaningful cross-sections showing the fluid saturations of FIELD α are represented. Dates have been chosen after time 4 years to be coherent with what said above.

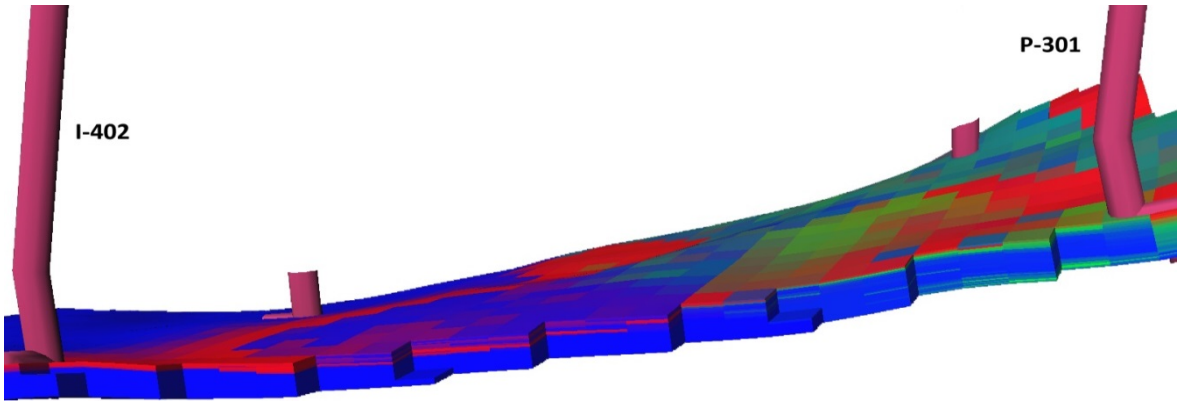

Figure 4 . 23 – P-301/I-402 cross section at 01/01/2020 (saturations of gas (red), oil (green) and water (blue))

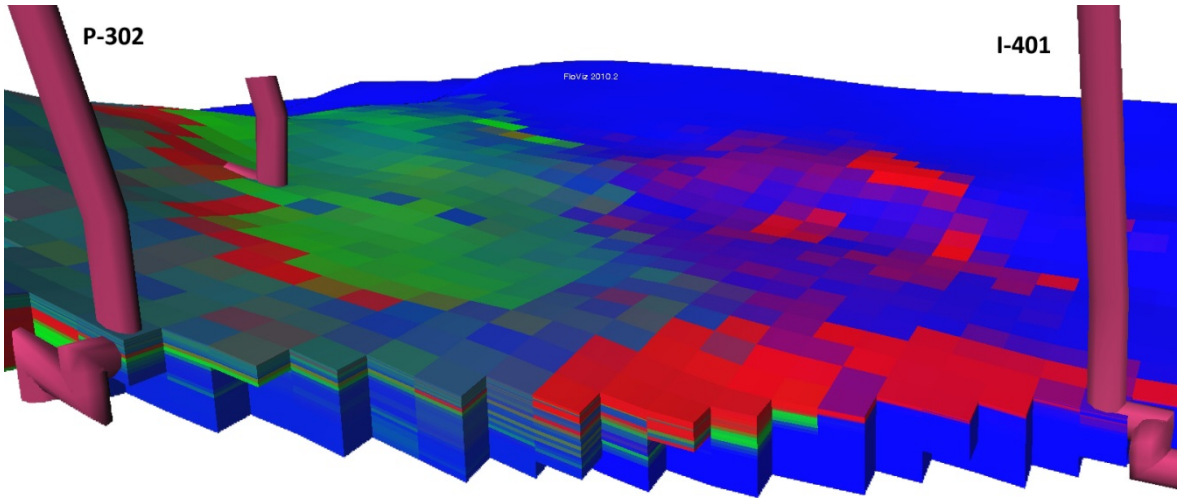

Figure 4 . 24 – P-302/I-401 cross section at 01/01/2021 (saturations of gas (red), oil (green) and water (blue))

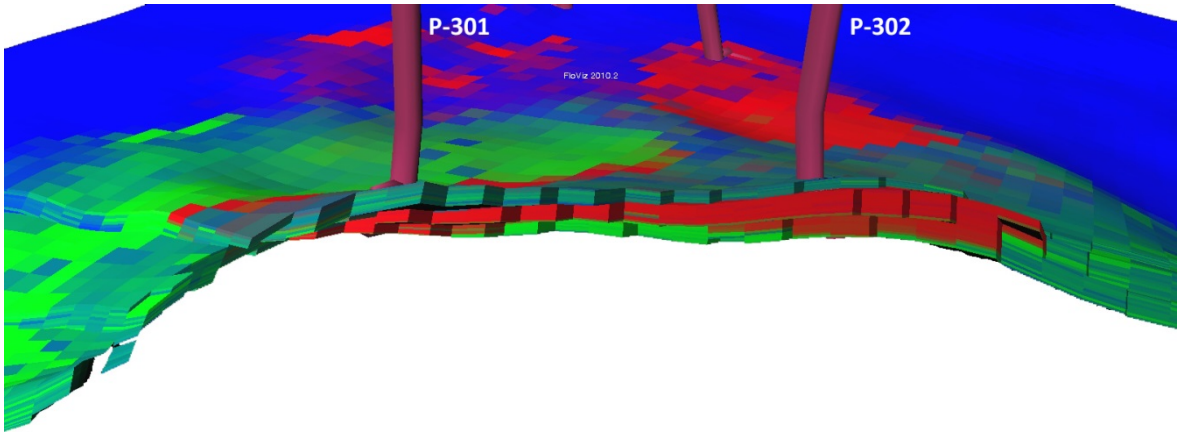

Figure 4 . 25 – P-301/P-302 cross section at 01/01/2021 (saturations of gas (red), oil (green) and water (blue))

Fig. 4.23 shows a cross the layers between the producer P-301 and the injector I-402 at the end of the 1-year-long gas slug injected by I-402. It is noticeable that the gas (red) flows directly to P-301 following a gravity-override-pattern, as it flows above water (blue) and above oil (green) in the near-producer area. This fact is not really evident when dealing with the other producer and injector (P-302 and I-401 in *Fig. 4.24*), as they are not really directly connected with good facies as previously shown in *Fig. 4.3*. In fact, just gasified top-layers near well I-401 are visible, while it seems that P-302 is not experiencing gas-related issues. But, the third figure (*Fig. 4.25*) illustrates that a highly gas saturated area is present between the two producers and over the oil saturated layers, reflecting what said about the good-facies-characterized channel connecting producers and injectors. Thus, both the producers are experiencing gas-breakthrough due to gravity over-ride problems, as foreseen. This is sufficient to allow a deeper study concerning a possible foam application.

5. Foam Assisted WAG Optimization

5.1. Foam model

The physics of the foam flooding process is very complex. The ECLIPSE Foam Model does not attempt to model the details of foam generation and collapse. Foam is modeled as tracer which may be transported with either the gas or the water phase with account taken of adsorption on to the rock surface and decay over time.
Although foam is essentially a mixture of gas, water and surfactant, ECLIPSE models it as an effective concentration of surfactant transported in either the gas or the water phase. Hence, the foam concentration can be thought of as the surfactant concentration existing in foam form. Since the functional gas mobility reduction model (which will be introduced in the following pages) is only available if the transport phase is defined to be water, the distribution of the injected foam for each cell is solved by the following conservation equation [44]:

$$\frac{d}{dt}\left(\frac{VS_wC_f}{B_w}\right)+\frac{d}{dt}\left(V\rho_rC_f^{ads}\frac{1-\phi}{\phi}\right)= \\ =\sum_{i=1}^{n}\left[\frac{Tk_{rw}}{B_w\mu_w}(\delta P_w-\rho_w g D_z)\right]_i C_f+Q_wC_f-\lambda(S_w,S_o)VC_f \tag{5.1}$$

where
C_f denotes the foam concentration;
ρ_w denotes the water density;
n denotes the number of neighboring cells;
C_f^{ads} denotes the adsorbed foam concentration;
μ_w denotes the water viscosity;
D_z is the cell center depth;
B_w is the water formation volume factor;
T is the transmissibility;
k_{rw} is the water relative permeability;
S_w is the water saturation;
V is the block pore volume;
Q_w is the water production rate;
P_w is the water pressure;
λ is the rate decay parameter function of oil and water saturation;
g is the gravity acceleration.

The foam concentrations are solved in each Newton iteration and used to update the flow properties for the subsequent iterations. The adsorption of foam is assumed to be instantaneous and its isotherm is specified as a look-up table of adsorbed foam as a function of the flowing foam concentration, thus just a single variable is identified since the simulator interpolates linearly between 0, corresponding to a null value of local foam concentration in the solution surrounding the rock, and the variable value (C^{ads}) of adsorbed foam at a local foam concentration of 2 lb/StB, depending on the local value of rock surfactant concentration considered for the cell.

Foam effectiveness will typically reduce over time, even in conditions very favorable to foam stability. This reduction in effectiveness may be accelerated in the presence of water and/or oil and it is modeled by foam decay $\lambda(S_w, S_o)$. However, this effect is not taken into account in this work as it is usually neglected in the literature and no significant studies have been carried out at reservoir conditions.

The foam modifies the gas mobility Λ, defined as gas permeability k_g divided by its viscosity μ_g, by means of a multiplier supplied as a function of foam concentration (that is the effective surfactant concentration). The mobility modification is applied explicitly, that is, the modification associated with the conditions at the end of each iteration or time step is applied at the subsequent one. It is evident then, that modifying the permeability, as usually reported in the literature, or the viscosity, will lead to equivalent results.

A functional empirical model expression for the mobility reduction factor M_{rf}, which scales the gas relative permeability curve, is chosen in ECLIPSE along the same lines of the model used by STARS [55-56]:

$$M_{rf} = \frac{1}{1 + M_r^{ref} F_w F_s F_o F_c} \tag{5.2}$$

This is the most common model used for simulation purposes after the outgrowth of the success in predicting and well simulating several field-foam pilots [57].

Reference mobility reduction factor, M_r^{ref}

This term corresponds to the normalized resistance to flow of a minimum-size bubble in the absence of factors increasing its size [58].

Mobility reduction factor component due to water saturation, F_w

This term represents the dependence upon water saturation by capturing the impact of changes in foam strength as foam quality increases and the foam itself dries out [59]. The gas mobility increases sharply as water saturation decreases towards this limiting value, i.e. low water saturations weaken the foam. The function is expressed as:

$$F_w = 0{,}5 + \frac{atan\left[f_w(S_w - S_w^{lim})\right]}{\pi} \tag{5.3}$$

where
S_w is the water saturation;
S_w^{lim} is the limiting water saturation below which the foam ceases to be effective;
f_w is a weighting factor which controls the sharpness in the change in mobility, i.e. the abruptness of the foam collapse. Small values give a gradual transition between the high and low quality flow regimes, while larger values yield a sharper, albeit still continuous transition. Reservoir simulators cannot work properly with discontinuities in fluid properties, thus this parameter is usually constrained to not excessively slow down the simulations

Mobility reduction factor component due to surfactant concentration, F_s

This term represents the dependence upon foam (effective surfactant) concentration by the following power-law relationship:

$$F_s = \left(\frac{C_s}{C_s^{ref}}\right)^{e_s} \tag{5.4}$$

where
C_s is the effective surfactant concentration;
C_s^{ref} is the reference surfactant concentration;
e_s is an exponent which controls the steepness of the transition about the point $C_s = C_s^{ref}$.

The significance of F_s is determined by the reference surfactant concentration above which the presence of surfactant becomes significant in the creation of foam. For low surfactant concentrations $C_s < C_s^{ref}$ (weak foam), the value of F_s will be less than 1 and will tend to 0 as the surfactant concentration decreases to 0. Conversely, for high surfactant concentrations $C_s > C_s^{ref}$ (strong foam), the value of F_s will be greater than 1 and will increase with increasing surfactant concentration. The steepness and curvature of F_s versus C_s and the rate of change about the point where $C_s = C_s^{ref}$ are determined by the value of e_s [44].

Mobility reduction factor component due to oil saturation, F_o

This term represents the dependence upon oil saturation, which can reduce the foam stability by increasing the degree of foam coalescence, leading to an increase of the foam bubble size and, as a consequence, to a higher gas mobility [61]. It is expressed as:

$$F_o = \begin{cases} \left(\frac{S_o^m - S_o}{S_o^m}\right)^{e_o} & S_o \leq S_o^m \\ 0 & S_o > S_o^m \end{cases} \quad (5.5)$$

where
S_o is the oil saturation;
S_o^m is the maximum oil saturation above which the foam ceases to be effective;
e_o is the exponent which controls the steepness of the transition about the point $S_o = S_o^m$.

The maximum value of F_o is 1 and occurs when $S_o = 0$. For values of $S_o < S_o^m$, the value of F_o will decrease with increasing S_o. The rate of decrease is controlled by the value of the exponent e_o, which makes F_o only if larger than unity. For values of $S_o \geq S_o^m$, the value of $F_o$will be 0 and will completely eliminate any gas mobility reduction irrespective of the values of the other multiplicative factors, i.e. the oil factor has a killing effect on the foam.

Mobility reduction factor component due to gas velocity (capillary number), F_c

This term represents the dependence upon the capillary number, i.e. it alters gas mobility to account for shear thinning (non-Newtonian) behavior (decrease in viscosity with increasing rate of shear) in the low-quality regime [36]. Its power-law expression is the following one:

$$F_c = \left(\frac{N_c^r}{N_c}\right)^{e_c} \quad (5.6)$$

where
N_c is the capillary number;
N_c^r is the reference capillary number;
e_c is the exponent which controls the steepness of the transition about the point $N_c = N_c^r$.

The capillary number is a dimensionless parameter which provides a measure of the ratio of viscous to capillary forces and is calculated according to the expression [44]:

$$N_c = \frac{|K \cdot gradP|}{\sigma_{wg}} C_{unit} \quad (5.7)$$

where
K is the rock permeability;
P is the pressure;
σ_{wg} is the gas water interfacial tension;
C_{unit} is the conversion factor which depends upon the units used, as N_c is dimensionless.

As noticeable, the capillary number is a function of the pressure gradient, thus the foam gets weaker as the pressure gradient increases. Anyway, this function is not taken into account within this work (i.e. $F_c = 1$ is assumed) as it has been usually neglected in the literature as well and, as a consequence, not enough data have been provided to create a reliable range of values to analyze. This is not a too strict assumption to make because the

amount of gas injected into FIELD α (see Table B 5) is very high (gas produced in addition to gas coming from other neighboring Angolan fields), supporting most likely a high quality regime, and as said, the capillary number affects only the low quality regime, i.e. the flow regime occurring at low amounts of gas compared to water injected.

5.2. Analysis setup

Once that the foam model has been introduced, it is worthwhile to well structure the upcoming steps in order to not lose the two main objectives of the possible foam application, that is to say:

- ***reduce the gas produced***

  FIELD α has been selected as a good candidate for gas disposal purposes. As the gas coming from other fields is a variable not controllable, the efficacy of the disposal, i.e. how much gas is trapped into the reservoir, lies in the produced amount of gas, which has to be minimized.

- ***maximize the oil produced***

  To guarantee the feasibility of the foam application, it is clear that the oil produced has to be maximized and cannot drop below the amount simulated for the best WAG scenario, otherwise the advantages obtained by a reduction in the gas production will be nullified by the decrease in oil produced.

In this case the foam injection has to be applied to a field scale, thus an In-Depth Mobility Control Foam (MCF, see Section 3.1) has to be used in order to guarantee the best propagation all the way from injectors to producers without decaying. Moreover, a SAG generation method is chosen to avoid a plugging effect inside the reservoir (which could be anyway solved by a methanol injection dissolving the foam). As a consequence, C_{14}-C_{16} alpha-olefin-sulfonate surfactants have been selected at ENI labs and are being studied for a foam application.

Figure 5 . 1 – Steps analyzed throughout this section

The reported scheme shows the following steps before entering inside the core analysis of the optimization problem.

5.2.1. Variables selection and problem formalization

In order to rationally face this concrete problem, it is necessary to properly express its essential components. The system independent variables within the circle of influence, which can be used to steer the behavior of the response, are called **decision** (or **control**) **variables** $d_1, d_2, \dots, d_n$. In addition, all the others independent variables, which can take more than a single value on and represent the uncertainty characterizing the relationship between decision variables and objective functions, are called **uncertain variables** $u_1, u_2, \dots, u_m$. The goal is to select a set of optimal decision variables $\hat{d}_1, \hat{d}_2, \dots, \hat{d}_n$that minimize or maximize the **objective functions** $f_i(d_1, d_2, \dots, d_n, u_1, u_2, \dots, u_m)$, where i can be 1 or more in case of multi-objective analyses, subject to a certain number p of constraints [62]:

$$g_1(d_1, d_2, \dots, d_n, u_1, u_2, \dots, u_m) \leq c_1$$

$$g_2(d_1, d_2, \dots, d_n, u_1, u_2, \dots, u_m) \geq c_2$$

$$\vdots$$

$$g_p(d_1, d_2, \dots, d_n, u_1, u_2, \dots, u_m) <> c_p$$

Thus, on the basis of what said in the previous sections and in this subsection, it is possible to distinguish three main groups of parameters reported in the following hierarchy diagrams.

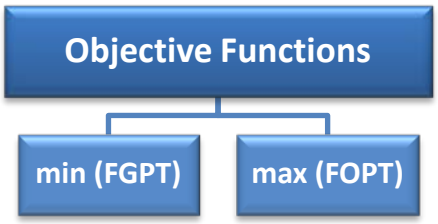

Figure 5 . 2 – List of objective functions

Two objectives represent the aim of the foam application: reduction of the field gas produced (FGPT) and maximization of the field oil produced (FOPT), as previously introduced. It is expectable that these two objectives will be somehow weakly or strongly related and, as a consequence, an extremely big reduction of gas produced should be avoided in order to guarantee the production of a certain amount of oil which makes the project feasible as an improvement of the WAG application.

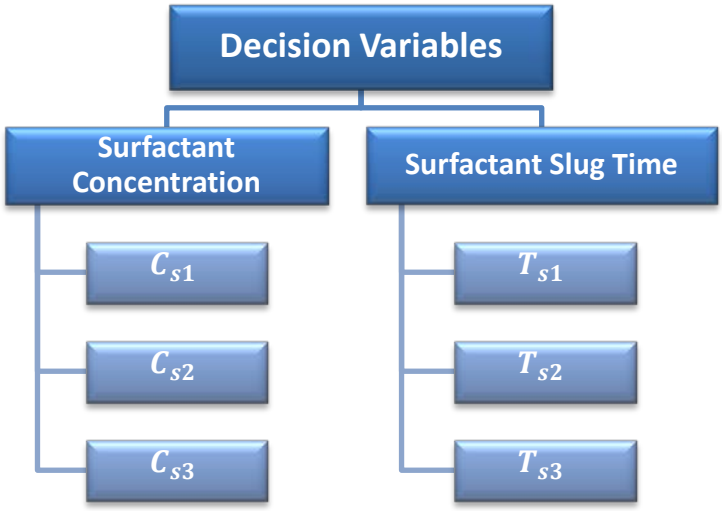

Figure 5 . 3 - List of decision variables

Two main groups of decision “operative” variables have then been selected: concentration (C_s) and time-length of the injected surfactant slug (T_s) which takes place at the end of the water injected slug (i.e. the sum of the water and surfactant slug time-lengths totals 365 days). Thus, three slugs of surfactant are analyzed at the moment and will be verified as necessary to guarantee the profitability of the foam application. As a consequence, since each surfactant slug is characterized by concentration and time-length of the injection, six decision variables are analyzed.

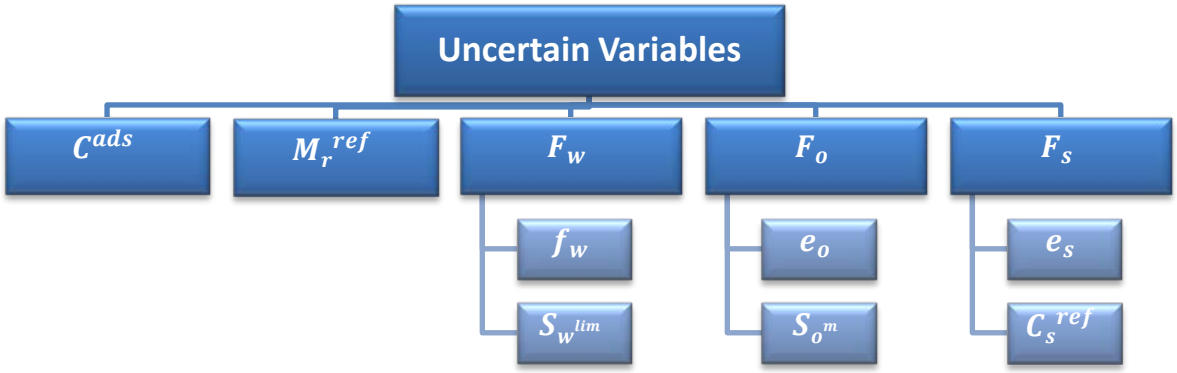

Figure 5 . 4 - List of uncertain variables

On the other hand, each uncertain variable derives from the foam model and the assumptions presented in Section 5.1. By reasonably neglecting the foam decay and the capillary number related factor component, five main groups of uncertain variables are taken into account in this work: adsorbed concentration (C^{ads}), reference mobility reduction factor (M_r^{ref}), surfactant concentration-related (F_s) and water and oil saturations-related mobility reduction factor components (F_w, F_o). Then, each of these three last mobility reduction factor components carries two variables, i.e. eight main uncertain variables are analyzed.

5.2.2. Range selection

So far, the usual approaches to calculate the parameters needed to simulate the foam flow behavior inside the reservoir consist in either measuring an apparent foam viscosity in labs and matching the obtained profile with the foam model based profile taking into account at most two or three variables (hypothesizing the others) [33, 36, 38, 43-44, 56, 59-60, 63-66] or, in an even less accurate way (as variables dependences are not taken into account), making an a posteriori sensitivity analysis and matching, in this way, one variable at a time [61]. Thus, a probabilistic approach is proposed here, in which ranges for all the considered variables are identified through data both reported in the literature and supplied by early experiments conducted at ENI laboratories. In this way, every possible application of foam in a suitable reservoir candidate can be analyzed and roughly evaluated before any advanced core analyses.

All the variables included in both the “uncertain” and “decision” categories are represented through uniform distributions $U(a, b)$, taking into account in such a way the maximum level of possible uncertainty concerning each variable and avoiding the possibility of giving an unreliable or unexplained weight to certain values. For the uncertain variables, only a few variable-outliers [64-65] have been excluded from the work because of unexplained deviations from “reasonable” values, as they differ of even two orders of magnitude from suggested threshold values given by ECLIPSE or STARS User Manuals

[44, 56], while some other ranges (such as the M_r^{ref} values) have been slightly improved, hypothesizing that surfactants generating too weak foams (for instance with $M_r^{ref} < 50$ or $C^{ads} > 0{,}00005\ {}^{lb}/_{StB}$) can be replaced (see Table 10). On the other hand, the ranges for the decision variables have been chosen taking into account also the fact that the surfactant cannot be injected for more than 5 days because of the impossibility of guaranteeing a reliable and continuous connection between the FPSO and the vessel carrying the surfactant for a larger time frame. Moreover, it would be senseless to inject surfactant at concentrations lower than 0,5 lb/StB due to the proximity of the reference surfactant concentration and because it is quite reasonable to assume that a low concentration could be slightly compensated by a lower slug time-length instead (as verified in the next subsection).

As can be noticed from Table 10, in addition to the extreme values (maximum and minimum,(a, b)) characterizing the support of the probability density function, a column representing a "*base case*" is given. This is the column of rounded average values which is used for sensitivity analyses in order to possibly simplify the problem by neglecting the variation of certain variables, thus not exact values but values making physical sense are rather needed.

	Variable	Min	Base	Max
Decision Variables	C_{s1} [lb/StB]	0,05	2	3
	C_{s2} [lb/StB]	0,05	2	3
	C_{s3} [lb/StB]	0,05	2	3
	T_{s1} [days]	0	3	10
	T_{s2} [days]	0	3	10
	T_{s3} [days]	0	3	10
Uncertain Variables	M_r^{ref} (fmmob)	100	200	500
	f_w (epdry)	50	200	1000
	S_w^{lim} (fmdry)	0,1	0,2	0,3
	e_o (epoil)	0,5	1	2
	S_o^m (fmoil)	0,2	0,3	0,4
	e_s (epsurf)	0,5	1	4
	C_s^{ref} [lb/StB] (fmsurf)	0,01	0,02	0,1
	C^{ads} [lb/StB] (ad)	0,00001	0,00002	0,00005

Table 10 - Ranges of the variables analyzed in the work

The various terms are expressed also in the STARS' notation (within parentheses) as in some upcoming images they are expressed through this notation.

5.2.3. Problem split

Once that the ranges have been selected for each variable, it is possible to proceed with a split of the problem into two parts to facilitate and speed up the multi-objective research, as it would otherwise require a too long computational time:

- ***FOPT Analysis***

  The total field oil produced is the only objective, so that the steps included in the analysis and optimization should be carried taking into account only its values.

- ***Complete Robust Analysis***

  The total field gas produced is analyzed by reducing the ranges of the decision variables on the basis of the results obtained in the FOPT Analysis in order to guarantee an FGPT minimization which will not obstruct the oil production. Then, the robust analysis is implemented by taking into account both of the outcomes by building two proxies.

The upcoming sections will represent an accurate description of each part introduced above.

5.3. FOPT Analysis

The analysis of the optimization of the oil produced globally is carried following the below represented scheme:

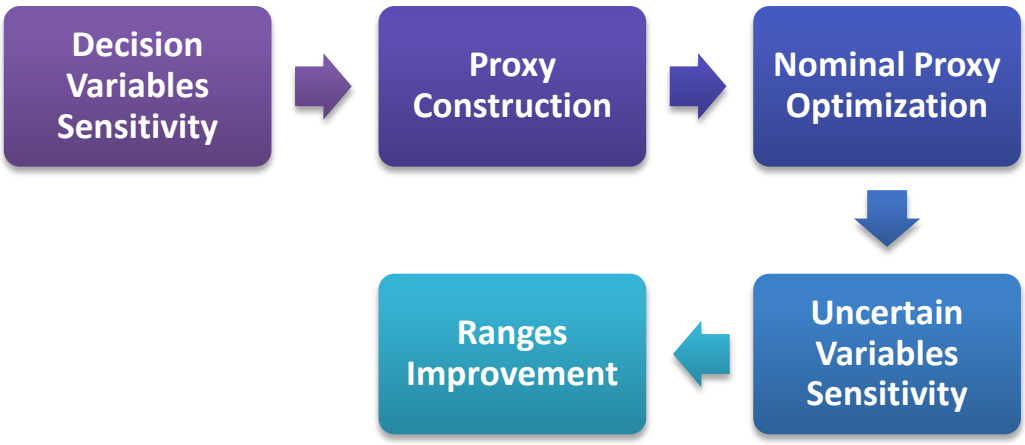

Figure 5 . 5 - Scheme representing the steps throughout the FOPT-analysis

The following subsections explain accurately each one of the above represented steps to achieve the optimization.

5.3.1. Decision variables sensitivity

To assess the effects of the decision variables on the objective function (FOPT) and to statistically neglect insignificant variables for the optimization, a **stepwise regression** is applied by means of MATLAB software. Thus, the values for each uncertain variable are set to the *base case* reported in Table 10 and only concentration and time-length of the injected surfactant slugs are varied to determine relevant relationships between input and output.

Anyway, before proceeding with the relevance analysis, it is clearly necessary to have a good population of simulations. For this purpose, once again an LHS method has been used through MEPO software by running 150 simulations with 6 variables, that is the ratio $\frac{N}{K} > 20$ (see Eq. 4.8). In fact, to avoid possible corrupted simulations, it is better to well overstep the suggested minimum value of LHS strata [51], since the effects of the foam application on this particular reservoir has not been analyzed yet and the time required for each simulation exceeds two hours in some cases (it would be time-expensive to restart an LH sampling). The following figure (*Fig. 5.6*) represents the FOPTs for each simulated dataset.

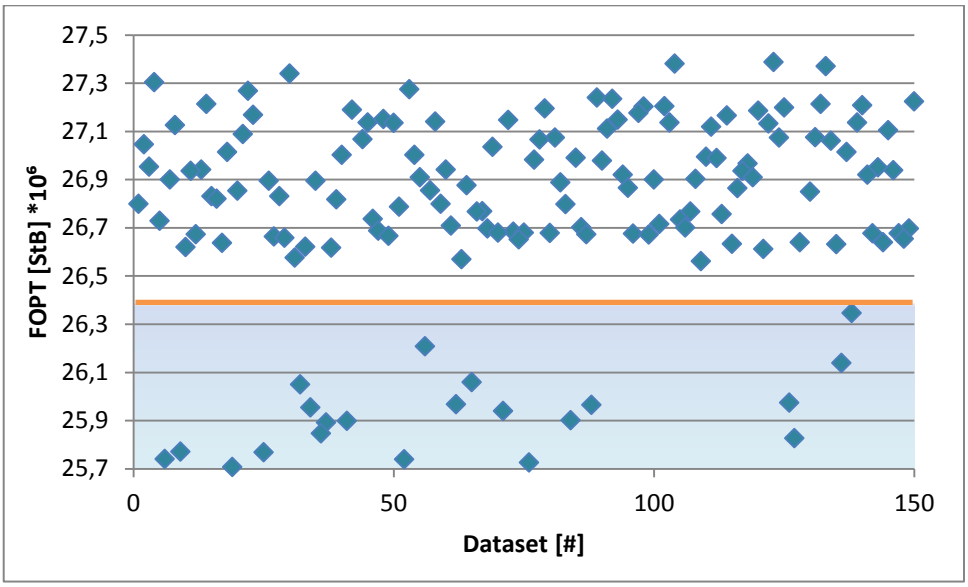

Figure 5 . 6 - Plot showing the 150 LHS runs with the threshold at 26,4 million StB

As proactively presumed, 21 simulations distance themselves from the "common" and reasonable values and 3 others are not represented due to computational interruptions that made them outliers in terms of FOPTs. By going in deeper details through the outcomes (data files), it is found that the production well P-302 shuts-off prematurely because of a

too strong foam causing a plug within the reservoir that cannot be balanced by injectors because of the injection constraints (see Table 3). Thus, since unrealistic simulations would cause an invalid analysis, only those with $FOPT > 26{,}5 \cdot 10^6\ StB$ are kept, i.e. 126 runs out of 150 are used, keeping anyways a ratio $\frac{N}{K} > 20$.

Once that a good amount of samples with different valid datasets is available, it is possible to perform the sensitivity analysis to see if there are any negligible variations of the variables. Thus, the MATLAB statistical tool already mentioned performs a stepwise regression of the input data to uncover statistically significant relationships, which involves, at each step, the computation of the *p*-value (i.e. the probability of obtaining a test statistic result at least as extreme or as close to the one that was actually observed, assuming that the null hypothesis is true) of an *F*-test (statistical test in which the test statistic has an *F*-distribution under the null hypothesis) to analyze the model with and without a potential term. The terms represented by the two groups of decision variables (C_{si}, T_{si}) and their product $(C_{si} \cdot T_{si})$ have been analyzed as it is supposed that an increase in the injected surfactant concentration could be balanced by a decrease in the injected time-length and vice versa. Thus, at each step a straight line approximating the trend is hypothesized with a certain intercept and slope coefficient. If a term is not currently in the model, the null hypothesis is that the term would have a zero coefficient if added to the model. If there is sufficient evidence to reject the null hypothesis, the term is added to the model. Conversely, if a term is currently in the model, the null hypothesis is that the term has a zero coefficient. If there is insufficient evidence to reject the null hypothesis, the term is removed from the model. The method proceeds as follows [67]:

1. If any terms not in the model have *p*-values less than an entrance tolerance (that is, if it is unlikely that they would have zero coefficient if added to the model), add the one with the smallest *p*-value and repeat this step;
2. If any terms in the model have *p*-values greater than an exit tolerance (that is, if it is unlikely that the hypothesis of a zero coefficient can be rejected), remove the one with the largest *p*-value and go to step 2, otherwise end.

The method terminates when no single step improves the model. The minimum *p*-value above which the considered term can be excluded is set to 0,03, while the maximum *p*-value below which a term is recommended to be added is set to 0,01 . *Figure 5.7* shows the first and the last steps computed during the stepwise regression. Any variable that is determined should be kept in the final model is colored blue, while those variables that are not kept are colored red and the horizontal bars indicate 90% confidence intervals.

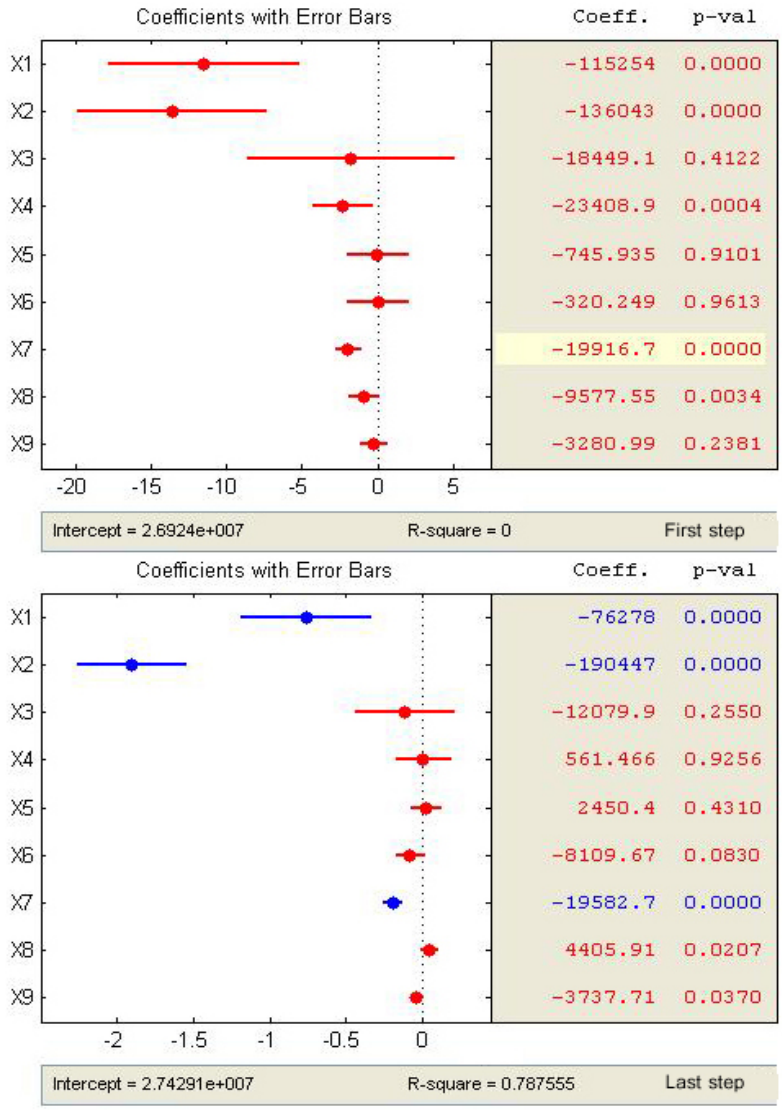

Figure 5 . 7 – First (top) and last (bottom) steps of the stepwise regression analysis, where [X1,…,X9]=[Cs1, Cs2, Cs3, Ts1, Ts2, Ts3, Cs1·Ts1, Cs2·Ts2, Cs3·Ts3]

Where R-square is the coefficient of determination $\left(R^2 = 1 - \frac{\Sigma(y_i - \bar{y})^2}{\Sigma(y_i - \hat{y}_i)^2}\right)$ and provides a measure of how well observed outcomes are replicated by the model (as it gets closer to unity), while the other terms have been previously explained. The components of a X-vector are represented on the y-axis of the figure, containing the analyzed variables:

$$X = \begin{bmatrix} X_1 \\ \vdots \\ X_9 \end{bmatrix} = \begin{bmatrix} C_{s1} \\ C_{s2} \\ C_{s3} \\ T_{s1} \\ T_{s2} \\ T_{s3} \\ C_{s1} \cdot T_{s1} \\ C_{s2} \cdot T_{s2} \\ C_{s3} \cdot T_{s3} \end{bmatrix}$$

As can be noticed, only the first and the second slugs have a reasonable relationship with the trend of the simulations. In particular, the most relevant terms are the concentration of the two slugs C_{s1} and C_{s2} and the product $C_{s1} \cdot T_{s1}$, endorsing what previously said about the combination of slug time length and concentration of surfactant. This can be visualized by plotting the FOPT as function of each combination C_{si} versus T_{si} (*Fig. 5.8*).

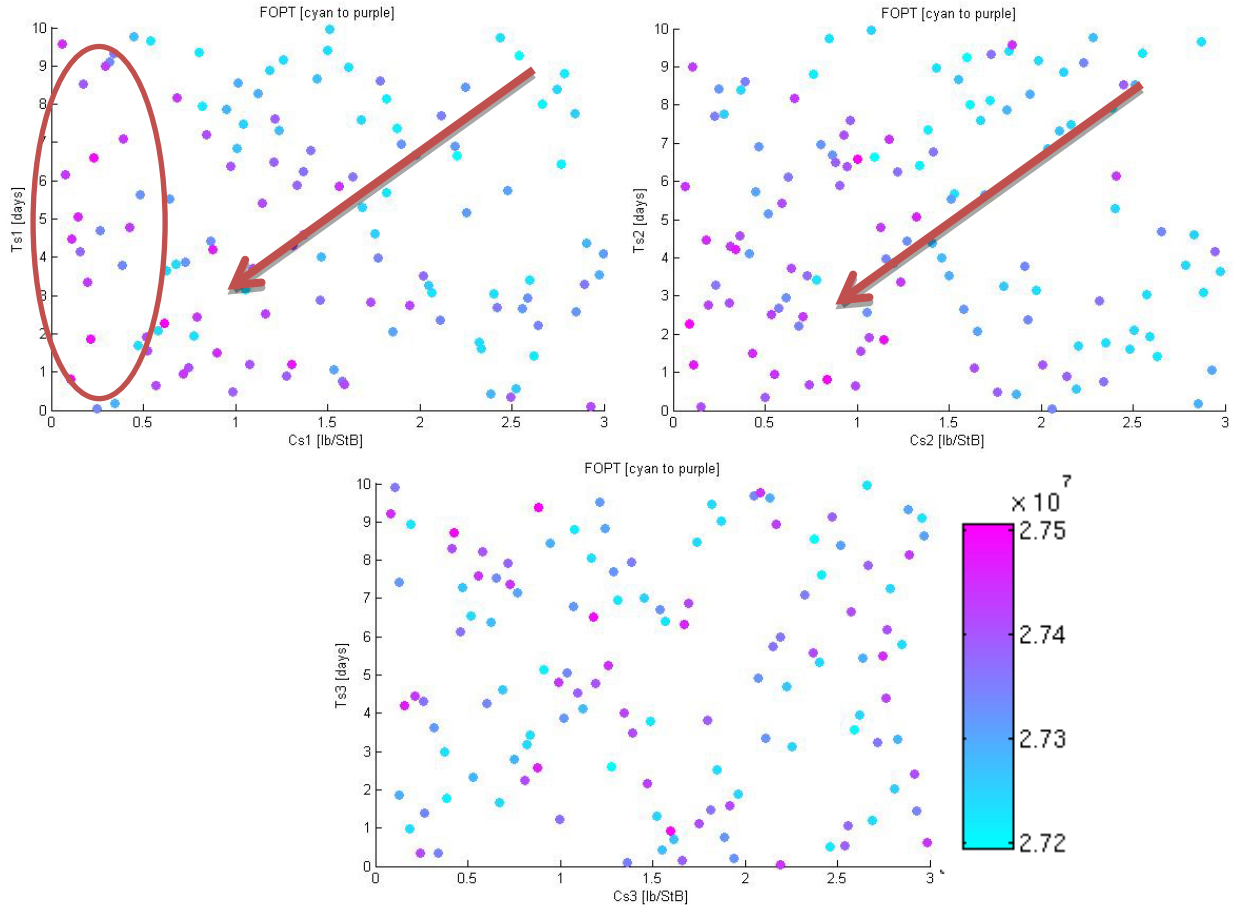

Figure 5 . 8 - Representation of FOPTs as functions of slug time-length and concentration for: 1st slug (upper-left), 2nd slug (upper right), 3rdslug (bottom)

As can be seen, for the second slug (upper-right plot) the FOPT increases (from cyan, with lower, to purple, with higher values) as both the surfactant concentration C_{s2} and the slug time-length T_{s2} decrease, following the red arrow. On the other hand, for the first slug (upper-left plot) this trend is not perfectly evident as for the second, but it is clear that a decreasing concentration C_{s1} usually leads to higher recoveries and that, as previously said through the stepwise analysis, an increasing value of the slug time-length T_{s1} can be compensated by low values of concentration (red circle). Finally, for the third slug, no particular relationships have been found through the stepwise regression and, in fact, the distribution of the FOPTs in the lower plot is absolutely random.

Up to this point, on the basis of what said, it is reasonable to neglect the variation of the parameters characterizing the third slug and to set them to a constant value. As a matter of fact, the missing relationship between the trend of the data and the parameters does not

indicate that it would be worthless to consider C_{s3} and T_{s3}, but it rather indicates that it is possible to neglect the variations. To further endorse this fact, the 10 best simulations have been selected (see Table B6) and then, the same 10 best cases have been re-simulated without C_{s3} and T_{s3} as input variables. Thus, as noticeable, the recoveries obtained in the case of neglecting the third slug are, on average, 1,02% lower than those obtained considering the last slug. This decrease of FOPT could affect the feasibility of the FAWAG project since it is necessary to stay above the value obtained for the best WAG scenario.

Once that a check about whether to use or to neglect C_{s3} and T_{s3} has been done, it is possible to proceed with the following step of the FOPT analysis by considering only the ranges of the four variables C_{s1}, C_{s2}, T_{s1} and T_{s2}. For this purpose, the average values of C_{s3} and T_{s3}, coming from the 10 "best cases" used for the last check, are selected (Table B6) after rounding them to the second decimal digit for the fractional part:

C_{s3} [lb/StB]	T_{s3} [days]
1,00	6,00

5.3.2. Proxy construction

A **nominal optimization** is implemented to find the best values of the four selected variables and, in this way, to reduce at least the ranges of variation, neglecting for the moment the uncertainties associated to the uncertain variables. A practical approach to perform such optimization in terms of computational costs and analysis reliability is by applying a **proxy** modeling technique that recurs to an approximation of the objective function and, as a consequence, of the input-output relationship as well. Thus, a spatial interpolation method called Universal Kriging is selected.

On the basis of what reported by Nielsen *et al.* [68] and adapting the concepts to this application, the simulator deterministic responses are represented by an unknown function $y: D \in \mathbb{R}^n \rightarrow \mathbb{R}$, which is assumed to be one realization of a quadratically integrable random field Y and function of the input design model parameters $\boldsymbol{S} = [S_1 \dots S_m]^T$ with $S_i \in D$ (in this case $m = 4$). By denoting with $\boldsymbol{s_c} = [s_1 \dots s_d]^T$, where $s = s(\boldsymbol{S})$, the d design sites where y has already been evaluated, and by $\boldsymbol{y_c} = [y(s_1) \dots y(s_d)]^T$ the corresponding outputs, for any chosen $S_i \in D$, the Kriging method predicts an unknown deterministic response $y(s)$ through the adoption of a model $\hat{y}$, as a realization of a regression model $\mathcal{F}$ and a random stochastic process z assumed to have mean zero and expected value of $z(w)z(x)$

$$E[z(w)z(x)] = \sigma^2 \mathcal{R}(\theta, w, x) \tag{5.8}$$

between $z(w)$ and $z(x)$, where σ^2 is the process variance of the response, $\mathcal{R}(\theta, w, x)$ is the correlation model with parameters θ, w and x two random sites. Thus, z represents the

residual of the trend, i.e. it is a kind of correction of the trend so that if $\hat{y}(s)$ is evaluated in a known site ($s^* \in \boldsymbol{s_c}$), the result will be $\hat{y}(s^*) = y(s^*)$. The expression of $\hat{y}$ is:

$$\hat{y}(s) = \mathcal{F}(\beta_{:}, s) + z(s) \tag{5.9}$$

Where the used regression model $\mathcal{F}$ is a general proactively assigned combination (distinctive of the Universal Kriging method and polynomial in this case) of p chosen functions $f_j: D \in \mathbb{R}^n \rightarrow \mathbb{R}$:

$$\mathcal{F}(\beta_{:}, s) = \beta_1 f_1(s) + \cdots + \beta_p f_p(s) = [f_1(s) + \cdots + f_p(s)]\beta_{:} \equiv \boldsymbol{f}(s)^T \beta_{:} \tag{5.10}$$

And the coefficients β_k are regression parameters.

For the set $\boldsymbol{s_c}$ of design sites, the expanded $m \times p$ design matrix $\boldsymbol{F}$, with $F_{ij} = f_j(s_i)$, is defined:

$$\boldsymbol{F} = [f(s_1) \ldots f(s_d)]^T \tag{5.11}$$

Furthermore, the matrix $\boldsymbol{R}$ of stochastic-process correlations between z's at design sites is defined as:

$$R_{ij} = \mathcal{R}(\theta, s_i, s_j) \qquad i, j = 1, \ldots, d \tag{5.12}$$

It should be noticed that $\mathcal{R}$ (Eq. 5.8) weighs the possibility for z to move further or closer to the trend given by $\mathcal{F}$. So, it is an established function depending on θ's which weigh the correlation between random points.

At an untried point s let

$$\boldsymbol{r}(s) = [\mathcal{R}(\theta, s_1, s) \ldots \mathcal{R}(\theta, s_d, s)]^T \tag{5.13}$$

be the vector of correlations between z's at the design sites and s.

If a linear predictor is considered:

$$\hat{y}(s) = \boldsymbol{c}^T \boldsymbol{y_c} \tag{5.14}$$

with the vector $\boldsymbol{c} = \boldsymbol{c}(s) \in \mathbb{R}^d$ representing a kind of weights, the error is:

$$\hat{y}(s) - y(s) = \boldsymbol{c}^T \boldsymbol{y_c} - y(s) = \boldsymbol{c}^T \boldsymbol{Z} - z(s) + \left(\boldsymbol{F}^T \boldsymbol{c} - f(s)\right)^T \beta_{:}$$

where $\boldsymbol{Z} = [z_1, \ldots, z_d]^T$ is a vector containing all the errors evaluated at the design sites. To keep the predictor unbiased it is demanded that:

$$\boldsymbol{F}^T \boldsymbol{c} - f(s) = 0 \rightarrow \boldsymbol{F}^T \boldsymbol{c} = f(s) \tag{5.15}$$

Under this condition the mean squared error (MSE) of the predictor $\hat{y}(s)$ (Eq. 5.14) is

$$MSE(s) = E[(\hat{y}(s) - \mathrm{y(s)})^2] = \sigma^2(1 + \boldsymbol{c}^T\boldsymbol{R}\boldsymbol{c} - 2\boldsymbol{c}^T\boldsymbol{r}) \tag{5.16}$$

In order to minimize MSE and from the first order necessary conditions for optimality, the following system of equation must be solved

$$\begin{bmatrix} \boldsymbol{R} & \boldsymbol{F} \\ \boldsymbol{F}^T & \boldsymbol{0} \end{bmatrix} \begin{bmatrix} \boldsymbol{c} \\ \tilde{\boldsymbol{\lambda}} \end{bmatrix} = \begin{bmatrix} \boldsymbol{r} \\ \boldsymbol{f} \end{bmatrix} \tag{5.17}$$

where $\tilde{\boldsymbol{\lambda}}$ is defined as a vector containing the coefficients $\tilde{\boldsymbol{\lambda}} = [\beta_1, \dots, \beta_p]$.

So far, it is clear that the proxy construction process cannot exist itself without a validation stage. In fact, if a known point $s \in \boldsymbol{s_c}$ were selected, the outcome from $\boldsymbol{c}$ and $\tilde{\boldsymbol{\lambda}}$ would basically represent a perfect match, resulting in a straight line in case of plotting the estimated outcomes versus the data (FOPTs). For this purpose, the model is built based on a random sample of the dataset available (70%) coming from the LHS, representing the vector previously called $\boldsymbol{s_c}$, and the remaining 30% dataset is used to assess the accuracy of the model. In this way, 88 runs out of 126 are selected for the construction of the model, whereas the remaining 38 are kept for the validation. There are better experimental designs that can be used to build the proxy model through a reduced number of simulations, such as the Box-Behnken design which samples extreme values to best fit a hyper-plane on the data, but due to the shut-off of the of the producer P-302 the LHS design represents a valid solution if the number of sampled strata is big enough to be representative of the whole space of possible simulations.

The proxy is created by selecting all the four variables and their respective crosses ($C_{si}T_{sj}$, $C_{si}C_{sj}$ and $T_{si}T_{sj}$). As can be noticed from the graphical outcome of *Fig. 5.9*, the design sites (represented as blue diamond) lie on a bisector straight line, as previously highlighted, while the validation dataset (green) shows that the error committed by the proxy on predicting values not included in 70% dataset used to build the model remains within the range delimited by the two red lines representing a 1% error. It is also possible to evaluate an error related to the maximum range of FOPT variation, as will be presented in Eq. 5.21. In this case that error equals the maximum value of 23%, but the proxy can be anyhow considered valid. Obviously, the validity of this analysis relies on the hypothesis that the simulation model is perfect and exempt from errors, i.e. $y(s)$ corresponds to the exact real value of FOPT.

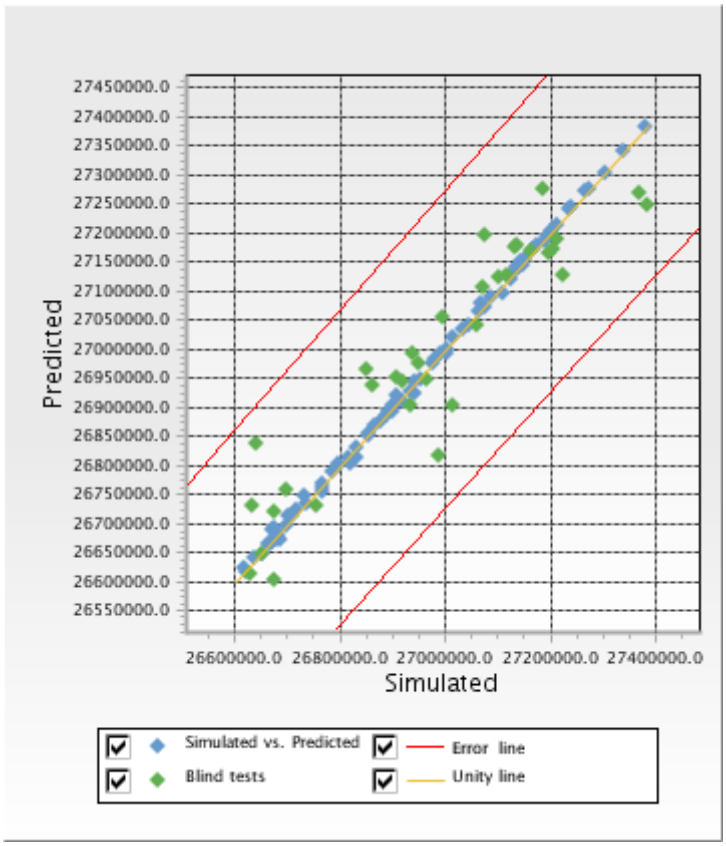

Figure 5 . 9 – Illustration of predicted vs. simulated data and 1% error lines

Now that the proxy has been proven to be valid, it is possible to proceed with the nominal optimization of the decision variables.

5.3.3. Nominal proxy optimization

A proxy model allows the approximation of a very large number of simulated experiments with a very limited computational cost. In fact, the "fictitious" results obtained by the proxy require a very short time and, as a consequence, an extended evaluation of samples can be easily carried without any computational problems. Thus, 10000 experiments are added to the experiment list and evaluated using a Latin Hypercube design to avoid possible slowdowns that can occur with an evolutionary algorithm and since the localization of promising regions can be made in a simple way. Subsequently, the best approximated experiments are selected to be really simulated in order to obtain the optimal results. In this case, 40 simulations are run and the 10 best cases out of these "best" experiments are selected to find a *base case* that should be used for further analyses. *Fig. 5.10* shows the outcomes:

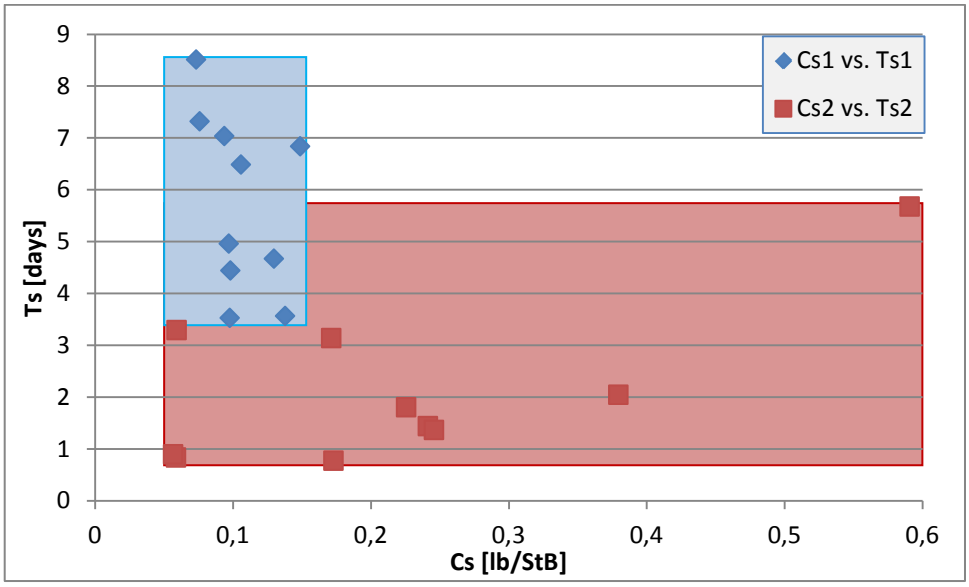

Figure 5 . 10 – Illustration of Cs versus Ts of the two slugs for the 10 best simulated cases

As noticeable, the ranges for the concentrations are much reduced to a maximum value below 0,6 lb/StB. In particular, the first slug has a very restricted range of variability for these optimal cases, while the second slug presents an improved range of time-length. A reasonable way to select a base case for the four variables, is by averaging the obtained data, resulting in the following values:

C_{S1} [lb/StB]	C_{S2} [lb/StB]	C_{S3} [lb/StB]	T_{S1} [d]	T_{S2} [d]	T_{S3} [d]	FOPT [StB]
0,106	0,26	1	5,735	2,127	6	**27.460.514**

Table 11 – Averaged best values after the proxy optimization

Also the average FOPT of the 10 cases has been reported and, if compared to the value averaged over the 126 simulations coming from the first LHS (26935275 StB), represents a 1,95% increase in the total oil produced, endorsing a weak optimization (it would be an error to compare only the maximum values of the two dataset, as it would not be representative of the efficacy of the optimization process). A sensitivity analysis, which is carried in the following subsection, aims to find the relevant uncertain variables.

5.3.4. Uncertain variables sensitivity

The sensitivity analysis is applied to the uncertain variables by means of an experimental design method called OVAT (One-Variable-At-a-Time), which basically consists of a base case and levels of each input parameter used just to generate simulations by varying one input parameter at a time and keeping the others at the base values. In this case, the levels are the upper and the lower values of the correspondent uniform distribution of the uncertain variables, once the decision variables have been set to the values represented in Table 10. Since $m = 8$ parameters are considered, MEPO runs $2m + 1 = 17$ simulations

to perform the OVAT analysis. The results can be represented by a tornado plot (*Fig. 5.11*), showing the simulations at three different periods (6,16 and 8,16 years in addition to the final values at the end of the time-frame of 10 years) to avoid the neglect of any particular trends and to check time-step specific sensitivity patterns.

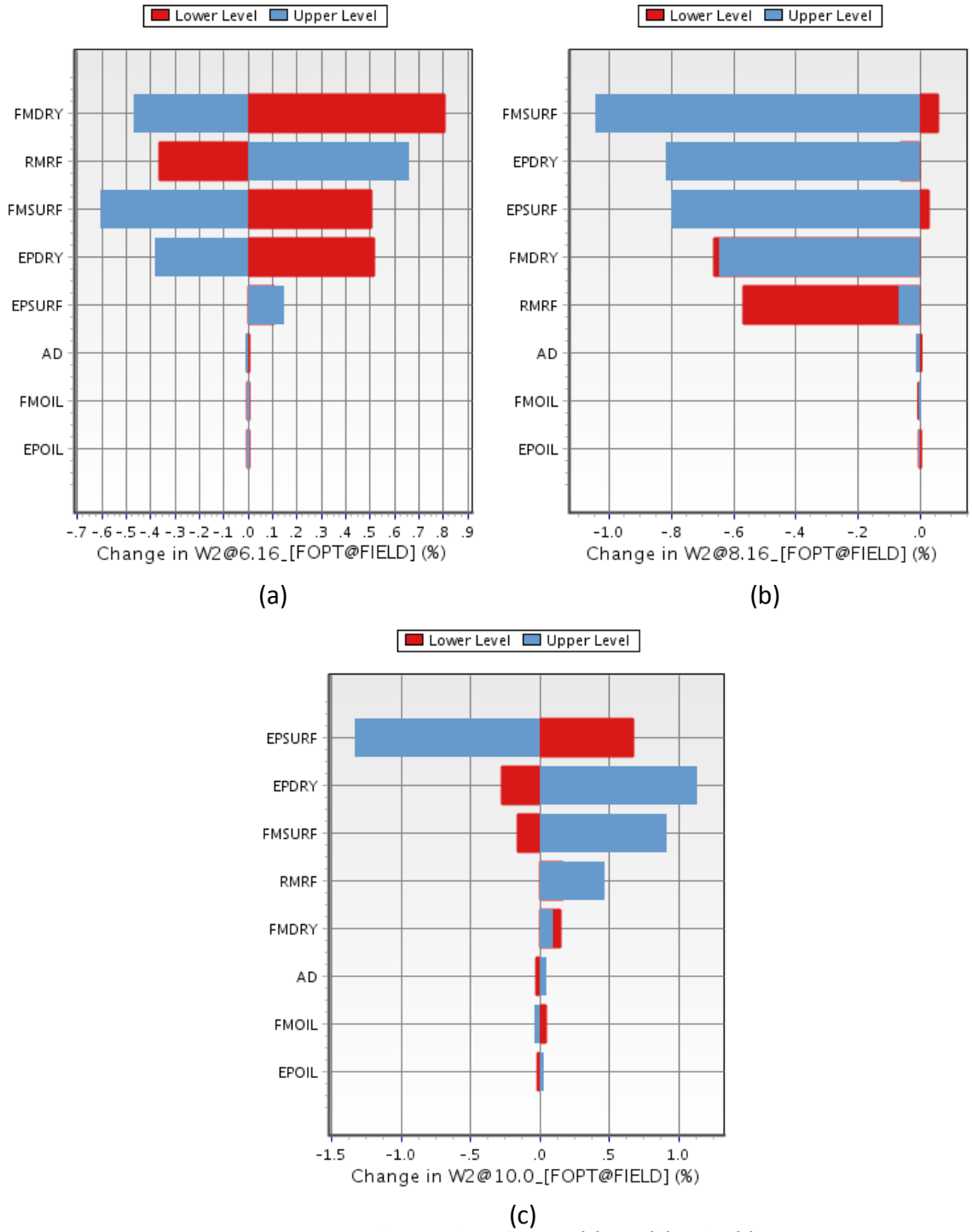

Figure 5 . 11 – OVAT analysis conducted at 6,16 (a), 8,16(b) and 10(c) years

As visible, some bars are located in the same side of the graph, supporting the fact that some variables should be better explained by a stepwise regression as done in the previous subsection to show what is happening within the limiting values of the ranges. Anyway, as the overall changes of FOPT squeak by 1% of variation, any other analyses made only for the oil produced would be worthless in this case. In fact, the process leading to the robust optimization can be thought as implying a reduction in the optimal reachable values of FOPTs, as the model should find a good solution adaptable to all the variables (both decision-type and uncertain). Due to this fact and since the nominal-optimal values of FOPT are already pretty close to the best WAG scenario, the possible increased values of FOPT would become comparable to the error associated to the simulation model that is not taken into account in this work.

5.3.5. Ranges improvement

Based on the 10 best cases obtained by the proxy optimization of the FOPT, the ranges of the decision variables are improved as shown in *Fig. 5.10* through the rectangular areas. Thus, for the upcoming analyses, the values reported in Table 10 are changed to the following ones:

Variable	Min	Max
C_{s1} [lb/StB]	0,05	0,15
C_{s2} [lb/StB]	0,05	0,8
T_{s1} [days]	3,5	8,5
T_{s2} [days]	0,7	5,7

Table 12 – New values selected for the decision variables

As can be noticed through a quick comparison, the ranges have been extremely reduced, especially for the surfactant concentrations, supporting the fact that a too strong foam would plug the reservoir as the volume available for the gas to flow is reduced due to the high level of water present in the reservoir which raises gradually. Anyway, it is necessary to verify that the variations of the same variables neglected for the FOPT analysis are negligible also in the case of a FGPT analysis.

5.4. Complete robust analysis

The complete robust analysis follows a scheme similar to the one shown for the FOPT in section 5.3, but, in this case, the nominal optimization is skipped as the results obtained for the FOPT are used to improve the analysis here and, thus, the following illustration shows the logic approach used:

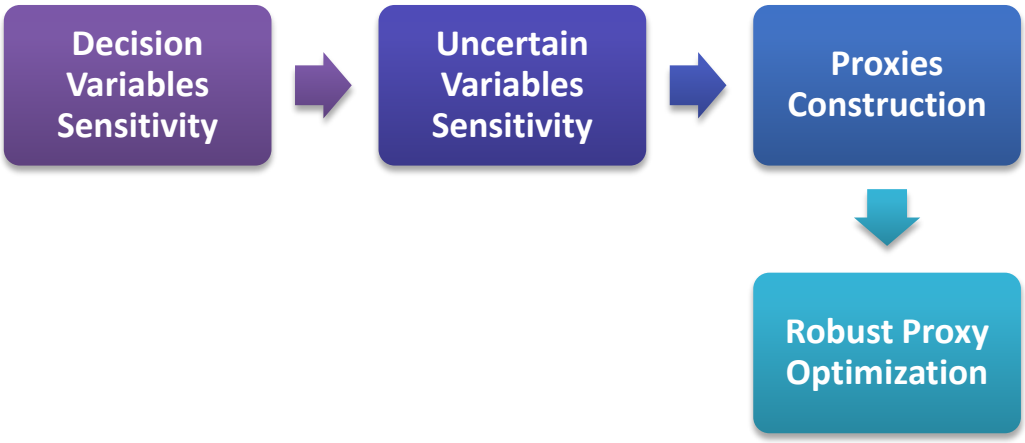

Figure 5 . 12 – Scheme representing the steps throughout the FGPT-analysis

The following subsections explain accurately each one of the represented steps.

5.4.1. Decision variables sensitivity

As done for the FOPT, it is required to check the effect of the decision variables on the FGPT values to verify whether it is reasonable to neglect the variation of the parameters characterizing the third slug. Thus, the data coming from the LHS used in the last section is recalled for the analysis of the gas produced. As the theory behind the process has already been introduced, it is possible to go straight to the outcomes of the stepwise regression. Once again, the minimum and maximum *p*-values are set to 0,03 and 0,01 respectively and *Figures 5.13* and *5.14* show respectively the first and last steps computed during the stepwise regression and a graphical representation of how the decision variables affect the FGPT values. The components of the X-vector represented on the y-axis of *Fig. 5.13* are the same shown in subsection 5.3.1 and in the same order. As can be noticed, once again only C_{s1}, C_{s2} and the product $C_{s1} \cdot T_{s1}$ are relevant terms. But, in this case, the R-square value at the final step is higher than the one found for the FOPT stepwise analysis (0,877 versus 0,788), i.e. a hypothetical model which took into account only C_{s1}, C_{s2} and $C_{s1} \cdot T_{s1}$ would explain the trend of the data in a better way than what would be found for the FOPT.

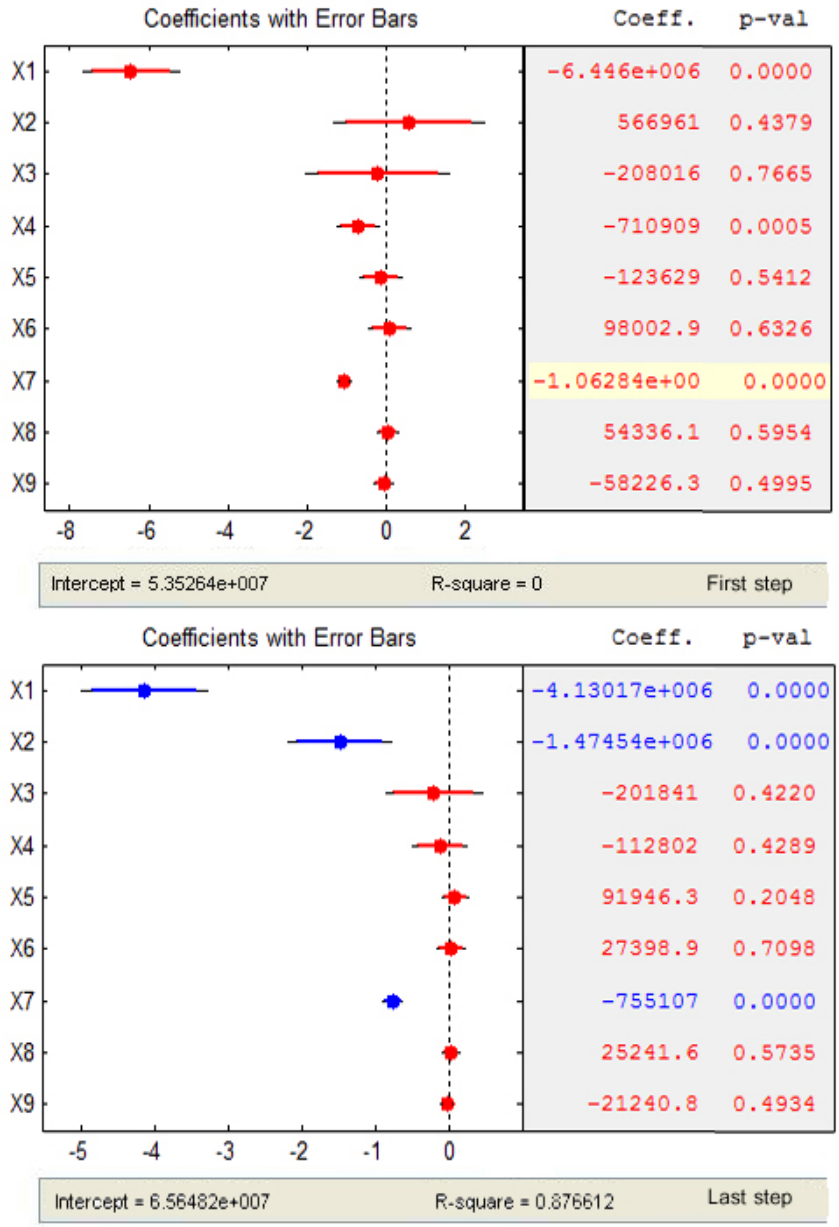

Figure 5 . 13 - First (top) and last (bottom) steps of the stepwise regression analysis, where [X1,…,X9]=[Cs1, Cs2, Cs3, Ts1, Ts2, Ts3, Cs1·Ts1, Cs2·Ts2, Cs3·Ts3]

These considerations can be also graphically visualized by scatter-plotting the FOPT as a function of each combination C_{si} versus T_{si} (*Fig. 5.14*), as previously done in the last section. It is evident that the relationships obtained through the stepwise regression between FGPT and decision variables are respected, since, for the first slug (upper-left scatterplot), both a high surfactant concentration and a high slug time-length lead to high reductions in gas produced. Anyway, as during the stepwise regression the first predominant term has been found to be the product $C_{s1}T_{s1}$ whereas the concentration C_{s1} has been the second one, the trend, visualized as a color gradient going from cyan (lower values of FGPT) to purple (higher values), is more oriented to the top-right side of

the plot in terms of optimal direction. This fact is highlighted by the arrow, which as noticeable points to the opposite side of the frame compared to the FOPT-related findings.

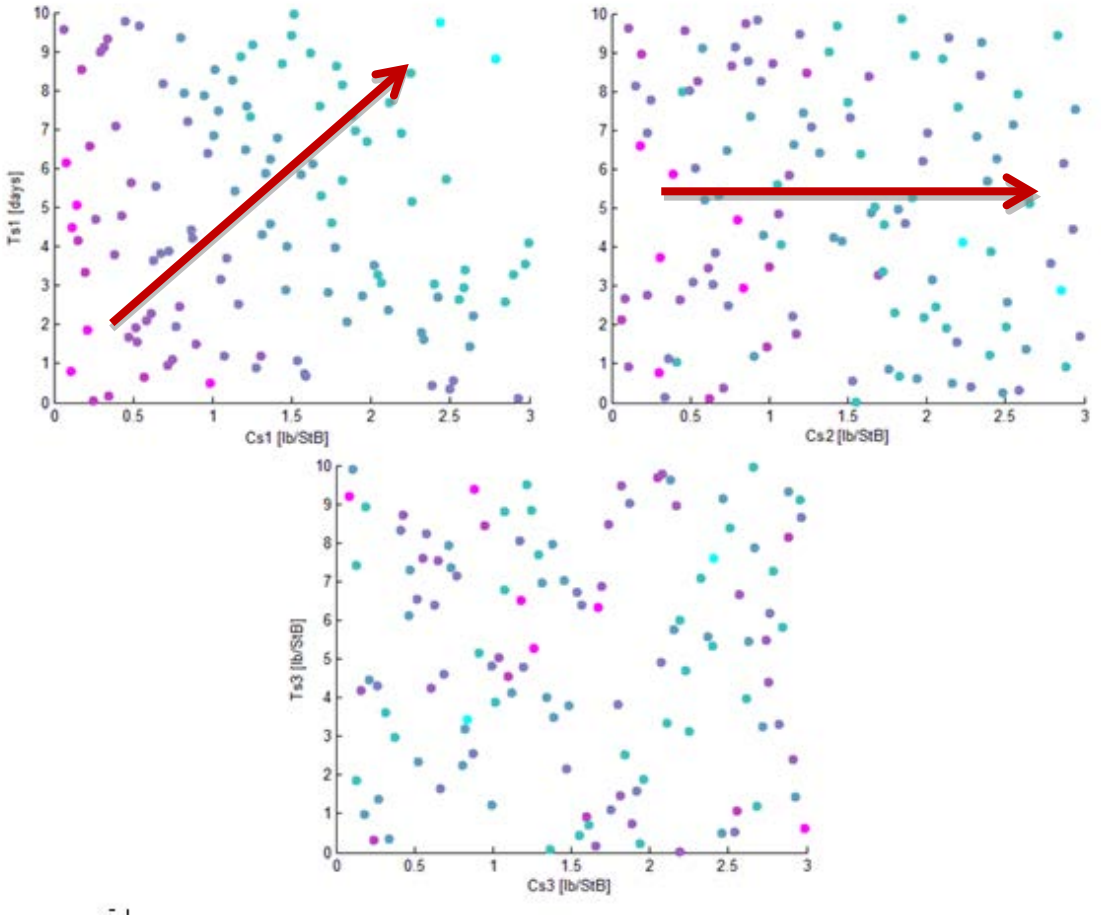

Figure 5 . 14 – Representation of FGPTs as functions of slug time-length and concentration for: 1st slug (upper-left), 2nd slug (upper right), 3rdslug (bottom)

On the other hand, the second slug (upper-right scatterplot) shows a weaker relationship between concentration of surfactant and FGPT (it was the last term added during the stepwise regression indeed), but still visible through the color gradient. Finally, the third slug, as seen in the case of FOPT, does not show any kind of trend, supporting the hypothesis of neglecting the C_{s3} and T_{s3} variations.

So far, it is clear the trade-off between the FGPT and FOPT optimizations, as imaginable from the fact that the foam strength directly affect the gas mobility through the model previously introduced. Thus, the application of the ranges found during the FOPT analysis will surely limit the optimization of the FGPT, but this is a necessary step in order to guarantee the feasibility of the project and to avoid the plug of the reservoir due to a too strong foam.

5.4.2. Uncertain variables sensitivity

Once again, the sensitivity analysis is applied to the uncertain variables by means of an OVAT design (see subsection 5.3.4), in which 17 simulations are run to check the relevance of the 8 considered variables. The results are represented by three tornado plots (*Fig. 5.15*), showing the simulations at 6,16 8,16 and 10 years.

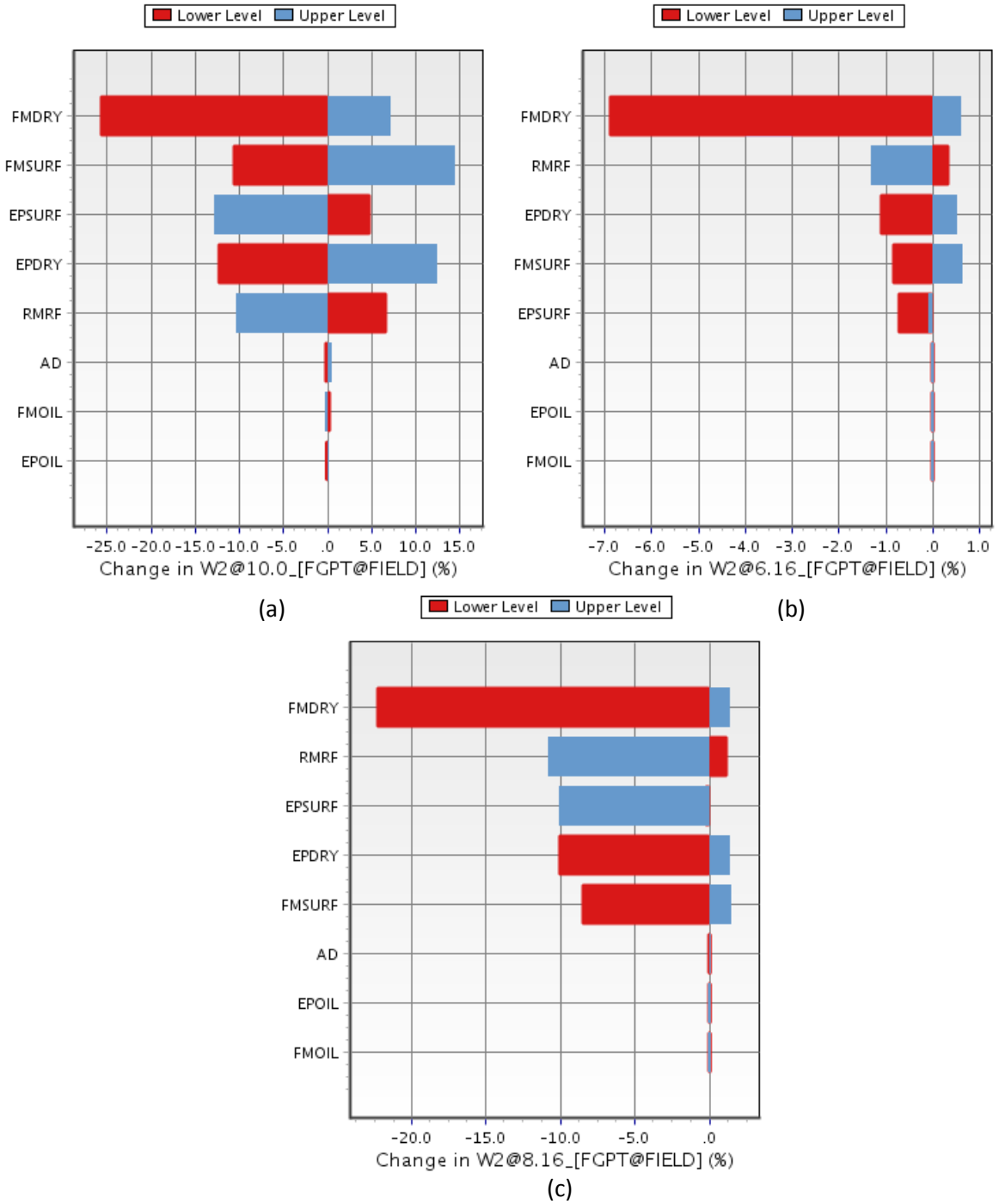

Figure 5 . 15 – OVAT analysis conducted at 6,16 (a), 8,16(b) and 10(c) years

It is immediately noticeable as the adsorption and oil-related terms are again negligible due to their very weak effect on the FGPT values. On the other hand, if compared to the OVAT applied to the FOPT, this time the percent change in the output (FGPT) due to variations of the uncertain variables is much higher and can even exceeds 25% of reduction compared to the base case (which is set to the same values exhibited in Table 10). Moreover, the tornado plots are much more oriented to the left-side, i.e. apparently the beneficial effects given by the variables are more likely and/or heavier in terms of resulting FGPT values than the negative effects. Once again, a stepwise regression would be redundant as the aim of this analysis is just to check the influence of each variable on the output and the results are pretty satisfying to build the basis for the construction of the proxies presented in the following subsection.

5.4.3. Proxies construction

Differently from what has been done in the previous section, here the proxy-construction process aims to robustly-optimize the FGPT handling the feasibility of the project due to "good" FOPT values. Thus, the optimization will take into account the uncertainties related to the deterministic variability of what has been presented as uncertain variables. As seen, a proxy modeling technique such as the Universal Kriging would be worthwhile for this purpose, but since the complexity and, as a consequence, the time required are increased due to the robust-optimization (9 variables to consider instead of 4, i.e. a calibration of the model with 9 parameters θ (Eq. 5.8) would be needed), the modeling technique is simplified to a polynomial proxy technique.

For this purpose, a very large number of simulations must be available as the problem now takes into account 9 variables at the same time (4 decision variables and 5 uncertain variable) and the proxy is going to be built on these variables. Moreover, the FOPT and FGPT values will represent a sorting factor for the simulations in order to improve and facilitate the analysis. In fact, even though the ranges of variation for the decision variables have been highly improved, it is expected that most of the resulting values of outcomes will surely not be included in the "wanted" ranges of FOPT and FGPT because the uncertainties are significantly high. Thus, it is necessary to have a large amount of runs and, as a consequence, a total number of 2000 cases has been simulated in a required considerable long time by means of a LH sampling design, as a reasonable compromise between computational cost and statistical sampling requirements (6 hours per run versus 1 hour per run for the WAG cases). Out of these 2000 cases, 10 resulted to be corrupted due to computational problems and have been consequently excluded from the analysis. *Figure 5.16* in the following page represents a plot of the 1990 simulations in terms of FOPT versus FGPT values and, on the basis of this graph, a few observation can be outlined. First of all, it can be noticed that the resulting simulations follow a well-defined trend, that is to say roughly high values of FOPT correspond to high values of FGPT. Within this trend, three main areas with a dense distribution of simulated runs are evident. In particular, the

upper-right cluster presents a discontinuity from the remaining body of data. This is due to the fact that in the "body" of simulations, only one or both of the producers experience a shut-off at some point due to the too high strength of the foam, while the upper-right cluster goes on producing for the whole time frame of 10 years.

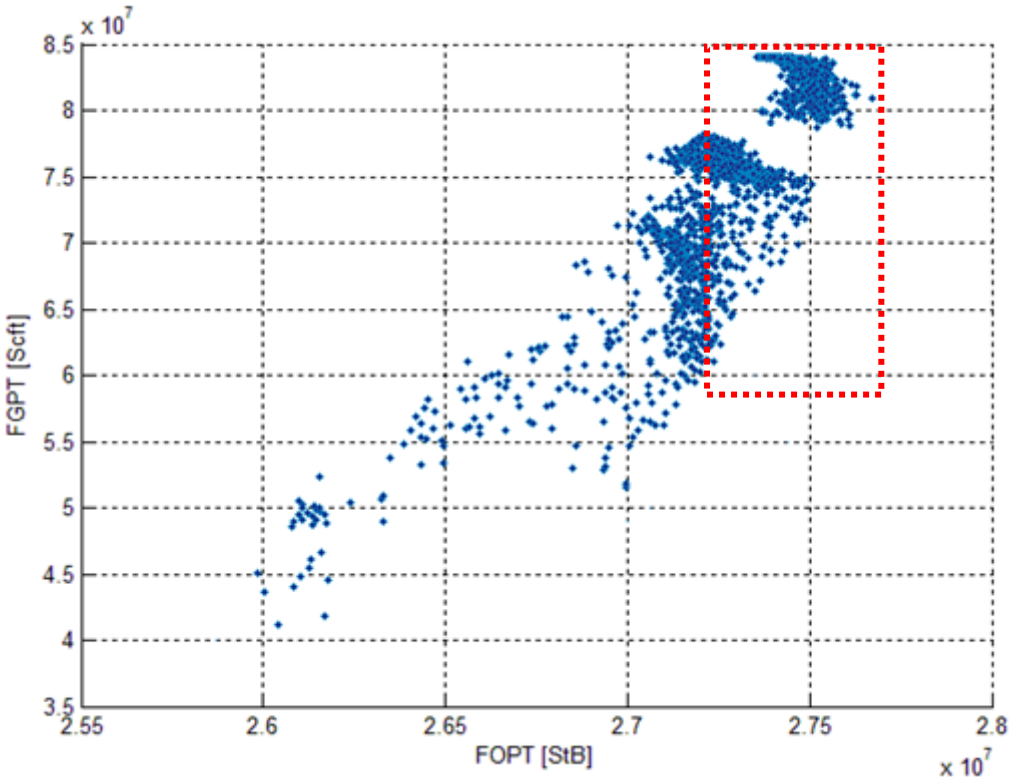

Figure 5 . 16 – Illustration of the FGPT and FOPT values resulting from the 1990 simulations run

To be more precise, the centered cluster is the one, as imaginable, in which the producer P-302 experiences a shut-off within the considered time-frame, while the lower cluster and the simulations lying below that area experience a shut-off of the other producer or of both of them, which occurs obviously more pre-maturely when the FGPT and FOPT have lower values. Anyway, the information available is not enough to explain why an empty area in the lower part of the body is present and of course it would be senseless to repeat the simulations including more information in outputs slowing down the already long lasting runs, but it is something that would be interesting to analyze.

It is worthwhile to have a deeper look inside the data and analyze how both the uncertain and the decision variables are distributed within the simulations. For this purpose, *Fig. 5.17* shows the FGPTs versus FOPTs as functions of each variable represented as color gradients (see color bars in the right-side of each graph). The only decision variable showing a weak relationship with the trend of the runs is C_{s1}, which commonly reaches higher values in the bottom-right side of the body of simulations, while the second slug concentration C_{s2} apparently has medium-high values when both the FGPTs and FOPTs are low. The other two decision variables (T_{s1} and T_{s2}) do not show any particular trends

related to the variation of outcomes. Anyway, the robust optimization will average the uncertainties in order to make the analysis robust on the uncertain side and this will probably improve the problems related to possible lack of trends of the decision variables.

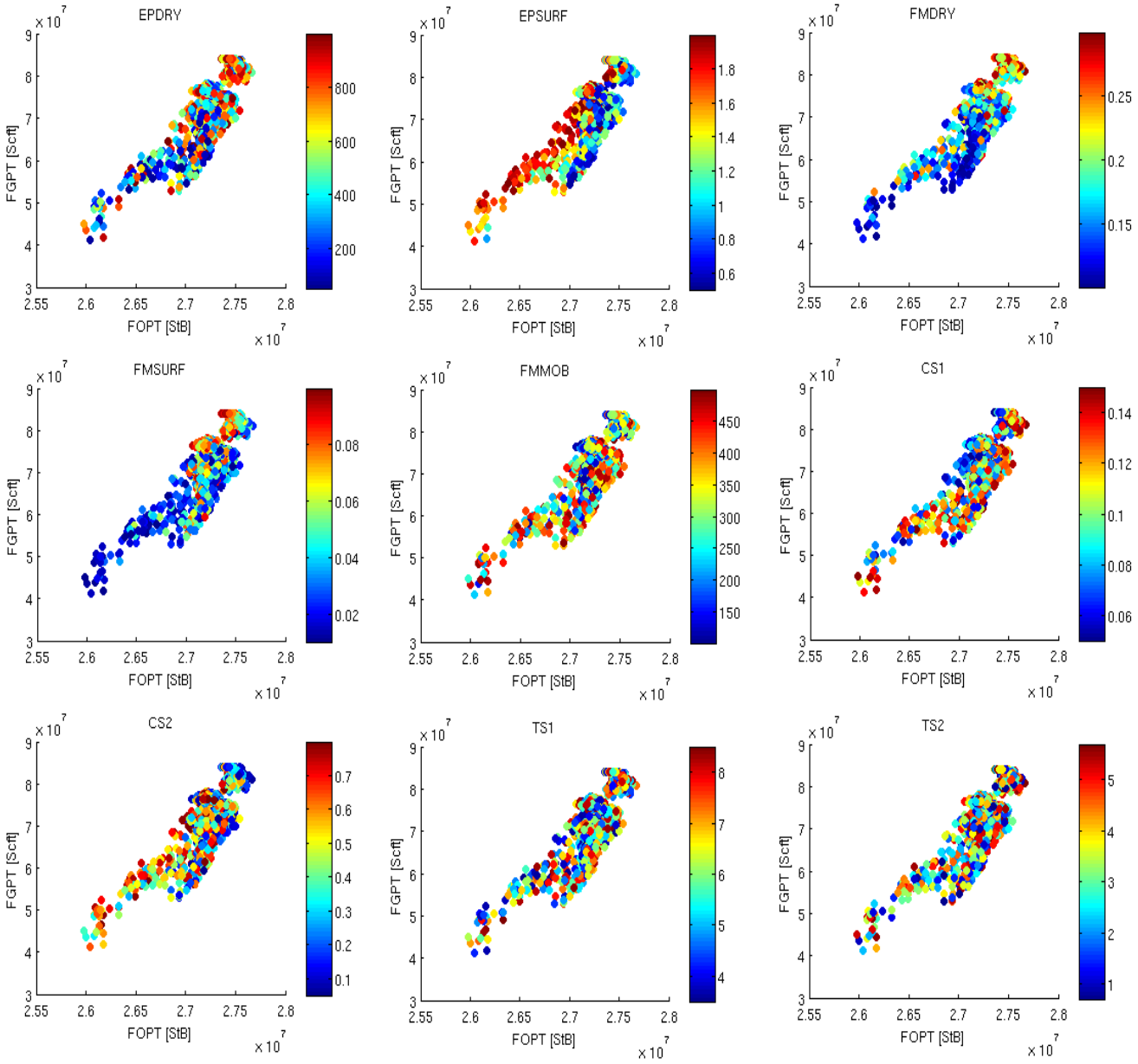

Figure 5 . 17 – FOPTs and FGPTs as functions of each variable

On the other hand, it is interesting that some uncertain variables show visible direct effects on the outcomes depending on their values. In fact, foremost for S_w^{lim} (fmdry) and less evidently for C_s^{ref} (fmsurf), low (blue circles) and high (red circles) values correspond to low and high values of the outcomes respectively. A similar trend is noticeable for the variable e_s (epsurf) but, in this case, the relationship is more related to the FOPT instead of both the outcomes, as demonstrated by the color gradient which is more horizontal than sloping.

Up to this point, it is clear that the effect of uncertain variables is relatively large and more definite than the effect of the decision variables. Moreover, most of the simulations lie outside the frame of interests (red dotted rectangle in *Fig. 5.16*). Thus, the proxies will be built on the whole range of data but then only the frame of interest will be analyzed. First and foremost, it is necessary to bring into focus this frame in terms of promising ranges of values. Thus, *Figure 5.18* shows a section of the previous graph with a limiting lower value for FOPT set to about $2{,}72 \cdot 10^7\ StB$ for the reasons later exposed.

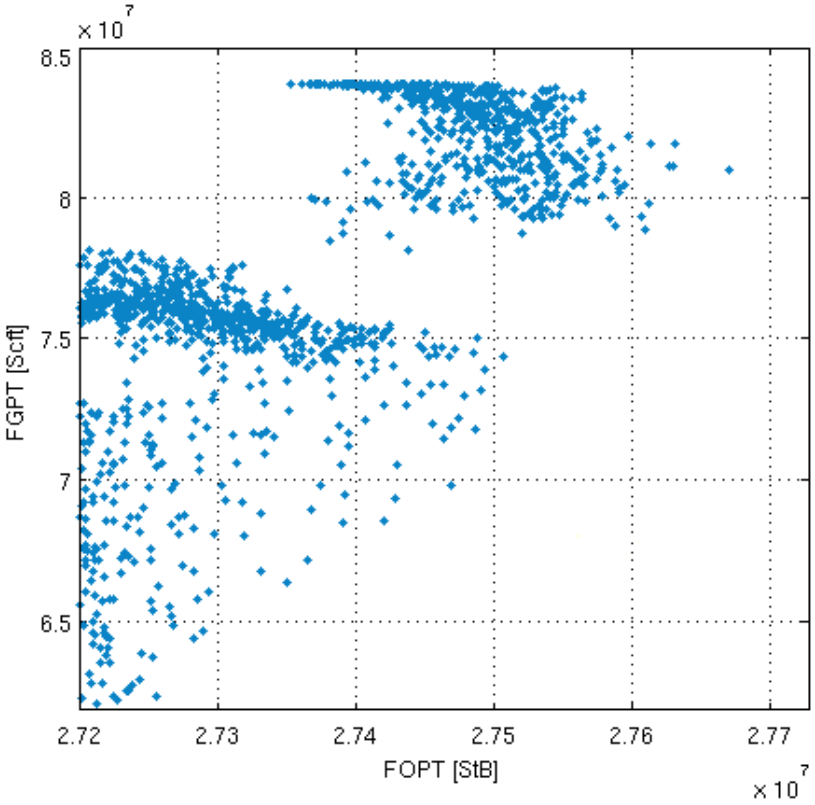

Figure 5 . 18 – Illustration of the FGPT and FOPT values within the frame of interest

The dense clusters of data will probably cause problems to the proxies which will be not that accurate, but, in order to avoid problems of interpolation, all the data are going to be considered for the construction and subsequently, after the optimization, only the frame of interest will be taken into account. Thus, on this basis, it is possible to build a proxy for both of the outcomes by a **multilinear regression** modeling technique applied to all the input variables (both uncertain and decision-type).

The multilinear regression attempts to model the relationship between two or more explanatory variables and a response variable by fitting a linear equation to observed data and each value of the independent variable x is associated with a value of the dependent variable $y: D \in \mathbb{R}^n \rightarrow \mathbb{R}$, which is one realization of a random field Y and function of the input model parameters $\boldsymbol{S} = [S_1 \dots S_m]^T$ with $S_i \in D$ (in this case $m = 9$). For any chosen $S_i \in D$, the multilinear regression predicts an unknown deterministic response y through

the adoption of a model $\hat{y}$, as a realization of a regression model μ and a deviation ε assumed to have mean zero and standard deviation σ.

The regression model μ is a linear combination of the p explanatory variables $\boldsymbol{X} = [x_1, \dots, x_p]^T$:

$$\mu(\beta_{:}, \boldsymbol{X}) = \beta_0 + \beta_1 x_1 + \cdots + \beta_p x_p \tag{5.18}$$

where the coefficients β_k are regression parameters and the explanatory variables are the input variables themselves ($\boldsymbol{S}$) and their quadratic combinations $S_i \cdot S_j$ in order to improve the accuracy of the model. Thus, formally the model, given d design sites is:

$$y_i(\beta_{:}, \boldsymbol{X}) = \beta_0 + \beta_1 x_{i1} + \cdots + \beta_p x_{ip} + \varepsilon_i \qquad for\ i = 1, \dots, d \tag{5.19}$$

Then, the best-fitting line for the observed data is calculated by minimizing the sum of the squares of the vertical deviations from each data point to the line. The least-squares estimates $b_0 + \cdots + b_p$ of the p regression coefficients β lead to the model $\hat{y}$:

$$\hat{y}_i(b_{:}, \boldsymbol{X}) = b_0 + b_1 x_{i1} + \cdots + b_p x_{ip} \qquad for\ i = 1, \dots, d \tag{5.20}$$

and the residuals are equal to $y_i - \hat{y}_i$ which add up to zero. The resulting outputs coming from a best-construction which minimizes the errors of the predictions compared to the simulations (by means of empirically findings) are shown in *Fig. 5.19* and *Fig. 5.20*. Also for the polynomial regression model the input experiments are divided into two subsets: the construction sites, which are represented as blue diamond, and the validation sites, which are represented in red. A straight bisector line (green) indicates the "ideal" trend of the predicted values versus the simulated ones, i.e. they should coincide in the case of a perfect proxy. Anyway, it is clear that the proxy built for the FOPT is much rougher than the one used to predict the FGPT values. This is a difference that could have been expected since the foam model (see section 5.1) implies that the effect of the foam directly affects the mobility of the gas and, as a consequence, any effect on the oil is indirect. This fact can be evaluated by measuring the distances of the design sites from the straight line, which represent the difference between the predicted $\hat{y}_i$ and the simulated y_i outcomes, and then compare those values with the maximum range of variation for the values $(\max(y) - \min(y))$, obtaining a normalized error e:

$$e_i = \frac{|y_i - \hat{y}_i|}{\max(y) - \min(y)} \tag{5.21}$$

Eq. 5.21 has been used to find a good proxy in terms of computational time by putting a maximum threshold on the values of the error, and the one applied to the FOPT proxy (40%) is much higher than the one used to build the FGPT proxy (20%). Thus, single optimized predicted values of FOPT may correspond to different values once that those sites will be really simulated, but this problem may be overcome in terms of robustness over the uncertainties. Moreover, as noticeable in *Fig. 5.19*, the highest deviations from the

predictions are located in a region with low values of FOPT, where there are a lot of overestimates of the outcome, and since they are not representative of the frame of interest, possible predictions occurring in this area would generate errors that are not taken into account as well as the predicted sites.

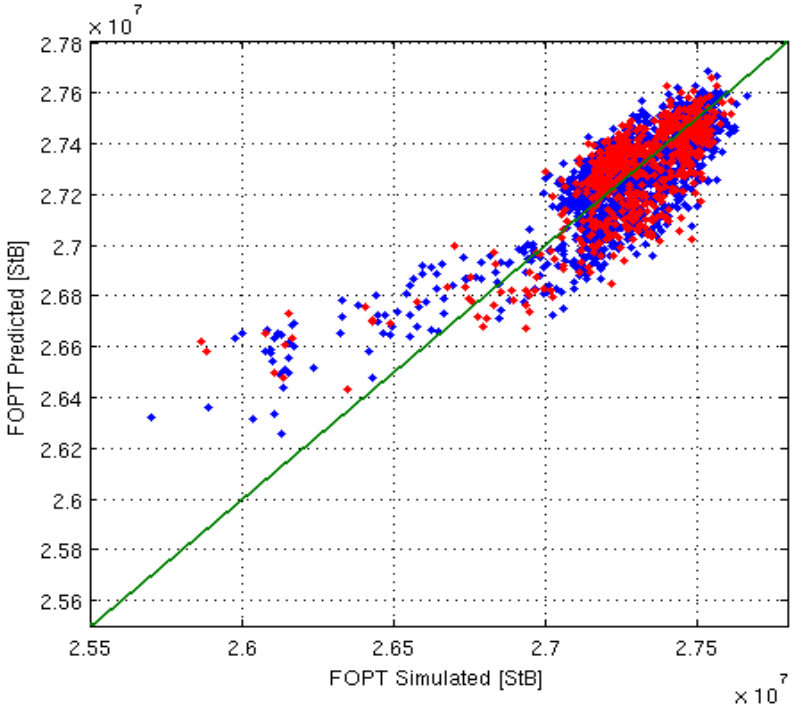

Figure 5 . 19 – FOPT values simulated and predicted by the proxy and validation sites (red)

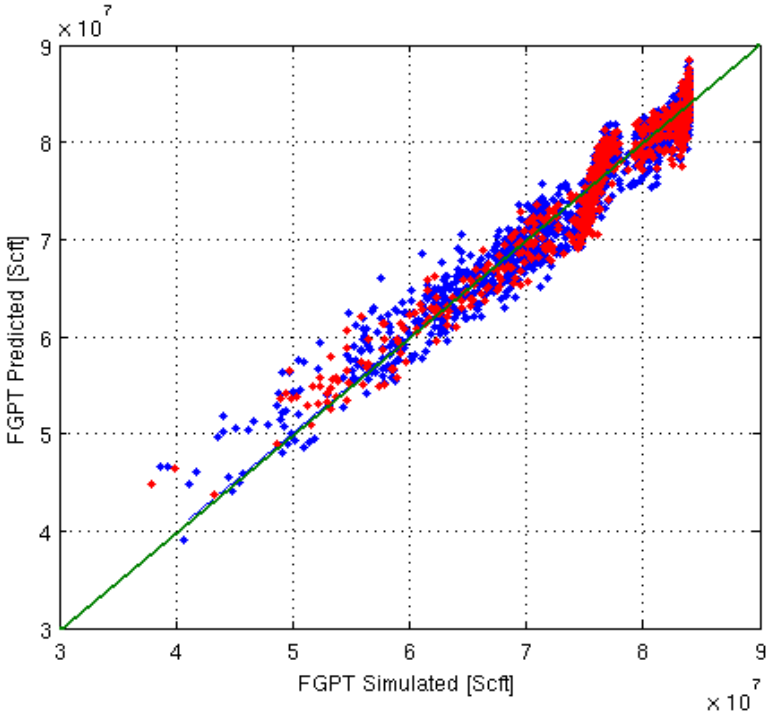

Figure 5 . 20 – FGPT values simulated and predicted by the proxy and validation sites (red)

Anyhow, it is interesting to see that the proxy worsens as the FOPT values decrease, but this is probably a negligible problem as the frame of interest lies well above those sites and as the robust optimization calculates average values of the outcomes. Moreover, the validation sites do not lie in outlier-positions compared to the design sites, supporting the fact that the proxies very weakly exceed (it does not even happen for the FGPT) the maximum error (Eq. 5.21) imposed to be built through the design sites while predicting new values. This is visible from Table 13, where the maximum values of error e_{max} and the coefficients of determination R^2 are exhibited:

Proxies	e_{max}	R^2
FOPT	0,4451	0,6790
FGPT	0,1965	0,9334

Table 13 – Maximum errors and coefficients of determination for each proxy

The reported values have been computed by evaluating both the validation and the design sites, since the purpose is to evaluate the goodness of the predictor.

Once that the building process has been completed and, consequently, 55 regression coefficients have been generated (taking into account linear, cross and square values), it is possible to proceed with the optimization stage.

5.4.4. Robust proxy optimization

The global optimal design depends on the objective functions and constraints restricting the design space (see subsection 5.2.1). However, these functions always represent approximations of the real world and as long as one does not have detailed knowledge of the errors contained in the model, it cannot be inferred that the model optimum can be mapped to the true optimum. Thus, being too precise might waste time and resources reusable at possible later design stages [69].

The considered "system" is to be designed in such a way that it generates desired outputs $f_i(\boldsymbol{d}, \boldsymbol{u})$ of which behavior can be controlled only to a certain extent by the design variables $\boldsymbol{d} = d_1, d_2, \dots, d_n$, due to the several uncertainties $\boldsymbol{u} = u_1, u_2, \dots, u_m$ beyond the direct control of the designer. These uncertainties have been mathematically modeled, as seen, in a probabilistic way, i.e. probability distributions (uniform) have been initially chosen to describe the likelihood by which the uncertain parameters vary.

The aim of a single-objective robust optimization is to find the values of the decision variables $\boldsymbol{d}$ which lead to an optimal value of the only objective function $f(\boldsymbol{d}, \boldsymbol{u})$ and are robust in respect to the uncertain variables $\boldsymbol{u}$. Thus, let us consider for the moment that the function f corresponds to the FOPT. The process is done by computing the expected values (E) of FOPT in respect to $\boldsymbol{u}$ (as said) and seeking out the set of $\widehat{\boldsymbol{d}}$ that maximizes those values ($argmax_{\boldsymbol{d}}$ refers to the $\boldsymbol{d}$ "arguments" characterizing the maximized function). So, the robust optimization is formalized as:

$$\hat{\boldsymbol{d}} = argmax_{\boldsymbol{d}}\left[E_{\boldsymbol{u}}\left(FOPT(\boldsymbol{u},\boldsymbol{d})\right)\right] \tag{5.22}$$

where the expectations of FOPT can be approximated by computing a sample average as follows:

$$\hat{\boldsymbol{d}}_{\boldsymbol{a}} = \overline{FOPT}_{\boldsymbol{u}} = argmax_{\boldsymbol{d}}\left[\frac{1}{N_{\boldsymbol{u}}}\sum_{i=1}^{N_{\boldsymbol{u}}}\left(FOPT(\boldsymbol{u}_i,\boldsymbol{d})\right)\right] \tag{5.23}$$

and $\hat{\boldsymbol{d}}_{\boldsymbol{a}}$ represents the approximated value of $\hat{\boldsymbol{d}}$ and $N_{\boldsymbol{u}}$ is the number of samples generated by varying the uncertain variables and setting the decision ones to random values which are subsequently explored to seek out the optimal combination.

Anyhow, the field of *robust multi-objective optimization* is entered here as in this case there is a trade-off between maximum values of FOPT and minimum values of FGPT (see *Fig. 5.16*). This does not introduce a loss of generality for the problem since the minimization of the $FGPT(\boldsymbol{u}_i,\boldsymbol{d})$ equals the maximization of the function $-FGPT(\boldsymbol{u}_i,\boldsymbol{d})$. It is usually possible to establish a relationship of dominance between two decisions according to Pareto. In a maximization problem, a set of decision variables $\boldsymbol{d_A}$ is said to dominate the set of decision variables $\boldsymbol{d_B}$ if, for each objective function f, the value of the function in $\boldsymbol{d_A}$ is higher than, or at most equal to, the value of the function evaluated in $\boldsymbol{d_B}$ and at least one relationship of inequality must be true in the strict sense within the functions. Since $n = 2$ objective functions ($FGPT$ and $FOPT$) are analyzed here, the concept of dominance can be expressed in mathematical terms as:

$$\begin{cases} FOPT(\boldsymbol{d_A}) \geq FOPT(\boldsymbol{d_B}) \\ FGPT(\boldsymbol{d_A}) < FGPT(\boldsymbol{d_B}) \end{cases} \vee \begin{cases} FOPT(\boldsymbol{d_A}) > FOPT(\boldsymbol{d_B}) \\ FGPT(\boldsymbol{d_A}) \leq FGPT(\boldsymbol{d_B}) \end{cases} \tag{5.24}$$

where the decision $\boldsymbol{A}$ is said to dominate the decision $\boldsymbol{B}$.

A decision is said *optimal according to Pareto* when it is not dominated by other decisions and the values of the objective functions deriving from all the Pareto optimal decisions form the *Pareto frontier*. Thus, during the optimization process, the Pareto optimal decisions are desired [70]. These concepts are shown in *Fig. 5.21* by selecting the "body" of data inside the frame of interest (*Fig. 5.18*).

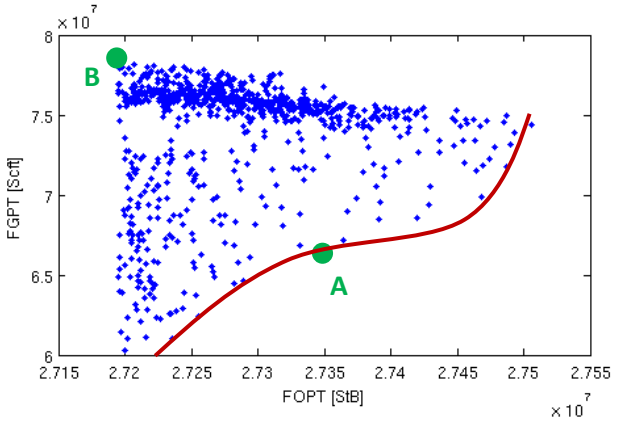

Figure 5 . 21 – Illustration of the concept of dominance

By hypothesizing that the Pareto frontier will be the one represented by a red line, it can be inferred that the decision $\boldsymbol{A}$ dominates all the other decisions belonging to the represented area and is not dominated by any others as a Pareto optimal, while the decision $\boldsymbol{B}$ is dominated by all the other decisions of the area.

The approach selected to carry the multi-objective optimization is recurring to the *aggregate objective function* F, where the partial objective functions are combined by weighed sums to build an unique function [71]:

$$F = \lambda_1 f_1 + \cdots + \lambda_n f_n \tag{5.25}$$

where λ is the relative weight and again f an objective function.

Thus, the problem can be formalized as follows:

$$\widehat{\boldsymbol{d}} = argmax_{\boldsymbol{d}}\left[E_{\boldsymbol{u}}\left(F(\boldsymbol{u},\boldsymbol{d})\right)\right] = argmax_{\boldsymbol{d}}\left[E_{\boldsymbol{u}}\left(FOPT(\boldsymbol{u},\boldsymbol{d}) - \lambda \cdot FGPT(\boldsymbol{u},\boldsymbol{d})\right)\right] \tag{5.26}$$

where for simplicity the weight associated to the FOPT has been set to 1 and only the one associated to the FGPT is used, carrying all the information about the balance. Obviously, the expected values can be approximated as shown in Eq. 5.23 and at varying values of λ several sites should be found lying on the Pareto frontier.

Up to this point, it is clear that many "random" values of both decision and uncertain variables are needed. Thus, the Latin Hypercube Sampling is once again applied here to compute $N_{\boldsymbol{d}} = 100$ random combinations of decision variables and $N_{\boldsymbol{u}} = 100$ random combinations of uncertain variables as well uniformly distributed. After executing the sampling process, each set of decision variables $\boldsymbol{d}$ is combined with all the sets of uncertain variables $\boldsymbol{u}$, so that a total of $N_{\boldsymbol{u}} \cdot N_{\boldsymbol{d}} = 10000$ sites are predicted. Then, for each dataset $\boldsymbol{d}$, the FOPT and FGPT values are averaged over the uncertain variables, obtaining 100 values of $\overline{FOPT}_{\boldsymbol{u}}$ and just as many of $\overline{FGPT}_{\boldsymbol{u}}$. The results are plotted in *Fig. 5.22*.

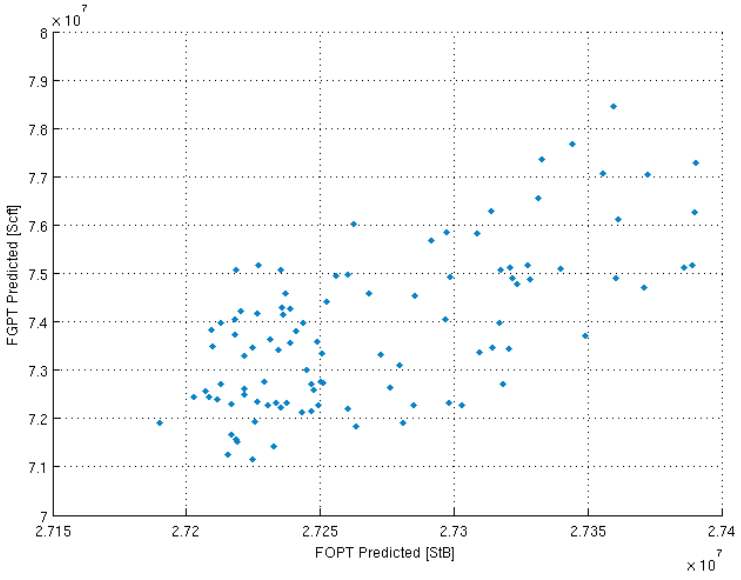

Figure 5 . 22 – Average predicted values of FOPT and FGPT plotted

As noticeable, this robust averaging process led to a big reduction of the ranges characterizing the variations of the outcomes, endorsing the fact that the main cause of such a big frame of variation (see *Fig. 5.16*) is due to the uncertainties. Moreover, it is interesting to look at how the decision variables are now distributed among the averaged predicted sites (see *Fig. 5.23*).

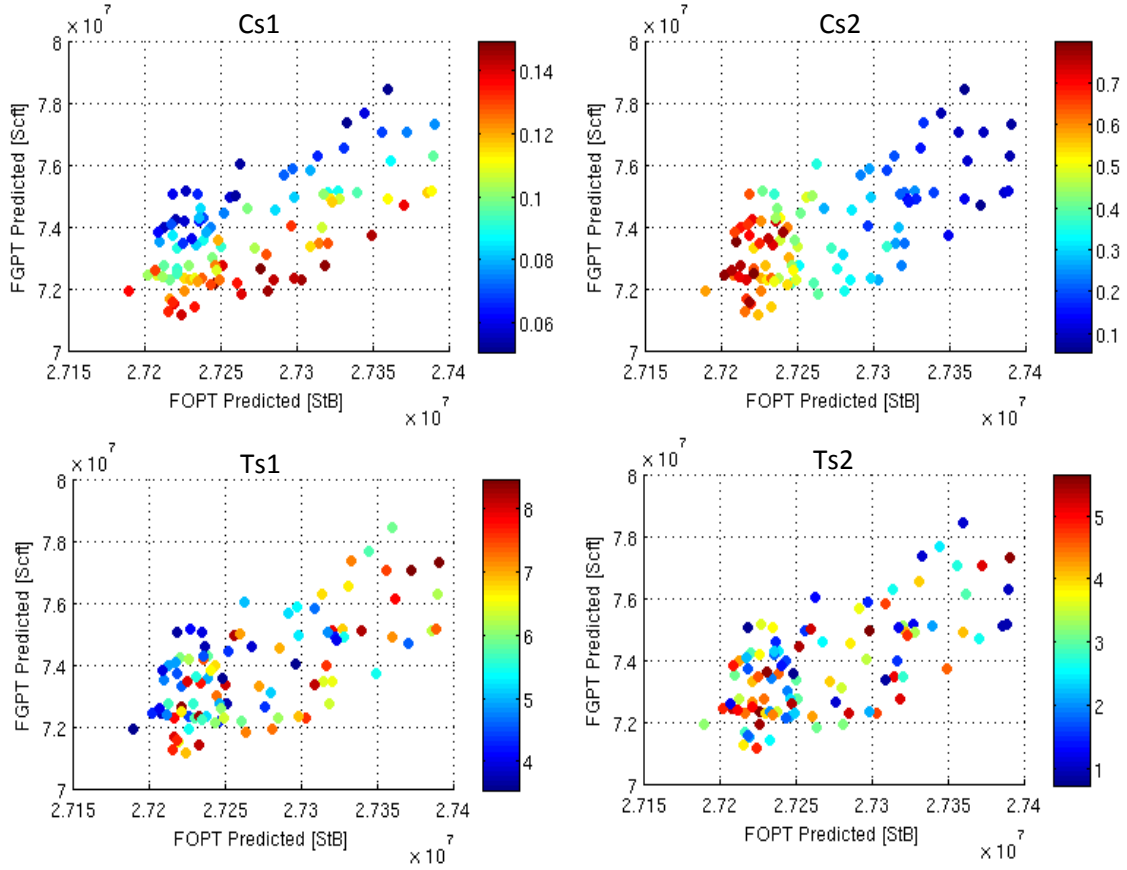

Figure 5 . 23 – Illustration of the averaged predicted sites as functions of the decision variables

Apparently, the concentrations of both the first and second slugs highly impact on the trend of the sites. In fact, it is clear from the color gradient that high values of concentration for the first slug correspond to low values of FGPT, while it seems that the FOPT is only weakly affected by this parameter. The opposite considerations can be inferred for the second slug, where it appears evident that low concentrations lead to high values of FOPT while the gas is less affected by this trend. It is anyway certain that a trade-off exists between FOPT and FGPT. On the other hand, the time-length of the first slug shows a weaker relationship with the trend of the predicted sites, but it is still noticeable a certain color gradient (blue sites characterized by short slugs are not found amongst the highest-FOPT sites), while the variable T_{s2} does not show any particular relationship and the colors of the sites appear definitely randomly dispersed. It has to be highlighted that these observations are possible because of the drastic reduction of uncertainties given by the averaging process.

Thus, according to Eq. 5.26, a set of values for the coefficient λ is to be computed now in order to find the optimal values lying on the frontier. In order to solve this task, it has been considered that a standard cubic meter of oil might correspond to, in terms of economic benefits, 5-to-100 standard cubic meters of reduced gas (having taken into account the conversion factor from standard cubic feet to cubic meters) and the maximum of the function F (Eq. 5.25) has been found amongst the computed predicted sites:

$$F_{max} = \max(\overline{FOPT}_{\boldsymbol{u}} - \lambda \cdot \overline{FGPT}_{\boldsymbol{u}}) \tag{5.27}$$

The resulting Pareto-optimal sites are shown in *Fig. 5.24* and highlighted through a red dotted line. It is interesting to notice that for the whole range of reasonable values of λ selected, all the sites lie inside the frame of interest. Anyway, it can be inferred that, in descending order of FGPT (and FOPT) values, the first and the second slugs are dominated by the third one, as the oil recovered at the final step is almost the same, while the FGPT values change significantly (the scales of the axes are different). Similar observations can be inferred for the final site and are evident also in Table 14. In fact, as the equivalent volume of gas increases, the value of FOPT increases as well, since it becomes more and more important the reduction of oil produced compared to the gas reduced (Eq. 5.27 becomes a mere oil optimization when the equivalent volume is ∞, i.e. $\lambda = 0$), and case #1 and #2 have unlikely high values of equivalent volumes.

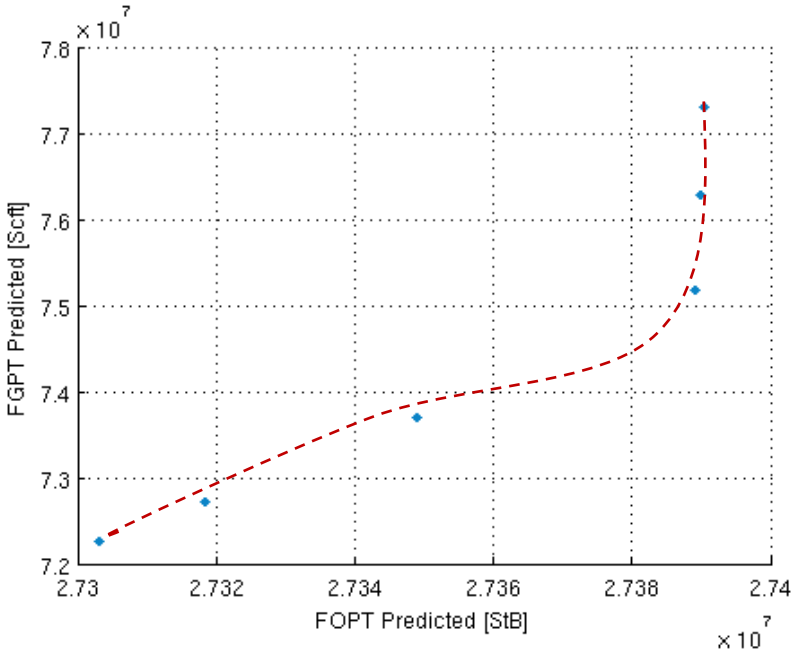

Figure 5 . 24 – Average values inside the frame of interest and approximated Pareto frontier (red)

The values are reported in the following table by exhibiting also the economic equivalence between volumes of oil produced and volume of gas reduced used to compute the λ's, the recovery factors (RF) and the percent reductions in total gas produced compared to the WAG best case$(\Delta FGPT_{WAG})$:

Case [#]	Eq. volume [Sm^3_{gas}/ Sm^3_{oil}]	Av. FOPT [StB]	Av. FGPT [Sft^3]	RF [%]	$\Delta FGPT_{WAG}$ [%]
1	>445	27.390.491	77.295.217	43,32	-8,11
2	255-444	27.390.038	76.277.238	43,32	-9,32
3	6,51-254	27.389.211	75.173.675	43,32	-10,63
4	5,71-6,5	27.349.177	73.707.362	43,25	-12,37
5	5,36-5,7	27.318.402	72.723.226	43,2	-13,54
6	<5,36	27.303.217	72.266.222	43,18	-14,08

Table 14 – Equivalent barrels of reduced gas for the computation of λ and corresponding average FOPT and FGPT

The reported results are highlighted in *Fig. 5.24* by a red curve representing the predicted frontier. Once that the process has been completed, it is necessary to validate the responses coming from proxies by a comparison with the outcomes really simulated. Since each obtained result has been averaged over 100 predicted sites, the validation is to be executed as an average of 100 simulations sampled through LHS design as well. For this purpose, the arguments (i.e. the decision-variables values) of three "inner" cases (the extreme sites are not simulated because of the required time needed and because are dominated by the others) reported in Table 14 are selected for the simulations and shown in the following table:

Case [#]	C_{s1}[lb/StB]	C_{s2} [lb/StB]	T_{s1} [days]	T_{s2} [days]
3	0,111	0,121	7,372	0,896
4	0,144	0,135	5,458	4,555
5	0,147	0,238	6,342	5,147

Table 15 – Decision parameters of the four Pareto-optimal sites used to generate the simulations

Thus, 300 simulations are run and the outcomes are averaged obtaining the following values:

Case [#]	Av. FOPT [StB]	Av. FGPT [Sft^3]	RF [%]	$\Delta FGPT_{WAG}$ [%]	ERR_{FOPT} [%]	ERR_{FGPT} [%]
3	27.373.973	75.456.304	43,29	-10,29	+0,056	-0,375
4	27.346.042	73.757.832	43,25	-12,31	+0,011	-0,068
5	27.325.381	72.958.856	43,21	-13,26	-0,026	-0,323

Table 16 – Decision parameters of the four Pareto-optimal sites used to generate the simulations

As can be noticed, the predicted average values do not match perfectly with the averaged simulated outcomes, especially for the case #3. Obviously, the recovery factors seem unvaried, but this is due to the fact that the considered ranges of FOPT are much smaller than the variations pertinent to the FGPT (as seen in the previous figures where the scales of the axes were considerably different). This fact also partly justifies why the errors of the proxies in predicting the values of FOPT, computed as:

$$ERR_{FOPT} = \frac{predicted\ av.\ value - simulated\ av.\ value}{simulated\ av.\ value} \tag{5.28}$$

and FGPT (ERR_{FGPT} is computed in the same way as the FOPT error) are one order of magnitude different. Better visual evidence is given by *Fig. 5.25* which compares the predicted Pareto-frontier with the three averaged sites forming the simulated frontier.

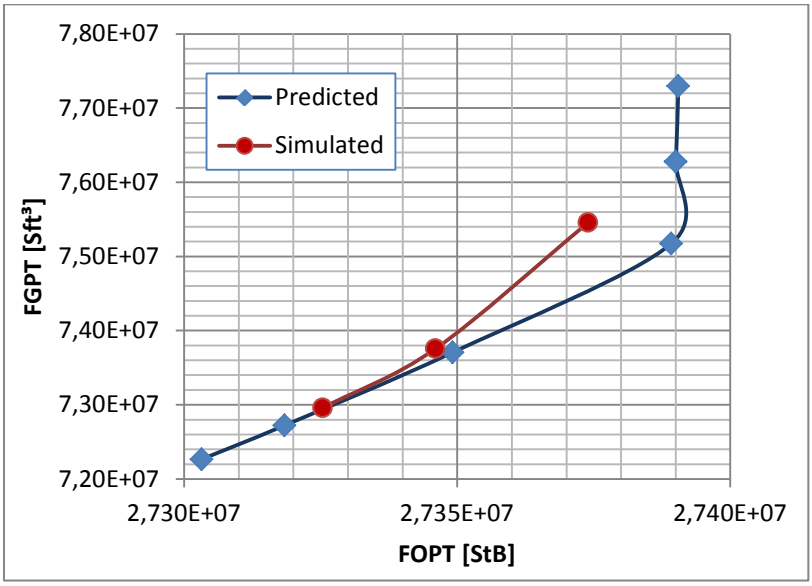

Figure 5 . 25 – Illustration of the comparison between simulated and predicted frontier

As can be seen, the simulated frontier distances itself from the predicted one for high values of FOPT and FGPT. By looking at the frame of interest and its consequent scales, it can be inferred that this is more a problem related to the predicted FOPT, which tends to be overestimated, than a problem related to the FGPT. This fact was slightly presumable from *Fig. 5.19*, where a representation of the proxy with its validation sites shows a denser cluster of sites lying above the straight bisector line, supporting an overestimate of predicted values. Furthermore, it is worthwhile to compare also both the outcomes in terms of average dispersion by the following estimate of the relative standard deviation (*RSD*):

$$RSD_{\%} = \frac{\left[\sqrt{\frac{\sum_{i=1}^{n}(x_i - \bar{x})^2}{n-1}}\right]}{\bar{x}} \cdot 100 \tag{5.29}$$

where:
x is the term constituting the sample, which is represented by either FOPT or FGPT;
n is the number of sites, i.e. 100 in this case;
$\bar{x}$ is the average value of either FOPT or FGPT.
Eq. 5.29 is evaluated for both simulated and predicted values to verify the accuracy of the proxies, since systematic errors could be neglected by the averaged values, and the results are reported in the following table:

	Simulated		Predicted	
Case [#]	**RSD_{FOPT} [%]**	**RSD_{FGPT} [%]**	**RSD_{FOPT} [%]**	**RSD_{FGPT} [%]**
3	0,51	11,73	0,66	12,16
4	0,96	13,75	0,78	13,67
5	1,00	13,98	0,81	13,94

Table 17 – relative standard deviations of FGPT and FOPT in both simulated and predicted cases

It is noticeable that, comparing the simulated and the predicted cases, the RSD_{FGPT} values match almost perfectly for cases #4 and #5, i.e. in addition to a good prediction of the average values also the dispersion of the sites is almost identical, while slight difference exists for the values of case #3. On the other hand, the difference between the values of RSD_{FOPT} consists of tenths of a percent (instead of hundredths in the case of FGPT case #4 and#5) which is not a big difference but not negligible since the required accuracy for the FOPT is higher if compared to the FGPT as noticeable from the scales represented in the previous figures.

Up to this point, what has been done through the analysis is an approximation of the Pareto frontier through a broader multi-objective screening to locate the most promising "areas". In fact, a formal optimization would require the application of optimization designs (such as genetic algorithms) leading to a specific optimal site, but since this is not worthwhile (λ's exist but not evaluated yet) and since the required computational time is extremely long (each sites would be the result of 100 averaged sites), the proposed approach is a good compromise between time and usefulness. Thus, taking into account the results obtained so far, it is possible to infer that a good reduction in gas produced by the field can be achieved compared to a standard WAG scenario, but the FOPT seems to almost not be affected by the foam, as the increase of the recovery factor is hundredths of a percent in terms of order of magnitude. As a consequence, the FOPT acts more like a constrain for the FGPT reduction (as drastic reductions in gas produced correspond to drastic reduction in oil produced as well) and, once that good estimates about the equivalent benefits arising from a produced-gas volume reduction in terms of produced-oil volumes (i.e. an estimated value of λ) will be available, a certain average Pareto-optimal value will be computable. The foam injection is then a solution which can be effective and lead to a beneficial reduction in terms of gas produced, especially where the gas has to be disposed inside the reservoir and its flow rates depend on the other fields in a not fully controllable way.

Anyhow, it is possible to examine in a deeper way the benefits deriving from the foam injection inside FIELD α representing a possible circumstance.

5.5. Foam-effects visualization

In order to analyze what are the results of the foam injection inside the reservoir, it is necessary to select a reasonable case to be simulated with all the possible outcomes to analyze (not available yet as the previous data files have been extremely simplified to minimize the computational time required). So, a case with FOPT and FGPT values close to the ones obtained for the averaged Pareto-frontier sites is chosen to be consistent with the previous analyses. In particular, the following parameters have been chosen, leading to outcomes similar to Case #4:

	Variable	Value
Decision Variables	C_{s1} [lb/StB]	0,147
	C_{s2} [lb/StB]	0,238
	C_{s3} [lb/StB]	1
	T_{s1} [days]	6,342
	T_{s2} [days]	5,147
	T_{s3} [days]	6
Uncertain Variables	M_r^{ref} (fmmob)	245,4
	f_w (epdry)	687,3
	S_w^{lim} (fmdry)	0,122
	e_o (epoil)	1
	S_o^m (fmoil)	0,3
	e_s (epsurf)	0,704
	C_s^{ref} [lb/StB] (fmsurf)	0,084
	C^{ads} [lb/StB] (ad)	0,00002

Table 18 – Values selected to run the simulation with the foam injection

Thus, a graphical comparison between the simulated foam-case and the best WAG scenario can be outlined and is shown in the following figures.

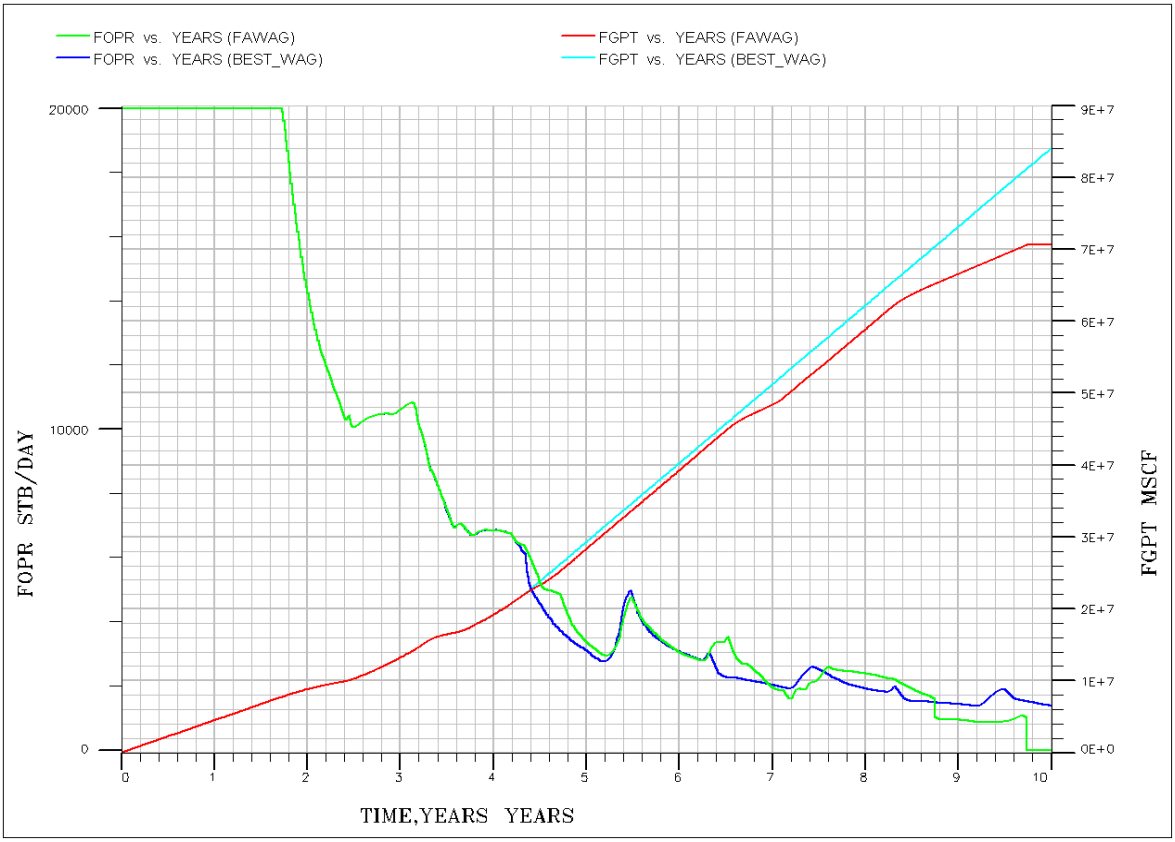

Figure 5 . 26 – Comparison between the foam-case and the best WAG case in terms of FOPR and FGPT

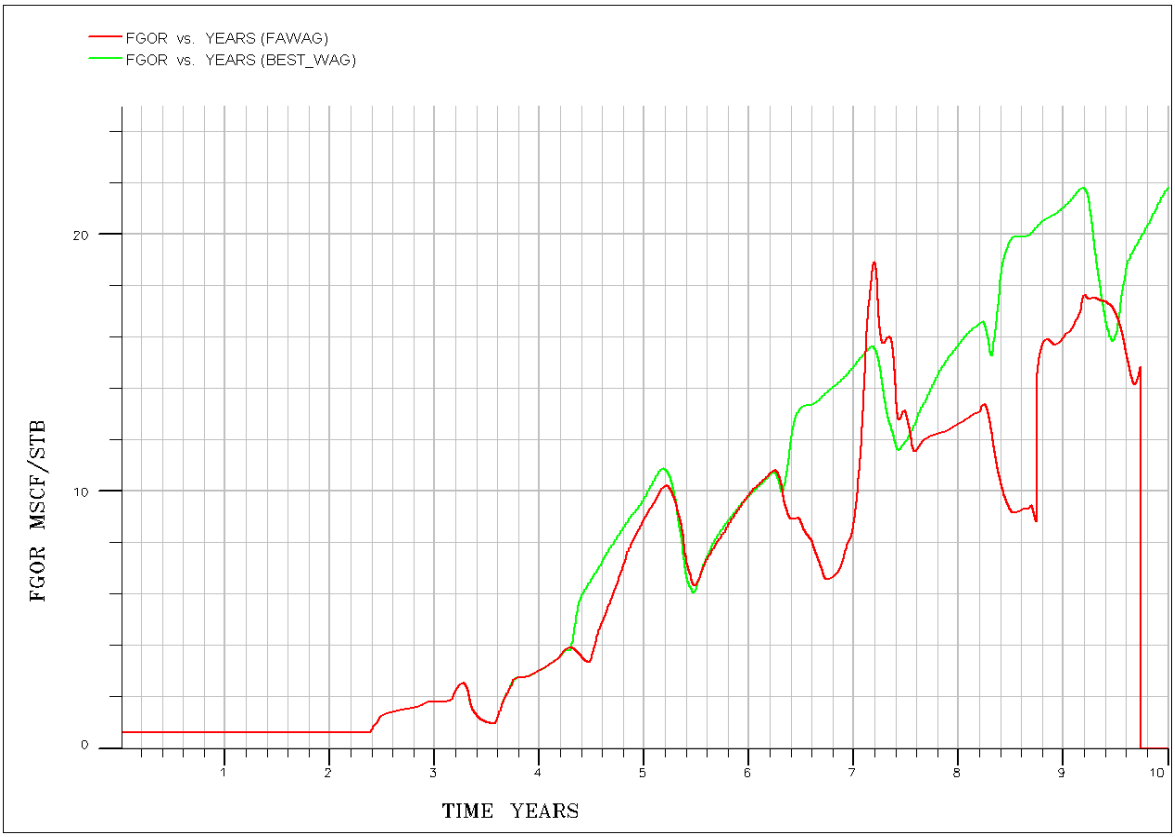

Figure 5 . 27 – Comparison between the foam-case and the best WAG case in terms of GOR

It is evident from the profiles shown in *Fig. 5.26* the reduction of gas produced, in terms of total volumes (FGPT – cyan and red lines) where a scissor shape is noticeable supporting the efficacy of the foam in blocking the gas inside the reservoir. It is also interesting to look at the gas-to-oil ratio (GOR) profiles in *Fig. 5.27*, where the FAWAG-line (red) lies almost continually below the WAG-line (green) except for a short period between the seventh and the eighth year after the surfactant injection occurring at 6,85 years, supporting a probable initial fingering that is gradually reduced. Moreover, it should be taken into account that gas coning effects are not fully represented by the model as in the WAG case the choking of the producers leads to a not realistic reduction in the oil produced, which should, but it does not, tend to tiny values once that the constrains on the wells are removed. Thus, the benefits generated by the foam application can be seen from an even more optimistic point of view.

Once that the beneficial effects of the foam on the gas have been visualized, it is possible to look at the oil profiles. For this purpose, *Fig. 5.26* shows the oil production rates within the 10-years range. As can be seen, the oil-rate profile of the FAWAG case (green) lies mostly above the one representing the best-WAG scenario, while it is overcome after 8,85 years and then it drops abruptly before reaching the tenth year, i.e. both the producers have been shut after that date. These problems start exactly when the third slug of surfactant is injected inside FIELD α, thus, it is worthwhile to look at the well water cuts shown in *Fig. 5.28* before drawing any conclusions.

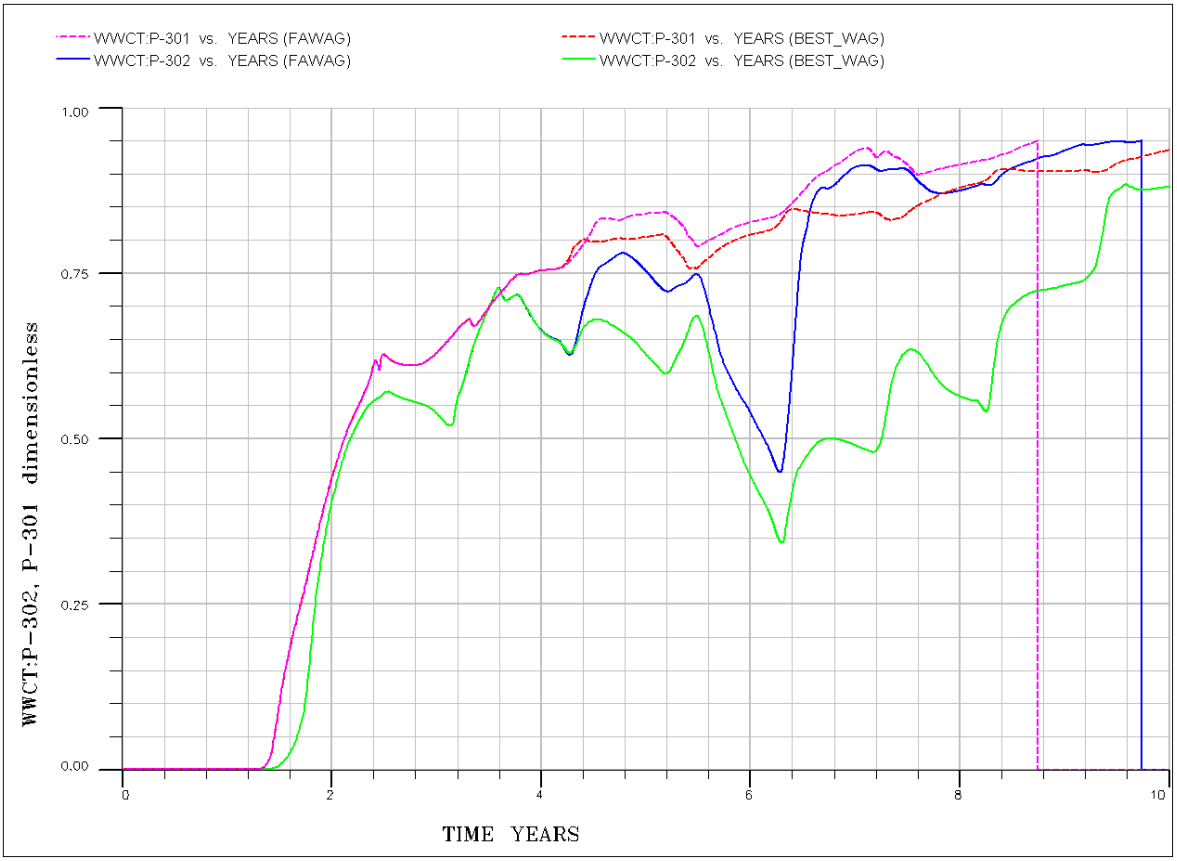

Figure 5 . 28 – Comparison between the foam-case and the best WAG case in terms of water cuts of each producer

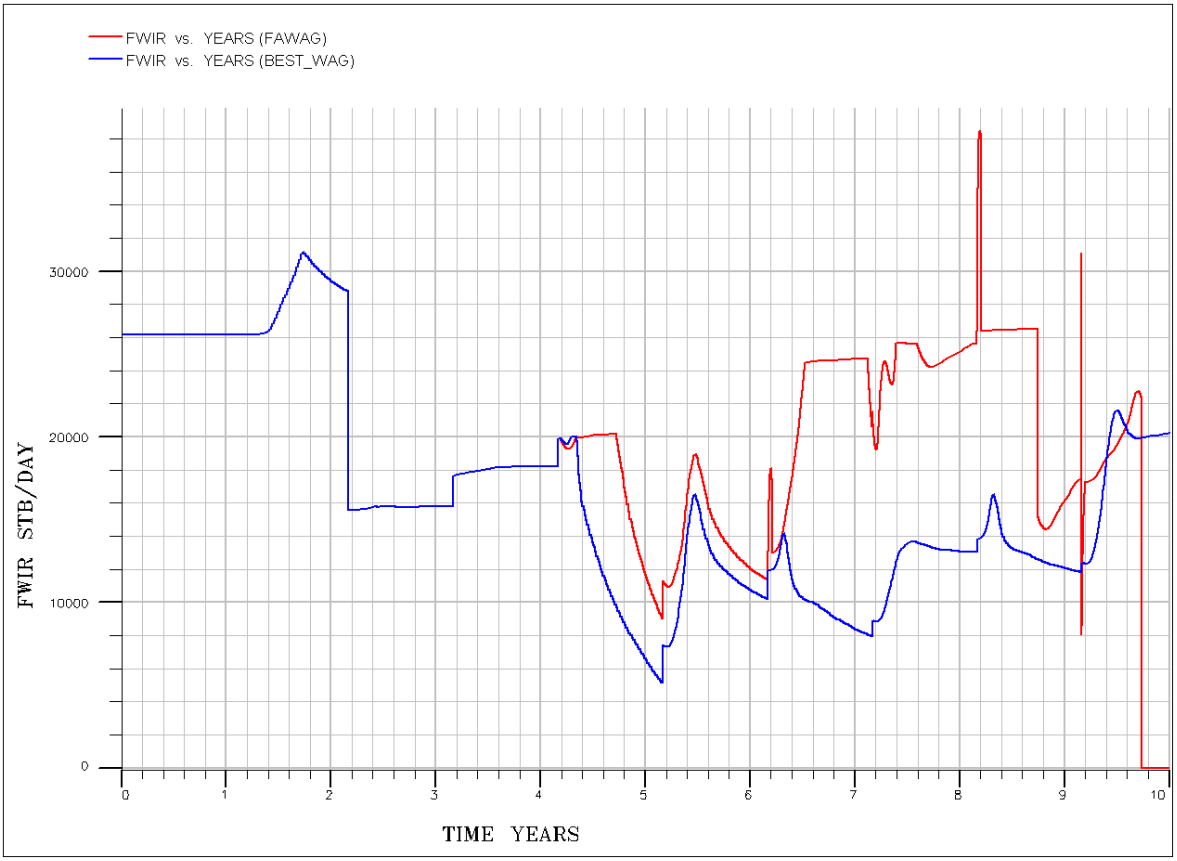

Figure 5 . 29 – Comparison between the foam-case and the best WAG case in terms of field water injection rates

It is immediately evident that the producer P-301 (purple dotted line) experiences a shut-off at time of the third surfactant slug injection and P-302 (blue line) is shut as well right before the tenth year because the water cut of each well reaches the limiting value of 95%. This is due to the fact that more water is injected and produced, compared to the WAG case (see *Fig. 5.28* and *Fig. 5.29*), to guarantee the voidage replacement, as more gas is "too effectively" entrapped inside the reservoir and, as a consequence, less gas is cycled (the volumes of injected gas are defined by the recycling and the amounts coming from the other fields). In fact, the injectors do not even experience problems with injectivity in terms of BHP (which does not reach constraint values), endorsing the fact that the problem is explained by what just said. Thus, further analyses concerning the third slug are needed once that a single optimal site can be computed, in order to avoid a shut off of both the producers and guarantee the optimality even after the end of the considered time frame.

5.6. Future developments

Up to this point, it can then be inferred that interesting results have been obtained and can be even improved if further analyses are conducted for the third slug. In fact, the "goodness" of the obtained results are valid within the considered time frame, but if the

frame is enlarged, it is probable that the FOPT simulated for the FAWAG cases will drop below the best WAG scenario, corrupting the optimality of the reported findings. Thus, what has been found so far has to be improved by better analyzing the characteristics of the third slug once that a single optimal value is available, since the randomly distributed findings for the third slug have not allowed a previous optimization.

The reported analysis can be highly improved once that reliable laboratory results are available. In fact, the uncertainties can be extremely reduced as three parameters (usually M_r^{ref}, f_w and S_w^{lim}) are computed after a best-fitting of the apparent viscosities for different foam qualities [33, 36, 38, 59-60, 63-66]. Furthermore, reliable tests are necessary to verify whether the selected surfactant and its interaction with the reservoir pore spaces generate parameters-values included within the chosen ranges, otherwise it will be necessary to seek out other, more effective, surfactants.

Then, after having verified the feasibility of the application by empirical results, the real full field application can be considered, as it would be impossible to isolate a pair of producer and injector for a pilot project because of the limited dimensions of the analyzed reservoir. Thus, serious attention should be paid to interventions on the reservoir to solve possible problems arising during the foam application, such as the injection of methanol to dissolve the foam formed inside the porous media in case of plugging phenomena. In fact, it is important to highlight that the reservoir is located offshore and that an FPSO unit will be used as operational base for the exploitation and, as a result, many problems could arise during the surfactant injection from an auxiliary vessel.

6. Conclusions

This dissertation is focused on the analysis of a Foam-Assisted-Water-Alternating-Gas (FAWAG) injection scenario to improve oil recovery and minimize gas production in a Angolan offshore reservoir (FIELD α).

The field is planned to be developed by means of WAG technologies. The development plan expects gas injection to increase oil recovery and dispose the gas itself, due to absence of gas export facilities. However, this scenario is associated to the risk of premature gas breakthrough jeopardizing oil production. The foam application would decrease the mobility of the gas, leading to a reduction of produced gas and to an increase of oil recovered. For this purpose, operational parameters, such as duration of gas and water cycles, have been tuned to obtain an optimal WAG scenario to be used as the base case.

The FAWAG optimization has been divided into different phases. Firstly, a set of parameters influencing the process have been classified into two main groups, on the basis of the empirical model used: uncertain and decision variables. Sensitivity analyses have then been carried out to sort the variables influencing the results. A first nominal optimization on produced oil has been completed, leading to a reduction of the parameters-range.

Secondly, a robust analysis on both produced oil and gas has been conducted to reduce the uncertainties through a multi-run-workflow (2000 simulations). A Pareto optimal frontier has been found, endorsing the trade-off characterizing the optimization process of produced oil and gas. Proxy models have been built and used for a multi-objective function optimization. Thus, a final set of simulations has been performed to confirm the accuracy of the proxies selected and to verify the benefits deriving from foam generation inside the reservoir.

From an analysis of the results, the produced gas has shown a significant volumes reduction (in terms of average values). On the other hand, the oil optimization has highlighted small increases with respect to the reference case. This fact is attributed to the strong effect of the water injection, which leads to high values of water cut for the producers after few years. Anyhow, oil-related results have been used to reduce decision parameters ranges. Within this environment, it has been possible to develop a robust analysis of both the objective functions simultaneously.

To allow a reasonable analysis in terms of computational time, only foam model related uncertainties have been considered. This aspect represents the main limitation of the work that might be anyway overcome by a thorough analysis of the uncertainties once that further information will be available (additional geological data from future drilling campaign, data from early production stage, economics of gas recycling, etc.).

Some observations can also be outlined about the optimization process. First and foremost, to improve the robustness of the analysis, also the variance of each objective function should be minimized. This improvement implies the addition of two objectives and, as a consequence, an increase of the complexity that is considered unmanageable. In fact, a variance minimization would be possible in case of less dominant uncertainties. But, in this case, since the accuracy of the oil-related proxy is low, the complexity of the problem would be unreasonably increased. Secondly, a possible improvement would be to optimize the net present value (NPV) instead of the total volumes produced (FOPT and FGPT).To perform this optimization more data, not currently available, are required. Furthermore, it would represent a significant added value to the analysis only in case of non-monotonic functions relating NPV to both FGPT and FOPT. But, as this is a quite seldom situation, the reported analysis is considered thorough.

Thus, it is clear that further analyses conducted in laboratories are required to verify the effectiveness of selected surfactants and to increase the accuracy of the computational analysis once that the benefits deriving from the foam application have been simulated positively. Moreover, the process applied to study FIELD α can be used as well to investigate possible applications of foam in other reservoirs.

Appendix A

A.1. ECLIPSE data file

```
--
-------------------------------------------------------------------------
RUNSPEC
--
-------------------------------------------------------------------------
TITLE
FIELD_ALPHA

FIELD

DIMENS
  118 107 45   /
VFPPDIMS
     20     10      10      10    10      3     /
VFPIDIMS
20  10  5  /

WELLDIMS
      5    200     1      10      /

START
  1 NOV 2014 /

DISGAS
WATER
OIL
GAS

ENDSCALE
  /

MULTOUT

TABDIMS
      3      1     25      25     1      25     25          /

EQLDIMS
    1                                 /

REGDIMS
   6  2*  3 2* 3                      /

FAULTDIM
1000 /

UNIFOUT
UNIFIN
```

```
NSTACK
25  /

MESSAGES
3* 10000 4* 100000 100000 /

FOAM

LICENSES
'foam' /
/

OPTIONS
187* 1 /

--
**********************************************************************
GRID
--
**********************************************************************
GRIDFILE
  0 0 /

INIT

NEWTRAN

NOECHO

INCLUDE
 '../INCLUDE/2012-1_UPSIDE_RUN1_GRID.GRDECL' /

INCLUDE
 '../INCLUDE/NTG_RISK_6.GRDECL' /

INCLUDE
 '../INCLUDE/PORO_RISK_6.GRDECL' /

INCLUDE
 '../INCLUDE/PERMX_RISK_6.GRDECL' /

INCLUDE
'../INCLUDE/FLUXNUM_RISK_6.GRDECL' /

COPY
'PERMX' 'PERMY' 1 118 1 107 1 45 /
'PERMX' 'PERMZ' 1 118 1 107 1 45 /
'FLUXNUM' 'OPERNUM' 1 118 1 107 1 45 /
/
MULTIREG
 PERMZ 0.01   1 F/
 PERMZ 0.114  2 F/
 PERMZ 0.703  3 F/
/
```

```
INCLUDE
'../INCLUDE/2012-1_UPSIDE_RUN1_PROP_ACTNUM.GRDECL' /

INCLUDE
'../INCLUDE/2012-1_UPSIDE_RUN1_FAULTS.GRDECL' /

 MULTFLT
'FAULTI_1'  0 /
'FAULTI_2'  0 /
'FAULTI_3'  0 /
'FAULTI_4'  0 /
'FAULTI_5'  0 /
'FAULTI_6'  0 /
/

MESSAGES
3* 10000 4* 100000 100000 /

EQUALS

NTG     0   1    118  1  107  1  15 /
NTG     0   1    42   1  107  1  45 /
NTG     0   110   118  1  107  1  45 /
NTG     0   1    118   1  24  1  45 /
NTG     0   1    118   78  107  1  45 /
/


--
************************************************************************
EDIT
--
************************************************************************
--
************************************************************************
PROPS
--
************************************************************************

NOECHO

INCLUDE
'../INCLUDE/SWL_RISK_6.GRDECL' /

MAXVALUE
SWL  0.819  1  118  1 107 1 45  /
/

INCLUDE
'../INCLUDE/PVT.GRDECL'/

INCLUDE
'../INCLUDE/SCAL.INC'/
```

```
OPERATE
SGU   1  118  1 107 1 45   'MULTA'  SWL   -1   1  /
/

EQUALS
'SGL'     0.00    1  118  1 107 1 45 /
'SGCR'    0.03    1  118  1 107 1 45  /
/

COPY
SWL  SWCR   1  118  1 107 1 45   /
/

EQUALREG
 SOWCR 0.134  1 F /
 SOWCR 0.112  2 F /
 SOWCR 0.107  3 F /
/

EQUALREG
 KRWR 0.038  1 F /
 KRWR 0.216  2 F /
 KRWR 0.461  3 F /
/

EQUALREG
 KRO 0.196  1 F /
 KRO 0.585  2 F /
 KRO 0.820  3 F /
/

OPERATER
SOWCR 1 'MAXLIM' SOWCR 0.18 /
SOWCR 2 'MAXLIM' SOWCR 0.18 /
SOWCR 3 'MAXLIM' SOWCR 0.18 /
/

MESSAGES
3* 10000 4* 100000 100000 /

FOAMOPTS
WATER FUNC /

FOAMFRM
__FMMOB__ /
__FMMOB__ /
__FMMOB__ /

FOAMFSC
__FMSURF__  __EPSURF__ /
__FMSURF__  __EPSURF__ /
__FMSURF__  __EPSURF__ /

FOAMFSO
__FMOIL__  __EPOIL__ /
```

```
__FMOIL__  __EPOIL__  /
__FMOIL__  __EPOIL__  /

FOAMFSW
__FMDRY__  __EPDRY__  /
__FMDRY__  __EPDRY__  /
__FMDRY__  __EPDRY__  /

FOAMROCK
1  143.584 /
1  143.584 /
1  143.584 /

FOAMADS
0.000  0.0
2  __AD__  /
/
0.000  0.0
2  __AD__  /
/
0.000  0.0
2  __AD__  /
/
--
************************************************************************
REGIONS
--
************************************************************************
NOECHO

COPY
  'FLUXNUM' 'SATNUM'  1 118 1 107 1 45 /
/

INCLUDE
'../INCLUDE/FIPNUM_REGIONS.GRDECL' /

EQLNUM
 568170*1 /

MESSAGES
3* 10000 4* 100000 100000 /

--
************************************************************************
SOLUTION
--
************************************************************************
NOECHO

EQUIL
    8343.83    3769.3     8547.24   0    100     0     1     1*
10 /
RSVD
8664.7    0.615
```

```
8800      0.615
/

MESSAGES
3* 10000 4* 100000 100000 /

RPTRST
  BASIC=5 FIP FREQ=6 /

RPTSOL
  RESTART=2 FIP=2 /

--
************************************************************************
SUMMARY
--
************************************************************************
NOECHO

INCLUDE
'../INCLUDE/SUMMARY.INC' /

MESSAGES
3* 10000 4* 100000 100000 /

--
************************************************************************
SCHEDULE
--
************************************************************************
NOECHO

RPTRST
BASIC=5 FIP FREQ=6  /

MESSAGES
3* 10000 4* 100000 100000 /

INCLUDE
'../INCLUDE/VLP/NOV_2012/LM20_301_op1.Ecl' /


INCLUDE
'../INCLUDE/VLP/NOV_2012/LM20_302_op2.Ecl' /

INCLUDE
'../INCLUDE/VLP/NOV_2012/I401.Ecl' /

INCLUDE
'../INCLUDE/VLP/NOV_2012/I402.Ecl' /

INCLUDE
'../INCLUDE/VLP/NOV_2012/I401_tbg 5 1-2_gas10000.Ecl' /
INCLUDE
'../INCLUDE/VLP/NOV_2012/I402_tbg 5 1-2_gas10000.Ecl' /
```

```
TUNING

HRUPT
   1*     5   1*    1*   1*      1*    1*     1* /

   0.1   0.001  1.0E-7 0.0001  10.0   0.01  1.0E-6  0.001 0.001  /

   12      1      1*     1      8     8   /

GRUPTREE
  'GROUP 1' FIELD /
/

WELSPECS
   P-301 'GROUP 1' 64 49 1* OIL /
   P-302 'GROUP 1' 70 57 1* OIL /
   I-401 'GROUP 1' 80 49 1* WATER /
   I-402 'GROUP 1' 83 42 1* WATER /
/
COMPDAT
  P-301 65 49 1 1 OPEN 1* 2.1456E+001 0.82292 14267.78 0.50 1* Z 27.70 /
  P-301 65 49 2 2 OPEN 1* 1.1932E+001 0.82292 7699.43  0.50 1* Z 24.09 /
  P-301 64 49 4 4 OPEN 1* 4.5041E-002 0.82292 21.73    0.50 1* Z 7.60 /
  P-301 64 49 5 5 OPEN 1* 8.8350E-001 0.82292 509.69   0.50 1* Z 14.84 /
  P-301 64 49 6 6 OPEN 1* 3.1499E-002 0.82292 16.98 0.50 1* Z 11.34 /
  P-301 64 49 7 7 OPEN 1* 1.8581E-001 0.82292 105.16 0.50 1* Z 13.74 /
  P-301 64 49 8 8 OPEN 1* 1.0398E+000 0.82292 591.83 0.50 1* Z 14.05 /
  P-301 64 49 9 9 OPEN 1* 3.5669E-001 0.82292 225.34 0.50 1* Z 21.89 /
  P-301 63 49 9 9 OPEN 1* 2.0279E-001 0.82292 119.50 0.50 1* Z 16.20 /
  P-301 63 49 10 10 OPEN 1* 2.0274E+001 0.82292 13161.99 0.50 1* Z 24.77/
  P-301 63 49 11 11 OPEN 1* 1.4483E+001 0.82292 9630.12 0.50 1* Z 27.68 /
  P-301 63 48 11 11 OPEN 1* 2.1075E+001 0.82292 13852.77 0.50 1* Z 26.23/
  P-301 63 48 12 12 OPEN 1* 1.4252E+001 0.82292 9131.55 0.50 1* Z 23.32 /
  P-301 63 48 13 13 OPEN 1* 2.3457E+001 0.82292 15219.88 0.50 1* Z 24.70/
  P-301 63 48 14 14 OPEN 1* 1.8232E+001 0.82292 11831.71 0.50 1* Z 24.72/
  P-301 63 48 15 15 OPEN 1* 1.7684E+001 0.82292 11444.80 0.50 1* Z 24.42/
  P-301 63 48 16 16 OPEN 1* 2.3149E+001 0.82292 15051.06 0.50 1* Z 24.94/
  P-301 63 48 17 17 OPEN 1* 1.9166E+001 0.82292 12461.74 0.50 1* Z 24.94/
  P-301 63 48 18 18 OPEN 1* 1.3984E+001 0.82292 9166.61 0.50 1* Z 25.90 /
  P-301 63 48 19 19 OPEN 1* 5.9237E+000 0.82292 3796.08 0.50 1* Z 23.34 /
  P-301 63 48 20 20 OPEN 1* 5.2868E-001 0.82292 338.71 0.50 1* Z 23.31 /
  P-301 62 48 20 20 OPEN 1* 1.6631E+001 0.82292 10966.86 0.50 1* Z 26.63/
  P-301 62 48 21 21 OPEN 1* 4.7307E+000 0.82292 3063.27 0.50 1* Z 24.48 /
  P-301 62 48 22 22 OPEN 1* 7.3422E+000 0.82292 4749.91 0.50 1* Z 24.37 /
  P-301 62 48 23 23 OPEN 1* 1.5558E+001 0.82292 10231.93 0.50 1* Z 26.30/
  P-301 62 48 24 24 OPEN 1* 1.9922E+001 0.82292 13258.19 0.50 1* Z 27.80/
  P-301 62 48 25 25 OPEN 1* 1.6782E+001 0.82292 11063.59 0.50 1* Z 26.59/
  P-301 62 48 26 26 OPEN 1* 9.2085E+000 0.82292 6074.01 0.50 1* Z 26.66 /
  P-301 62 48 27 27 OPEN 1* 1.0380E+001 0.82292 6808.73 0.50 1* Z 25.98 /
  P-301 62 48 28 28 OPEN 1* 1.3127E+001 0.82292 8728.17 0.50 1* Z 27.68 /
  P-301 62 48 29 29 OPEN 1* 2.0361E+000 0.82292 1326.87 0.50 1* Z 25.21 /
  P-301 62 48 30 30 OPEN 1* 8.7924E+000 0.82292 5799.43 0.50 1* Z 26.66 /
  P-301 62 48 31 31 OPEN 1* 9.9487E+000 0.82292 6522.76 0.50 1* Z 25.92 /
  P-301 62 48 32 32 OPEN 1* 9.0522E+000 0.82292 5959.69 0.50 1* Z 26.43 /
  P-301 62 48 33 33 OPEN 1* 1.3531E+001 0.82292 9050.11 0.50 1* Z 28.46 /
  P-301 62 48 34 34 OPEN 1* 8.4020E+000 0.82292 5539.90 0.50 1* Z 26.61 /
  P-301 62 48 35 35 OPEN 1* 4.1022E+000 0.82292 2658.93 0.50 1* Z 24.59 /
  P-301 62 48 36 36 OPEN 1* 2.8792E+000 0.82292 1887.04 0.50 1* Z 25.88 /
```

```
  P-301 62 48 37 37 OPEN 1* 1.5137E+001 0.82292 10131.55 0.50 1* Z 28.56/
  P-301 62 48 38 38 OPEN 1* 7.4163E+000 0.82292 4908.00 0.50 1* Z 27.08 /
  P-301 62 48 39 39 OPEN 1* 4.3296E+000 0.82292 2820.33 0.50 1* Z 25.16 /
  P-301 62 48 40 40 OPEN 1* 2.3814E-001 0.82292 145.12 0.50 1* Z 18.68 /
  P-301 62 48 41 41 OPEN 1* 9.5753E+000 0.82292 6356.15 0.50 1* Z 27.47 /
  P-301 62 48 42 42 OPEN 1* 6.4576E+000 0.82292 4256.49 0.50 1* Z 26.57 /
  P-301 61 48 42 42 OPEN 1* 1.7417E+000 0.82292 1161.48 0.50 1* Z 28.07 /
  P-301 61 48 43 43 OPEN 1* 4.2836E+000 0.82292 2850.35 0.50 1* Z 27.78 /
  P-301 61 48 44 44 OPEN 1* 3.7496E+000 0.82292 2433.67 0.50 1* Z 24.74 /
  P-301 61 48 45 45 OPEN 1* 2.2703E+000 0.82292 1470.67 0.50 1* Z 24.52 /
  P-302 68 59 26 26 OPEN 1* 1.1360E+001 0.82292 7526.17 0.50 1* Z 27.21/
  P-302 68 59 27 27 OPEN 1* 1.7653E+001 0.82292 11684.22 0.50 1* Z 27.10/
  P-302 68 59 28 28 OPEN 1* 1.6738E+001 0.82292 11155.21 0.50 1* Z 27.99/
  P-302 68 59 29 29 OPEN 1* 1.5102E+001 0.82292 10210.58 0.50 1* Z 29.97/
  P-302 68 60 29 29 OPEN 1* 1.2056E+001 0.82292 8154.82 0.50 1* Z 30.03 /
  P-302 68 60 30 30 OPEN 1* 1.6380E+001 0.82292 11030.34 0.50 1* Z 29.40/
  P-302 68 60 31 31 OPEN 1* 1.1981E+001 0.82292 7960.20 0.50 1* Z 27.58 /
  P-302 68 60 32 32 OPEN 1* 1.9859E+001 0.82292 13525.42 0.50 1* Z 31.04/
  P-302 68 60 33 33 OPEN 1* 3.1559E+000 0.82292 2055.75 0.50 1* Z 25.16 /
  P-302 68 60 34 34 OPEN 1* 1.7123E+000 0.82292 1116.50 0.50 1* Z 25.27 /
  P-302 68 60 35 35 OPEN 1* 1.4202E+001 0.82292 9539.73 0.50 1* Z 29.05 /
  P-302 68 60 36 36 OPEN 1* 7.9808E+000 0.82292 5389.67 0.50 1* Z 29.80 /
  P-302 67 60 36 36 OPEN 1* 1.2618E+001 0.82292 8661.89 0.50 1* Z 32.25 /
  P-302 67 60 37 37 OPEN 1* 3.2565E+001 0.82292 22494.60 0.50 1* Z 33.24/
  P-302 67 60 38 38 OPEN 1* 1.4569E+001 0.82292 9938.87 0.50 1* Z 31.28 /
  P-302 67 60 39 39 OPEN 1* 8.0559E+000 0.82292 5444.90 0.50 1* Z 29.92 /
  P-302 67 60 40 40 OPEN 1* 1.7100E+001 0.82292 11748.32 0.50 1* Z 32.38/
  P-302 67 60 41 41 OPEN 1* 7.0951E+000 0.82292 4745.71 0.50 1* Z 28.47 /
  P-302 67 60 42 42 OPEN 1* 2.9322E+001 0.82292 20274.68 0.50 1* Z 33.41/
  P-302 67 60 43 43 OPEN 1* 1.5620E+001 0.82292 10755.88 0.50 1* Z 32.74/
  P-302 67 60 44 44 OPEN 1* 1.2547E+001 0.82292 8650.97 0.50 1* Z 32.94 /
  P-302 67 60 45 45 OPEN 1* 1.6066E+001 0.82292 11111.78 0.50 1* Z 33.45/
  I-401 85 49 16 16 OPEN 1* 1.3405E+001 0.82292 8274.65 0.50 1* Z 19.75 /
  I-401 85 49 17 17 OPEN 1* 5.2473E-001 0.82292 286.68 0.50 1* Z 11.95 /
I-401 85 49 18 18 OPEN 1* 2.3603E+001 0.82292 14673.41 0.50 1* Z 20.38 /
  I-401 85 49 19 19 OPEN 1* 1.8245E+001 0.82292 11296.29 0.50 1* Z 20.02/
  I-401 85 49 20 20 OPEN 1* 1.4804E+001 0.82292 9181.59 0.50 1* Z 20.17 /
  I-401 85 49 21 21 OPEN 1* 2.0968E+001 0.82292 13038.35 0.50 1* Z 20.40/
  I-401 85 49 22 22 OPEN 1* 1.2068E-002 0.82292 4.84 0.50 1* Z 4.28 /
  I-401 85 49 23 23 OPEN 1* 1.3593E+001 0.82292 8390.68 0.50 1* Z 19.75 /
  I-401 85 49 24 24 OPEN 1* 2.1704E+001 0.82292 13498.31 0.50 1* Z 20.42/
  I-401 85 49 25 25 OPEN 1* 2.0338E+001 0.82292 12649.82 0.50 1* Z 20.42/
  I-401 85 49 26 26 OPEN 1* 2.3365E+001 0.82292 14367.43 0.50 1* Z 19.43/
  I-401 85 49 27 27 OPEN 1* 1.3297E+001 0.82292 8226.03 0.50 1* Z 19.95 /
  I-401 86 49 27 27 OPEN 1* 1.4211E+001 0.82292 8719.83 0.50 1* Z 19.25 /
  I-401 86 49 28 28 OPEN 1* 6.3533E+000 0.82292 3908.33 0.50 1* Z 19.46 /
  I-401 86 50 28 28 OPEN 1* 2.1570E+001 0.82292 13264.99 0.50 1* Z 19.43/
  I-401 86 50 29 29 OPEN 1* 3.6987E+001 0.82292 22764.39 0.50 1* Z 19.50/
  I-401 86 50 30 30 OPEN 1* 2.7320E+001 0.82292 16788.51 0.50 1* Z 19.37/
  I-401 86 50 31 31 OPEN 1* 2.2796E+001 0.82292 13993.73 0.50 1* Z 19.29/
  I-401 86 50 32 32 OPEN 1* 3.2576E+001 0.82292 20167.29 0.50 1* Z 20.01/
  I-401 87 50 32 32 OPEN 1* 2.1326E+001 0.82292 13154.55 0.50 1* Z 19.69/
  I-401 87 50 33 33 OPEN 1* 1.9378E+001 0.82292 11891.59 0.50 1* Z 19.26/
  I-401 87 50 34 34 OPEN 1* 2.2473E+001 0.82292 13801.40 0.50 1* Z 19.32/
  I-401 87 50 35 35 OPEN 1* 3.8374E+001 0.82292 23728.40 0.50 1* Z 19.91/
  I-401 87 50 36 36 OPEN 1* 7.1382E+001 0.82292 44464.07 0.50 1* Z 20.56/
  I-401 87 50 37 37 OPEN 1* 3.2568E+001 0.82292 20162.24 0.50 1* Z 20.01
  I-401 88 50 37 37 OPEN 1* 6.9110E+000 0.82292 4263.88 0.50 1* Z 19.71 /
  I-401 88 50 38 38 OPEN 1* 5.6375E+001 0.82292 34893.86 0.50 1* Z 19.99/
  I-401 88 50 39 39 OPEN 1* 9.7805E-001 0.82292 531.63 0.50 1* Z 11.72 /
```

```
  I-401 88 50 40 40 OPEN 1* 8.7014E+001 0.82292 54158.48 0.50 1* Z 20.49/
  I-401 88 50 41 41 OPEN 1* 4.7724E+001 0.82292 29508.65 0.50 1* Z 19.90/
  I-401 88 50 42 42 OPEN 1* 5.6489E+001 0.82292 35171.49 0.50 1* Z 20.52/
  I-401 89 50 42 42 OPEN 1* 6.7300E+000 0.82292 4128.26 0.50 1* Z 19.22 /
  I-401 89 50 43 43 OPEN 1* 3.7421E+001 0.82292 23080.53 0.50 1* Z 19.69/
  I-401 89 50 44 44 OPEN 1* 4.6207E+001 0.82292 28564.57 0.50 1* Z 19.88/
  I-401 89 50 45 45 OPEN 1* 2.3076E+001 0.82292 14175.11 0.50 1* Z 19.34/
  I-402 87 40 16 16 OPEN 1* 1.0626E+001 0.82292 6677.21 0.50 1* Z 21.38 /
  I-402 87 40 17 17 OPEN 1* 1.2857E+001 0.82292 8123.36 0.50 1* Z 21.90 /
  I-402 87 40 18 18 OPEN 1* 4.0893E+000 0.82292 2525.01 0.50 1* Z 19.78 /
  I-402 87 40 19 19 OPEN 1* 8.7382E+000 0.82292 5512.53 0.50 1* Z 21.75 /
  I-402 87 39 19 19 OPEN 1* 5.6259E+000 0.82292 3556.14 0.50 1* Z 21.94 /
  I-402 87 39 20 20 OPEN 1* 1.5294E+001 0.82292 9667.43 0.50 1* Z 21.95 /
  I-402 87 39 21 21 OPEN 1* 7.5236E+000 0.82292 4691.59 0.50 1* Z 20.66 /
  I-402 87 39 22 22 OPEN 1* 1.0850E+001 0.82292 6830.32 0.50 1* Z 21.55 /
  I-402 87 39 23 23 OPEN 1* 1.0159E+001 0.82292 6396.38 0.50 1* Z 21.56 /
  I-402 87 39 24 24 OPEN 1* 1.3441E+001 0.82292 8406.39 0.50 1* Z 20.93 /
  I-402 87 39 25 25 OPEN 1* 5.8459E+000 0.82292 3629.34 0.50 1* Z 20.26 /
  I-402 87 39 26 26 OPEN 1* 8.2402E+000 0.82292 5172.34 0.50 1* Z 21.27 /
  I-402 88 39 26 26 OPEN 1* 3.5026E+000 0.82292 2169.87 0.50 1* Z 20.07 /
  I-402 88 39 27 27 OPEN 1* 2.2834E+001 0.82292 14331.58 0.50 1* Z 21.26/
  I-402 88 39 28 28 OPEN 1* 1.8237E+001 0.82292 11408.03 0.50 1* Z 20.95/
  I-402 88 39 29 29 OPEN 1* 3.0052E+001 0.82292 18982.53 0.50 1* Z 21.87/
  I-402 88 39 30 30 OPEN 1* 1.8631E+001 0.82292 11683.97 0.50 1* Z 21.18/
  I-402 88 39 31 31 OPEN 1* 1.2691E+001 0.82292 7890.32 0.50 1* Z 20.39 /
  I-402 88 39 32 32 OPEN 1* 2.8110E+001 0.82292 17765.46 0.50 1* Z 21.93/
  I-402 88 39 33 33 OPEN 1* 2.9514E+001 0.82292 18655.84 0.50 1* Z 21.94/
  I-402 88 39 34 34 OPEN 1* 1.1788E+001 0.82292 7328.45 0.50 1* Z 20.38 /
  I-402 88 39 35 35 OPEN 1* 1.3480E+001 0.82292 8399.08 0.50 1* Z 20.58 /
  /

COMPORD
 P-301  INPUT  /
 P-302  INPUT  /
 I-401  INPUT  /
 I-402  INPUT  /
/

WCONPROD
    P-301 1* GRUP  11000 1*  15000  3*   1450  1  0.6 /
    P-302 1* GRUP 9000  1*  15000  3*  1450  2  0.4 /
/

WECON
  P-301  200 1* 0.9500 1* 1* WELL /
  P-302 200 1* 0.9500 1* 1* WELL /

 /
 --INJ1-2
 WCONINJE
     'I-401'     WATER     1*     GRUP     1*     1*     5100
3000     1     /
     'I-402'     WATER     1*     GRUP     1*     1*     5100
3000     2     /
/

GCONINJE
```

```
'GROUP 1' WATER VREP 1* 1* 1* 1.0 /
/
GCONPROD
  FIELD ORAT 20000 1* 30000 25000 RATE /
/

DRSDT
 0.0 /

TSTEP
120 120 125 61 366 /

--INJ3
GCONSUMP
 'GROUP 1' 7500 17641/
/

WCONINJE
   'I-401'     WATER     1*     GRUP     1*     1*     5100
3000     1     /
   'I-402'     GAS       1*     GRUP     1*     1*     5100
5000     4  /
 /

GCONINJE
'FIELD'  'GAS'     'REIN'  60000   1*  1   /
'GROUP 1' WATER VREP 1* 1* 1* 1.0 /
/
TSTEP
365 /

--INJ4
GCONSUMP
 'GROUP 1' 7500 15220 /
/

WCONINJE
     'I-402'     WATER     1*     GRUP     1*     1*     5100
3000     2     /
     'I-401'     GAS     1*     GRUP     1*     1*     5100
5000     3  /
 /

 TSTEP
365 {-} __TS1__ /

WFOAM
I-402  __CS1__ /
/

TSTEP
__TS1__ /

--INJ5
GCONSUMP
```

```
 'GROUP 1' 7500 12974 /
/

WCONINJE
   'I-401'     WATER     1*     GRUP     1*     1*     5100
3000     1     /
   'I-402'     GAS       1*     GRUP     1*     1*     5100
5000     4  /
 /

TSTEP
365 /

--INJ6
GCONSUMP
 'GROUP 1' 7500 9897 /
/
WCONINJE
     'I-402'     WATER     1*     GRUP     1*     1*     5100
3000     2     /
     'I-401'     GAS     1*     GRUP     1*     1*     5100
5000     3  /
 /
TSTEP
365 {-} __TS2__ /

WFOAM
I-402  __CS2__ /
/

TSTEP
__TS2__  /

--INJ7
GCONSUMP
 'GROUP 1' 7500 7503 /
/

WCONINJE
   'I-401'     WATER     1*     GRUP     1*     1*     5100
3000     1     /
   'I-402'     GAS       1*     GRUP     1*     1*     5100
5000     4  /
 /

TSTEP
365 /

--INJ8
GCONSUMP
 'GROUP 1' 7500 6200 /
/

WCONINJE
```

```
     'I-402'      WATER      1*      GRUP      1*      1*      5100
3000      2      /
     'I-401'      GAS      1*      GRUP      1*      1*      5100
5000      3   /
 /

TSTEP
365 {-} __TS3__ /

WFOAM
I-402   __CS3__ /
/

TSTEP
__TS3__ /

--INJ9
GCONSUMP
 'GROUP 1' 7500 5151 /
/

WCONINJE
   'I-401'      WATER      1*      GRUP      1*      1*      5100
3000      1      /
   'I-402'      GAS        1*      GRUP      1*      1*      5100
5000      4   /
 /

TSTEP
365 /

--INJ10
GCONSUMP
 'GROUP 1' 7500 4405 /
/

WCONINJE
     'I-402'      WATER      1*      GRUP      1*      1*      5100
3000      2      /
     'I-401'      GAS      1*      GRUP      1*      1*      5100
5000      3   /
 /

TSTEP
305 /

END
```

A.2. MATLAB data file

```
data = xlsread('OUTCOMES_SIMULATIONS.xls');
UncSamp = data(:,3:7);
DecSamp = [data(:,1:2) data(:,8:9)];
FOPT = data(:,10);
FGPT = data(:,11);

% Design matrix building
X = [ ones(nprg,1) UncSamp(rgpt,:) DecSamp(rgpt,:)];
Y = FOPT(rgpt);
XL = X;
for i=2:10,
    for j=i:10,
    XL = [XL X(:,i).*X(:,j)];
    end
end
BO = regress(Y,XL);
FOPTest = XL*BO;

% Validation matrix building
Xv = [ ones(size(valpt,1),1) UncSamp(valpt,:) DecSamp(valpt,:)];
XLv = Xv;
for i=2:10,
    for j=i:10,
    XLv = [XLv Xv(:,i).*Xv(:,j)];
    end
end
FOPTval = XLv*BO;

Y = FGPT(rgpt);
BG = regress(Y,XL);
FGPTest = XL*BG;
FGPTval = XLv*BG;

rangeO=max(FOPT(sel2))-min(FOPT(sel2));
rangeG=max(FGPT(sel2))-min(FGPT(sel2));
checkO=0.4.*ones(nprg,1);
checkG=0.2.*ones(nprg,1);

while      sum((((abs(FGPT(rgpt)-FGPTest))./rangeG)>checkG))>0||
sum((((abs(FOPT(rgpt)-FOPTest))./rangeO)>checkO))>0
    % Validation versus building selection
    rgpt  = randperm(size(FOPT,1));
    nprg  = round(0.7.*size(FOPT,1));
    valpt = rgpt(nprg+1:end)';
    rgpt  = rgpt(1:nprg)';
    % Design matrix building
    X = [ ones(nprg,1) UncSamp(rgpt,:) DecSamp(rgpt,:)];
    Y = FOPT(rgpt);
    XL = X;
    for i=2:10,
```

```
      for j=i:10,
      XL = [XL X(:,i).*X(:,j)];
      end
    end
    BO = regress(Y,XL);
    FOPTest = XL*BO;

    % Validation matrix building
    Xv = [ ones(size(valpt,1),1) UncSamp(valpt,:)
DecSamp(valpt,:)];
    XLv = Xv;
    for i=2:10,
        for j=i:10,
        XLv = [XLv Xv(:,i).*Xv(:,j)];
        end
    end
    FOPTval = XLv*BO;
    Y = FGPT(rgpt);
    BG = regress(Y,XL);
    FGPTest = XL*BG;
    FGPTval = XLv*BG;
end
UNC = xlsread('UNCERTAIN_VARIABLES.xls');
DEC = xlsread('DECISION_VARIABLES.xls');
for i=1:size(DEC,1)
    for j=1:size(UNC,1)
        VAR = [1 UNC(j,:) DEC(i,:)];
        V=VAR;
        for k=2:10,
            for l=k:10,
            V = [V VAR(1,k).*VAR(1,l)];
            end
        end

        FOPTp(i,j) = V*BO;
        FGPTp(i,j) = V*BG;
    end

end

for i=1:size(UNC,1)
    FOPTm(i)=mean(FOPTp(i,:));
    FGPTm(i)=mean(FGPTp(i,:));
end
LAMBDA=[0:0.0001:0.05];
mass=LAMBDA;
RES=[];
for i=1:size(LAMBDA,2)
    RES = [RES; FOPTm-LAMBDA(i).*FGPTm];
    mass(i)=max(RES(i,:));
    ind(i)=find(RES(i,:)==max(RES(i,:)));
end
a=unique(ind);
```

Appendix B

	2014	2015/2016/2017								2018				2019				2020				2021				2022				2023				2024			
			Dis1							Dis2				Dis3				Dis4				Dis5				Dis6				Dis7				Dis8			
CASE 1 [3 mon]	IN1	IN2	IN3	IN4	IN5	IN6	IN7	IN8	IN9	IN10	IN11	IN12	IN13	IN14	IN15	IN16	IN17	IN18	IN19	IN20	IN21	IN22	IN23	IN24	IN25	IN26	IN27	IN28	IN29	IN30	IN31	IN32	IN33	IN34	IN35	IN36	IN37
Time length [d]	426	91	91	92	92	90	91	92	92	90	91	92	92	90	91	92	92	91	91	92	92	90	91	92	92	90	91	92	92	90	91	92	92	91	91	92	31
Start-up day	1/11	1/1	1/4	1/7	1/10	1/1	1/4	1/7	1/10	1/1	1/4	1/7	1/10	1/1	1/4	1/7	1/10	1/1	1/4	1/7	1/10	1/1	1/4	1/7	1/10	1/1	1/4	1/7	1/10	1/1	1/4	1/7	1/10	1/1	1/4	1/7	1/10
I-401	W	W	W	G	W	G	W	G	W	G	W	G	W	G	W	G	W	G	W	G	W	G	W	G	W	G	W	G	W	G	W	G	W	G	W	G	W
I-402	W	W	G	W	G	W	G	W	G	W	G	W	G	W	G	W	G	W	G	W	G	W	G	W	G	W	G	W	G	W	G	W	G	W	G	W	G
CASE 11 [3 mon]	IN1	IN2	IN3	IN4	IN5	IN6	IN7	IN8	IN9	IN10	IN11	IN12	IN13	IN14	IN15	IN16	IN17	IN18	IN19	IN20	IN21	IN22	IN23	IN24	IN25	IN26	IN27	IN28	IN29	IN30	IN31	IN32	IN33	IN34	IN35	IN36	IN37
Time length [d]	426	91	91	92	92	90	91	92	92	90	91	92	92	90	91	92	92	91	91	92	92	90	91	92	92	90	91	92	92	90	91	92	92	91	91	92	31
Start-up day	1/11	1/1	1/4	1/7	1/10	1/1	1/4	1/7	1/10	1/1	1/4	1/7	1/10	1/1	1/4	1/7	1/10	1/1	1/4	1/7	1/10	1/1	1/4	1/7	1/10	1/1	1/4	1/7	1/10	1/1	1/4	1/7	1/10	1/1	1/4	1/7	1/10
I-401	W	W	G	W	G	W	G	W	G	W	G	W	G	W	G	W	G	W	G	W	G	W	G	W	G	W	G	W	G	W	G	W	G	W	G	W	G
I-402	W	W	W	G	W	G	W	G	W	G	W	G	W	G	W	G	W	G	W	G	W	G	W	G	W	G	W	G	W	G	W	G	W	G	W	G	W
CASE 2 [4 mon]	IN1	IN2	IN3	IN4	IN5	IN6	IN7			IN8	IN9	IN10		IN11	IN12	IN13		IN14	IN15	IN16		IN17	IN18	IN19		IN20	IN21	IN22		IN23	IN24	IN25		IN26	IN27	IN28	
Time length [d]	426	121	123	122	120	123	122			120	123	122		120	123	122		121	123	122		120	123	122		120	123	122		120	123	122		121	123	61	
Start-up day	1/11	1/1	1/5	1/9	1/1	1/5	1/9			1/1	1/5	1/9		1/1	1/5	1/9		1/1	1/5	1/9		1/1	1/5	1/9		1/1	1/5	1/9		1/1	1/5	1/9		1/1	1/5	1/9	
I-401	W	W	W	G	W	G	W			G	W	G		W	G	W		G	W	G		W	G	W		G	W	G		W	G	W		G	W	G	
I-402	W	W	G	W	G	W	G			W	G	W		G	W	G		W	G	W		G	W	G		W	G	W		G	W	G		W	G	W	
CASE 12 [4 mon]	IN1	IN2	IN3	IN4	IN5	IN6	IN7			IN8	IN9	IN10		IN11	IN12	IN13		IN14	IN15	IN16		IN17	IN18	IN19		IN20	IN21	IN22		IN23	IN24	IN25		IN26	IN27	IN28	
Time length [d]	426	121	123	122	120	123	122			120	123	122		120	123	122		121	123	122		120	123	122		120	123	122		120	123	122		121	123	61	
Start-up day	1/11	1/1	1/5	1/9	1/1	1/5	1/9			1/1	1/5	1/9		1/1	1/5	1/9		1/1	1/5	1/9		1/1	1/5	1/9		1/1	1/5	1/9		1/1	1/5	1/9		1/1	1/5	1/9	
I-401	W	W	G	W	G	W	G			W	G	W		G	W	G		W	G	W		G	W	G		W	G	W		G	W	G		W	G	W	
I-402	W	W	W	G	W	G	W			G	W	G		W	G	W		G	W	G		W	G	W		G	W	G		W	G	W		G	W	G	
CASE 3 [5 mon]	IN1	IN2	IN3	IN4	IN5	IN6				IN7	IN8	IN9	IN10	IN11	IN12	IN13		IN14	IN15	IN16		IN17	IN18	IN19		IN20	IN21	IN22		IN23	IN24	IN25	IN26	IN27	IN28	IN29	
Time length [d]	426	152	153	151	153	122				31	150	153	31	120	153	92		60	153	153		151	153	61		90	153	122		31	150	153	31	121	153	31	
Start-up day	1/11	1/1	1/6	1/11	1/4	1/9				1/1	1/2	1/7	1/12	1/1	1/5	1/10		1/1	1/3	1/8		1/1	1/6	1/11		1/1	1/4	1/9		1/1	1/2	1/7	1/12	1/1	1/5	1/10	

Appendix B

I-401	W	W	W	G	W	G				G	W	G	W	W	G	W		W	G	W		G	W	G		G	W	G		G	W	G	W	W	G	W	
I-402	W	W	G	W	G	W				W	G	W	G	G	W	G		G	W	G		W	G	W		W	G	W		W	G	W	G	G	W	G	
CASE 13 [5 mon]	IN1	IN2	IN3	IN4	IN5	IN6				IN7	IN8	IN9	IN10	IN11	IN12	IN13		IN14	IN15	IN16		IN17	IN18	IN19		IN20	IN21	IN22		IN23	IN24	IN25	IN26	IN27	IN28	IN29	
Time length [d]	426	152	153	151	153	122				31	150	153	31	120	153	92		60	153	153		151	153	61		90	153	122		31	150	153	31	121	153	31	
Start-up day	1/11	1/1	1/6	1/11	1/4	1/9				1/1	1/2	1/7	1/12	1/1	1/5	1/10		1/1	1/3	1/8		1/1	1/6	1/11		1/1	1/4	1/9		1/1	1/2	1/7	1/12	1/1	1/5	1/10	
I-401	W	W	G	W	G	W				W	G	W	G	G	W	G		G	W	G		W	G	W		W	G	W		W	G	W	G	G	W	G	
I-402	W	W	W	G	W	G				G	W	G	W	W	G	W		W	G	W		G	W	G		G	W	G		G	W	G	W	W	G	W	
CASE 4 [6 mon]	IN1	IN2	IN3	IN4	IN5					IN6	IN7			IN8	IN9			IN10	IN11			IN12	IN13			IN14	IN15			IN16	IN17			IN18	IN19		
Time length [d]	426	182	184	181	184					181	184			181	184			182	184			181	184			181	184			181	184			182	123		
Start-up day	1/11	1/1	1/7	1/1	1/7					1/1	1/7			1/1	1/7			1/1	1/7			1/1	1/7			1/1	1/7			1/1	1/7			1/1	1/7		
I-401	W	W	W	G	W					G	W			G	W			G	W			G	W			G	W			G	W			G	W		
I-402	W	W	G	W	G					W	G			W	G			W	G			W	G			W	G			W	G			W	G		
CASE 14 [6 mon]	IN1	IN2	IN3	IN4	IN5					IN6	IN7			IN8	IN9			IN10	IN11			IN12	IN13			IN14	IN15			IN16	IN17			IN18	IN19		
Time length [d]	426	182	184	181	184					181	184			181	184			182	184			181	184			181	184			181	184			182	123		
Start-up day	1/11	1/1	1/7	1/1	1/7					1/1	1/7			1/1	1/7			1/1	1/7			1/1	1/7			1/1	1/7			1/1	1/7			1/1	1/7		
I-401	W	W	G	W	G					W	G			W	G			W	G			W	G			W	G			W	G			W	G		
I-402	W	W	W	G	W					G	W			G	W			G	W			G	W			G	W			G	W			G	W		
CASE 5 [7 mon]	IN1	IN2	IN3	IN4	IN5					IN6	IN7	IN8		IN9	IN10			IN11	IN12	IN13		IN14	IN15	IN16		IN17	IN18			IN19	IN20			IN21	IN22	IN23	
Time length [d]	426	213	212	214	92					120	214	31		181	184			31	213	122		90	214	61		151	214			212	153			60	214	31	
Start-up day	1/11	1/1	1/8	1/3	1/10					1/1	1/5	1/12		1/1	1/7			1/1	1/2	1/9		1/1	1/4	1/11		1/1	1/6			1/1	1/8			1/1	1/3	1/10	
I-401	W	W	W	G	W					W	G	W		W	G			G	W	G		G	W	G		G	W			G	W			W	G	W	
I-402	W	W	G	W	G					G	W	G		G	W			W	G	W		W	G	W		W	G			W	G			G	W	G	
CASE 15 [7 mon]	IN1	IN2	IN3	IN4	IN5					IN6	IN7	IN8		IN9	IN10			IN11	IN12	IN13		IN14	IN15	IN16		IN17	IN18			IN19	IN20			IN21	IN22	IN23	
Time length [d]	426	213	212	214	92					120	214	31		181	184			31	213	122		90	214	61		151	214			212	153			60	214	31	
Start-up day	1/11	1/1	1/8	1/3	1/10					1/1	1/5	1/12		1/1	1/7			1/1	1/2	1/9		1/1	1/4	1/11		1/1	1/6			1/1	1/8			1/1	1/3	1/10	
I-401	W	W	G	W	G					G	W	G		G	W			W	G	W		W	G	W		W	G			W	G			G	W	G	
I-402	W	W	W	G	W					W	G	W		W	G			G	W	G		G	W	G		G	W			G	W			W	G	W	

CASE 6 [8 mon]	IN1	IN2	IN3	IN4						IN5	IN6			IN7	IN8			IN9	IN10			IN11	IN12			IN13	IN14			IN15	IN16			IN17	IN18		
Time length [d]	426	244	242	245						243	122			120	245			244	122			120	245			243	122			120	245			244	61		
Start-up day	1/11	1/1	1/9	1/5						1/1	1/9			1/1	1/5			1/1	1/9			1/1	1/5			1/1	1/9			1/1	1/5			1/1	1/9		
I-401	W	W	W	G						W	G			G	W			G	W			W	G			W	G			G	W			G	W		
I-402	W	W	G	W						G	W			W	G			W	G			G	W			G	W			W	G			W	G		
CASE 16 [8 mon]	IN1	IN2	IN3	IN4						IN5	IN6			IN7	IN8			IN9	IN10			IN11	IN12			IN13	IN14			IN15	IN16			IN17	IN18		
Time length [d]	426	244	242	245						243	122			120	245			244	122			120	245			243	122			120	245			244	61		
Start-up day	1/11	1/1	1/9	1/5						1/1	1/9			1/1	1/5			1/1	1/9			1/1	1/5			1/1	1/9			1/1	1/5			1/1	1/9		
I-401	W	W	G	W						G	W			W	G			W	G			G	W			G	W			W	G			W	G		
I-402	W	W	W	G						W	G			G	W			G	W			W	G			W	G			G	W			G	W		
CASE 7 [9 mon]	IN1	IN2	IN3	IN4						IN5	IN6			IN7	IN8			IN9	IN10			IN11	IN12			IN13	IN14			IN15	IN16			IN17	IN18		
Time length [d]	426	274	273	184						90	275			273	92			182	184			90	275			273	92			181	184			91	214		
Start-up day	1/11	1/1	1/10	1/7						1/1	1/4			1/1	1/10			1/1	1/7			1/1	1/4			1/1	1/10			1/1	1/7			1/1	1/4		
I-401	W	W	W	G						G	W			G	W			W	G			G	W			G	W			W	G			G	W		
I-402	W	W	G	W						W	G			W	G			G	W			W	G			W	G			G	W			W	G		
CASE 17 [9 mon]	IN1	IN2	IN3	IN4						IN5	IN6			IN7	IN8			IN9	IN10			IN11	IN12			IN13	IN14			IN15	IN16			IN17	IN18		
Time length [d]	426	274	273	184						90	275			273	92			182	184			90	275			273	92			181	184			91	214		
Start-up day	1/11	1/1	1/10	1/7						1/1	1/4			1/1	1/10			1/1	1/7			1/1	1/4			1/1	1/10			1/1	1/7			1/1	1/4		
I-401	W	W	G	W						W	G			W	G			G	W			W	G			W	G			G	W			W	G		
I-402	W	W	W	G						G	W			G	W			W	G			G	W			G	W			W	G			G	W		
CASE 8 [10 mon]	IN1	IN2	IN3	IN4						IN5	IN6			IN7	IN8			IN9	IN10			IN11	IN12			IN13	IN14			IN15	IN16			IN17	IN18		
Time length [d]	426	305	304	122						181	184			120	245			60	306			304	61			243	122			181	184			121	184		
Start-up day	1/11	1/1	1/11	1/9						1/1	1/7			1/1	1/5			1/1	1/3			1/1	1/11			1/1	1/9			1/1	1/7			1/1	1/5		
I-401	W	W	W	G						G	W			W	G			G	W			G	W			W	G			G	W			W	G		
I-402	W	W	G	W						W	G			G	W			W	G			W	G			G	W			W	G			G	W		
CASE 18 [10 mon]	IN1	IN2	IN3	IN4						IN5	IN6			IN7	IN8			IN9	IN10			IN11	IN12			IN13	IN14			IN15	IN16			IN17	IN18		
Time length [d]	426	305	304	122						181	184			120	245			60	306			304	61			243	122			181	184			121	184		

Appendix B

Start-up day	1/11	1/1	1/11	1/9						1/1	1/7			1/1	1/5			1/1	1/3			1/1	1/11			1/1	1/9			1/1	1/7			1/1	1/5		
I-401	W	W	G	W						W	G			G	W			W	G			W	G			G	W			W	G			G	W		
I-402	W	W	W	G						G	W			W	G			G	W			G	W			W	G			G	W			W	G		
CASE 9 [11 mon]	IN1	IN2	IN3	IN4						IN5	IN6			IN7	IN8			IN9	IN10			IN11	IN12			IN13	IN14			IN15	IN16			IN17	IN18		
Time length [d]	426	335	335	61						273	92			243	122			213	153			181	184			151	214			120	245			91	214		
Start-up day	1/11	1/1	1/12	1/11						1/1	1/10			1/1	1/9			1/1	1/8			1/1	1/7			1/1	1/6			1/1	1/5			1/1	1/4		
I-401	W	W	W	G						G	W			W	G			G	W			W	G			G	W			W	G			G	W		
I-402	W	W	G	W						W	G			G	W			W	G			G	W			W	G			G	W			W	G		
CASE 19 [11 mon]	IN1	IN2	IN3	IN4						IN5	IN6			IN7	IN8			IN9	IN10			IN11	IN12			IN13	IN14			IN15	IN16			IN17	IN18		
Time length [d]	426	335	335	61						273	92			243	122			213	153			181	184			151	214			120	245			91	214		
Start-up day	1/11	1/1	1/12	1/11						1/1	1/10			1/1	1/9			1/1	1/8			1/1	1/7			1/1	1/6			1/1	1/5			1/1	1/4		
I-401	W	W	G	W						W	G			G	W			W	G			G	W			W	G			G	W			W	G		
I-402	W	W	W	G						G	W			W	G			G	W			W	G			G	W			W	G			G	W		
CASE 10 [12 mon]	IN1	IN2	IN3							IN4				IN5				IN6				IN7				IN8				IN9				IN10			
Time length [d]	426	366	365							365				365				366				365				365				365				305			
Start-up day	1/11	1/1	1/1							1/1				1/1				1/1				1/1				1/1				1/1				1/1			
I-401	W	W	W							G				W				G				W				G				W				G			
I-402	W	W	G							W				G				W				G				W				G				W			
CASE 20 [12 mon]	IN1	IN2	IN3							IN4				IN5				IN6				IN7				IN8				IN9				IN10			
Time length [d]	426	366	365							365				365				366				365				365				365				305			
Start-up day	1/11	1/1	1/1							1/1				1/1				1/1				1/1				1/1				1/1				1/1			
I-401	W	W	G							W				G				W				G				W				G				W			
I-402	W	W	W							G				W				G				W				G				W				G			

Table B 1 – Possible WAG injection scenarios analyzed

FOPT [StB]	VRR1	VRR2	VRR3	VRR4	VRR5	VRR6	VRR7	VRR8
27449968	1,00	1,00	1,30	1,20	1,30	1,20	1,00	1,10
27449446	1,00	1,00	1,30	1,20	1,10	1,30	1,00	1,20
27448590	1,00	1,00	1,20	1,00	1,10	1,00	1,00	1,30
27448334	1,00	1,00	1,10	1,20	1,30	1,10	1,00	1,10
27445704	1,00	1,00	1,20	1,10	1,30	1,10	1,20	1,20
27445500	1,00	1,00	1,30	1,20	1,20	1,30	1,30	1,20
27445150	1,00	1,00	1,20	1,00	1,30	1,00	1,10	1,20
27444888	1,00	1,00	1,30	1,30	1,10	1,30	1,20	1,20
27444684	1,00	1,00	1,30	1,30	1,20	1,00	1,20	1,20
27444354	1,00	1,00	1,10	1,20	1,20	1,10	1,30	1,00

Table B 2 – First 10 best scenarios for Case #10 (12 months-slugs)

	I-402 starting gas injection				I-401 starting gas injection			
Slug Duration [months]	**FOPT [StB]**	**Case**	**VRR**	**$\Delta_{VRR:1,3-1}$**	**FOPT [StB]**	**Case**	**VRR**	**$\Delta_{I402-I401}$**
3	24650702	1	1,0	1997832	24633136	11	1,0	17566
3	26648534	1	1,3		26633086	11	1,3	15448
4	24927544	2	1,0	1747898	24942074	12	1,0	-14530
4	26675442	2	1,3		26661266	12	1,3	14176
5	25300596	3	1,0	1443296	25221780	13	1,0	78816
5	26743892	3	1,3		26726936	13	1,3	16956
6	25575826	4	1,0	1269052	25445042	14	1,0	130784
6	26844878	4	1,3		26814098	14	1,3	30780
7	26592068	5	1,0	345562	26519560	15	1,0	72508
7	26937630	5	1,3		26891194	15	1,3	46436
8	26859626	6	1,0	173530	26794980	16	1,0	64646
8	27033156	6	1,3		26968230	16	1,3	64926
9	26969970	7	1,0	130462	26980084	17	1,0	-10114
9	27100432	7	1,3		27066628	17	1,3	33804
10	27101014	8	1,0	73592	27080298	18	1,0	20716
10	27174606	8	1,3		27078380	18	1,3	96226
11	27186724	9	1,0	8740	27190972	19	1,0	-4248
11	27195464	9	1,3		27212564	19	1,3	17100
12	27297784	10	1,0	982	27245110	20	1,0	52674
12	27298766	10	1,3		27246314	20	1,3	52452

Table B 3 – Case-comparison for wells I-401 and I-402 starting gas injection

Appendix B

				VRR = 1							LHS OPTIMAL						
TIME [yrs]	YR	$r_{o,Brent}$ [$/StB]	$r_{o,FIELD}$ [$/StB]	FOPT [10^3 StB]	FWPT [10^3 StB]	FWIT [10^3 StB]	FOAPR [StB/d]	FWAPR [StB/d]	FWAIR [StB/d]	NPVi [10^6 $]	FOPT [10^3 StB]	FWPT [10^3 StB]	FWIT [10^3 StB]	FOAPR [StB/d]	FWAPR [StB/d]	FWAIR [StB/d]	NPVi [10^6 $]
0,329	15	104,9	105,6	2400	0,02	3139	20013,7	0,16	26177,3	233,85	2400	0,02	3139	20013,7	0,17	26177,3	233,85
0,657	15	104,9	105,6	4800	0,04	6279	20013,7	0,18	26186,7	227,46	4800	0,04	6279	20013,7	0,18	26186,7	227,46
0,999	15	104,9	105,6	7300	0,063	9550	20013,7	0,17	26189,8	231,16	7300	0,063	9550	20013,7	0,17	26189,8	231,16
1,166	16	99,5	100,2	8520	0,079	11147	20013,7	0,24	26191,0	105,49	8520	0,079	11147	20013,7	0,24	26191,0	105,49
2,168	17	99,3	100,0	15124	1807	21597	18055,5	4940,9	28572,0	511,15	15123	1807	21597	18055,5	4940,9	28572,0	511,15
3,168	18	101,5	102,2	19010	7046	27341	10654,4	14362,9	15748,4	266,04	18803	7252	28842	10087,6	14929,1	19863,1	242,98
4,167	19	105,2	105,9	21764	13418	33936	7550,1	17469,2	18079,4	161,11	21396	13785	35845	7110,3	17911,0	19199,1	146,58
5,166	20	109,3	110,0	23326	17881	38246	4282,4	12237,5	11817,7	83,68	23051	20524	44289	4536,6	18474,6	23150,0	67,92
6,168	21	114,0	114,7	24621	21692	42516	3540,0	10420,5	11673,2	65,72	24498	27358	51123	3956,4	18684,3	18685,8	57,03
7,168	22	118,8	119,5	25462	24662	46204	2305,6	8141,0	10111,7	37,72	25430	33276	58713	2555,2	16225,6	20806,1	22,58
8,167	23	124,0	124,7	26249	28224	50789	2158,6	9765,1	12569,7	29,42	26305	40264	65765	2399,4	19158,4	19334,3	17,23
9,166	24	129,2	129,9	26818	31923	55605	1560,2	10142,9	13204,8	14,11	26926	46674	73284	1701,0	17574,7	20615,7	2,46
10	24	134,2	134,9	27298	36469	61255	1573,8	14912,7	18536,4	4,54	27450	53257	80428	1718,3	21597,2	23438,6	-2,10
										1971,5							**1863,8**

Table B 4 – NPV calculated for the analyzed optimal cases with VRR=1 and the one coming from the LHS design

Year	Gas from other fields [Sft^3/d]	Gas from other fields [Sm^3/d]
2017	17641	500
2018	15220	431
2019	12974	367
2020	9897	280
2021	7503	212
2022	6200	176
2023	5151	146
2024	4405	125

Table B 5 – Gas rates coming from other fields to be disposed into FIELD α

C_{S1} [lb/StB]	C_{S2} [lb/StB]	C_{S3} [lb/StB]	T_{S1} [d]	T_{S2} [d]	T_{S3} [d]	FOPT [StB]	FOPT (No C_{S3} & T_{S3}) [StB]	Δ [%]
0,62	0,09	0,43	2,27	2,67	8,72	27386594	27051108	-1,23
0,11	0,84	0,59	0,81	2,96	9,39	27380330	27097818	-1,03
0,23	1,00	1,60	6,59	3,48	0,93	27369896	27116280	-0,93
0,21	1,15	1,18	1,85	2,23	6,52	27339242	27046692	-1,07
1,30	0,11	0,16	1,21	0,93	4,60	27303268	27044142	-0,95
0,88	0,34	0,87	4,20	0,13	2,57	27274584	27064588	-0,77
0,15	1,32	1,27	5,06	6,41	6,32	27266966	26995756	-0,99
0,11	0,18	0,09	4,47	6,60	9,21	27239594	26959116	-1,03
0,90	0,43	2,54	1,49	2,65	6,49	27234792	26945284	-1,06
0,06	1,84	1,26	9,56	9,87	5,26	27223562	26907056	-1,16
		1,00			**6,00**			**-1,02**

Table B 6 – Best 10 cases selected for the computation of reasonable average value of Cs3 and Ts3

References

[1] U.S. Department of Energy – Office of Fossil Energy. Available: http://www.energy.gov/fe/science-innovation/oil-gas/enhanced-oil-recovery

[2] RIGZONE Website – "What Is EOR, and How Does It Work?". Available: http://www.rigzone.com/training/insight.asp?insight_id=313&c_id=4

[3] Green, D.W. and Willhite, G.P. – "Enhanced Oil Recovery", Henry L. Doherty Memorial Fund of AIME, SPE, pp. 3-4, 1998.

[4] Christensen, J.R., Stenby, E.H., and Skauge, A. – "Review of WAG Field Experience", SPE Reservoir Evaluation & Engineering, pp. 97-106, April 2001.

[5] Hinderaker, L., Utseth, R.H., Hustad, O.S., Akervoll, I., Dalland, M., Kvanvik, B.A., Austad, T., and Paulsen, J.E. – "RUTH – A Comprehensive Norwegian R&D program on IOR", SPE European Petroleum Conference, October 1996.

[6] Smalley, P.C., Ross, B., Brown, C.E., Moulds, T.P., and Smith, M.J. – "Reservoir Technical Limits: A Framework for Maximizing Recovery From Oil Fields", SPE Reservoir Evaluation & Engineering, pp. 610-617, August 2009.

[7] Petrobras' IOR strategy for the Lula production pilot injection tests. Available: http://www.offshore-mag.com/articles/print/volume-71/issue-10/deepwater-field-development/petrobras-addresses-unknowns-of-pre-salt-drilling-and-production.html

[8] Sohrabi, M., Henderson, G.D., Tehrani, D.H. and Danesh, A. – "Visualization of Oil Recovery by Water Alternating Gas (WAG) Injection Using High Pressure Micromodels – Water-Wet System", SPE Annual Technical Conference and Exhibition, 1-4 October 2000.

[12] Arogundade, O., Shahverdi, H. and Sohrabi, M. – "A Study of Three Phase Relative Permeability and Hysteresis in Water Alternating Gas (WAG) Injection", SPE Enhanced Oil Recovery Conference, 2-4 July 2013.

[13] Christensen, J.R., Larsen M. and Nicolaisen, H. – "Compositional Simulation of Water-Alternating-Gas Processes", SPE Annual Technical Conference and Exhibition, 1-4 October 2009.

[10] Kulkarni, M.M. and Rao, D.N. – "Experimental Investigation of Various Methods of Tertiary Gas Injection", SPE Annual Technical Conference and Exhibition, 26-29 September 2004.

[11] Virnovsky, G.A., Helset, H.M. and Skjæveland, S.M. – "Stability of Displacement Fronts in WAG Operations", SPE Annual Technical Conference and Exhibition, 25-28 September 1994.

[9] Skauge, A. – "Simulation studies of WAG using three-phase relative permeability hysteresis models", paper 015, European Symposium on Improved Oil Recovery, The Hague, 20-22 October 1997.

[14] Danesh, A. – "PVT and phase behaviour of petroleum reservoir fluids", Developments in Petroleum Science 47, 2007.

[15] Shahverdi, H. – "Characterization of Three-phase Flow and WAG Injection in Oil Reservoirs", Ph.D. Thesis, Department of Petroleum Engineering at Heriot-Watt University, February, 2012.

[16] Skauge, A. and Sorbie, K. – "Status of Fluid Flow Mechanisms for Miscible and Immiscible WAG", SPE EOR Conference, 31 March – 2 April, 2014.

[17] Sohrabi, M., Danesh, A. and Tehrani, D.H. – "Oil Recovery by Near-Miscible SWAG Injection", SPE Europec/EAGE Annual Conference, 13-16 June, 2005.

[18] Sorbie, K.S. and van Dijke, M.I.J. – "The Mechanism of Oil Recovery by Water-Alternating-Gas Injection at Near-Miscible Conditions in Mixed Wet Systems", SPE Improved Oil Recovery Symposium, 26-28 April, 2010.

[19] van Dijke, M.I.J., Danesh, A., Sohrabi, M. and Sorbie, K.S. – "Three-Phase Flow WAG Processes in Mixed-Wet Porous Media: Pore-Scale Network Simulations and Comparison With Water-Wet Micromodel Experiments", SPE Journal, pp. 57-66, March, 2004.

[20] van Dijke, M.I.J., Lorentzen, M., Sohrabi, M. and Sorbie, K.S. – "Pore-Scale Simulation of WAG Floods in Mixed-Wet Micromodels", SPE Journal, pp. 238-247, March, 2010.

[21] Righi, E.F., Royo, J., Gentil, P., Castelo, R., Del Monte, A. and Bosco, S. – "Experimental Study of Tertiary Immiscible WAG Injection", SPE/DOE 14th Symposium on Improved Oil Recovery, 17-21 April, 2004.

[22] Faisal, A., Bisdom, K., Zhumabek, B., Zadeh, A.M. and Rossen, W.R. – "Injectivity and Gravity Segregation in WAG and SWAG Enhanced Oil Recovery", SPE Annual Technical Conference and Exhibition, 4-7 October, 2009.

[23] Mohammad, J.D., Babak, M., Ghassem, Z., Afshin, J. and Gholam, H.M. – "Study of various water alternating gas injection methods in 4- and 5- spot injection patterns in an Iranian fractured reservoir", SPE, Trinidad and Tobago Energy Resources Conference, 27-30 June, 2010.

[24] Zahoor, M.K., Derahman, M.N. and Yunan, M.H. – "WAG Process Design – An Updated Review", Brazilian Journal of Petroleum and Gas, pp. 109-121, v.5, n°2, 2011.

[25] Jackson, D.D., Andrews, G.L. and Claridge, E.L. – "Optimum WAG Ratio vs. Rock Wettability in CO2 Flooding", SPE Annual Technical Conference and Exhibition, 22-25 September, 1985.

[26] Sohrabi, M. and Jamiolahmady, M. – "Mechanism of Injectivity Loss During Water-Alternating-Gas (WAG) Injection", 3rd IASME/WSEAS Int. Conf. on Fluid Dynamics and Aerodynamics, pp. 287-292, 20-22 August, 2005.

[27] Khanifar, A., Alian, S.S, Demiral, B. and Darman, N. – "Study of Asphaltene Precipitation and Deposition Phenomenon during WAG Application", SPE, Enhanced Oil Recovery Conference, 19-21 July, 2011.

[28] Rønningsen, H.P. – "Transportation of Waxy Crudes in Multiphase Pipelines", Presentation, Department of Petroleum Engineering and Applied Geophysics, Norwegian University of Science and Technology, Trondheim, pp. 52, 2006.

[29] Gudmundsson, J.S. – "Natural Gas Hydrate", Presentation, Department of Petroleum Engineering and Applied Geophysics, Norwegian University of Science and Technology, Trondheim, 22 October, 2013.

[30] Surguchev, L.M., Coombe, D.A., Hanssen, J.E. and Svorstøl, I. – "Simulation of WAG and Gas Injection with Potential Sweep Improvement by Application of Foam", 8th European IOR – Symposium, 15-17 May, 1995.

[31] Turta, A.T and Singhal, A.K. – "Field Foam Applications in Enhanced Oil Recovery Projects: Screening and Design Aspects", SPE, International Conference and Exhibition, 2-6 November, 1998.

[32] Sheng, J. – "Enhanced Oil Recovery Field Case Studies", Gulf Professional Publishing, April, 2013.

[33] Reme, A.B. - Diploma Thesis, March, 1999.

[34] Farzaneh, S.A. and Sohrabi, M. – "A Review of the Status of Foam Applications in Enhanced Oil Recovery", SPE, EAGE Annual Conference & Exhibition, 10-13 June, 2013.

[35] Chambers, K.T. and Radke, C.J. – "Interfacial Phenomena in Petroleum Recovery", Morrow, N.R. (Ed.), Dekker, pp 191-256, 1991.

[36] Cheng, L., Reme, A.B., Shan, D., Coombe, D.A. and Rossen, W.R. – "Simulating Foam Processes at High and Low Foam Qualities", SPE, 2000 SPE/DOE Improved Oil Recovery Symposium , 3-5 April, 2000.

[37] Osterloh, W.T. and Jante, M.J. – "Effects of Gas and Liquid Velocity on Steady-State Foam Flow at High Temperature", SPE, 1992 SPE/DOE Improved Oil Recovery Symposium, 22-24 April, 1992.

[38] Farajzadeh, R., Lotfollahi, M., Boeije, C.S., Rossen, W.R. and Hirasaki, G.J.H. – "Effect of permeability on foam-model parameters and the limiting capillary pressure", 2014.

[39] Holt, T., Vassenden, F. and Svorstøl, I. – "Effects of Pressure on Foam Stability; Implications for Foam Screening", SPE, 1996 SPE/DOE Tenth Symposium on Improved Oil Recovery, 21-24 April, 1996.

[40] Cateel, J.F. and Djbbarah, N.F. – "Sweep Improvement in CO2 Flooding by Use of Foaming Agents", Journal of Reservoir Engineering of Society of Petroleum Engineers, Vol 3, No 4, 1988.

[41] Apaydin, O.G. and Kovscek, A.R. – "Transient Foam Flow in Homogeneous Porous Media: Surfactant Concentration and Capillary End Effects, 2000 SPE/DOE Improved Oil Recovery Symposium, 2000.

[42] Farajzadeh, R., Andrianov, A., Krastev, R., Hirasaki, G.J. and Rossen, W.R. – "Foam-Oil Interaction in Porous Media: Implications for Foam Assisted Enhanced Oil Recovery", SPE, EOR Conference at Oil and Gas West Asia, 16-18 April, 2012.

[43] Schramm, L.L. – "Surfactants: Fundamentals and Applications in the Petroleum Industry", Cambridge University Press, 2000.

[44] "ECLIPSE Technical Description 2010.2", Schlumberger, 2010.

[45] "ECLIPSE 100 User Course", GeoQuest, Schlumberger, 1999.

[46] República de Angola, Ministério dos Petróleos – "Lei Geral das Actividades Petroliferas, n°13/78", Assembleia Nacional.

[47] ENI Factbook, 2012.

[48] Vogel, J.V. – "Inflow Performance Relationships for Solution-Gas Drive Wells", Shell Oil Co., January, 1968.

[49] McKay, M. D., Conover, W. J. and Beckman, R. J. – "A Comparison of Three Methods for Selecting Values of Input Variables in the Analysis of Output From a

Computer Code", American Statistical Association and the American Society for Quality, 1979.

[50] Helton, J.C. and Davis, F.J. – "Latin Hypercube Sampling and the Propagation of Uncertainty in Analyses of Complex Systems", Reliability Engineering and System Safety, 81, pp. 23-69, 25 February 2003.

[51] Matala, A. – "Sample Size Requirement for Monte Carlo Simulations Using Latin Hypercube Sampling", Helsinki University of Technology, 20 May, 2008.

[52] Chen, C., Li, G. and Reynolds, A.C. – "Robust Constrained Optimization of Short and Long-Term NPV for Closed-Loop Reservoir Management", SPE, 2011 SPE Reservoir Simulation Symposium, 21-23 February, 2011.

[53] Seba, R.D. – "Economics of Worldwide Petroleum Production", 3rd Edition, OGCI and PetroSkills, April, 2008.

[54] Seba, R.D. – "Expanded Basic Petroleum Economics Exercises", PetroSkills, 2013.

[55] Mohammadi, S. S. and Coombe, D. A. – "Characteristics of Steam Foam Drive Process in Massive Multizone and Thin Single Zone Reservoirs," paper 113 presented at the 5th UNITAR/UNDP Conference on Heavy Crude and Tar Sands, Caracas, Venezuela, 4-9 August, 1991.

[56] "STARS, Advanced Process and Thermal Reservoir Simulator User's Guide", Computer Modelling Group, 2009.

[57] Kovscek, A.R. – "Reservoir Simulation of Foam Displacement Processes", 7th UNITAR International Conference of Heavy Crude and Tars, 27-31 October, 1998.

[58] Surguchev, L.M., Soegnesand, S., Skauge, A. and Aarra, M.G. – "Modeling and History Matching of Foam Field Pilot: Oseberg Field", 8th European IOR Symposium, vol. 2, pp. 29-38, 15-17 May, 1995.

[59] Abbaszadeh, M., Korrani, A.K.N., Lopez-Salinas, J.L., de la Garza, F.R., Pino, A.V. and Hirasaki, G. – "Experimentally-Based Empirical Foam Modeling", SPE, Improved Oil Recovery Symposium, 12-16 April, 2014.

[60] Boeije, C.S. and Rossen, W.R. – "Fitting Foam Simulation Model Parameters to Data", 17th European Symposium on Improved Oil Recovery, 16-18 April, 2013.

[61] Spirov, P., Rudyk, S.N. and Khan, A.A. – "Foam Assisted WAG, Snorre Revisit with New Foam Screening Model", SPE, North Africa Technical Conference and Exhibition, 20-22 February, 2012.

[62] Haimes, Y.Y. – "Risk Modeling, Assessment, and Management", Wiley-Interscience, 2nd Ed., 2004.

[63] Ma, K., Lopez-Salinas, J.L., Puerto, M.C., Miller, C.A., Biswal, S.L. and Hirasaki G.J. – "Estimation of Parameters for the Simulation of Foam Flow through Porous Media. Part 1: The Dry-Out Effect", ACS, American Chemical Society, 2013.

[64] Rossen, W.R. and Boeije, C.S. – "Fitting Foam Simulation Model Parameters for SAG Foam Applications", SPE, Enhanced Oil Recovery Conference, 2-4 July, 2013.

[65] Ma, K., Biswal, S.L. and Hirasaki, G.J. – "Estimation of Parameters for Simulation of Steady State Foam Flow in Porous Media", 8th Global Congress on Process Safety, 1-5 April, 2012.

[66] Ma, K., Lopez-Salinas, J.L., Farajzadeh, R., Miller, C.A., Biswal, S.L. and Hirasaki G.J. – "Estimation of Parameters for the Simulation of Foam Flow through Porous Media. Part 3: Non-Uniqueness, Numerical Artifact and Sensitivity", SPE, Enhanced Oil Recovery Conference, 2-4 July, 2013.

[67] Matlab R2014a Documentation: http://www.mathworks.it/it/help/stats/stepwise.html

[68] Nielsen, H.B., Lophaven, S.N. and Søndergaard, J. – "DACE, A Matlab Kriging Toolbox", Technical Report, Technical University of Denmark, Version 2.0, 1 August, 2002.

[69] Beyer, H.G. and Sendhoff, B. – "Robust Optimization – A Comprehensive Survey", Elsevier Science, 5 March, 2007.

[70] Cappello, D. – "Well Placement Under Uncertainty: Recovery Improvement and Risk Reduction with a Multi-Objective Optimization", Master's thesis, Politecnico di Torino, MOGI Dept. ENI.

[71] Messac, A., Suka, C.P. and Melachrinoudis E. – "Aggregate Objective Functions and Pareto Frontiers: Required Relationships and Practical Implications", Optimization and Engineering Journal, Kluwer Publishers, Vol. 1, no. 2, June 2000.